



Forschungszentrum Karlsruhe
in der Helmholtz-Gemeinschaft

Wissenschaftliche Berichte
FZKA 7078

CBBI-12

**Proceedings of the
12th International Workshop
on Ceramic Breeder Blanket
Interactions**

Karlsruhe, Germany

September 16 – 17, 2004

R. Knitter (Hrsg.)

**Institut für Materialforschung
Programm Kernfusion**

Dezember 2004

Forschungszentrum Karlsruhe

in der Helmholtz-Gemeinschaft

Wissenschaftliche Berichte

FZKA 7078

CBBI-12

Proceedings of the 12th International Workshop on
Ceramic Breeder Blanket Interactions

Karlsruhe, Germany

September 16 – 17, 2004

R. Knitter (Hrsg.)

Institut für Materialforschung

Programm Kernfusion

Forschungszentrum Karlsruhe GmbH, Karlsruhe

2004

Impressum der Print-Ausgabe:

**Als Manuskript gedruckt
Für diesen Bericht behalten wir uns alle Rechte vor**

**Forschungszentrum Karlsruhe GmbH
Postfach 3640, 76021 Karlsruhe**

**Mitglied der Hermann von Helmholtz-Gemeinschaft
Deutscher Forschungszentren (HGF)**

ISSN 0947-8620

urn:nbn:de:0005-070786

PREFACE

The Twelfth International Workshop on Ceramic Breeder Blanket Interactions was held – under the auspices of the International Energy Agreement for Nuclear Technology of Fusion Reactors (IEA-NFT) and Fusions Materials (IEA-FM) – in Karlsruhe, Germany on September 16-17, 2004 as a short form workshop. The workshop was attended by 19 Participants.

The CBBI-12 has provided a forum of specialists involved in the design, research, development and testing of materials and components for lithium ceramic based breeding blankets. The workshop was divided into 5 technical sessions that addressed the general topics of (1) progress in the design of ceramic breeder reactors, (2) breeder material properties, (3) thermal and mechanical behaviour of pebble beds, (4) progress in ceramic breeder material development, and (5) irradiation testing. The 15 presentation, which were given and discussed, are published in these Proceedings.

The workshop was hosted by the Institute of Reactor Safety (IRS) at the Forschungszentrum Karlsruhe (Karlsruhe Research Center).

Programme Advisory Committee

M. Abdou (UCLA), M. Akiba (JAERI), S. Berk (OFES, USA), L.V. Boccaccini (FZK), K. Hayashi (JAERI), J.-D. Lulewicz (CEA), J. van der Laan (NRG), and M. Yamawaki (Tokyo University)

Local Organizing Committee in FZK

L.V. Boccaccini, R. Knitter, J. Reimann (FZK)

TABLE OF CONTENTS

List of Participants Programme

1	Progress in the Design of Ceramic Breeder Reactors	1
1.1	Design of Solid Breeder Test Blanket Modules in JAERI	3
1.2	Recent Progress in the Design of the HCPB Blanket.....	15
2	Breeder Material Properties	33
2.1	Lithium Depletion vs. Oxygen Loss Correlation for Li_2TiO_3 Pebbles as Exposed to the HCPB “Hot Spot” Conditions. A Thermo-chemical (TG-DTA-XRD-XPS) and Kinetic (TPD-TPR) Study	35
2.2	Hydrogen Isotopes Behavior on Li_2TiO_3 Under Water Exposure and Deuterium Ion Irradiation	45
2.3	Release Behavior of Bred Tritium from Ceramic Breeder Materials.....	57
3	Thermal and Mechanical Behaviour of Pebble Beds	65
3.1	Recent Efforts on Solid Breeder Blanket Thermomechanics and ITER TBM Activities ..	67
3.2	Characterization of Orthosilicate ex Hydroxide Pebble Beds and Mechanical Cycling of Different Types of Ceramic Breeder Materials	85
3.3	Modelling of Ceramic Breeder and Beryllium Pebble Beds at FZK.....	97
3.4	Effect of Thermomechanical Load on Effective Thermal Conductivity of a Li_2TiO_3 Pebble Bed.....	109
4	Progress in Ceramic Breeder Material Development	117
4.1	Ceramic Foams: Inspiring New Solid Breeder Materials	119
4.2	Fabrication of Lithium Orthosilicate Pebbles by Melt-Spraying – Reproducibility and Yield	129
4.3	Preparation and Characterization of Li_2TiO_3 Pebble Using the Combustion Synthesis and the Dry-rolling Granulation Process	141
5	Irradiation Testing	151
5.1	Behaviour of Blanket Ceramic Materials under Irradiation at High Temperature	153
5.2	A High Fluence Irradiation of Ceramic Breeder Materials in HFR Petten, Test-matrix and Design of the Irradiation Capsule	167
5.3	In Pile Behavior of the Pebble Bed Assemblies in the HFR, Results and First Data Analyses.....	183

LIST OF PARTICIPANTS

Name	Affiliation	email
Akiba, Masato	JAERI	akiba@naka.jaeri.go.jp
Alm, Birgit	FZ Karlsruhe	birgit.alm@imf.fzk.de
Boccaccini, Lorenzo V.	FZ Karlsruhe	lorenzo.boccaccini@irs.fzk.de
Casadio, Sergio	ENEA Casaccia	sergio.casadio@casaccia.enea.it
Ezato, Koichiro	JAERI	ezatok@fusion.naka.jaeri.go.jp
Hegeman, Johannes	NRG Petten	hegeman@nrg-nl.com
Hermsmeyer, Stephan	FZ Karlsruhe	stephan.hermsmeyer@iket.fzk.de
Kamlah, Marc	FZ Karlsruhe	marc.kamlah@imf.fzk.de
Ķizāne, Gunta	University of Latvia	radchem@kfi.lu.lv
Knitter, Regina	FZ Karlsruhe	regina.knitter@imf.fzk.de
Lässer, Rainer	FZ Karlsruhe / EFDA	rainer.laesser@tech.efda.org
Magielsen, A. J.	NRG Petten	magielsen@nrg-nl.com
Nishikawa, Masabumi	Kyushu University	nishikaw@nucl.kyushu-u.ac.jp
Olivares, Ryan	University of Tokyo	ruolivares@q.t.u-tokyo.ac.jp
Park, Ji Yeon	KAERI	jypark@kaeri.re.kr
Reimann, Jörg	FZ Karlsruhe	joerg.reimann@iket.fzk.de
Sharafat, Robert Shahram	UCLA	shahrams@ucla.edu
Tanigawa, Hisashi	JAERI	tanigawh@fusion.naka.jaeri.go.jp
Ying, Alice	UCLA	ying@fusion.ucla.edu

PROGRAMME

12th International Workshop on CERAMIC BREEDER BLANKET INTERACTIONS

Thursday, September 16

8.30 - 9.00 Registration
9.00 - 9.30 Opening Addresses

1 Progress in the Design of Ceramic Breeder Reactors [chairman: M. Akiba]

9.30 - 10.00 **Design of Solid Breeder Test Blanket Modules in JAERI (P15)**
K. Ezato, Y. Nomoto, S. Suzuki, T. Hirose, D. Tsuru, H. Tanigawa, T. Hatano, M. Enoda, and M. Akiba

10.00 - 10.30 **Recent Progress in the Design of the HCPB Blanket (P16)**
L.V. Boccaccini, S. Hermsmeyer and R. Meyder

2 Breeder Material Properties [chairman: M. Nishikawa]

10.45 - 11.15 **Lithium Depletion vs. Oxygen Loss Correlation for Li₂TiO₃ Pebbles as Exposed to the HCPB “Hot Spot” Conditions. A Thermo-chemical (TG-DTA-XRD-XPS) and Kinetic (TPD-TPR) Study (P7)**
C. Alvani, S. Casadio, V. Contini, R. Giorni, R. Mancini, K. Tsuchiya, and H. Kawamura

11:15 - 11.45 **Hydrogen Isotopes Behavior on Li₂TiO₃ Under Water Exposure and Deuterium Ion Irradiation (P8)**
R. Olivares, T. Oda, Y. Oya, K. Tsuchiya and S. Tanaka

11:45 - 12.15 **Release Behavior of Bred Tritium from Ceramic Breeder Materials (P9)**
M. Nishikawa, T. Kinjyo, T. Ishizaka, S. Beloglazov, M. Enoda, and T. Tanifuji

3 Thermal and Mechanical Behaviour of Pebble Beds [chairman: J. Reimann]

13.30 - 14.00 **Recent Efforts on Solid Breeder Blanket Thermomechanics and ITER TBM Activities (P3)**
A. Ying, A. Ali, J. An, C. Patrick, T. Sketchley, S. Sharafat, M. Youssef, and M. Abdou

14.00 - 14.30 **Experimental and Theoretical Characterisation of Pebble Bed for Solid Breeding Blanket of Nuclear Fusion Reactor**
cancelled
D. Aquaro and N. Zaccari

- 14.30 -15.00 **Characterization of Orthosilicate ex Hydroxide Pebble Beds and Mechanical Cycling of Different Types of Ceramic Breeder Materials (P13)**
J. Reimann and H. Harsch
- 15.15 - 15.45 **Thermomechanical Modelling of Fusion Pebble Beds under Volumetric Heating (P6)**
 D. Hofer and M. Kamlah
- 15.45 - 16.15 **Preparation of the Benchmark Exercise for HELICA and HEXCALIBER Tests**
cancelled
G. Dell'Orco, P. A. Di Maio, M. Simoncini and G. Vella
- 16.15 - 16.45 **Effect of Thermomechanical Load on Effective Thermal Conductivity of a Li_2TiO_3 Pebble Bed (P14)**
H. Tanigawa, T. Hatano, M. Enoeda and M. Akiba

Friday, September 17

4 Progress in Ceramic Breeder Material Development [chairman: S. Casadio]

- 9.00 - 9.30 **Ceramic Foams: Inspiring New Solid Breeder Materials (P1)**
S. Sharafat, N. Ghoniem, A. Ying, M. Savan, B. Williams, and J. Babcock
- 9.30 - 10.00 **Fabrication of Lithium Orthosilicate Pebbles by Melt-Spraying – Reproducibility and Yield (P5)**
R. Knitter and P. Risthaus
- 10.00 -10.30 **Fabrication and Characterization of Li_2TiO_3 Pebble by the Combustion Synthesis and the Dry-rolling Granulation Process (P12)**
 Choong-Hwan Jung, Ji Yeon Park, Weon-Ju Kim, Sang-Jin Lee and Woo-Seog Ryu

5 Irradiation Testing [chairman: J.B.J. Hegeman]

- 10.45 -11.15 **Behaviour of Blanket Ceramic Materials under Irradiation at High Temperature (P2)**
G. Kizāne, J. Tīliks, A. Vītiņš and J. Tīliks Jr.
- 11.15 - 11.45 **A High Fluence Irradiation of Ceramic Breeder Materials in HFR Petten, Test-matrix and Design of the Irradiation Capsule (P10)**
J.B.J. Hegeman, J.G. van der Laan, S. Kamer, and S. de Groot
- 11.45 - 12.15 **In Pile Behaviour of the Pebble Bed Assemblies in the HFR, Results and First Data Analyses (P17)**
A.J. Magielsen, J.G. van der Laan, J.H. Fokkens and M.P. Stijkel

6 Conclusions

1 Progress in the Design of Ceramic Breeder Reactors

1.1 Design of Solid Breeder Test Blanket Modules in JAERI (P15)

K. Ezato, Y. Nomoto, S. Suzuki, T. Hirose, D. Tsuru, H. Tanigawa, T. Hatano, M. Enoeda, and M. Akiba

1.2 Recent Progress in the Design of the HCPB Blanket (P16)

L.V. Boccaccini, S. Hermsmeyer and R. Meyder

Design of Solid Breeder Test Blanket Modules in JAERI

Presented by: K. EZATO,

With contributions from Y. Nomoto, S. Suzuki, T. Hirose, D. Tsuru,
H. Tanigawa, T. Hatano, M. Enoeda, M. Akiba

Blanket Engineering Lab.,
Japan Atomic Energy Research Institute, JAERI

Contents

1. Outline of Blanket development in JAERI
2. Design of Water-cooled TBM
3. Design of He-cooled TBM
 - Design support analyses in each design
Temp. response and T-release breeder,
and Thermo-mechanics of FW

Blanket Development in Japan

Fusion Power Demonstration Plant

- National program confirmed the combined DEMO/Proto strategy and pursues earlier introduction of fusion into the market (Fusion Power Demonstration Plant)
- Multiple generations of blanket and materials will be studied in the Demonstration phase.

Blanket Development

- Universities and NIFS are developing advanced concepts: He-cooled, Li/V, molten salt, and LiPb will be attempted for the module testing in ITER and DEMO.
- **JAERI pursues solid breeder blanket concepts cooled with high pressure and temperature water and He.**

TBM testing in ITER is the most important milestone
for development DEMO blanket

Solid Breeder Test Blanket Module

1. JAERI is now perusing two types of Solid Breeder TBMs;
 - **Water-Cooled TBM** (Solid Breeder Pebble Bed and RAFS)
 - **Helium-Cooled TBM** (Solid Breeder Pebble Bed and RAFS)

2. Basic option of water condition is Pressurized Water(15 MPa).

3. Supercritical pressure water cooling (25 MPa) is under investigation and R&D, as the ambitious target of basic option and advanced option of solid breeder blanket.

4. He-cooled TBM has similar structure with water-cooled concept.
 - Provide data for a backup option of DEMO (He cooling).
 - Preliminary test for high temperature SiC-He cooled blanket.
 - Provide the simulated data of SCW TBM with high coolant temperature.

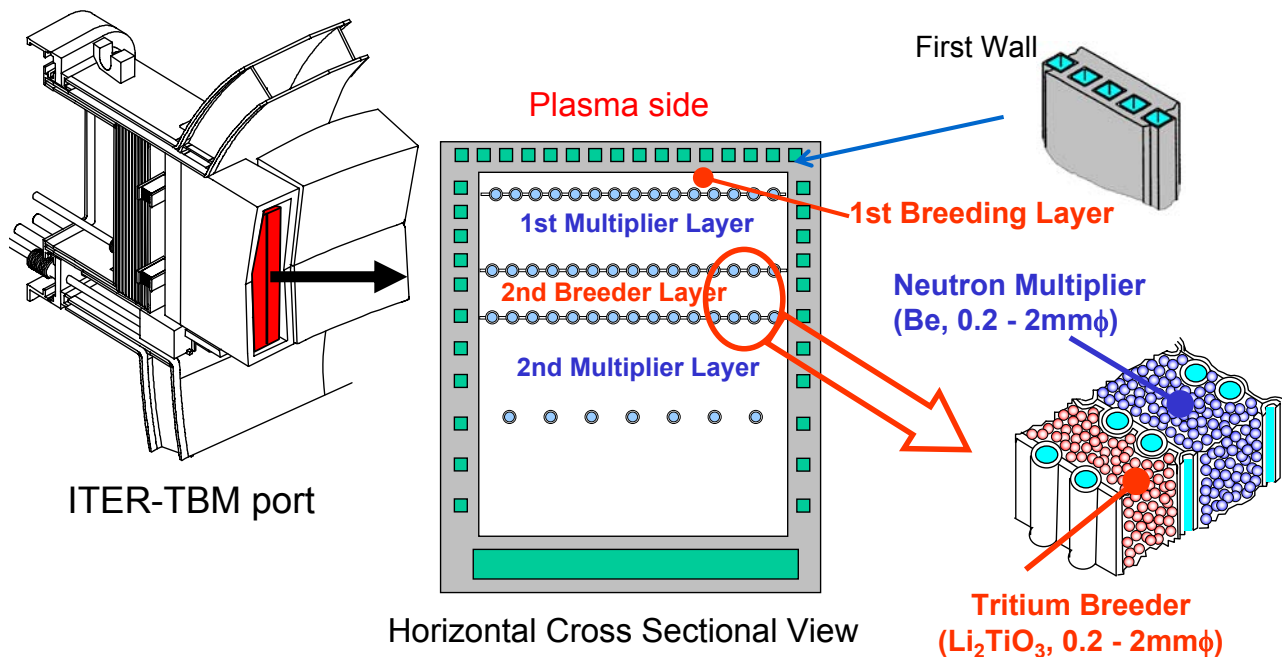
Design Conditions of solid breeder TBMs

Items	Unit	Water Cooled	He Cooled
Structural Material		F82H	F82H
Coolant		Water	He gas
Multiplier		Be, or Be ₁₂ Ti	Be, or Be ₁₂ Ti
Breeder		Li ₂ TiO ₃ , or other Li ceramics	Li ₂ TiO ₃ , or other Li ceramics
SHF (aver., max.)	MW/m ²	0.5	0.5
NWL (aver., max.)	MW/m ²	0.78	0.78
Area of FW	m ²	0.53 x 1.74	1.29 x 0.76
Coolant Pressure	MPa	15(25)	8.5
Coolant Inlet/Outlet Temp.	°C	280 /323 (360/380*)	300/432
Total Heat Deposit in TBM	MW	1.27	1.36
Total Tritium Production	g/FPD	0.156	0.180
Coolant Flow Rate	kg/s	5.3	2.0

Outlines of Solid Breeder TBM designed by JAERI

- (1) **Slit structure TBMs** are adopted to withstand electro magnetic force in VDE and internal over-pressure in case of failure of cooling tube.
- (2) **Thermo-mechanical analyses of FW** and **analyses of temperature distribution and tritium release performance** have been performed to show the feasibility of the TBM design.
- (3) **Detailed structures** are developed with consideration of fabrication procedure and welding lines. Coolant flow route is considered from the view points of hydraulics and heat transfer.
- (4) **Pressure relief route** is planned at the top and bottom of the module.
- (5) In cooling system, circulation pump is doubled to avoid loss of coolant.
- (6) Rear wall interface configuration is developed based on the structure design of TBM. Dimensions and structures of interfaces are clarified.

Configuration of Water-Cooled Solid Breeder TBM



Ceramic breeder(Li₂TiO₃) and Be neutron multiplier are packed in a form of small pebble bed in layered structure separated by cooling tube with wall

Design support analyses

□ Temperature response of breeder layer

- To evaluate whether TBM configuration can simulate temperature range in a DEMO breeder layer or not.
- 1D thermal analyses based on nuclear heating rate by ANIHEAT

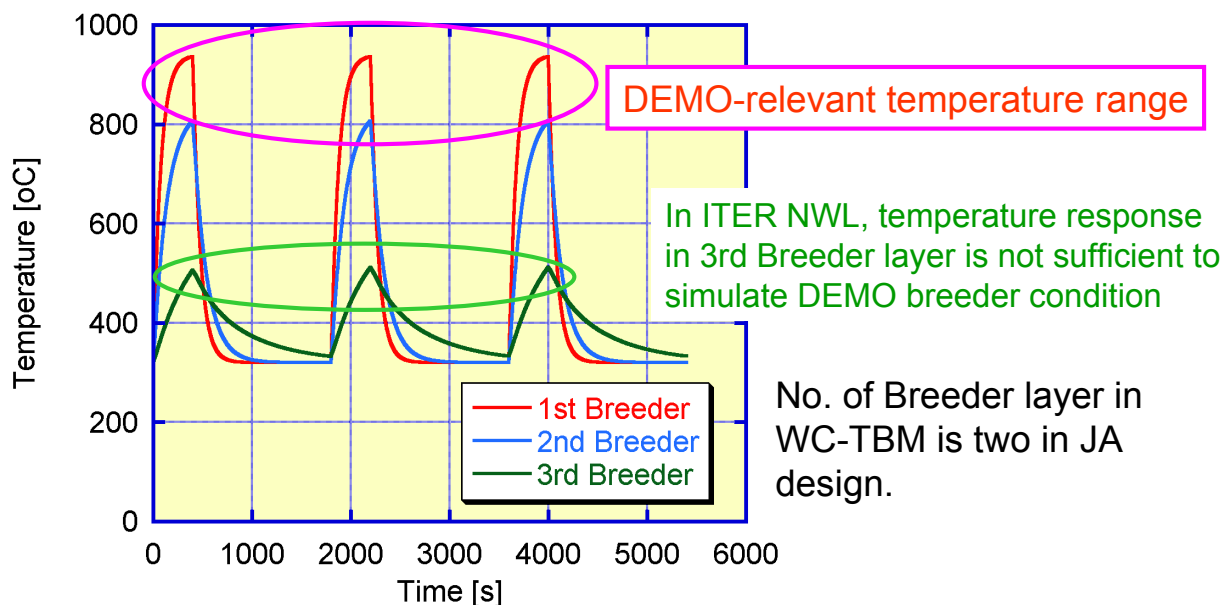
□ T-release response in breeder layer

- To obtain basic data on T production for ITER TBM testing and T-recovery system
- T-release model developed by Kyushu Univ. (Nishikawa, et al.,)

□ Thermo-mechanical feature of FW

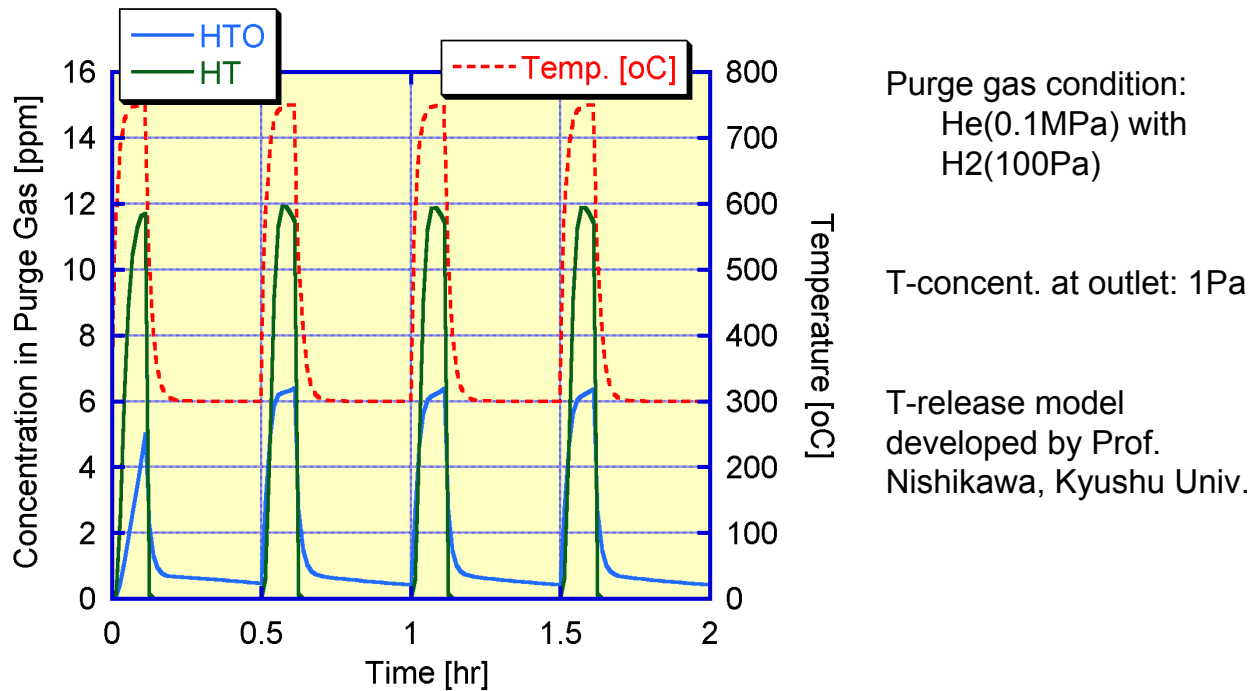
- To confirm whether max. temperature of FW made of F82H is less than 550°C.
- To confirm an excess of stress and strain does not occur.

Transient temperature response of Breeder layer



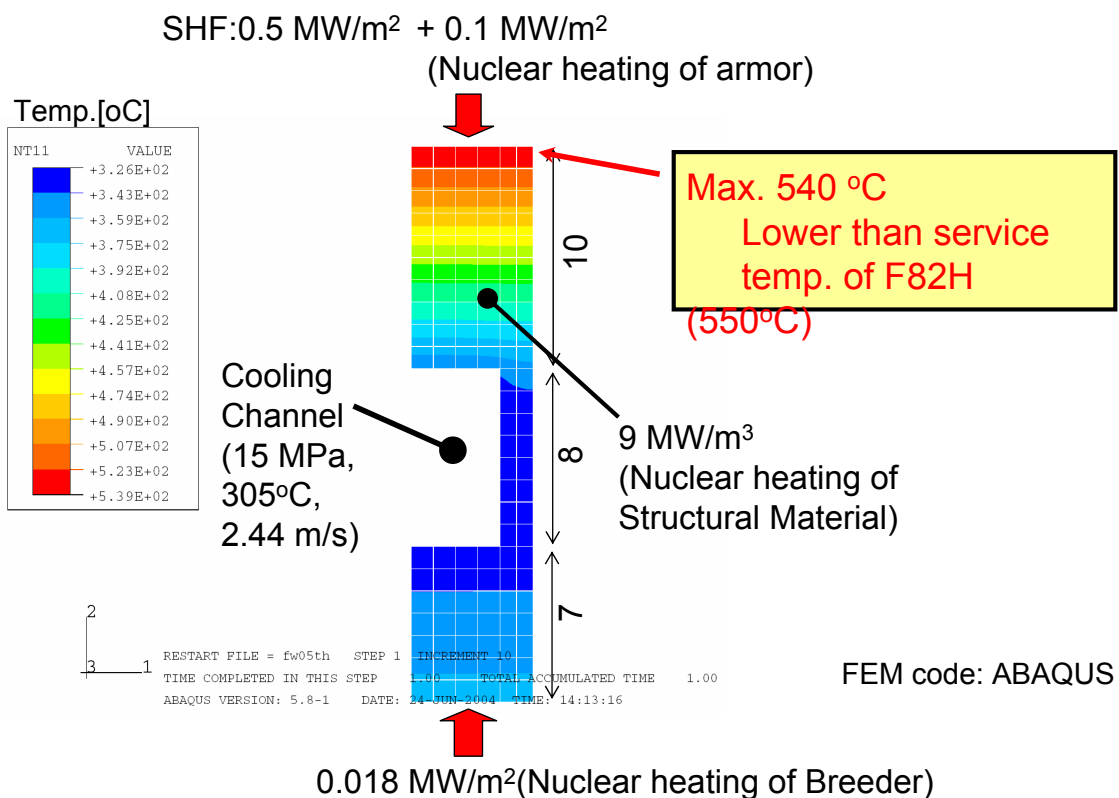
Time evolution of peak temperature of three breeder layers of water-cooled TBM with 400 sec burn/ 1400sec dwell cooled by 15MPa, 320°C water.

Transient tritium release behavior of 1st breeder layer



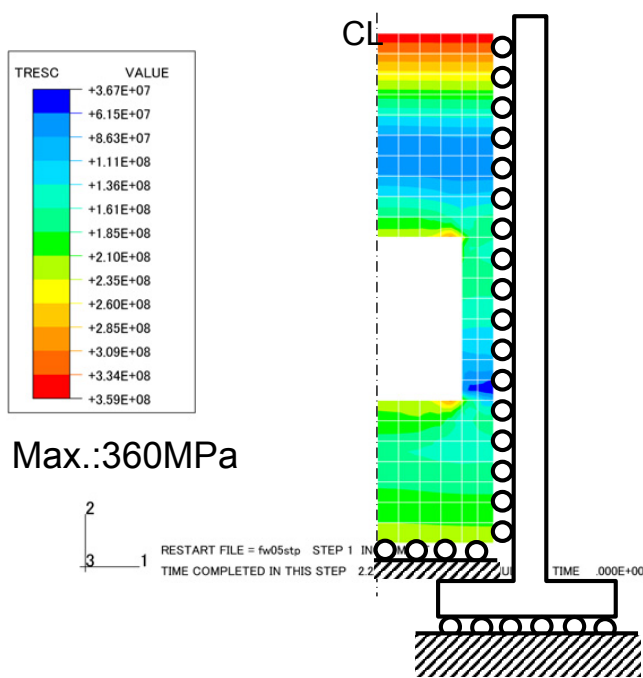
Tritium release from 1st breeder layer shows quick response due to high tritium generation rate and quick response of temperature transient (due to high nuclear heating rate). Performance of 2nd layer is similar.

Thermo-mechanical analysis of FW of Water-Cooled TBM



Stress Analysis of water-cooled FW

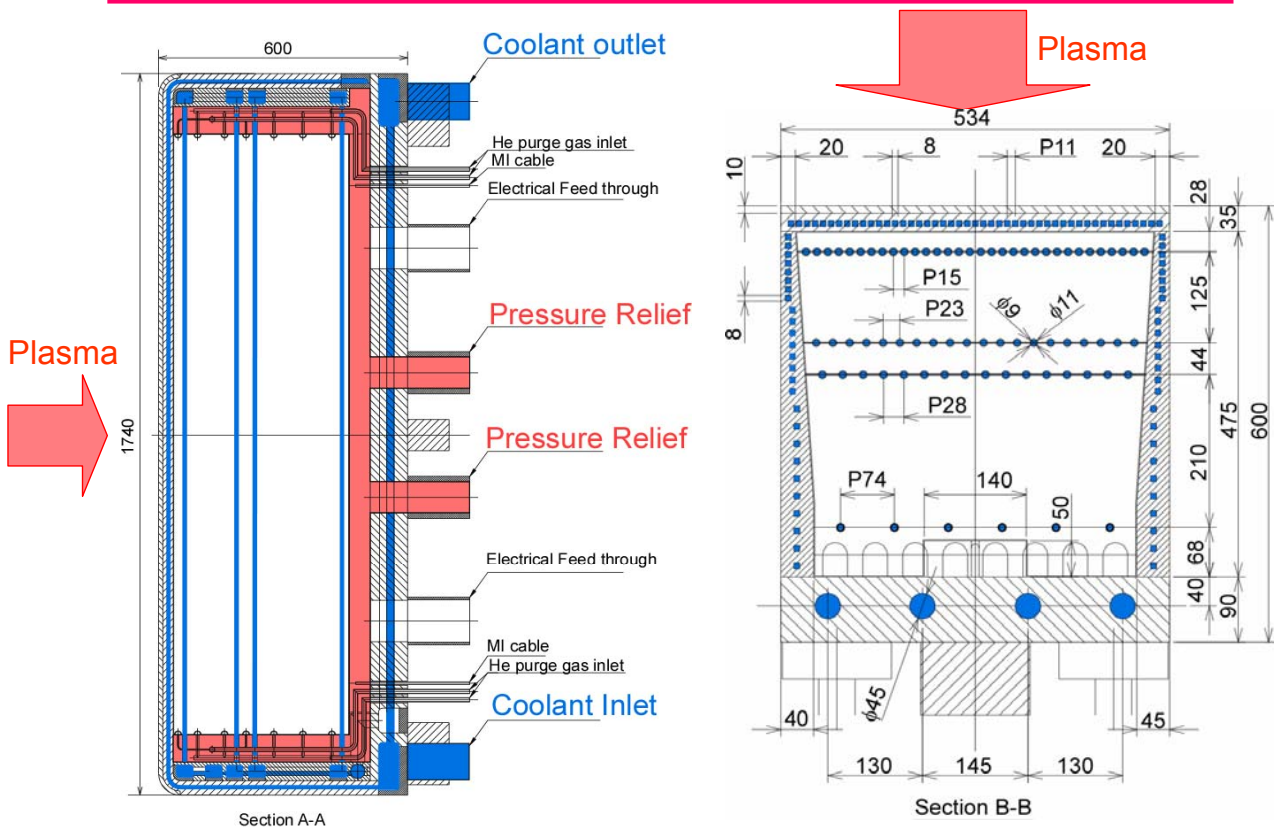
Equiv. Stress (Tresca) distribution



- 10-nodes generalized plane strain elements
(Out-of-plane bending was constrained.)

Stress field inside FW is within elastic range.

Structure of water-cooled TBM

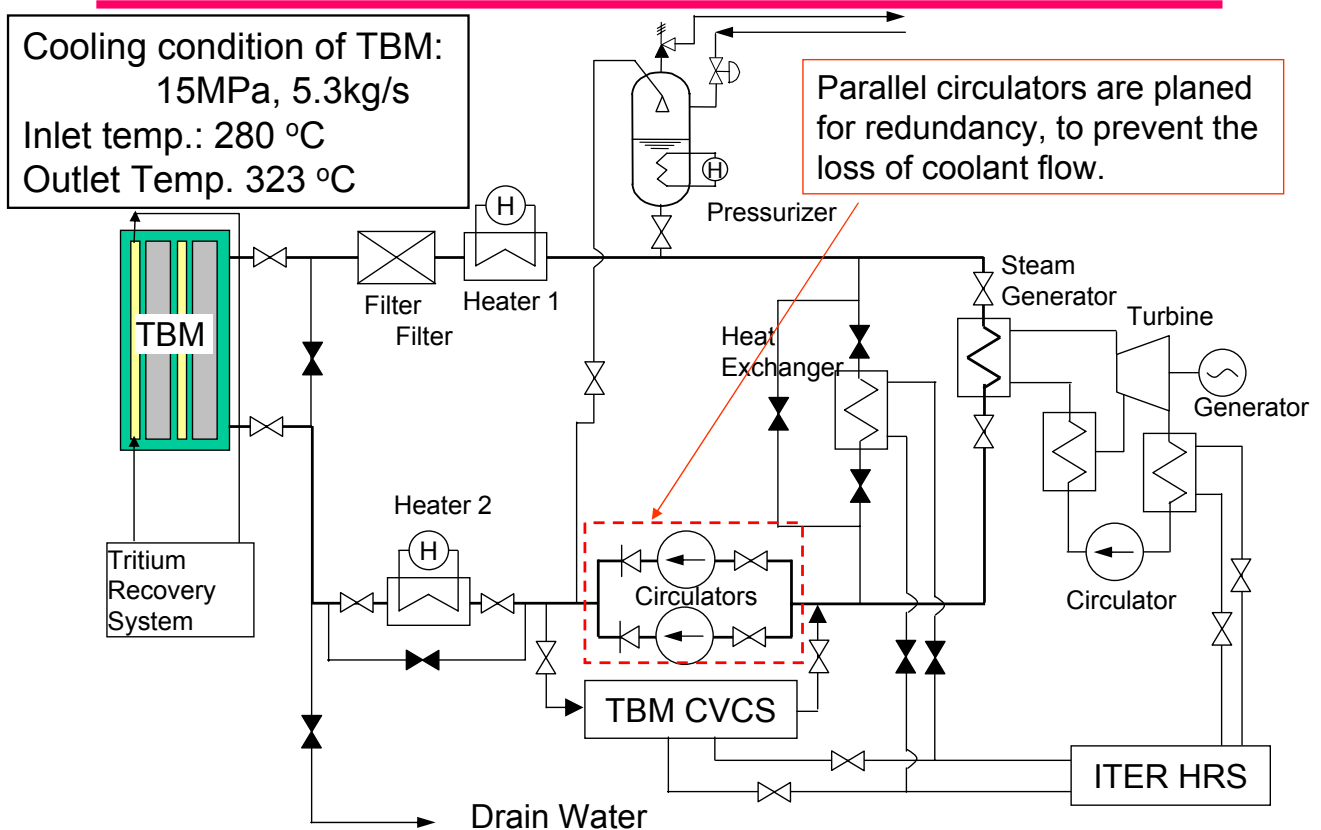


Cooling system design conditions for water-cooled test module

Requirement for Heat Rejection System

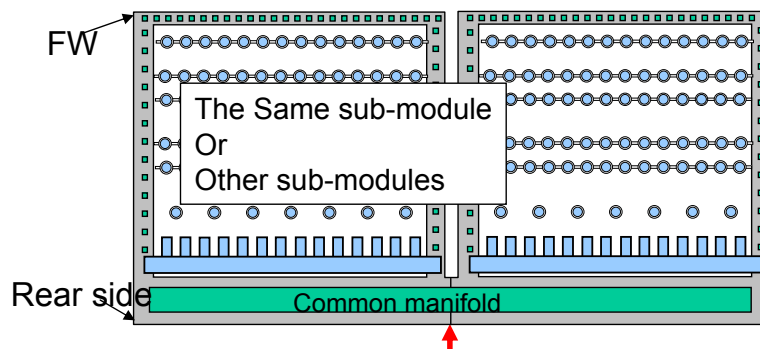
First wall area facing plasma	0.53 m ^W x 1.74 m ^H
Total removal heat	1.27 MW
Primary coolant	Water
Temperature (module in/out)	280/323 °C
Pressure	15 MPa
Flow rate	5.34 kg/s
Purification system (CVCS)	Bypass flow of primary coolant
Temperature (inlet/outlet)	280/40 °C
Pressure	15 MPa
Flow rate	0.27 kg/s
Secondary coolant	Water
Temperature (heat exchanger in/out)	35/75 °C
Pressure	0.5 MPa
Flow rate	9.48 kg/s

Flow Sheet of Water Cooling System



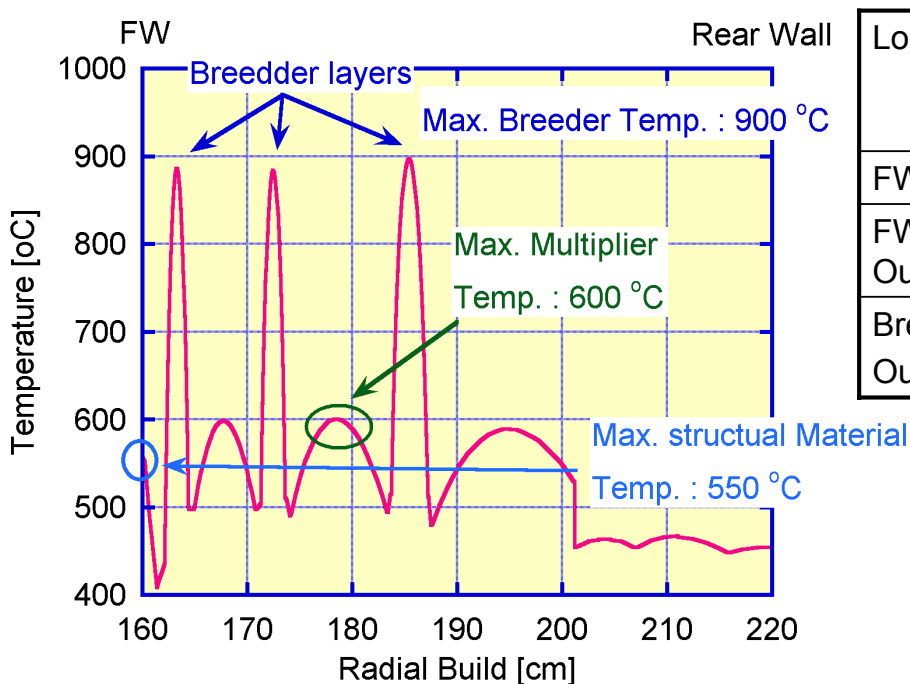
He -cooled TBM Concept

- From the viewpoint of EMF in DEMO blanket, **slit structure** is adopted. For this reason, sub-modules concept is the updated He-cooled TBM concept.
- From the results of temperature and tritium release transient analyses, **number of breeder layer is three**.
- From the viewpoint of cooling of FW against SHF 0.5 MW/m², coolant temperature is 300 °C. Total coolant He 1.99 kg/s is divided into two after TBM manifold. **Coolant He condition for one sub-module is 8.5MPa, Inlet:300°C, Outlet 432°C, 0.99 kg/s.**



Electron beam welding of two sub-modules. Then, common manifolds and rear wall equipments such as keys and flexible supports will be fabricated.

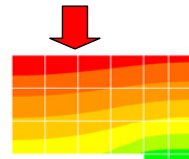
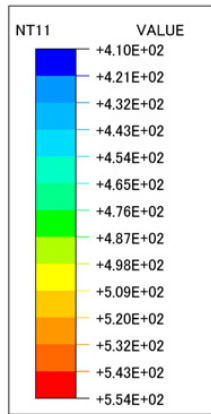
Temperature Distribution of FW and PB at 0.5 MW/m²



Location	He Temp. [°C]	Struct. Temp. [°C]
FW Inlet	300	
FW Outlet	370	548
Breeder Outlet	432	550

Thermal Analysis of He-cooled FW

SHF: $0.5 \text{ MW/m}^2 + 0.1 \text{ MW/m}^2$
(Nuclear heating of armor)



Max. $550 \text{ }^\circ\text{C}$
= service temp. of F82H

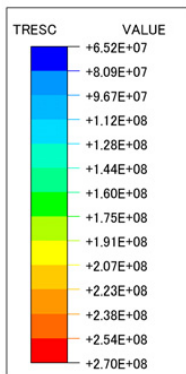
Cooling Channel
(8 MPa , $360 \text{ }^\circ\text{C}$,
 50 m/s)

10 MW/m^3
(Nuclear heating of
Structural Material)

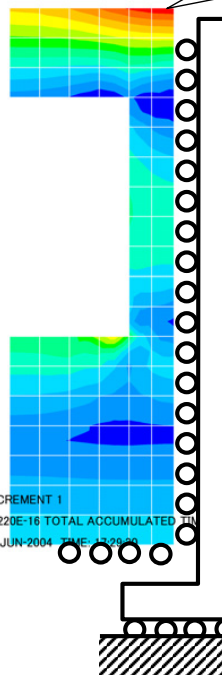
2
3 1
RESTART FILE = fw05th STEP 1 INCREMENT 6
TIME COMPLETED IN THIS STEP 1.00 TOTAL ACCUMULATED TIME 1.00
ABAQUS VERSION: 5.8-1 DATE: 30-JUN-2004 TIME: 16:42:26

0.110 MW/m^2 (Nuclear heating of Breeder)

Stress Analysis of FW



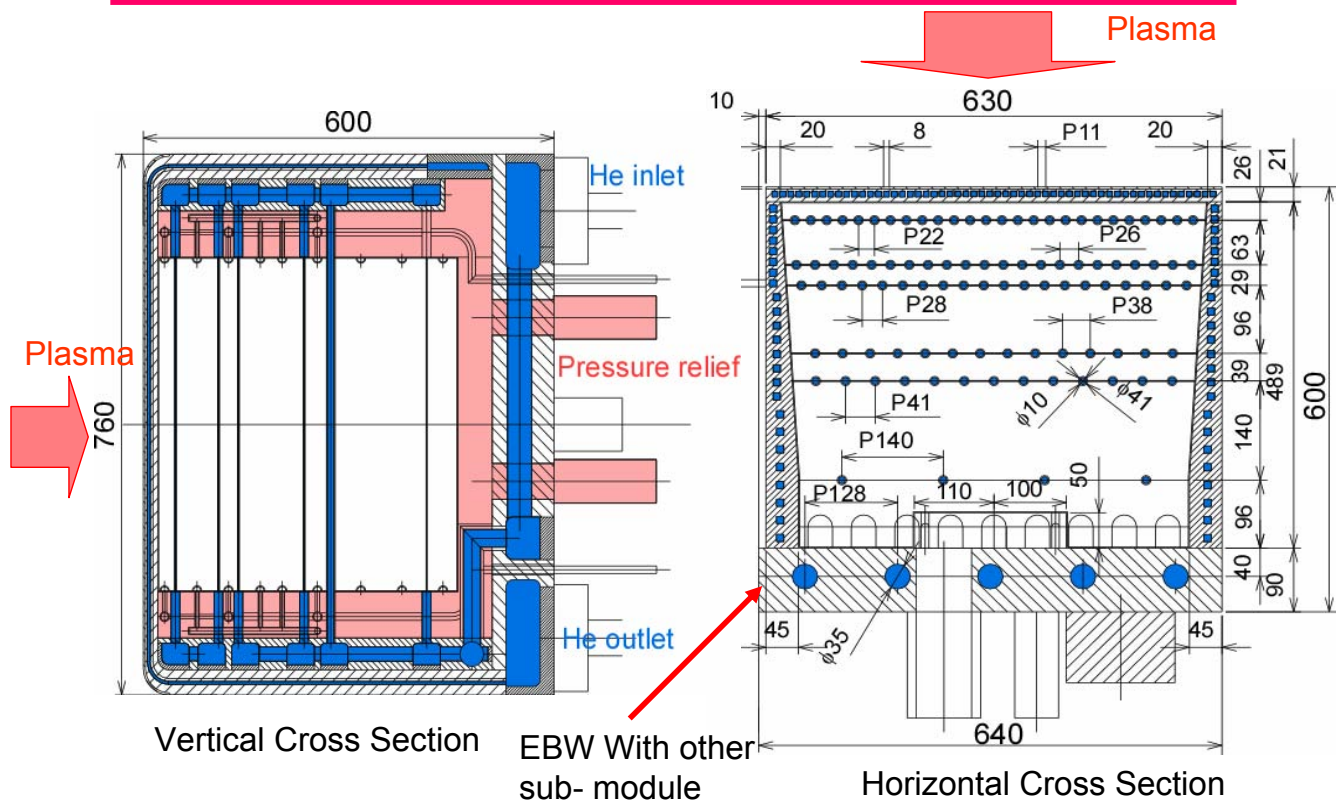
Tresca_{max.} = 270 MPa



Stress field inside FW is
within elastic range.

2
3 1
RESTART FILE = fw05st STEP 1 INCREMENT 1
TIME COMPLETED IN THIS STEP 2.220E-16 TOTAL ACCUMULATED TIME 2.220E-16
ABAQUS VERSION: 5.8-1 DATE: 30-JUN-2004 TIME: 11:29:00

Detailed Structure of Japanese He Cooled Sub-module

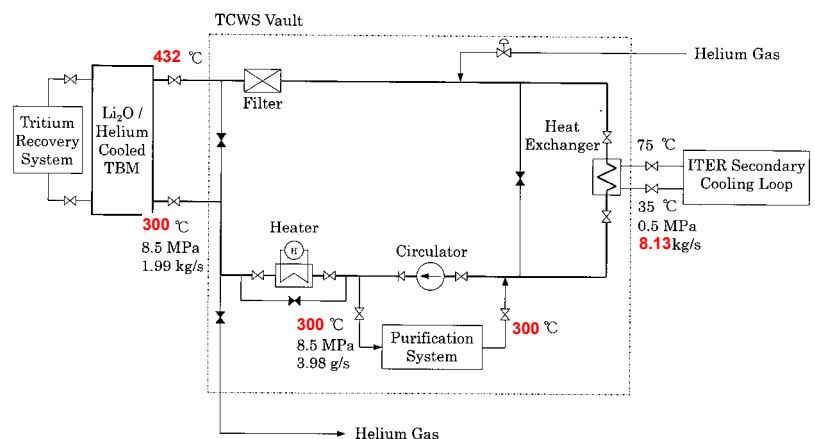


design conditions for He-cooled TBM

First wall area facing plasma	1.29 m ^w x 0.76 m ^h
Surface heat flux	0.5 MW/m²
Neutron wall load	0.78 MW/ m ²
Total removal heat	1.36 MW
Primary coolant	Helium
Temp.(module in/out)	300 / 432 °C
Pressure	8.5 MPa
Flow rate	1.99 kg/s
Purification system	MS Dryer + Cryo-MS Dryer
Temperature (inlet/outlet)	300/300 °C
Pressure	8.5 MPa
Flow rate	3.98 g/s
Secondary coolant	Water
Temp. (heat exchanger in/out)	35 / 75°C
Pressure	0.5 MPa
Flow rate	8.13 kg/s

He Cooling System

- Surface heat flux: 0.5 MW/m²
- Total heat removal: 1.36 MW/m²
- To design maximum temperature of FW structural material lower than 550 °C, inlet coolant temperature was changed to 300 °C.



Flow diagram of He-cooled TBM cooling system

Conclusion

- ❑ JAERI is now developing two concept of Solid Breeder TBM; Water-cooled and He-cooled TBMs.
 - In both concepts, ceramic breeder(Li_2TiO_3) and Be neutron multiplier are packed in a form of small pebble bed in layered structure separated by cooling tube with wall.

- ❑ Configurations of TBMs are simplified based on performance analyses of temperature response of breeder and T-release.
 - In water-cooled TBM, No. of breeder layer is reduced to two.

- ❑ The elemental technology phase has been almost completed.
 - One of them, thermo-mechanical feature of pebble bed will be presented at the last presentation by Dr. Tanigawa.
 - JAERI is taking further steps to engineering test phase including fabrication of scalable mock-ups of TBM to demonstrate its structural integrity.



Recent Progress in the Design of the HCPB Blanket

L.V. Boccaccini, S. Hermsmeyer, R. Meyder

**CBBI 12th
Karlsruhe, 16th-17th September, 2004**

slide # 1



Outline

- 1) Introduction**
- 2) HCPB TBM Design**
- 3) Testing in ITER**
- 4) Conclusion**

slide # 2

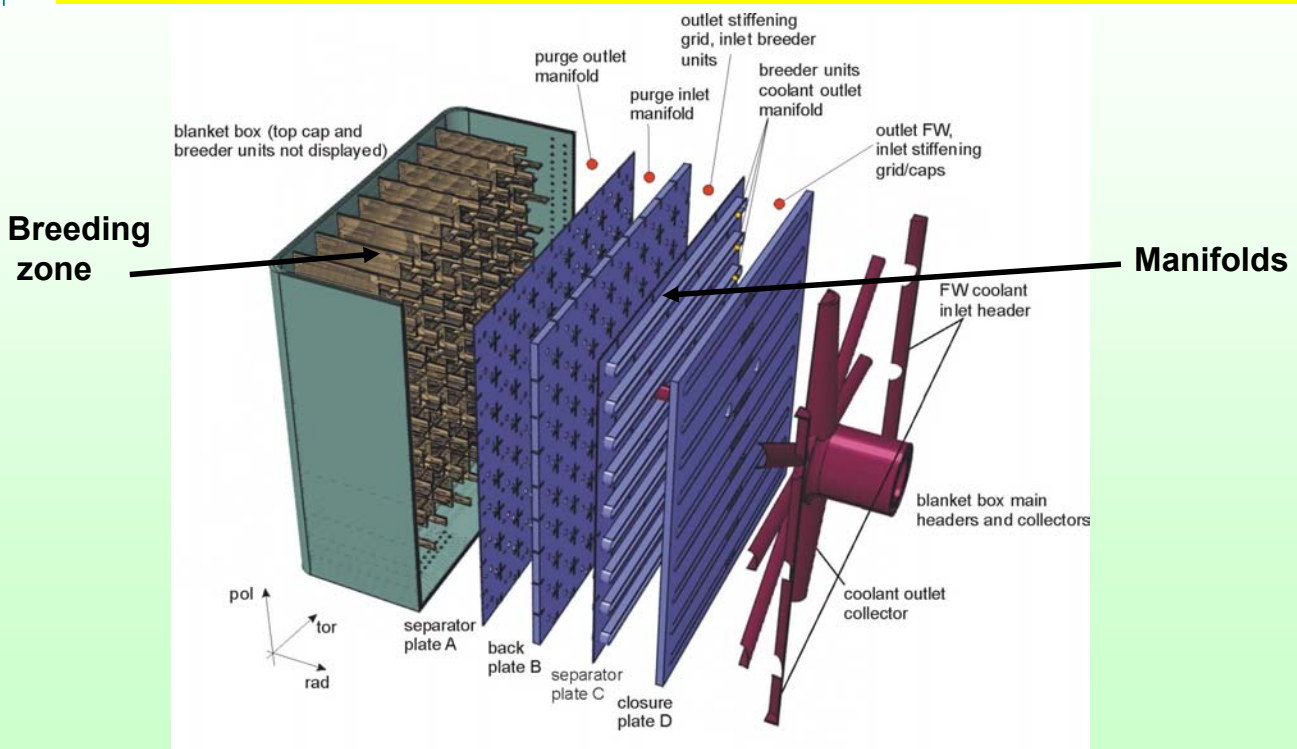


Introduction

slide # 3



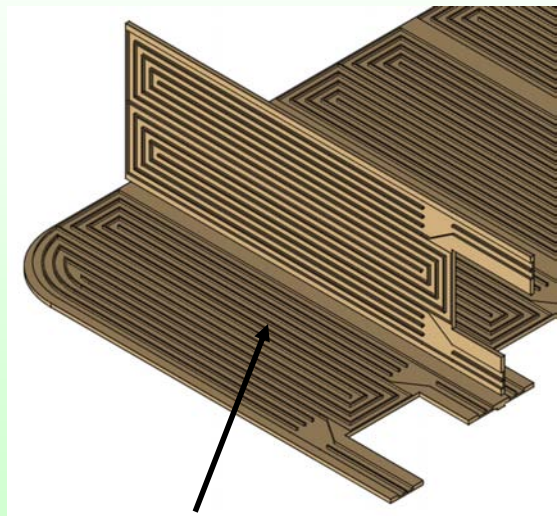
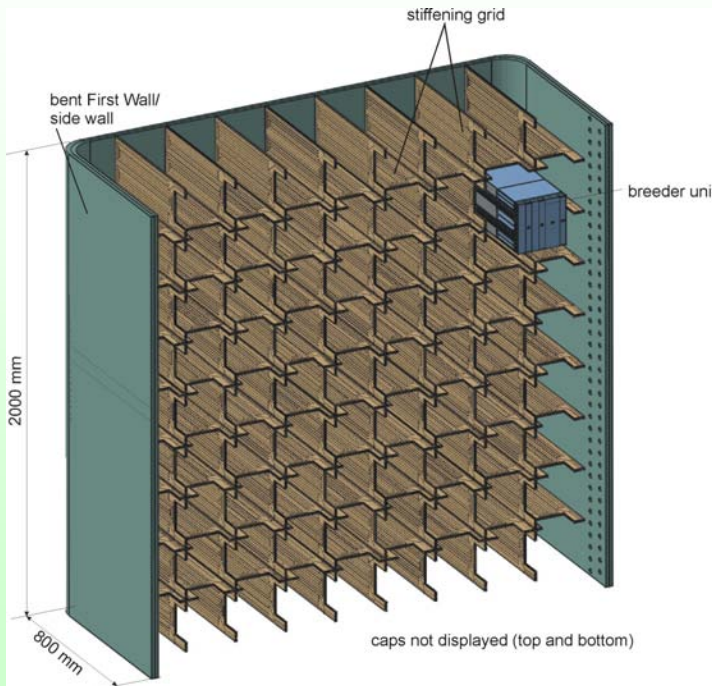
HCPB DEMO Concept



slide # 4



Grid system with Breeder Units

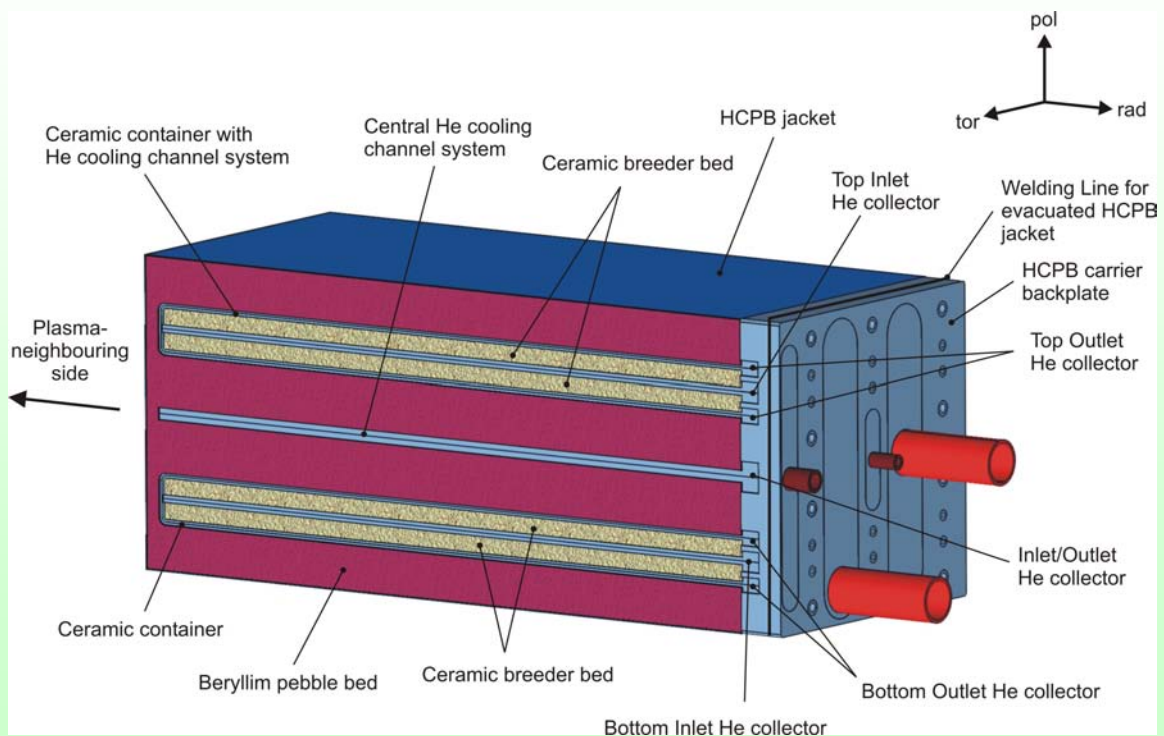


Steel structures have imbedded cooling channels

slide # 5



Breeder Unit for the HCPB Blanket



slide # 6



Breeder Unit for the HCPB Blanket

-Tritium breeding ratio

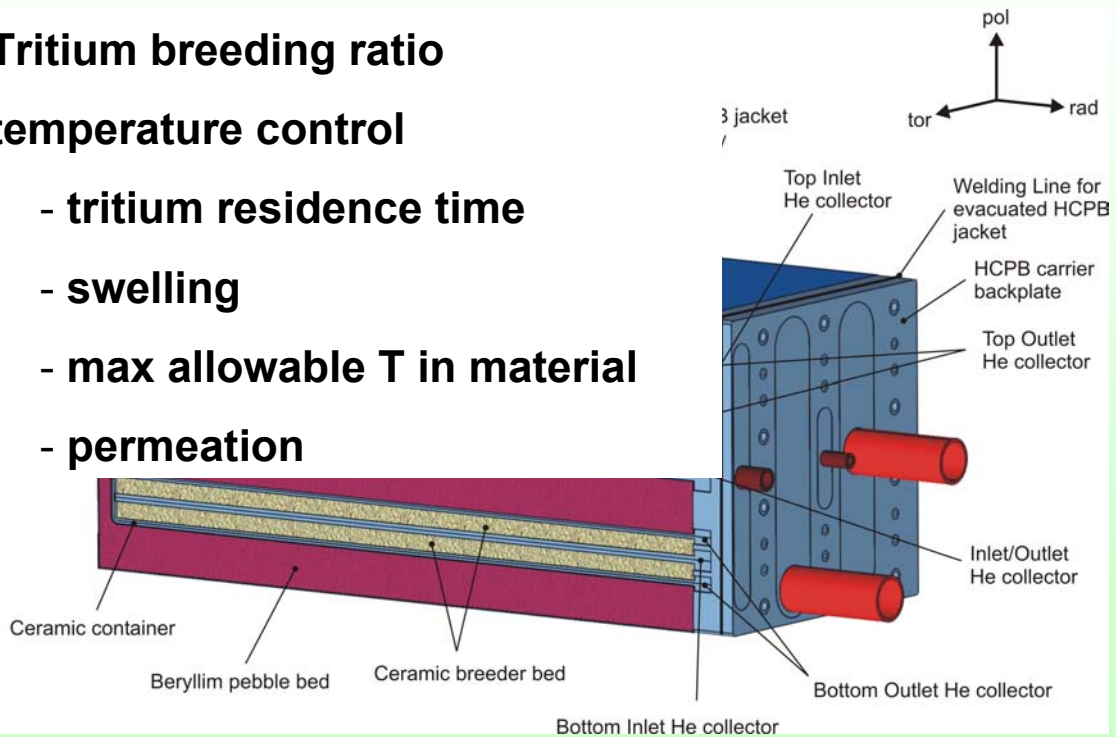
-temperature control

- tritium residence time

- swelling

- max allowable T in material

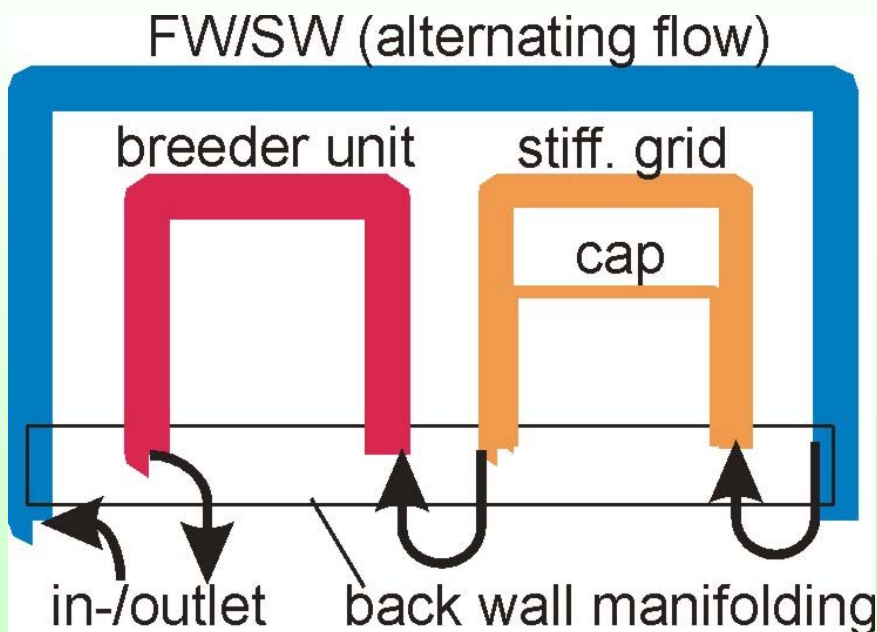
- permeation



slide # 7



DEMO HCPB coolant flow scheme



slide # 8

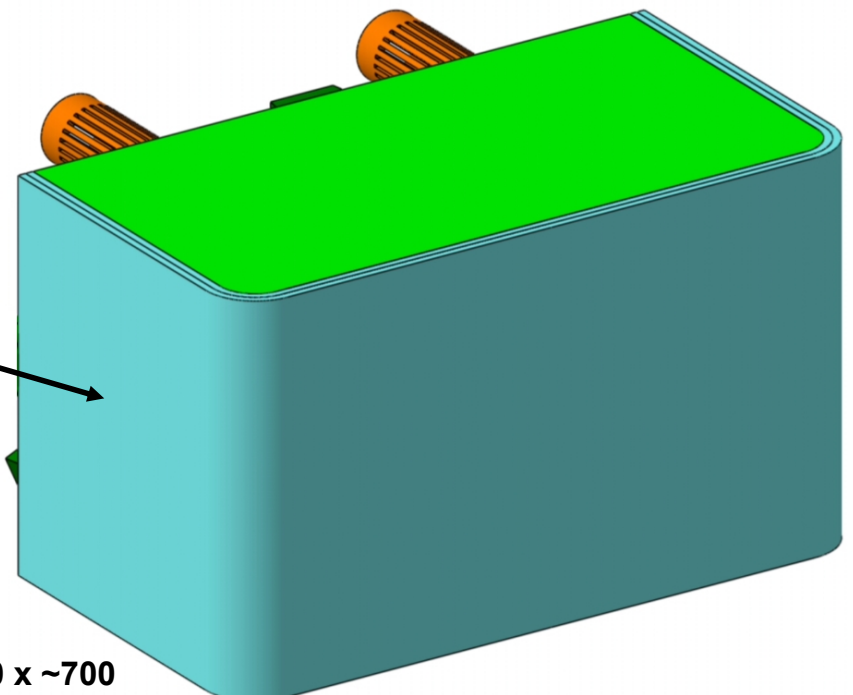
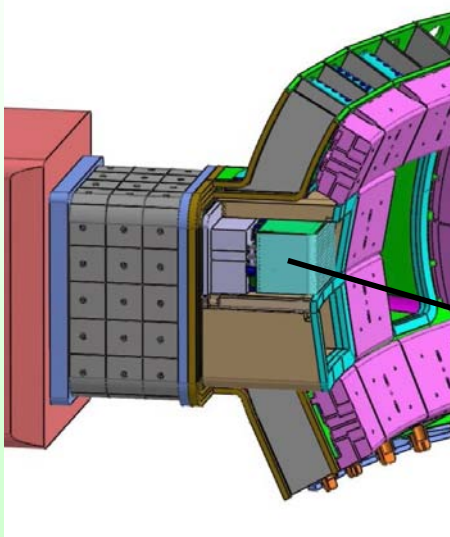


1. HCPB TBM Design

slide # 9



HCPB Test Blanket Module



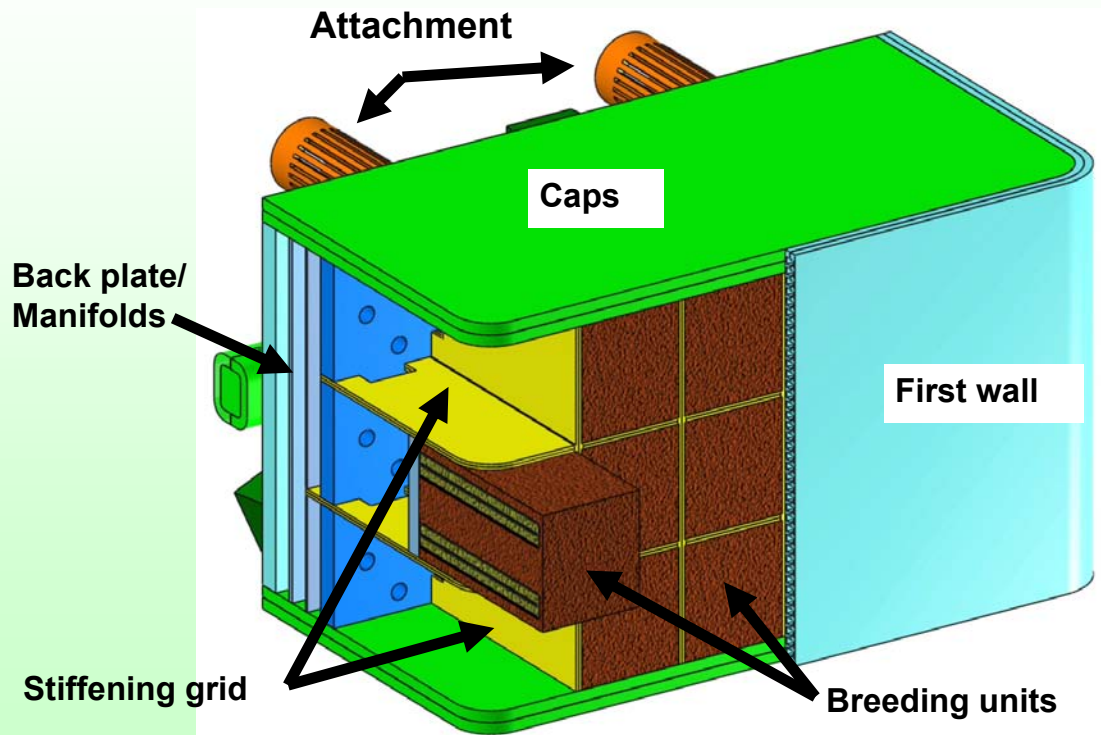
Orientation: horizontal

Dimensions (in mm): 740 x 1270 x ~700

slide # 10



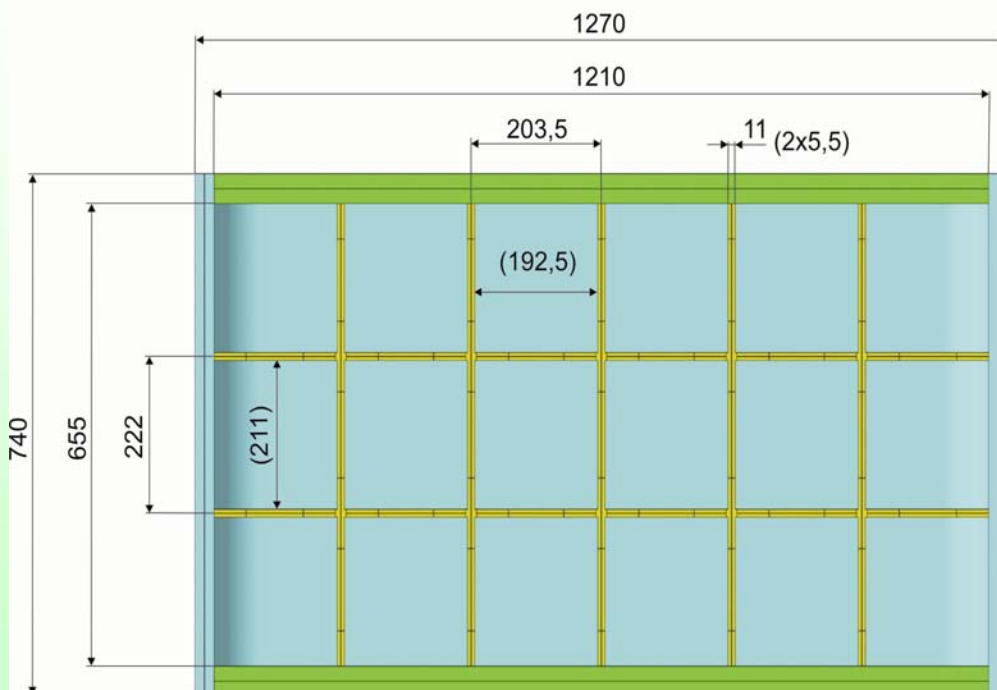
TBM Design 2003



slide # 11



Modular design (18 Breeder Units)

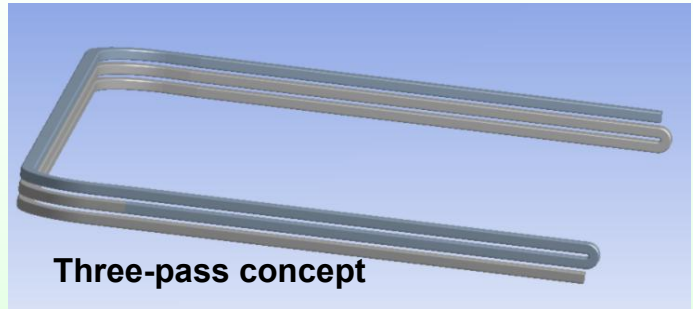


slide # 12

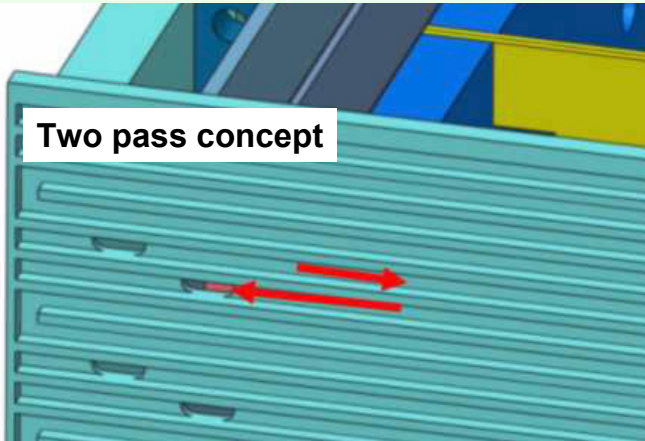


First Wall Lay-out

He velocity ~ 80 m/s
Max heat flux : 0.5 MW/m²

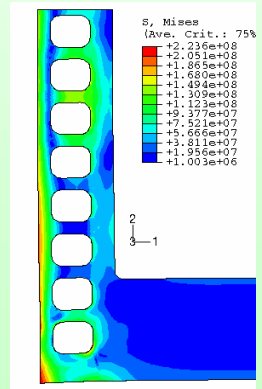


Three-pass concept

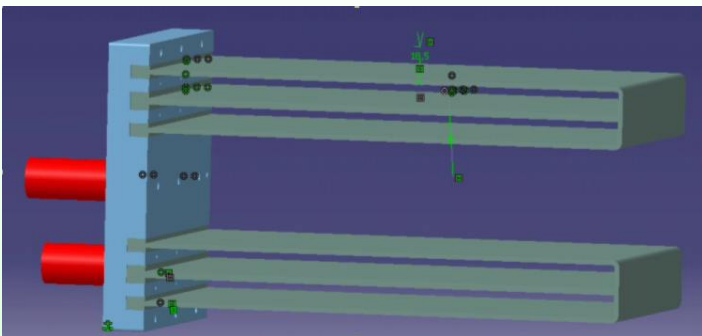


Two pass concept

Stress analysis for 3-pass concept indicates an acceptable stress level

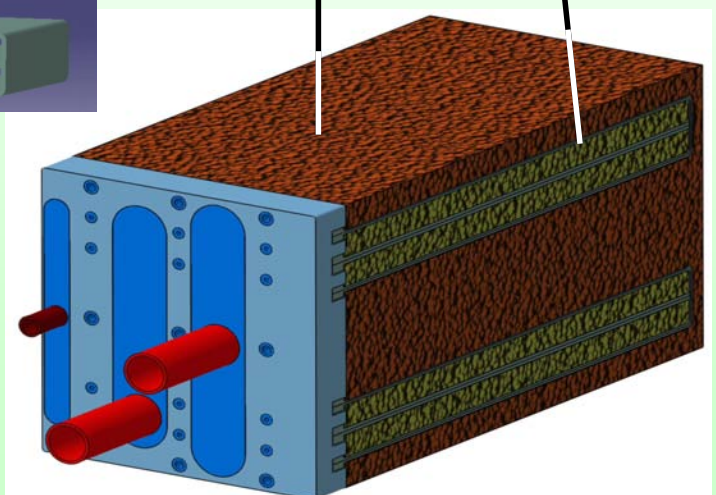


Breeder Unit



Ceramic Breeder

Beryllium

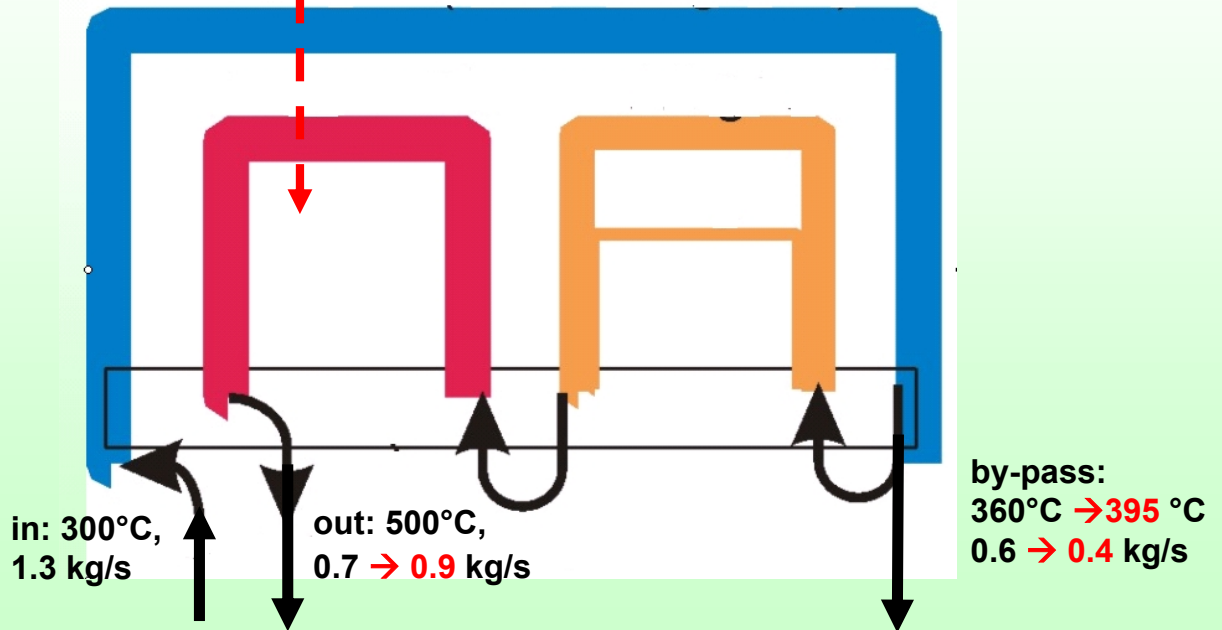




He coolant flow through the TBM

Neutron wall load
 0.78 MW/m^2

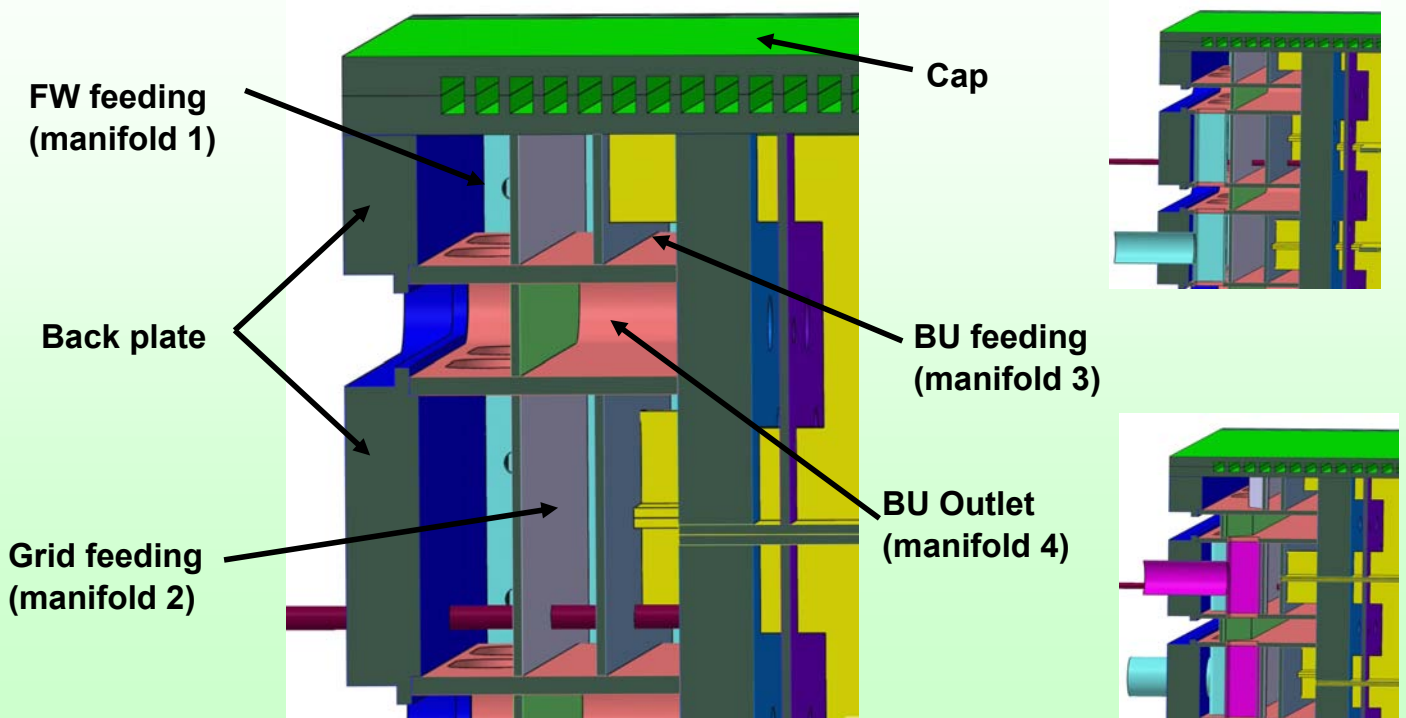
Surface heat flux
 $0.25 \text{ MW/m}^2 \rightarrow 0.5 \text{ MW/m}^2$



slide # 15



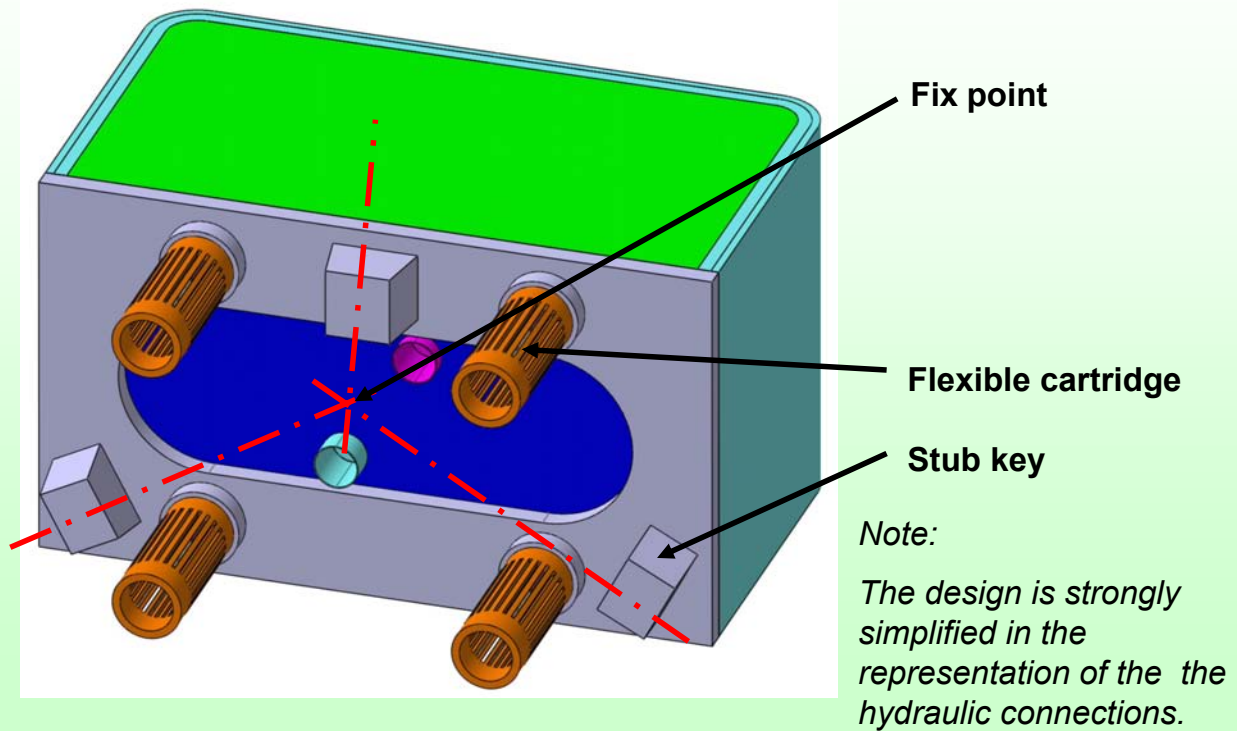
Back plate & Helium coolant manifolds



slide # 16



Mechanical Attachment



slide # 17



3. Testing in ITER

slide # 18



Test blanket modules planned for ITER

- 1. Electro magnetic module (EM) during the H-H phase**
to test the overall system in not irradiated environment
to investigate electro magnetic behavior during disruptions
- 2. Neutron and Tritium module (NT) during the D-D and LD - D-T phase**
to investigate neutron spectra in a BU, Tritium production
- 3. Thermo mechanic module (TM) during the D-T phase**
to investigate behavior of pebble beds
- 4. Plant integration module (PI) during the HD - D-T phase**
to investigate module behavior during long pulses and Tritium recovery

slide # 19



Scenarios for the TBM design

	1	2	3	4	5	6	7	8	9	10
	H-H			D-D	Low duty D-T			High duty D-T		
Equivalent standard pulses No.	0	0	0	1	750	1000	1500	2500	3000	3000
Tritium produced [mg]	0	0	0	0.510	382	510	765	1275	1530	1530
Type of pulses:										
•Short pulses										
•Standard pulses										
•Back-to-back										
•Long pulses										
Type of HCPB TBM:	EM-TBM			NT-TBM			TM-TBM		PI-TBM	

In the table a T production of about 510 μg during a standard pulse (0.11 g/FP-day for 400 s) has been assumed.

slide # 20



Scenarios for the TBM design

Short pulses: under the values of the standard pulses

Standard pulses:

- 500 MW Fusion Power
- 400 sec burn time
- 1800 sec minimum repetition time
- considered as insulated pulses

Back-to-back pulses:

- 500 MW Fusion Power
- 400 sec burn time
- 1800 sec repetition time
- 6 days duration (~ 288 pulses)

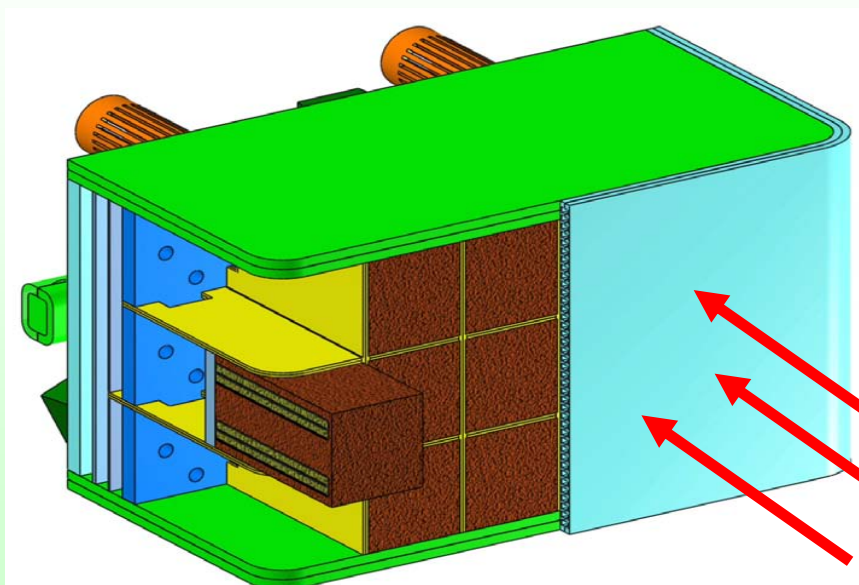
Long pulses:

- 500 MW Fusion Power
- 1000-3000 sec burn time
- 4000-12000 sec minimum repetition time
- considered as insulated pulses

slide # 21



1) Electromagnetic TBM



INSTRUMENTATION

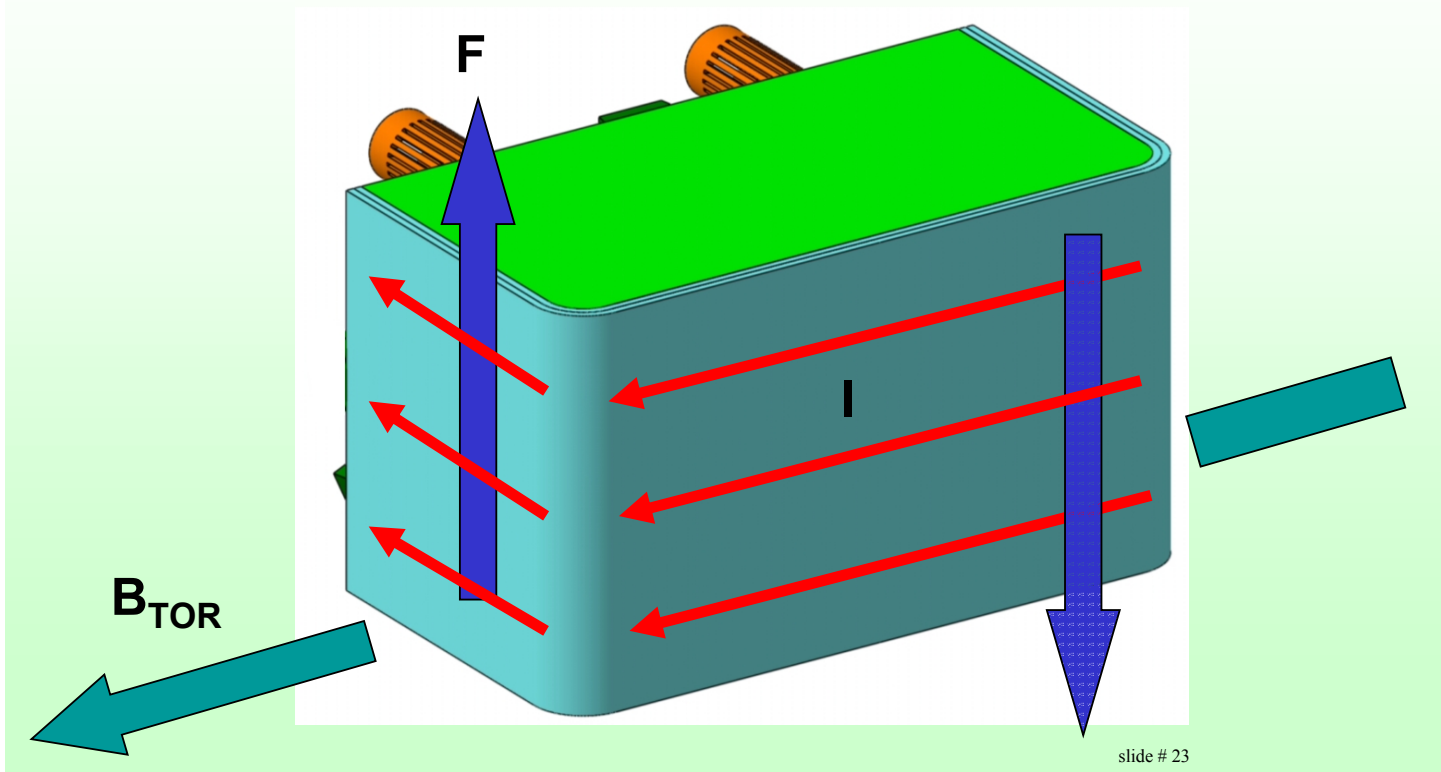
- flux coils
- Rogoski coils
- load cell

Only surface heating for the H-H phase

slide # 22



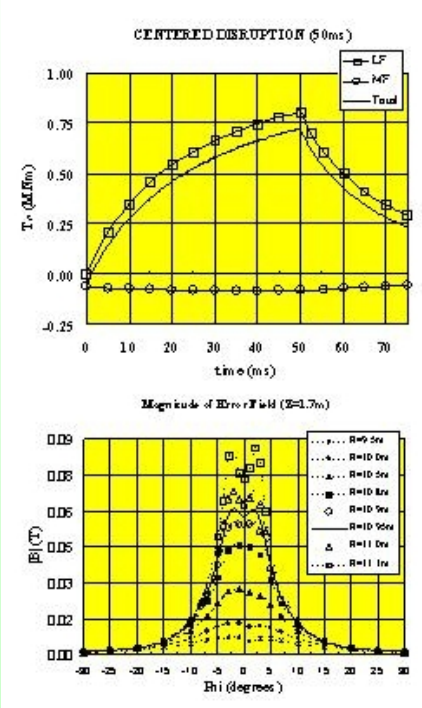
1) Electromagnetic TBM



slide # 23



1) Electromagnetic TBM



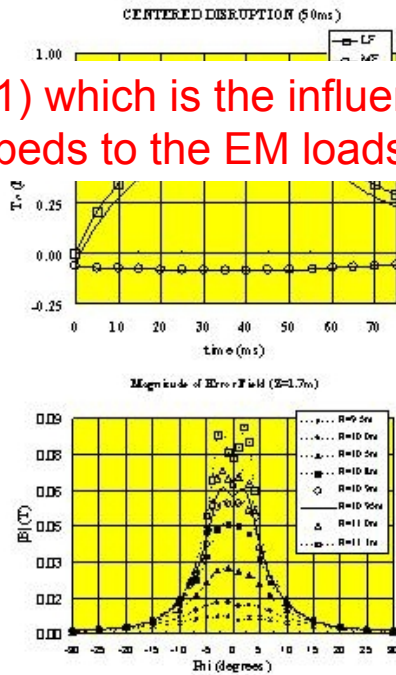
- Environmental measurements of electromagnetic field, eddy currents and electro-mechanical forces during EM transients.
- Investigation of the effects of ferromagnetic materials to the error fields of the magnetic confinement of ITER.
- Demonstration that the standard design of the TBM can withstand the mechanical effects of a major plasma disruption.

slide # 24



1) Electromagnetic TBM

1) which is the influence of pebble beds to the EM loads ?



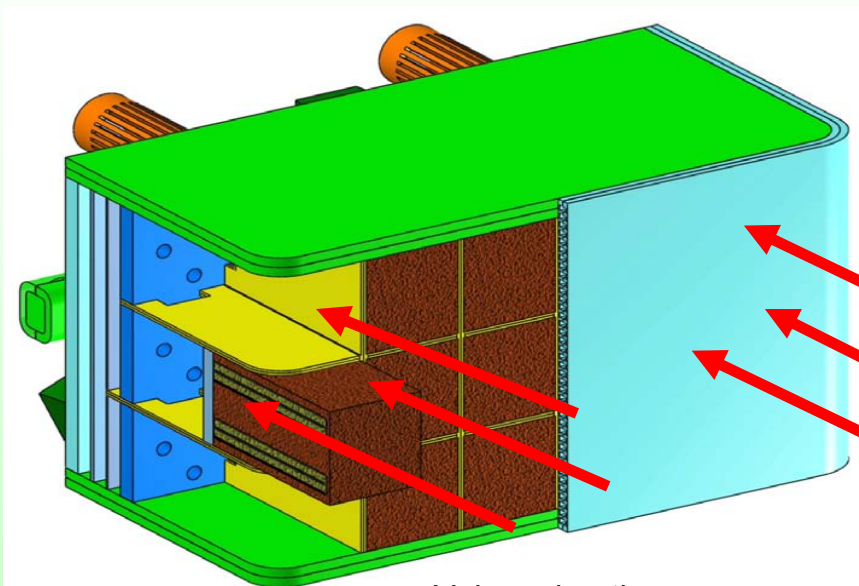
Experimental measurements of magnetic field, eddy currents and electro-mechanical forces during EM transients.

- Investigation of the effects of ferromagnetic materials to the error fields of the magnetic confinement of ITER

2) which can be the influence of the magnetic field on the processes in the pebble beds ?
plasma disruption.



2) Neutronics and Tritium Production TBM



INSTRUMENTATION

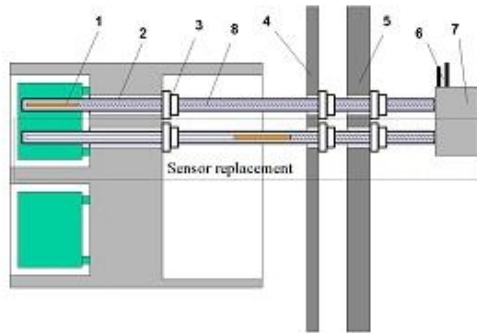
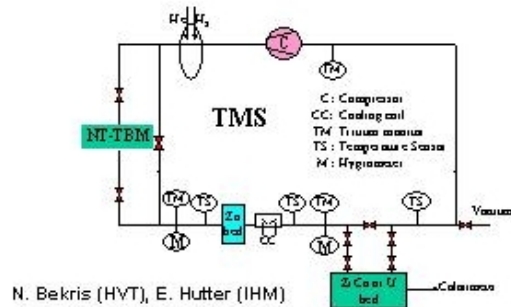
- activation foils, micro-chambers
- Tritium Measurement system

Surface heating up to 0.5 MW/m²

Volume heating corresponding to a neutron wall load of 0.78 MW/m²



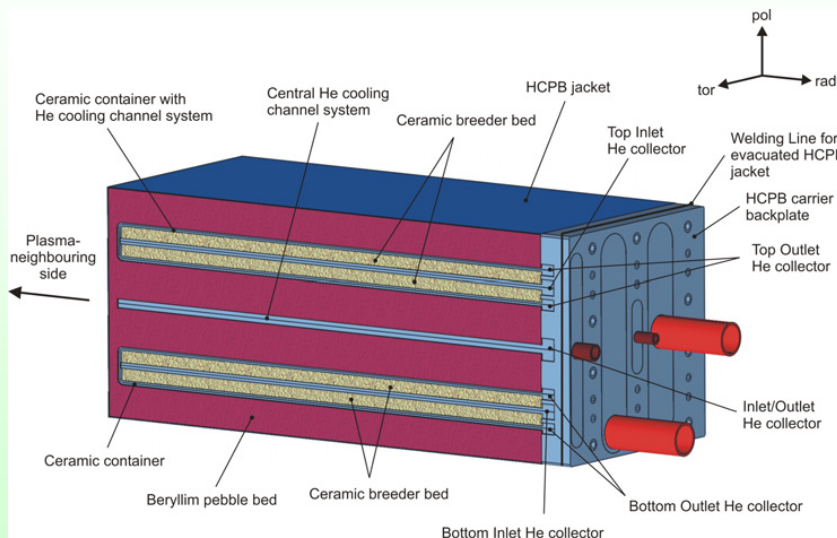
2) Neutronics and Tritium Production TBM



- To check and demonstrate the capability for tritium breeding. This can be achieved by directly comparing the calculated and measured tritium generated in the test blanket module over a given irradiation time.
- To check and validate the capability of the neutronic codes and data to predict the nuclear responses in the TBM. This includes the ability to accurately predict the tritium breeding in the TBM.



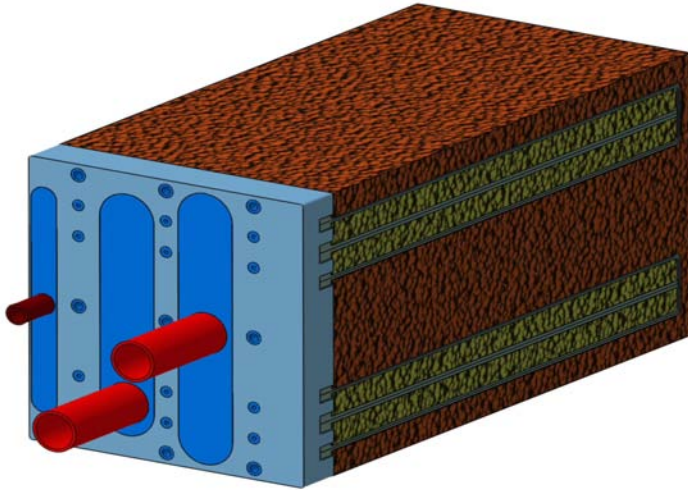
2) Neutronics and Tritium Production TBM



- 1) Phase: cold operation
He T=100°C – 300°C
Ceramic T < 450°C
- 2) Batch T recovery
He T ~ 500°C



3) Thermo-mechanics TBM

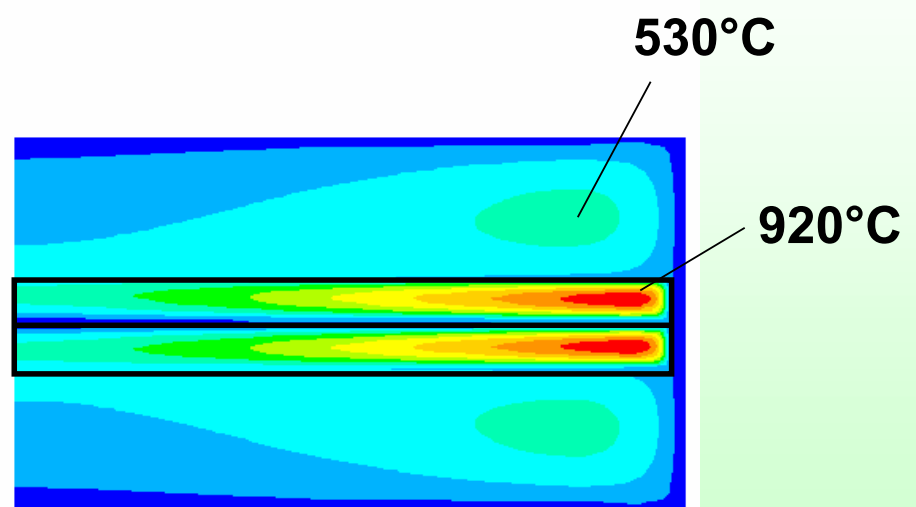
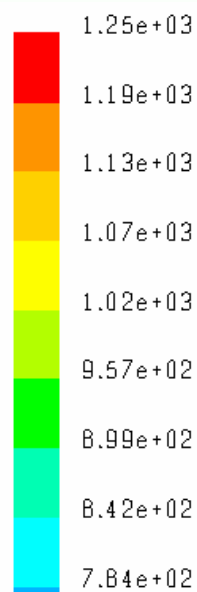


- Investigation of the pebble bed behaviour under the load conditions given by the thermal interference and the mechanical constraint
- Investigation of the consequences of thermal creep
- Investigation of the consequences of cyclic power operation
- Investigation of changes of the purge gas flow conditions in particular in the breeder pebble bed

slide # 29



3) Thermo-mechanics TBM

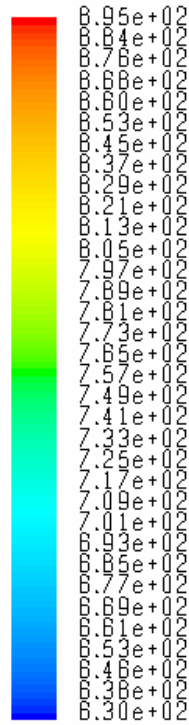


TM lay-out for relevant ceramic temperature

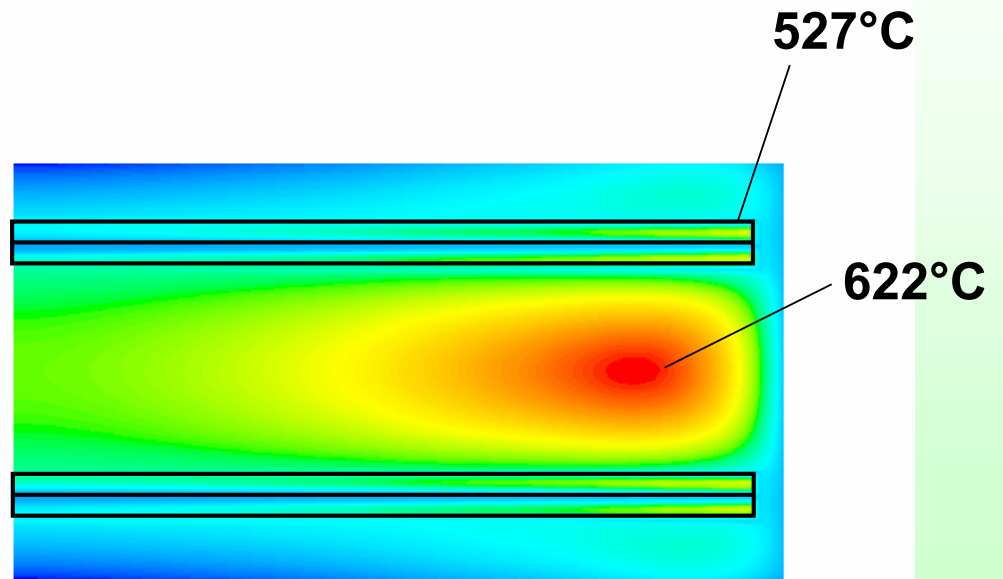
slide # 30



3) Thermo-mechanics TBM



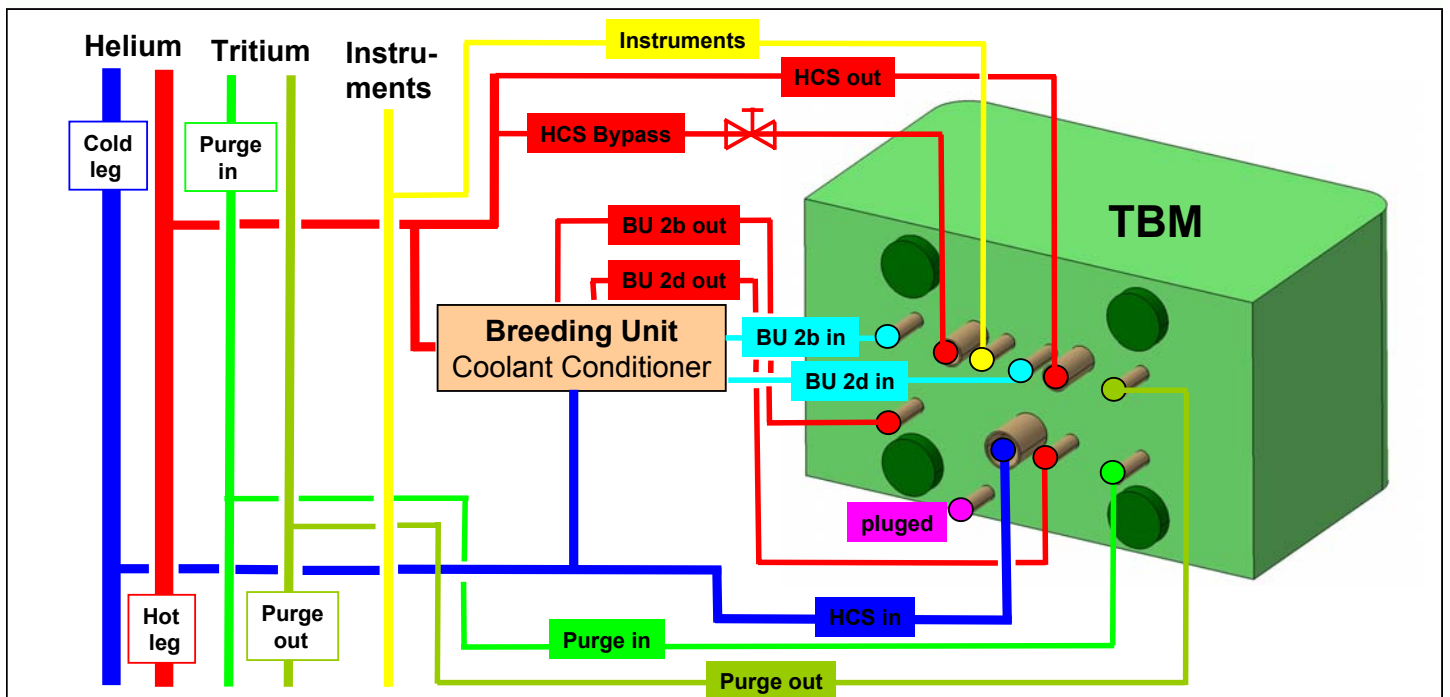
y



BU lay-out for relevant Be temperature



Integration pipes for TM-TBM in port cell



2 Breeder Material Properties

2.1 Lithium Depletion vs. Oxygen Loss Correlation for Li_2TiO_3 Pebbles as Exposed to the HCPB “Hot Spot” Conditions. A Thermo-chemical (TG-DTA-XRD-XPS) and Kinetic (TPD-TPR) Study (P7)

C. Alvani, S. Casadio, V. Contini, R. Giorni, R. Mancini, K. Tsuchiya, and H. Kawamura

2.2 Hydrogen Isotopes Behavior on Li_2TiO_3 Under Water Exposure and Deuterium Ion Irradiation (P8)

R. Olivares, T. Oda, Y. Oya, K. Tsuchiya and S. Tanaka

2.3 Release Behavior of Bred Tritium from Ceramic Breeder Materials (P9)

M. Nishikawa, T. Kinjyo, T. Ishizaka, S. Beloglazov, M. Enoda, and T. Tanifuji

Lithium depletion vs. Oxygen loss correlation for Li_2TiO_3 pebbles as exposed to the HCPB "hot spot" conditions.

A thermo-chemical and kinetic study

(by TPD-TPR-TG-DTA-XRD-XPS and SEM techniques)

and C. Alvani, V. Contini, R. Giorgi, R. Mancini (ENEA-Casaccia)
K. Tsuchiya, H. Hoshino (JAERI-Oarai), H. Kawamura (JAERI-Naka)

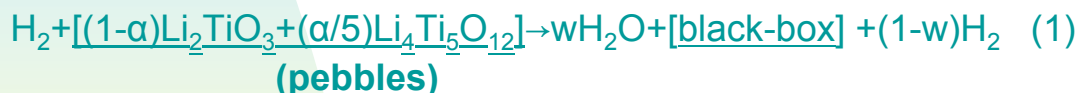
11/23/2004

S. Casadio

1

INTRODUCTION-1

The Li-depleted lithium titanate ceramic breeder pebbles are in principle two-phases composites: the monoclinic lithium metatitanate Li_2TiO_3 (main bulk phase) and spinel $\text{Li}_4\text{Ti}_5\text{O}_{12}$ (minor phase present at the grain boundary surfaces), hence the following reduction scheme was considered to hold :



This reaction was studied at 900°C by Temperature Programmed Desorption and Reduction (TPD -TPR) tests (pebbles and pellets) and at 1,000°C by thermo-analytical (TG-DTA) tests (powders) by exposing the specimens to flowing Ar+3% H_2 gas mixture.

Reaction products were analyzed by SEM, XRD and XPS

11/23/2004

S. Casadio

2

Five years ago reduced HCPB ref “black” pebbles (as annealed a week at 800°C in He + 0.1% H₂ and as shortly irradiated at low (below 80°C) temperature (NAA-mode) in TRIGA reactor) were found to trap tritium in sites characterized by high peak release rate temperature

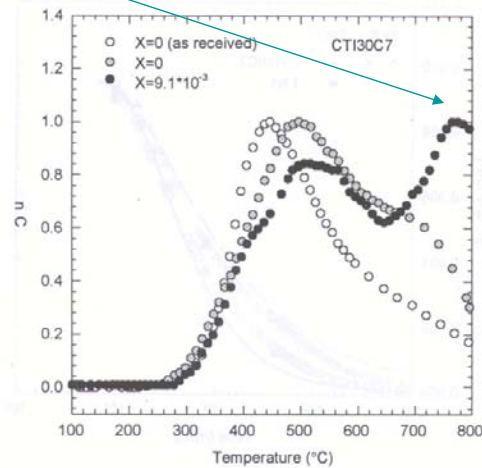
704

C. Alvani et al. / Fusion Engineering and Design 58–59 (2001) 701–705

ture during irradiation was close to room temperature. The irradiated specimens were tested out-of-pile for tritium release by exploiting a CREATE equipment in the typical TPD mode described elsewhere [4,6] using a linear heating rate $\beta = 5$ K/min from 200 °C (after isothermal anneal at this temperature for a few hours) up to 800 °C.

Fig. 2 shows the tritium release rate (normalized to the highest (peak) value observed during heating at the rate $\beta = 5$ K/min for the specimens ‘as received’ (no treated at all), annealed at 800 °C in R-purge and re-oxidized in pure O₂ under the conditions reported in the captions.

‘As received’ specimens, with adsorbed moisture and CO₂ on the surface, show tritium release at lower temperatures than those annealed previously in He or R-gas purge.



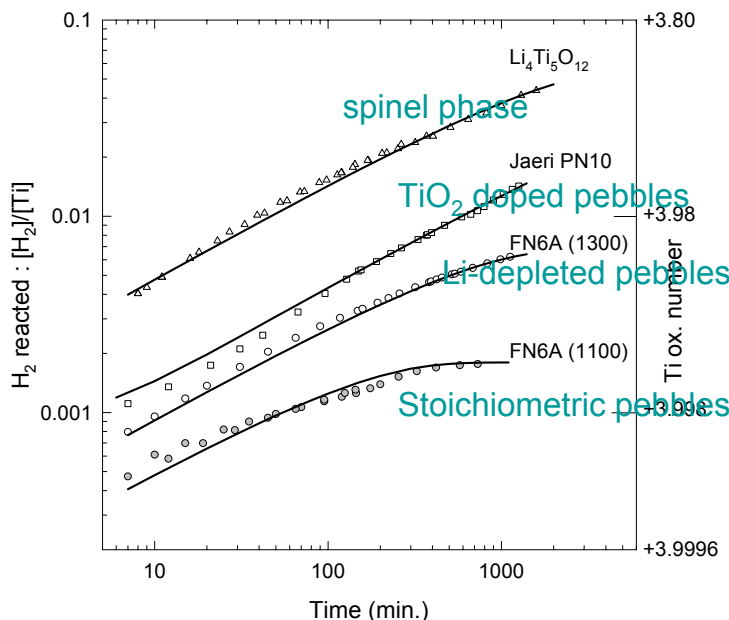
The irradiation and the TPD test was then made on re-oxidized pebbles. This trapping site was not observed but the original (as received) TPD signal was not recovered, that suggested the occurring of a remarkable grain boundary surface modification due to this thermal-chemical cycle.

S. Casadio

3

Within the frame of JAERI-ENEA cooperation (IEA, task F)

reactivity of H₂ (0.1%) at 900°C with different Li-Titanates samples

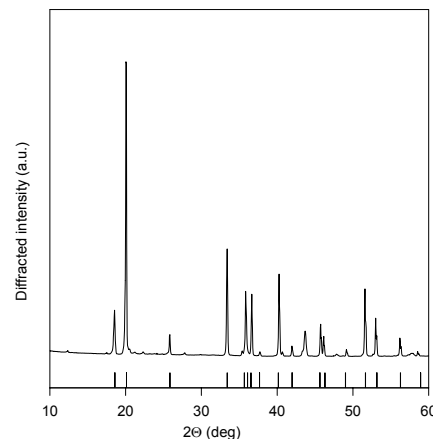
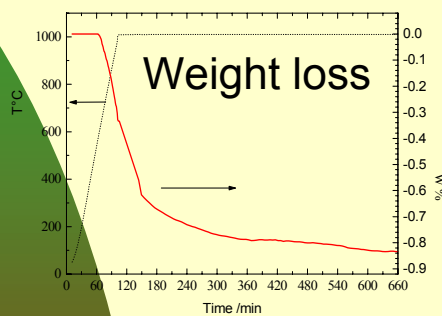


- Reduction (1) evolution of variously TiO₂ doped Li-titanates at 900°C (isothermal steps) under He+0.1% H₂ sweeping gas (S, Casadio et al. , CBBI-11 Tokyo 2003) showed the important role of the amount α of spinel phase presence in the specimens.
- Preliminary observation of this phenomenon (K. Tsuchiya, C. Alvani, et al., Fus. Eng. & Des. 69(2003)443) was so confirmed
- SEM analysis of the reduced surfaces showed the nucleation of a new phase

4

TG analysis of $\text{Li}_4\text{Ti}_5\text{O}_{12}$ powder reduction in flowing $\text{Ar}+3\%\text{H}_2$ at 1000°C

S. Casadio, CBBI-11. Tokyo-2003



Product XRD pattern. $\text{Li}_{0.14}\text{TiO}_2$ orthorhombic phase marks are reported on the 2θ axis: JCPDS card 82-1122.

S. Casadio

5

11/23/2004

OBJECTIVES OF THE PRESENT WORK

- to extend the high temperature ($900\text{-}1,000^\circ\text{C}$) $\text{Li}_2\text{TiO}_3\text{-Li}_4\text{Ti}_5\text{O}_{12}$ system reduction study to a wide range of environmental conditions,
- to use high H_2 concentration in the Ar purge (**3% by vol.**) to speed-up the slow pebbles reduction processes occurring in the reference type purge ($\text{Ar} + 0.1\% \text{H}_2$) by assuming the same final reaction products are generated.

MOTIVATION

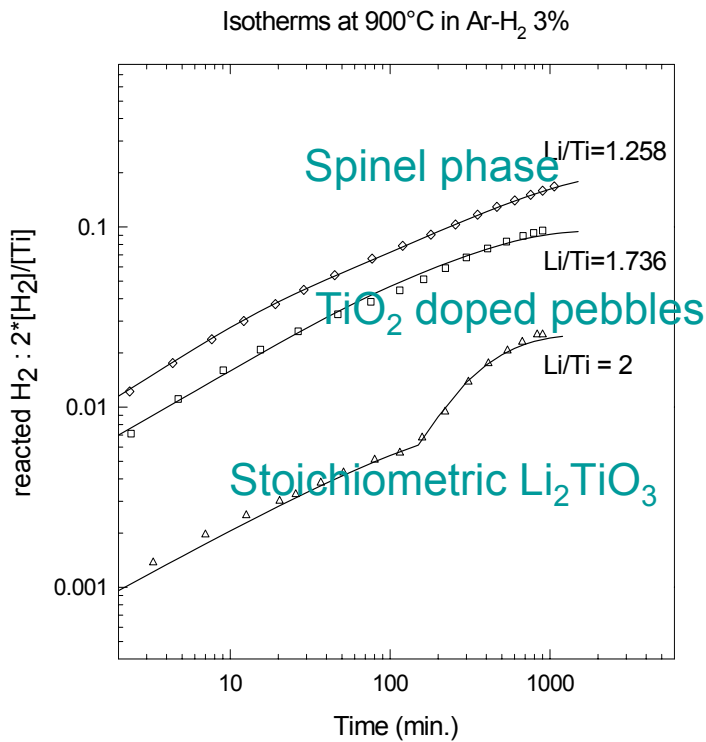
Possible connection between tritium release property and phase changing in the Li-titanate pebbles undergoing high BU

11/23/2004

S. Casadio

6

RESULTS -1) TPR test of Li-titanate pebbles under reduction-annealing at 900°C in flowing He + 3% H₂

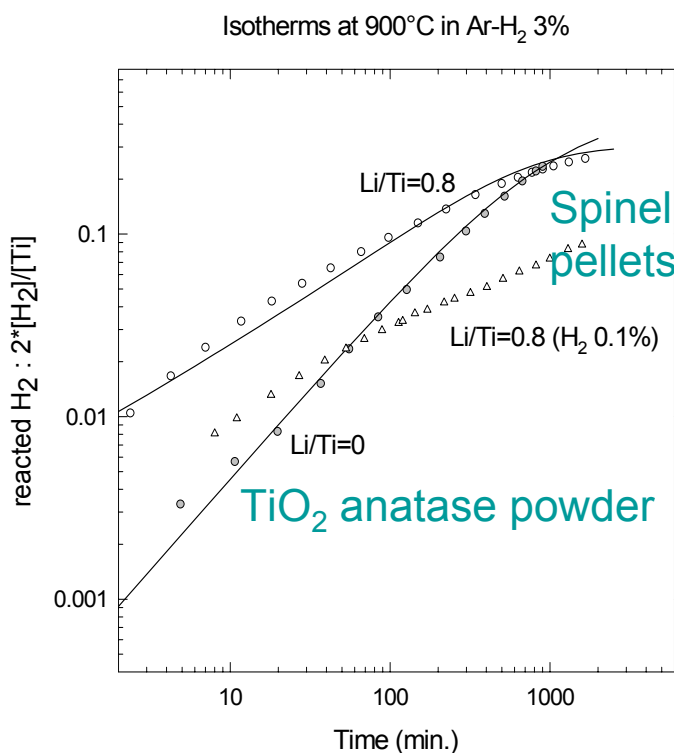


The pebbles reduction rate remarkably increased by increasing the H₂ concentration in the Ar purge gas

Some of the H₂ reacted to give Li metal vapors (Li-loss). The spinel phase reduction is accompanied by the formation of the orthorhombic Li_{0.14}TiO₂ “black” phase and to a Li-rich surface compound

7

RESULTS -2) TPR test of TiO₂ powder reduction at 900°C in flowing Ar + 3% H₂ as compared to that of spinel pellets



Pure TiO₂: the “extrapolated” Ti final valence resulted to be +3.5, corresponding to that of Ti₄O₇ Magneli phase.

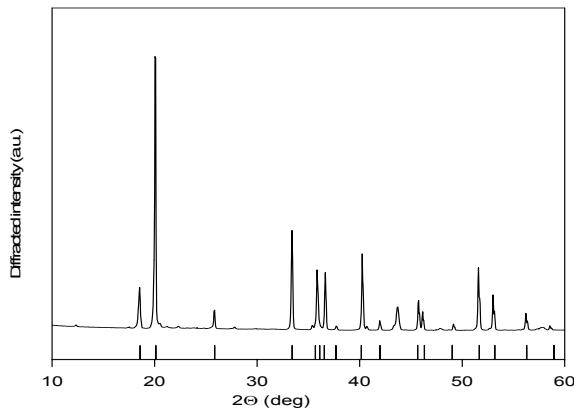
Pure spinel phase Li₄Ti₅O₁₂: no Li-loss was not observed. Reduction evolution reached the steady-state with a final Ti^{3.7+} valence.

The case for Ar + 0.1% H₂ purge is also reported for comparison.

A Li-rich reduced titanate (undetected by XRD) should be generated at the specimen surfaces (as observed by XPS)

8

RESULTS – 3) Phase changes in annealed (900°C x 16 h in flowing Ar+3% H₂) spinel pebbles



The density of the orthorhombic Li_{0.14}TiO₂ “black phase” is 3.83 g/cm³ while that of the spinel phase is 3.49 g/cm³. The reduction in volume must be accompanied by a Li expulsion from the lattice. Formal reaction scheme:



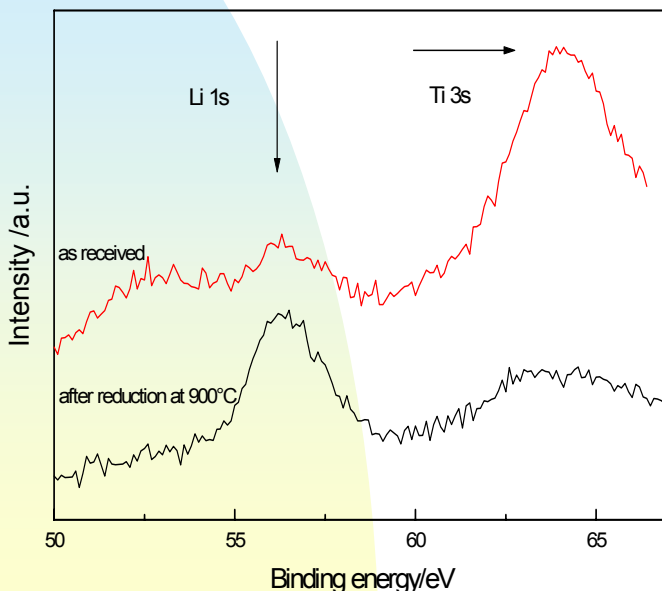
11/23/2004

S. Casadio

9

- Data reported in Tokyo (CBBI-11) for the spinel powder reduction at 1000°C x 16 h in flowing Ar + 3% H₂ are confirmed to occur also for pebbles at 900°C:
- XRD analysis show the formation of orthorhombic Li_{0.14}TiO₂ “black phase”.
- The resulting cell parameters are: a=4.99Å, b=9.58Å, c=2.94Å, β=100.5°; the cell volume results 140.80Å³ in fair agreement with the theoretical one 140.40Å³

RESULTS –4) X-ray Photoelectron Spectroscopy: spinel surface Li/Ti ratio changes after annealing at 900°C x 16 hours in flowing Ar + 3% H₂ gas



11/23/2004

S. Casadio

10

- The XPS Li(1s) over Ti(3s) signal ratio on the the spinel phase surface (for both pebbles and powders) is strongly enhanced by the reduction-annealing treatment.
- That is in agreement with the expected Li expulsion from the lattice undergoing Li_{0.14}TiO₂ “black phase” the spinel→orthorhombic Li_{0.14}TiO₂ (“black phase”) transformation.
- This behavior could not be observed for the lithium metatitanate pebbles, generally showing a very low Li(1s) signal.

RESULTS –5) The Ti valence evolution in the reduced annealed titanate specimens

- Li_2TiO_3 and $\text{Li}_4\text{Ti}_5\text{O}_{12}$ are Ti^{4+} valence ion compounds.
- In $\text{Li}_{0.14}\text{TiO}_2$ (clearly confirmed to be one of the final products) Ti is in (average) $\text{Ti}^{3.86+}$ valence state.
- The reduced product of TiO_2 in equilibrium conditions was found to have $\text{Ti}^{3.5+}$ valence state corresponding to that of the Ti_4O_7 Magneli phase.
- This $\text{Ti}^{3.5+}$ valence state is assumed to hold also for the lithium titanate at steady-state reduction.
- Under this assumption the following table shows the fraction of the different phases (characterized by different Ti-valence states) generated by the reduction-annealing treatment at 900°C in $\text{Ar}+3\%\text{H}_2$ in the considered specimens.

11/23/2004

S. Casadio

11

RESULTS –6) Ti valence, Li/Ti ratio and phase composition of the reduction annealed pellets and pebbles (900°C x 16 hours in $\text{He}+3\%\text{H}_2$)

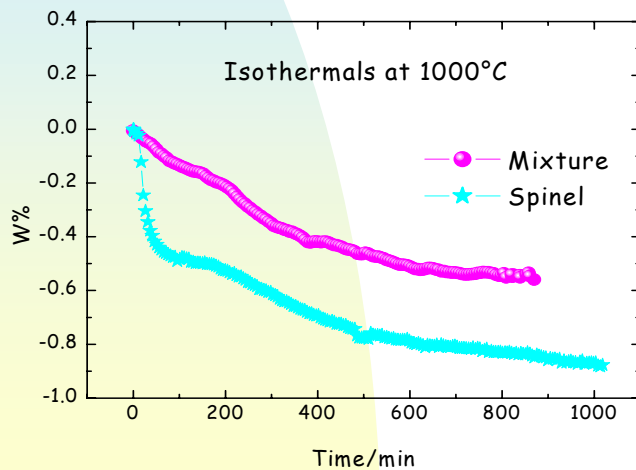
Sample	Li_2TiO_3 (Ti^{4+})	$\text{Li}_{0.14}\text{TiO}_2$ ($\text{Ti}^{3.86+}$)	$(\text{Li}_2\text{TiO}_{2.75})$ ($\text{Ti}^{3.5+}$)	Final Li/Ti	Ti average valence		
					calculated	measured	extrap.
JPLT-SP	0.000	0.645	0.355	0.800	3.732	3.745	3.700
JPLT-30	0.373	0.405	0.223	1.247	3.832	3.843	3.810
JPLT-20	0.557	0.286	0.157	1.458	3.881	3,869	3.860
JPLT-10	0.775	0.145	0.080	1.731	3.940	3.910	3.910
JPBL-10	0.817	0.118	0.065	1.781	3.951	3.931	3.931
JPBL-5	0.888	0.073	0.040	1.865	3.970	3.951	3.951
JPBL-2.5	0.938	0.040	0.022	1.926	3.984	3.977	3.977
JPBL-0	0.986	0.009	0.005	1.983	3.996	3.990	3.990
JPLT-0	0.986	0.009	0.005	1.983	3.996	3.992	3.992

11/23/2004

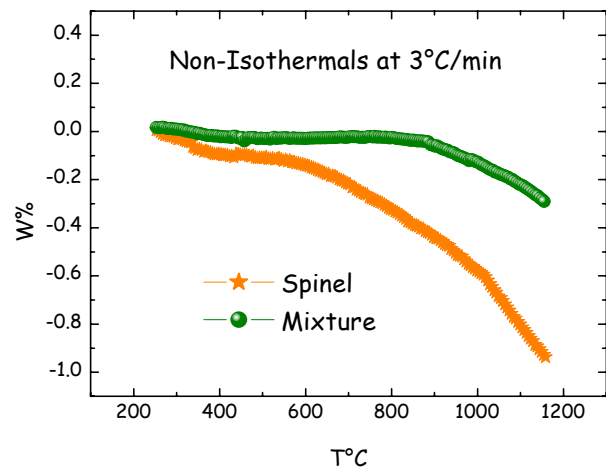
S. Casadio

12

- The reduction of spinel $\text{Li}_4\text{Ti}_5\text{O}_{12}$ and $\text{Li}_4\text{Ti}_5\text{O}_{12} - \text{Li}_2\text{TiO}_3$ with mixture of $\text{Ar} + 3\% \text{H}_2$ was studied by using
- Isothermal (1000°C) and Non-Isothermal (heating ramp 3°C/min).



11/23/2004

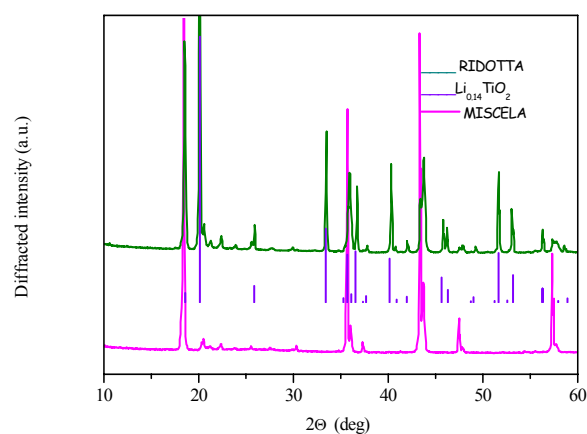
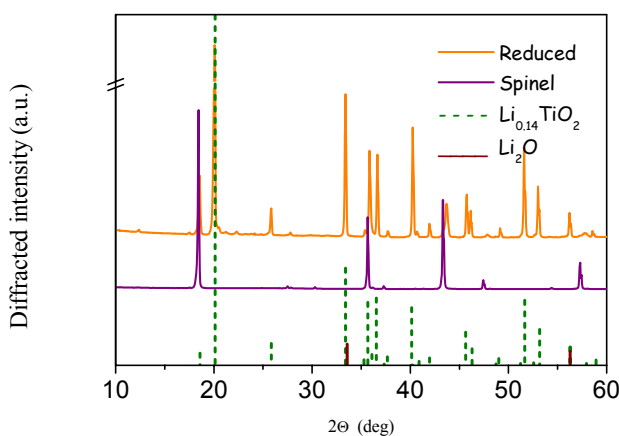


S. Casadio

13

XRD ANALYSIS of the reaction products

Pure $\text{Li}_4\text{Ti}_5\text{O}_{12}$ and $\text{Li}_4\text{Ti}_5\text{O}_{12} + \text{Li}_2\text{TiO}_3$ powder mixture (45-55 mol %) reduction in flowing $\text{Ar} + 3\% \text{H}_2$ at 1000°C x 16 hours



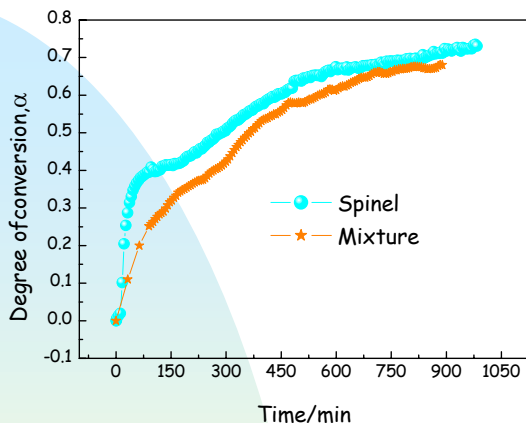
- The presence of Li-metatitanate does not change the spinel phase reduction product formed by pure $\text{Li}_4\text{Ti}_5\text{O}_{12}$ phase-powder reduction:
- the orthorhombic $\text{Li}_{0.14}\text{TiO}_2$ “black” phase and Li_2O (confirming XPS analysis) were found to be the main reaction products.

11/23/2004

S. Casadio

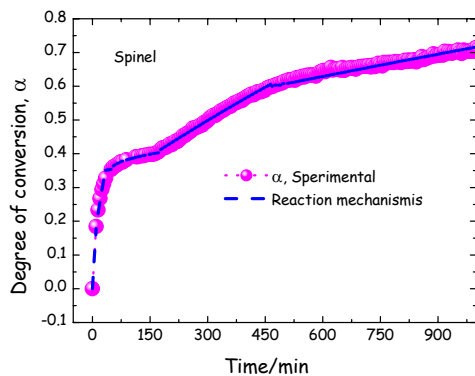
14

Li₄Ti₅O₁₂ powder reduction kinetics-1



- Isothermal method (1000°C)
- The time evolution of the degree of fractional conversion α show the complex nature of the reaction. It was possible to evaluate average rate constant K values

Spinel	
$0 < \alpha < 0.34$	$k=3.220 \cdot 10^{-4} \pm 8.91 \cdot 10^{-6} \text{ min}^{-1}$
$0.34 < \alpha < 0.40$	$k=2.269 \cdot 10^{-6} \pm 3.10 \cdot 10^{-8}$
$0.41 < \alpha < 0.60$	$k=2.406 \cdot 10^{-4} \pm 1.06 \cdot 10^{-6}$
$0.60 < \alpha < 0.72$	$k=1.136 \cdot 10^{-4} \pm 7.73 \cdot 10^{-6}$
Mixture	
$0 < \alpha < 0.34$	$k=5.639 \cdot 10^{-4} \pm 5.35 \cdot 10^{-6} \text{ min}^{-1}$
$0.34 < \alpha < 0.41$	$k=3.001 \cdot 10^{-4} \pm 4.84 \cdot 10^{-6}$
$0.41 < \alpha < 0.54$	$k=3.854 \cdot 10^{-4} \pm 4.37 \cdot 10^{-6}$
$0.54 < \alpha < 0.7$	$k=1.280 \cdot 10^{-4} \pm 1.36 \cdot 10^{-6}$

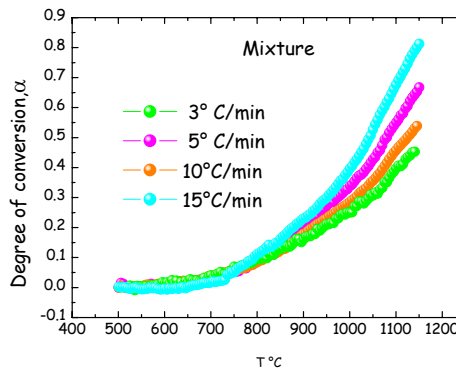
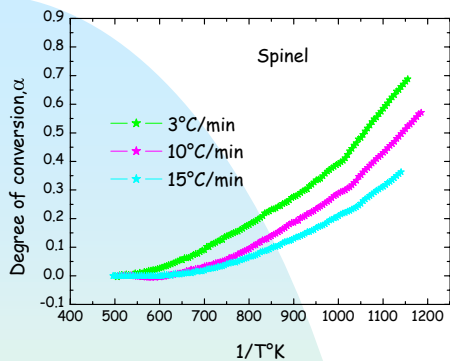


11/23/2004

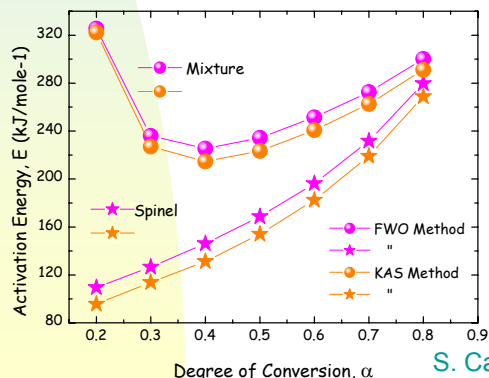
S. Casadio

15

Li₄Ti₅O₁₂ powder reduction kinetics-2



Non isothermal method. The elaboration of the degree of fractional reaction conversion α at various heating rates β gave activation energy (E_a kJ/mol) vs α plots



11/23/2004

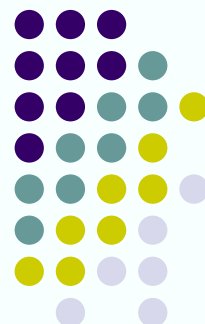
S. Casadio

16

- The high temperature (900 -1,000°C) reaction of H₂ (doping the He purge) with lithium titanate pebbles was performed in reference environment (Ar + 0.1% H₂) and mainly by accelerated tests (using Ar + 3% H₂) on TiO₂ doped (Li-depleted) pellets and pebbles.
- In any case the extend of the reduction was found to increase with the amount of the Li₄Ti₅O₁₂ spinel phase inside the specimens
- The maximum of transformation was observed for pure Li₄Ti₅O₁₂ spinel phase pebbles (900°C) and powders (1000°C) for which the reduction was found to be almost completed after 16 hours with the formation of the orthorombic Li_{0.14}TiO₂ phase pushing a Li-rich compound toward the specimen surface (well revealed by XPS and detected by XRD analysis as Li₂O only for the pure powder specimen).
- The spinel phase reduction as mixed with metatitanate Li₂TiO₃ powder gave the same products of the pure phase powder, but at a slightly slower rate.
- By the obtained kinetic parameters very conservative extrapolations show that the rate of the process is so low to be not significant below 650°C.
- The high temperature (800 - 1,000°C) lithium titanate pebble transformation mechanism (as induced by the H₂ of the purge gas) may be understood and evaluated by knowing the Li-depletion (spinel phase) level in the specimens.

Hydrogen Isotopes Behavior on Li_2TiO_3 under H_2O exposure and D_2^+ irradiation

R. Olivares, T. Oda, Y. Oya, K. Tsuchiya and S. Tanaka
The University of Tokyo



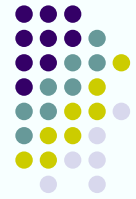
Contents

- 1. Introduction**
- 2. Methodology**
 - 2.1 Photoelectron Spectroscopy (XPS/UPS)**
 - 2.2 FT-IR Spectroscopy**
 - 2.3 Quantum Chemical Calculation (DFT)**
- 3. Results and Discussion**
 - 3.1 Surface Nature**
 - 3.2 Hydrogen Isotope Behavior on the Surface**
- 4. Conclusions**



1. Introduction

Background/Purpose



In R&D for D-T fusion reactor, production of a sufficient amount of T is an essential task.

T breeding in a blanket: ${}^6\text{Li} + n \rightarrow {}^4\text{He} (2.1 \text{ MeV}) + \text{T} (2.7 \text{ MeV})$

Li_2O , LiAlO_2 , Li_4SiO_4 , Li_2ZrO_3 , Li_2TiO_3 ...

Li_2TiO_3 is the promising candidate due to its excellent tritium release performance.

However, *detailed tritium behavior* in Li_2TiO_3 is not understood:

“How tritium exists in the bulk or on the surface ?”
 “What kind of influence tritium is received from radiation defects ? ”

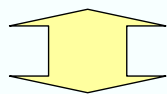


Elucidate the **surf. nature** of Li_2TiO_3 and
 the **hydrogen isotope behavior** on the surf.

2. Methodology



To understand the hydrogen isotope behavior on Li_2TiO_3 :



Observe the surface nature and the hydrogen isotope behavior **directly**.

Surface composition and chemical states of constitutional element.
 High sensitivity to surface -OH

Photoelectron Spectroscopy (XPS/UPS)

Ar^+ sputtering,
 Heating
 H_2O exposure

identify various chemical states of hydrogen isotopes on the surface.

Fourier Transform Infrared Spectroscopy (FTIR)

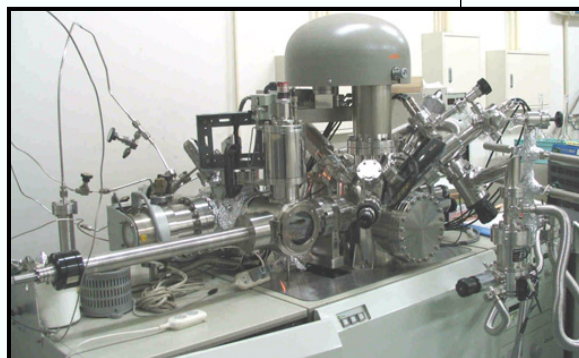
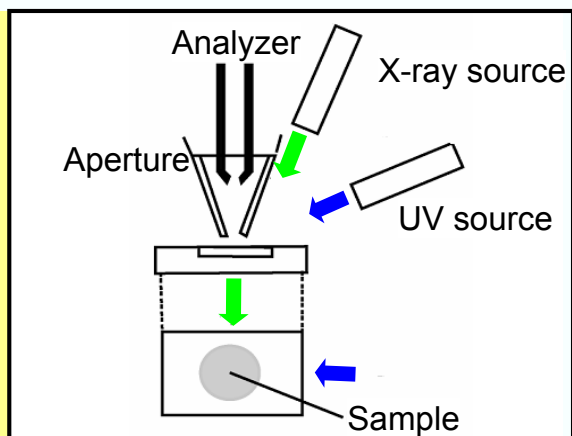
D_2^+ ion irradiation
 D_2O exposure

Valence band comparison

DOS calculation

Quantum Chemical Calculation (DFT)

2.1 Photoelectron Spectroscopy (XPS/UPS)



Apparatus: JPS-9800 (JEOL)
X-ray: Mg K α (1253.6 eV)
UV: He II (40.8eV)
Pressure: 2x10⁻⁷ / 1x10⁻⁶ Pa (XPS/UPS)
Sample: Li₂TiO₃ pellet (JAERI)

Analysis is sensitive to surface nature.

XPS (Core electrons)
Surface composition/chemical states

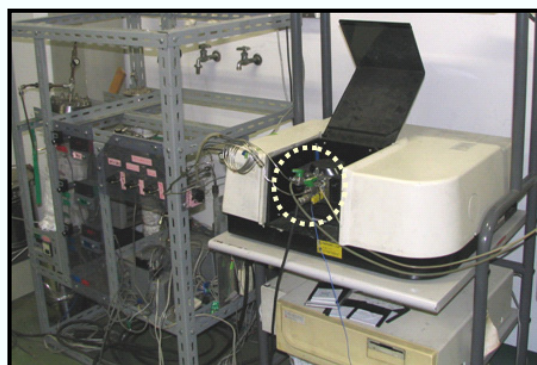
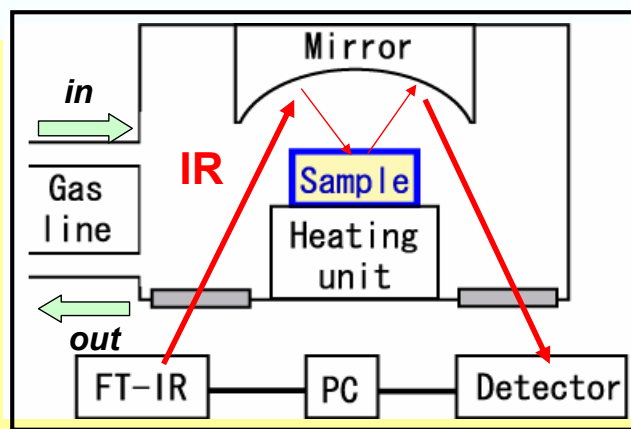
UPS (Valence electrons)
High sensitivity to surface-OH

hydrogen behavior and the surface nature can be analyzed

2.2 Fourier transform infrared spectroscopy (FT-IR) with diffuse reflectance Unit



a) High pressure system



Shimadzu FT-IR 8100
Li₂TiO₃ powder (purity: 99-99.9%)
Purge gas: dry N₂ gas (100-200 cc/min)
Pressure: 1 atm.

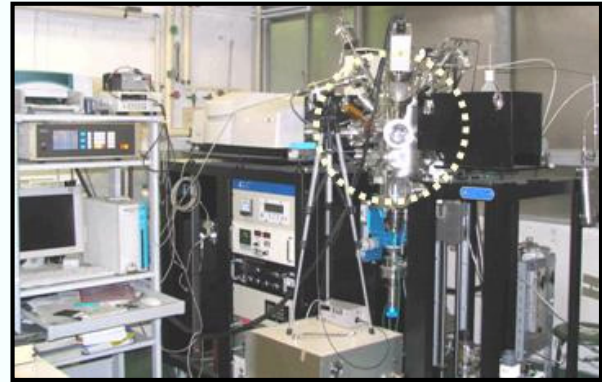
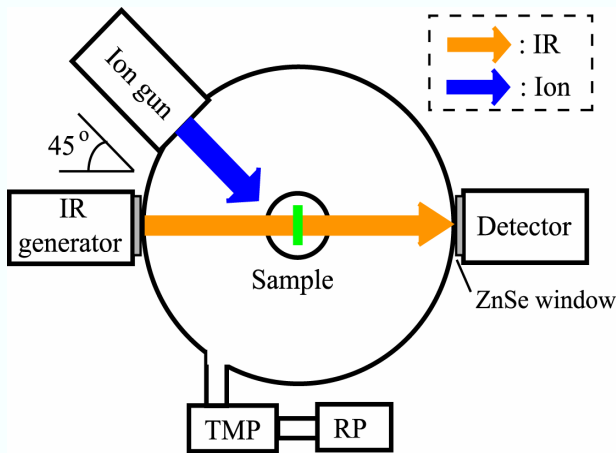
FT-IR Existence state of surface O-D and Influence of surrounding conditions. (⇒ IR absorbing species show multiple peaks.)

Detailed information on surface O-D

Configuration of IR, ion gun and the sample in ion irradiation FT-IR



a) Low pressure system



Mattson Infinity Gold

Li₂TiO₃ powder (purity: 99-99.9%)

Pressure: 10⁻⁶Pa; during D₂⁺Irradiation: 5x10⁻³ Pa

Ion Flux: 1.3x10¹⁷ D₂⁺ m⁻² s⁻¹

Ion Fluence: 1.0x10²² D₂⁺ m⁻²

By FT-IR under D₂⁺ irradiation

- influence of radiation defects
- variation of hydrogen behavior

Information on radiation damage

2.2 Quantum Chemical Calculation (DFT)



DFT technique provided by CASTEP code

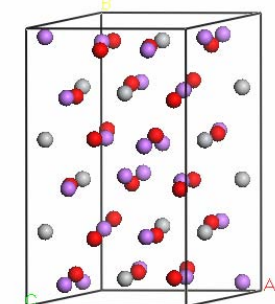
Approximation: **GGA**

Functional: **RPBE**

- To treat properly the relaxation on the surface, **all atoms were permitted to move.**

- Calculation cost was reduced using **plane wave pseudopotential method.** (O for He core, Ti for Ne core).

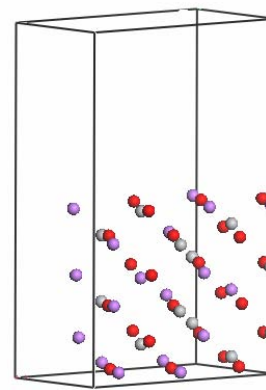
Li: ● O: ● Ti: ●



Conventional cell

Slab tech.

Model a surface



(010) surface

3. Results and Discussion

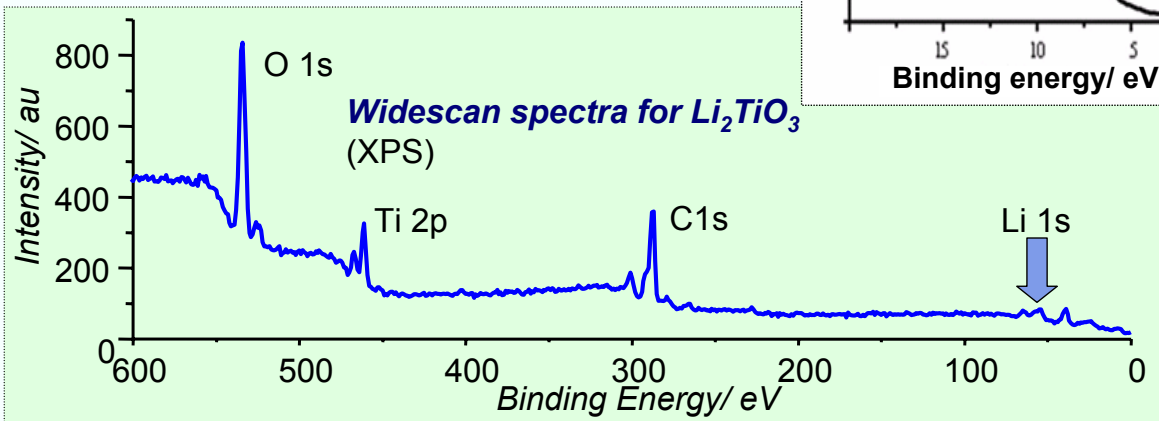
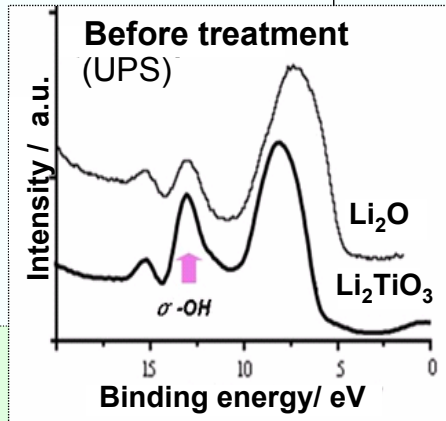


3.1. Surface Nature

3.1.1 As-received sample (XPS/UPS)

Consistent results in the case of O 1s were indicated. Surface tends to be covered by -OH, largely as LiOH

UPS spectra before sputtering is Li₂O- like surface

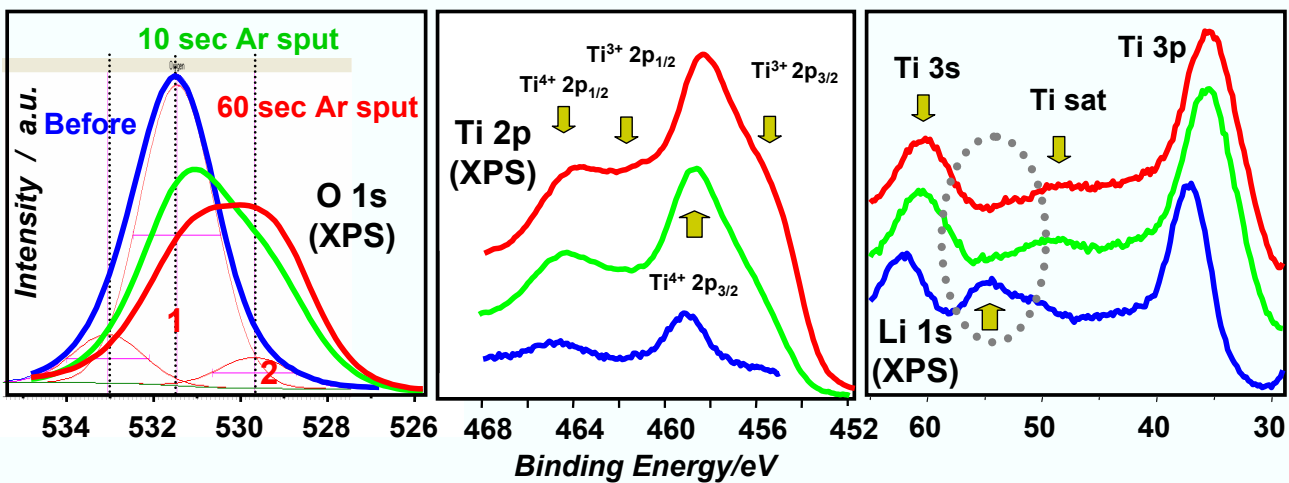


3.1. Surface Nature

3.1.2 Ar ion sputtering (XPS)



Ar sputtering rate: 30 nm/min in SiO₂



<Oxygen>
LiOH (1) decreased and
Li₂TiO₃ (2) appeared.

<Titanium>
Ti was reduced
from Ti⁴⁺ to Ti³⁺.

<Lithium>
Li disappeared.

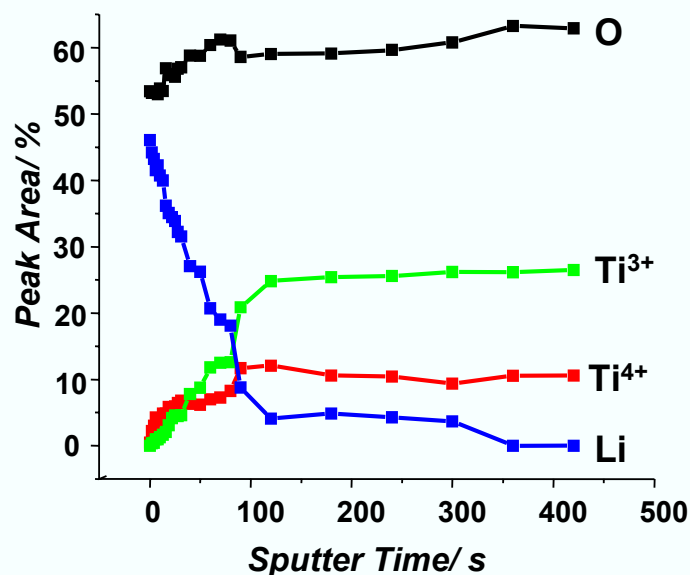


3.1. Surface Nature

3.1.2 Ar ion sputtering

Effect of Ar ion bombardment on composition (XPS)

Ar sputtering rate: 30 nm/min in SiO₂



- Selective sputtering occurs:
Li > O > Ti

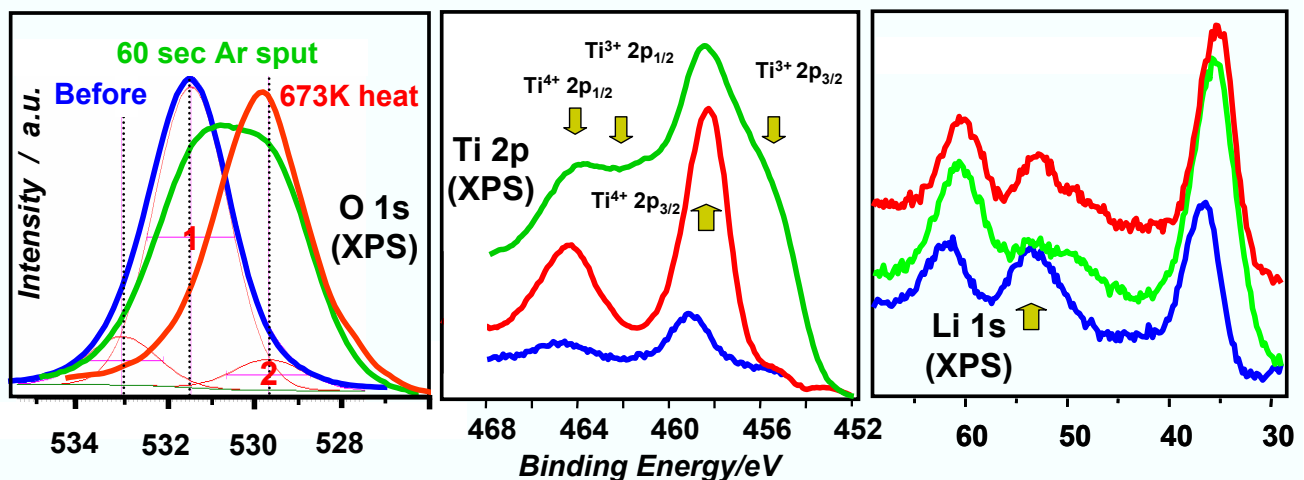
- It induces:
Li and O deficiency & Ti reduction

- The selective sputtering finished at 65 %-O, 25 %-Ti³⁺ and 10 %-Ti⁴⁺, where TiO₂-like and Ti₂O₃-like surfaces might coexist.

- Li was totally removed from the surface region by the sputtering.

3.1. Surface Nature

3.1.3 Effect of Heating (XPS)



<Oxygen>

LiOH (1) totally removed
Li₂TiO₃ (2) appeared.

<Titanium>

Ti was oxidized
from Ti³⁺ to Ti⁴⁺.

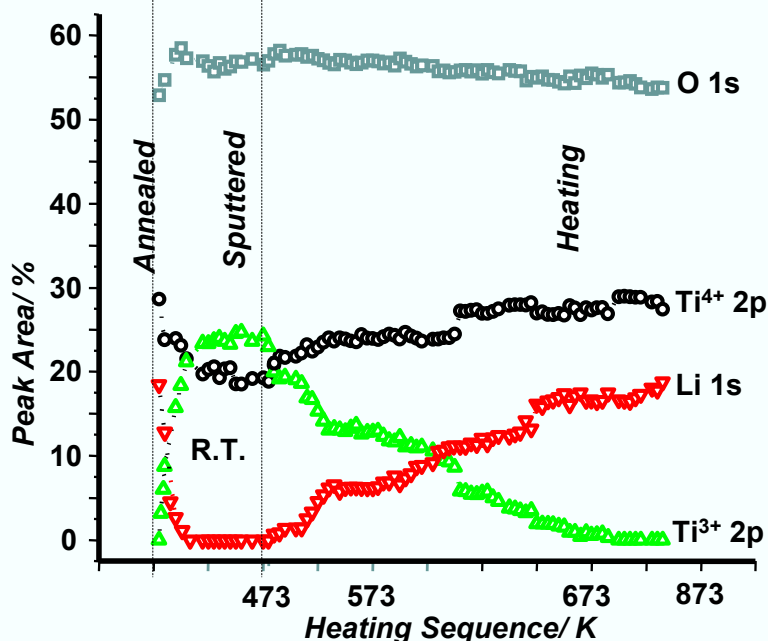
<Lithium>

Li emerged.

3.1. Surface Nature

3.1.2. Heating

Effect of heating on composition (XPS)



- Ti oxidation and Li recovery started at 473K.



Surface reconstruction is initiated at 473 K.

- The variation in spectra was almost finished at 673 K.

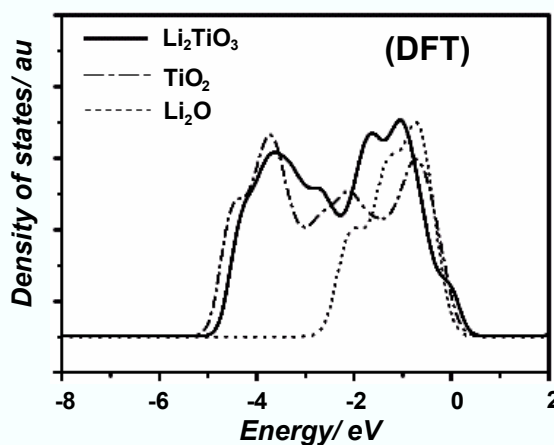
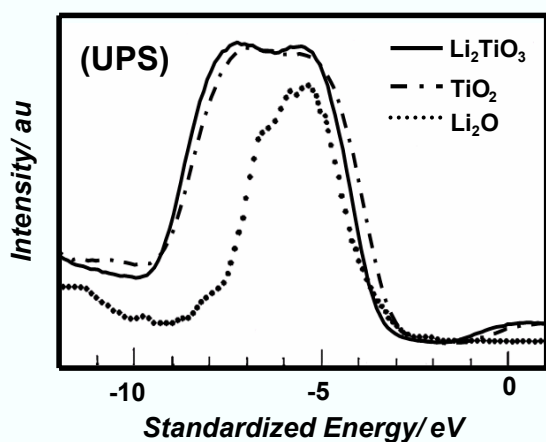


Total recovery of radiation induced damage is held at 673 K, and near-stoichiometric surface is obtained.

Surface reconstruction is observed at 673K. Surface is near stoichiometric.

3.1. Surface Nature

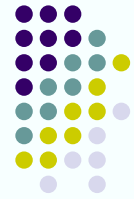
3.1.4 Comparison with TiO_2 and Li_2O Based on UPS and DFT results.



By DFT calculation **and the** valence band structure by UPS,

*Similarity in the structure between TiO_2 and Li_2TiO_3 .
Wide band spectra - O 2p and Ti 3d contributing factors in the valence band*

3.1. Surface Nature Section Summary



The surface nature of Li_2TiO_3 have been investigated by XPS, UPS and quantum chemical calculation.

The following have been derived from the results:

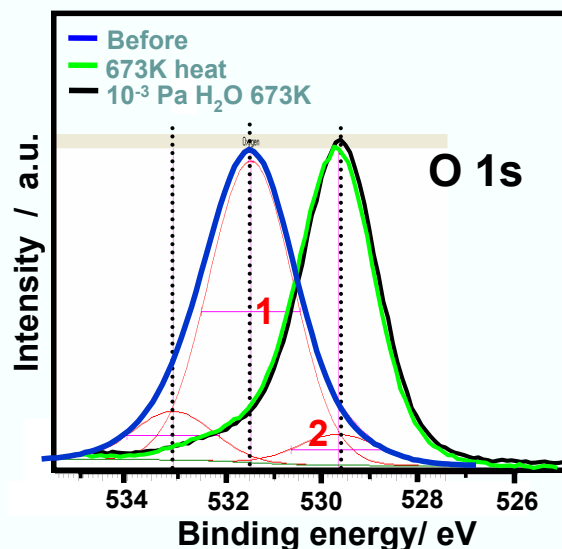
- i. Selective sputtering induced Li and O deficiency, and Ti reduction.*
- ii. Surface reconstruction, namely Li and O recovery and Ti oxidation, of sputtered surface is initiated at 473K and almost completed at 673 K. The surface seemed to be near stoichiometric at 673 K.*
- iii. Re-oxidation rate is rapid at 673-873K, and reduction is not strongly induced below 873 K.*
- iv. Based on valence electronic structure by UPS and DOS calculation, the surface nature of Li_2TiO_3 is similar with TiO_2 rather than Li_2O .*

3.2. Hydrogen Isotope Behavior

3.2.1 H_2O exposure on the annealed surface (XPS) (low pressure)



10^{-3} Pa H_2O exposure for 5 min at 300-673K.



- Another peak or peak broadening was not induced by the exposure.



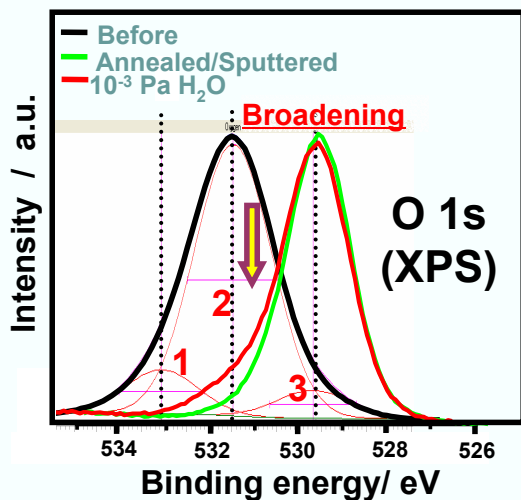
Water adsorption is non-existent on the near stoichiometric surface by the low pressure water exposure.

3.2. Hydrogen Isotope Behavior

3.2.2 H₂O exposure on the defective surface (XPS/UPS) (low pressure)



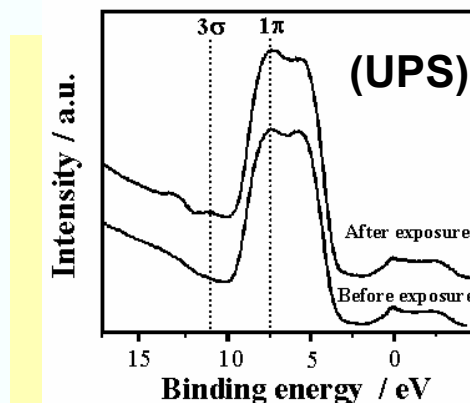
10⁻³ Pa H₂O exposure for 5 min at 300 K to the Ar sputtered surf.



- Peak Broadening at higher B.E.



Water dissociatively adsorbed.



- Additional peaks were formed associated with surface -OH; 3σ (~10.8 eV) and 1π (~7.6 eV).

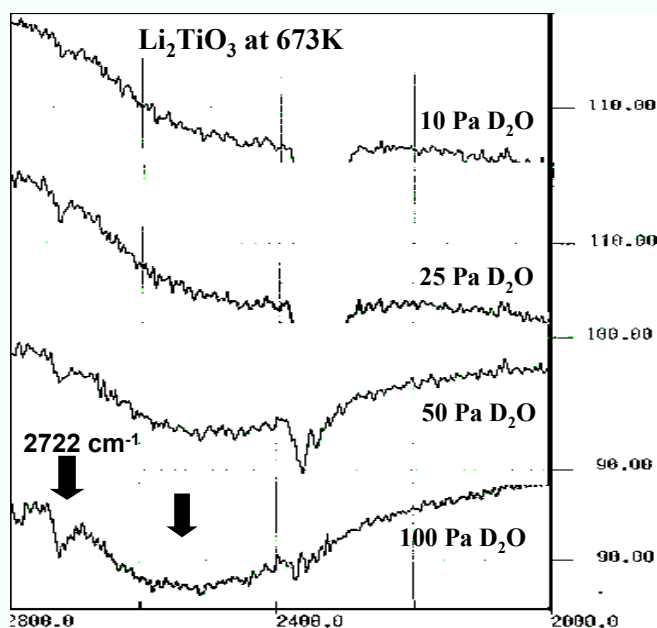


Water adsorption was clearly confirmed.

Dissociative adsorption of water is induced by surface defects.

3.2. Hydrogen Isotope Behavior

3.2.3 H₂O exposure on the annealed surface (FT-IR) (high pressure)



- Two -OD peaks appeared by 10-150 Pa D₂O exposures at 300-673 K, and their intensities increased at higher D₂O pressure.

- A sharp peak at 2722 cm⁻¹ has been evolved from the non-hydrogen bonded -ODs

- A broad peak at 2700-2500 cm⁻¹ was attributed to the surface ODs that were H-bonded with surrounding -ODs.



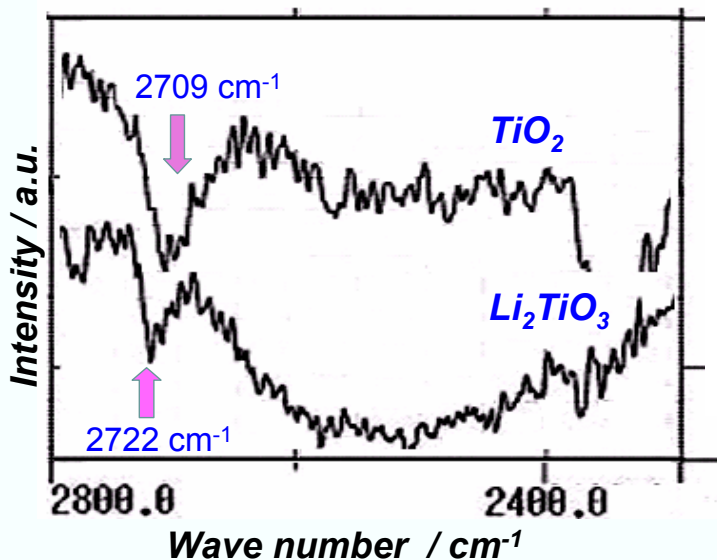
Hydrogen isotope takes mainly 2 existence states on Li₂TiO₃: 2722 cm⁻¹ and 2700-2500 cm⁻¹

3.2. Hydrogen Isotope Behavior

3.2.4 Comparison with TiO_2 (FT-IR measurement)



Absorption spectra of Li_2TiO_3 and TiO_2 obtained at 673 K with D_2O partial pressure of 100 Pa.



◆ TiO_2 showed two –OD peaks, the same as Li_2TiO_3 .

◆ A Sharp peak was found at 2709 cm^{-1} .



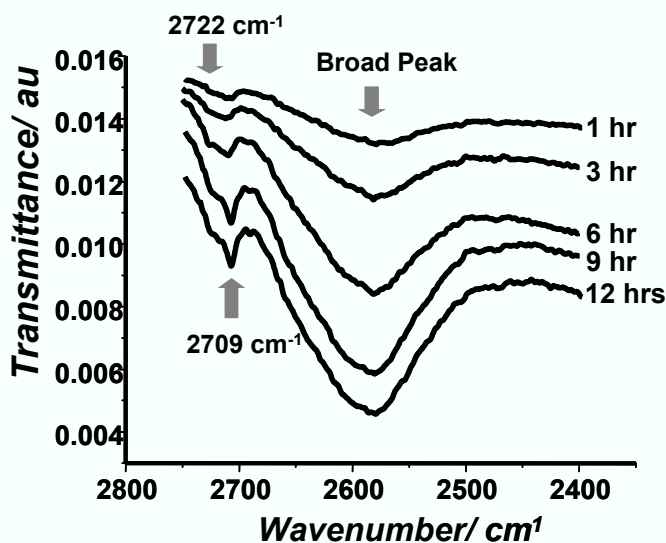
IR spectra were similar between in TiO_2 and in Li_2TiO_3 , except the positions of the sharp peaks; 2709 cm^{-1} (TiO_2) / 2722 cm^{-1} (Li_2TiO_3)

3.2. Hydrogen Isotope Behavior

3.2.5 Deuterium Ion Irradiation (FT-IR)



IR absorption spectra of Li_2TiO_3 during 3 keV D_2^+ irradiation at R.T.



2709 cm^{-1} – peak related with a defect, created by the D_2^+ irradiation.

- selective sputtering producing Li vacancy.
- Li deficient surface brought formation of the TiO_2 -like surface

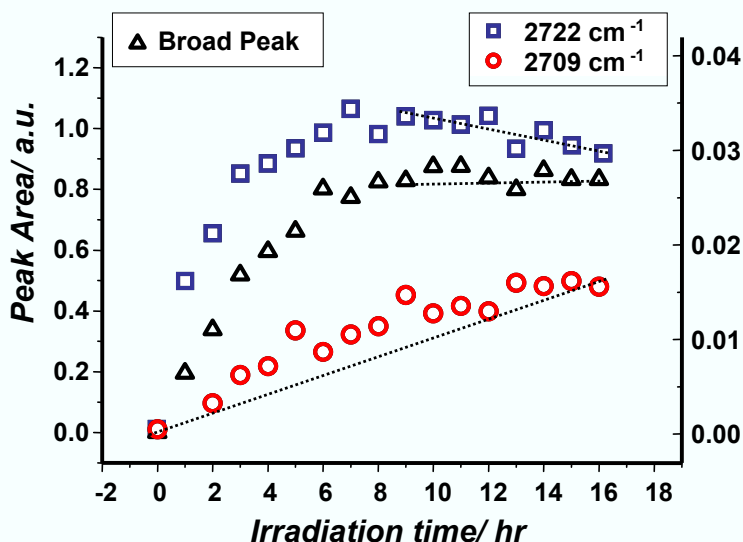
From this viewpoint, the peak at 2709 cm^{-1} seemed to be attributed from the O-D on the TiO_2 -like surface.

This consideration shows good agreement with respect to the peak position; an isolated O-D on Li_2TiO_3 is 2722 cm^{-1} ; and TiO_2 is 2709 cm^{-1}

3.2. Hydrogen Isotope Behavior

3.2.6 Deuterium Ion Irradiation

Dependence of peak area intensity with 3 keV D_2^+ irradiation time



- the broad peak and the peak at 2722 cm^{-1} increases with time and saturates at about 9 hours irradiation exposure.
- Absorption peak at 2709 cm^{-1} increases due to continues irradiation.

The increasing intensity of 2709 cm^{-1} is attributed to the increasing Ti active sites and increasing Li vacancies by continues irradiation, thus a decreasing behavior is observed with peak 2722 cm^{-1}

During the heating over 573 – 673 K, the intensity these peaks decreases abruptly after one hour.

3.1. Hydrogen Isotope Behavior Section Summary



The following summarizes the results obtained from D_2O/H_2O exposure and D_2^+ irradiation on Li_2TiO_3 :

- Dissociative adsorption*** of water hardly occurs without ***surface defects*** near ***R. T.*** Water has low affinity towards Li_2TiO_3
- At least ***two surface O-D states*** are possible above 573 K in the atmosphere of ***several tens Pa*** D_2O vapor pressure.
- Additional ***O-D state at 2709 cm^{-1}*** is observed by ***D_2^+ irradiation***, attributed to O-D from ***TiO_2 -like surface produce*** by radiation defects.
- OD/-OH states*** on the surface easily ***annihilated*** at 573 – 673 K.

4. Conclusions



The surface nature of Li_2TiO_3 and the hydrogen isotope behavior have been investigated using XPS/UPS and FT-IR. The similarity of Li_2TiO_3 surface with TiO_2 was clarified through the electronic states and the affinity with water vapor.

Irradiation damage is a known to have a large influence on tritium diffusion process, However, by the results, the stability of surface O-D was not so enhanced by the influence of radiation defects, and the reconstruction of surface defects brought by sputtering and irradiation rapidly occurs at lower temperature.

Release Behavior of Bred Tritium from Ceramic Breeder Materials with New Mass Transfer Resistance at Interface

M. Nishikawa, T. Kinjyo, T. Ishizaka, K. Nakashima,
S. Beloglazov*, M. Enoda** and T. Tanifuji**

Department of New Energy, Graduate School of Engineering Science, Kyushu University
Hakozaki 6-10-1, Higashi-ku, Fukuoka 812-8581, Japan

*Forschungszentrum Karlsruhe

**Japan Atomic Energy Research Institute

ABSTRACT

The present authors have proposed a model to explain tritium release behavior from irradiated solid breeder materials where the release curves were obtained in a series of experiments carried out using the out-pile temperature programmed desorption (TPD) techniques. Tritium release curves obtained for different purge gas compositions (dry N₂, N₂+H₂, N₂+H₂O) have been compared for selection of suitable condition to decide the tritium release behavior from solid breeder materials.

It has been pointed out by the present authors that not only diffusion of tritium in bulk of grain but also surface reactions on grain surface give profound effects on the tritium release behavior. In the model reported so far by the present authors, it is required to use so small reaction rates for the surface reactions as one several thousandth of the observed values reported in the previous papers to get the good fitting.

In this study the mass transfer resistance between grain surface and surface water is newly introduced because it is preferable to use the same reaction rate as that reported previously. The estimated values using the new model give good agreement with the observed tritium release curves and also with the release curves estimated using the model so far.

I. INTRODUCTION

A model to explain tritium release behavior from irradiated solid breeder materials has been proposed by the present authors where the release curves are obtained in a series of experiments carried out using the out-pile temperature programmed desorption techniques¹⁾⁻⁴⁾. Tritium release curves obtained for different purge gas composition (dry N₂, N₂ with H₂, N₂ with H₂O) have been compared for selection of suitable condition to decide the tritium release behavior from solid breeder materials and for discussion to evaluate parameters representing various tritium transfer steps.

It has been pointed out by the present authors that not only diffusion of tritium in bulk of grain but also surface reactions on grain surface give profound effects on the release behavior of bred tritium. It is assumed in the model by the present authors so far that the bred tritium arrives at the grain surface is transferred to the surface water on grain quickly and that mixing of tritium in the surface occurs instantaneously. Then, tritium is liberated to the purge gas from surface water through such surface reactions as desorption, isotope exchange reaction 1 and isotope exchange reaction 2. In the model reported so far by the present authors, it is required to use so small reaction rates for the surface reactions as one several thousandth of the observed values reported in the previous papers⁵⁾⁻⁸⁾ to get the good fitting²⁾⁻⁴⁾. The mass transfer resistance between grain surface and surface water is newly introduced in this paper because it is preferable to use the same reaction rate as that reported previously⁵⁾⁻⁸⁾. The estimated values using the new model give good agreement

with the observed tritium release curves and also with the release curves estimated using the model so far.

II. THEORY

It is considered that the following mass transfer processes contribute to the release of tritium bred in blanket materials: ^{9), 10)}

- 1) tritium formation reaction in crystal grain;
- 2) diffusion of tritium in crystal grain;
- 3) interaction of tritium with irradiation defects in crystal grains;
- 4) resistance for tritium transfer from inner bulk layer to surface water.
- 5) absorption of tritium into the bulk of crystal grain;
- 6) adsorption and desorption of tritium on grain surface;
- 7) isotope exchange reactions between gaseous hydrogen, H_2 , in the gas stream and tritium on grain surfaces (isotope exchange reaction 1)



- 8) isotope exchange reactions between water vapor, H_2O , in the gas stream and tritium on the grain surfaces (isotope exchange reaction 2)



- 9) water formation reactions in addition of H_2 to the blanket purge gas;
- 10) transfer of hydrogen isotopes and water through pores of sintered pellets;
- 11) transfer of hydrogen isotopes and water through boundary layer formed on the surface of a sintered pellets to the gas stream;

where step 4) is the newly introduced mass transfer resistance by the present authors.

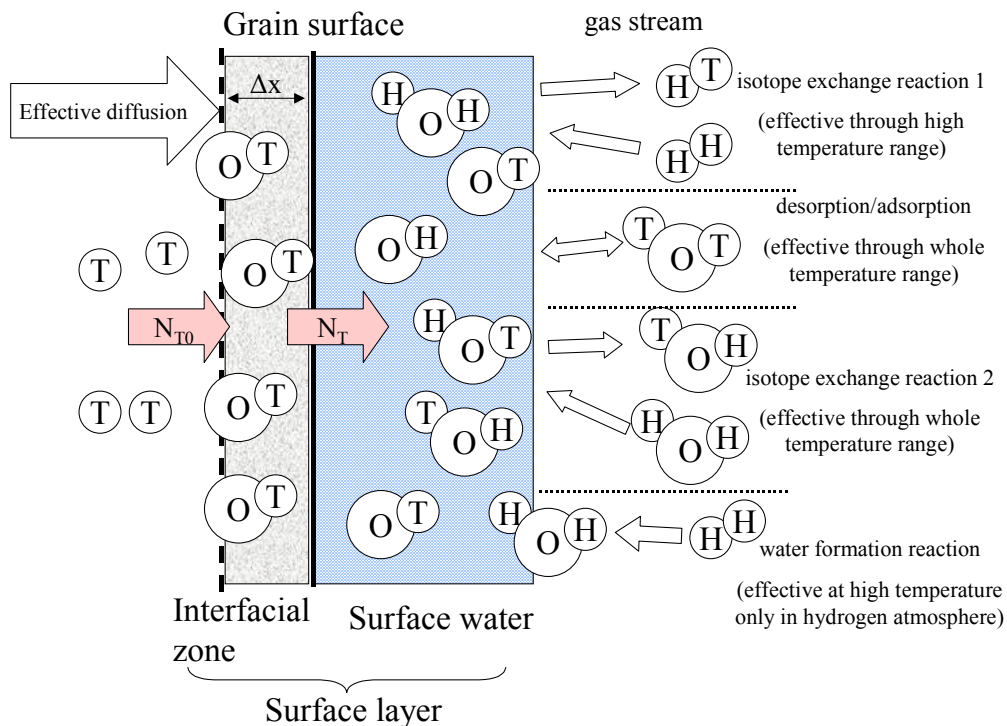


Fig.1 New model for tritium from solid breeder materials

Figure 1 shows a model of the tritium release from a grain of breeding ceramic considering that diffusion in bulk, mass transfer resistance between grain surface and surface water at the interfacial zone, and such surface reactions as adsorption/desorption, isotope exchange reactions and water formation reaction on the surface contribute in tritium release. It is assumed in this study that tritium is introduced to the interfacial

zone at the rate of N_{T0} [mol/m² sec] by diffusion and is transferred to the surface water at the rate of N_T [mol/m² sec]. The mass balance in the surface layer is expressed by the following equations imaging the isotope exchange reaction:

$$A\Delta x \frac{\partial C_T}{\partial t} = AN_{T0} - a_v V N_T$$

$$N_T = k \left(\frac{T}{T+H} - \frac{T_2O}{T_2O+H_2O} \right) C_T \quad (1)$$

where C_T [mol/m³] is tritium concentration in interfacial zone, a_v [m²/m³] is the specific surface area of packed bed, V [m³] is volume of interfacial zone in sample bed, $T/(T+H)$ [-] is isotopic ratio in grain, $T_2O/(T_2O+H_2O)$ [-] is isotopic ratio in surface water and k [m/sec] is rate constant.

Diffusion of tritium in a crystal grain and transfer of hydrogen, gaseous tritium, water vapor or tritiated water are expressed by mass balance equations explained in the previous paper by the present authors⁴⁾.

In the model presented so far by the present authors, the old model, the surface layer with perfect mixing was assumed. Then it was required the use so small reaction rates for the surface reactions as one several thousandth of the observed values to get the good fitting. In the model of this paper, the new model, the same reaction rates are used for the surface reactions as those reported in the previous papers⁵⁾⁻⁸⁾.

The present authors have observed that water vapor is absorbed into Li₂O at the higher blanket temperature though Li₂TiO₃, Li₂ZrO₃, LiAlO₂ and Li₄SiO₄ have no detectable absorption capacity of water or molecular form hydrogen. And the experimental observations about the tritium inventory so far indicate that effect of steps (9) and (10) are negligible.^{9), 10)}

III. EXPERIMENTAL

Pebbles of solid breeder materials such as Li₄SiO₄ (FzK), LiAlO₂ (JAERI), Li₂TiO₃ (CEA) and Li₂ZrO₃ (MAPI) were irradiated by the thermal neutron at the Kyoto University Reactor (KUR) or at the Japan Research Reactor 4 (JRR-4) in the Japan Atomic Energy Research Institute (JAERI) under the conditions of He atmosphere. The neutron flux was 1.65E13 [cm⁻²s⁻¹] at KUR and was 4.0E13 [cm⁻²s⁻¹] at JAERI.

Release curves of bred tritium from breeder material pebbles were obtained applying the out-pile temperature programmed desorption (TPD) techniques. Details of Experimental apparatus and experimental methods were explained in the previous paper⁴⁾.

IV. RESULTS AND DISCUSSION

Figure 2 shows comparison of tritium release curves estimated by old model or by new model with experimental tritium release curve obtained at KUR for Li₄SiO₄. Estimated curve (1) represented tritium introduction to the surface layer by diffusion where diffusion coefficient obtained in the previous paper⁴⁾ is used for estimation. Estimated release curves (2) and (3) obtained considering that both diffusion and surface reactions affected tritium release behavior show good agreement to the experimental curve, and curve (3) estimated by the new model gives better agreement as shown in Fig.2.

Comparison of mass transfer coefficients used for fitting is shown in **figure 3**. To get curve by using the old model, Curve (2) in fig.2 for example, it was required to use so small reaction rates for the surface reactions as shown by the curve (3) and (4) in fig.3. The mass transfer resistance between grain surface and surface water is newly introduced in this paper because it is preferable to use the same reaction rate as that reported previously.

In the experiment to estimate the rates of surface reactions, tritium was provided from the purge gas to the grain surface, though the bred tritium was provided from inside of the grain to surface. Accordingly, there is a possibility that some another phenomenon may contribute to lower the overall tritium transfer coefficient to large extent probably at the inner place than the place with the surface water.

Fitting parameters at new model are some as the values reported values as shown in Fig.3.

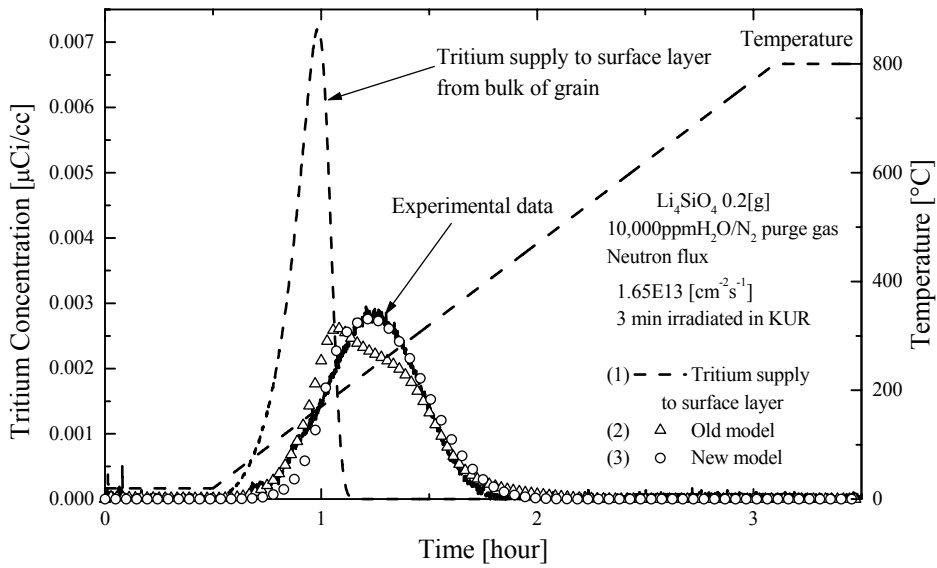


Fig.2 Tritium release curves for Li₄SiO₄ by 10,000ppmH₂O/N₂ purge gas

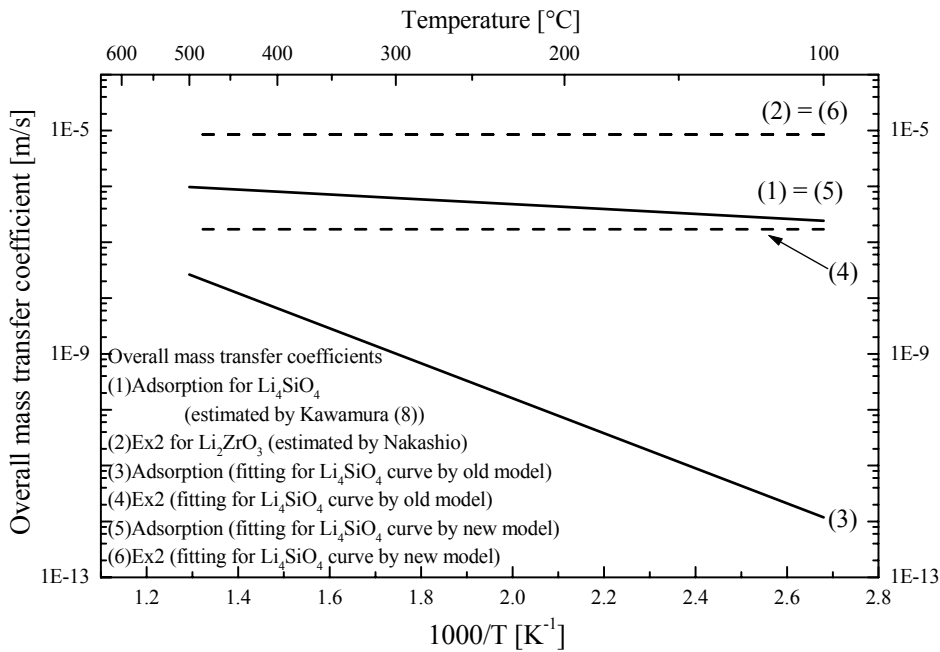


Fig.3 Fitting parameters for surface reactions

Figure 4 shows the estimated tritium release curves for experimental release curve of Li₄SiO₄ obtained at JAERI, which material was irradiated 100 minutes by neutron flux with 4.0E13 [1/cm²s]. Estimated release curve by the new model is more similar to the experimental curve than the curve estimated by the old model as compared in fig.4.

The parameters at numerical fitting for the release curve purged with humid gas are tritium effective diffusivity in grain and surface reaction rates representing adsorption and isotope exchange reaction 2 in the old model, but the fitting parameter which in the new model is only resistance between grain surface and

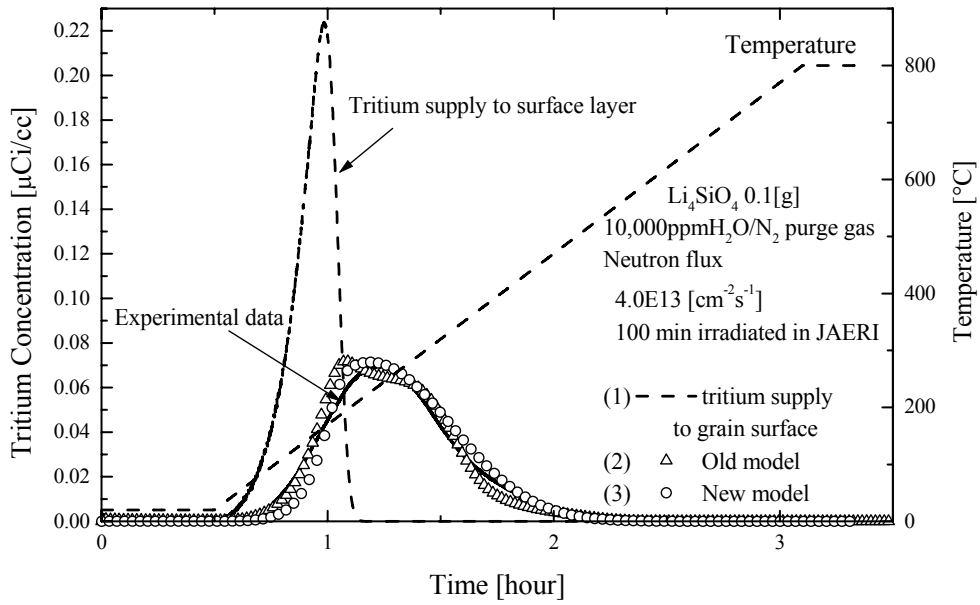


Fig.4 Tritium release curves for Li₄SiO₄ by 10,000ppmH₂O/N₂ purge gas

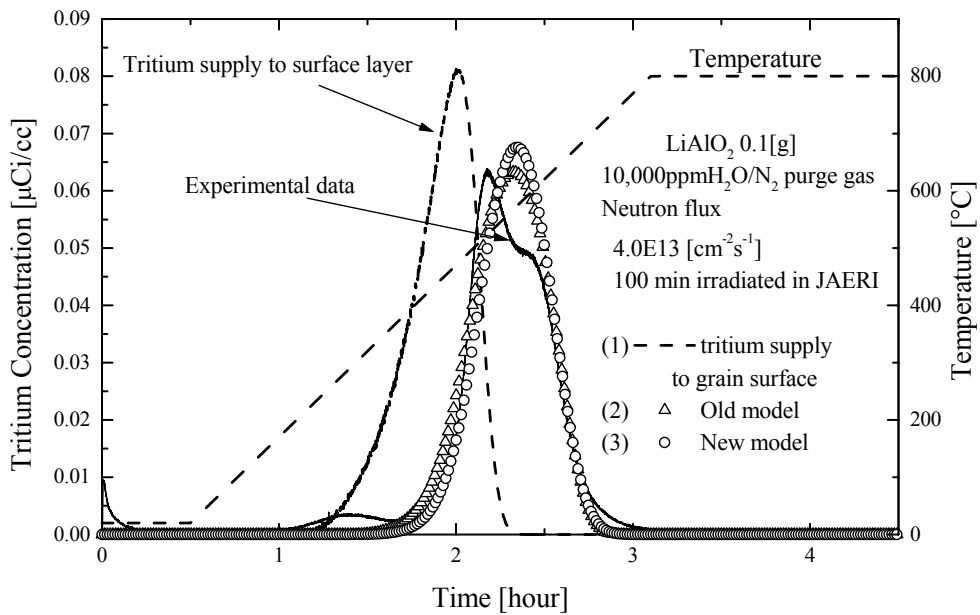


Fig.5 Tritium release curves for LiAlO₂ by 10,000ppmH₂O/N₂ purge gas

surface water when the effective diffusivity obtained by the old model is used. The tritium introduction rate to surface layer for fitting to experimental curve obtained by JAERI is a half of that of KUR. It is known that the effective diffusivity decreases with neutron fluence though quantitative discussion is insufficient.

Figure 5 shows the estimated tritium release curves for experimental release curve of LiAlO₂ obtained at JAERI. Curve estimated by the new model give good agreement with the experimental release curve and also the curve estimated by the old model reported previous paper²⁾. The effective diffusivity obtained by the old model²⁾ is used.

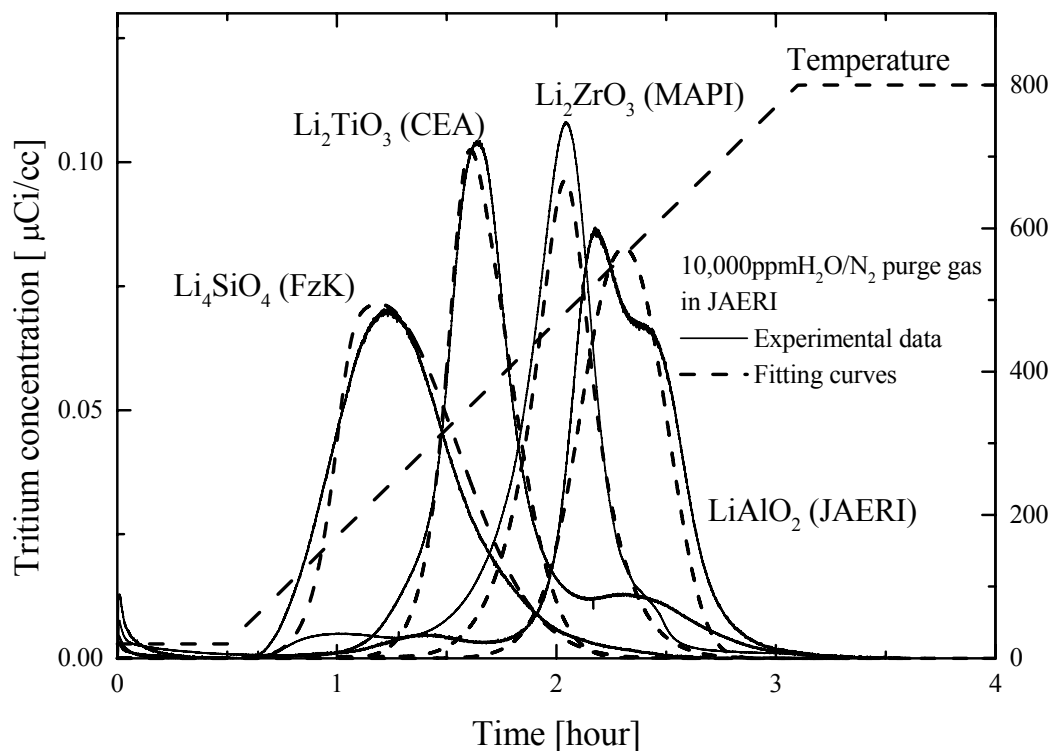


Fig.6 Estimated tritium release curves for solid breeder materials

Figure 6 shows fitting curves of experimental tritium release curves for LiAlO_2 , Li_2TiO_3 and Li_2ZrO_3 purged by 10,000ppm $\text{H}_2\text{O}/\text{N}_2$, which are estimated by new model. The estimated values using the new model give good agreement with the observed tritium release curves for various solid breeder materials.

V. CONCLUSION

In this study we propose the tritium release model, the new model, considering that 1) diffusion in bulk, 2) mass transfer resistance between grain surface and surface water at the interfacial zone, and such surface reactions as 3) adsorption/desorption, 4) isotope exchange reactions and 5) water formation reaction on the surface contribute in tritium release. The mass transfer step 2) is newly introduced because it is preferable to use the same surface reaction rate as that reported previously for fitting parameters.

The estimated values using the new model give good agreement with the observed tritium release curves and also with the release curves estimated by the old model so far.

ACKNOWLEDGMENT

The Li_4SiO_4 , LiAlO_2 , Li_2TiO_3 or Li_2ZrO_3 sample used in this study was kindly taken over from FzK, JAERI and CEA.

REFERENCES

- 1) M.Nishikawa, T.Kinjyo, Y.Nishida, "Chemical form of tritium released from solid breeder materials," *J.Nucl.Mater.*, **325**, 87-93 (2004).
- 2) M.Nishikawa, T.Kinjyo, Y.Nishida, T.Ishizaka, T.Takeishi, M.Enoeda, T.Tanifuji, "Release behavior of bred tritium from LiAlO_2 ," *J.Nucl.Mater.*, in press.
- 3) S.Beloglazov, M.Nishikawa, T.Tanifuji, "Modelling of tritium release from irradiated Li_2ZrO_3 ," *Fusion Sci. and Technol.*, **41**, 1049-1053 (2002).
- 4) T.Kinjyo, M.Nishikawa, "Tritium Release Behavior from Li_4SiO_4 ," *Fusion Sci. and Technol.*, in press.

- 5) Y.Kawamura, M.Nishikawa, K.Tanaka, H.Matsumoto, "Adsorption Characteristics of Water Vapor on Gamma-Aluminate," J.Nucl.Sci.Technol., **29**, 436-444 (1992).
- 6) Y.Kawamura, M.Nishikawa, "Adsorption characteristics of water vapor on Li_2ZrO_3 ," J.Nucl.Mater., **218**, 57-65 (1996).
- 7) Y.Kawamura, M.Nishikawa, K.Tanaka, "Adsorption characteristics of water vapor on Li_4SiO_4 ," J.Nucl.Mater., **230**, 308-312 (1996).
- 8) Y.Kawamura and M.Nishikawa, "Adsorption and desorption rate of water on the various ceramic breeder materials," Fusion Technol., **27**, 25-35 (1995).
- 9) M.Nishikawa, A.Baba, Y.Kawamura, "Tritium Inventory in LiAlO_2 blanket," J.Nucl.Mater., **246**, 1-8 (1997).
- 10) M.Nishikawa, A.Baba, "Tritium Inventory in Li_2ZrO_3 Blanket," J.Nucl.Mater., **257**, 162-171 (1998).

3 Thermal and Mechanical Behaviour of Pebble Beds

3.1 Recent Efforts on Solid Breeder Blanket Thermomechanics and ITER TBM Activities (P3)

A. Ying, A. Ali, J. An, C. Patrick, T. Sketchley, S. Sharafat, M. Youssef, and M. Abdou

3.2 Characterization of Orthosilicate ex Hydroxide Pebble Beds and Mechanical Cycling of Different Types of Ceramic Breeder Materials (P13)

J. Reimann and H. Harsch

3.3 Modelling of Ceramic breeder and Beryllium pebble beds at FZK (P6)

former title: Thermomechanical Modelling of Fusion Pebble Beds under Volumetric Heating

D. Hofer and M. Kamlah

3.4 Effect of Thermomechanical Load on Effective Thermal Conductivity of a Li_2TiO_3 Pebble Bed (P14)

H. Tanigawa, T. Hatano, M. Enoeda and M. Akiba

Recent Efforts on Solid Breeder Blanket Thermomechanics and ITER TBM Activities

Presented by
Alice Ying

With contributions from

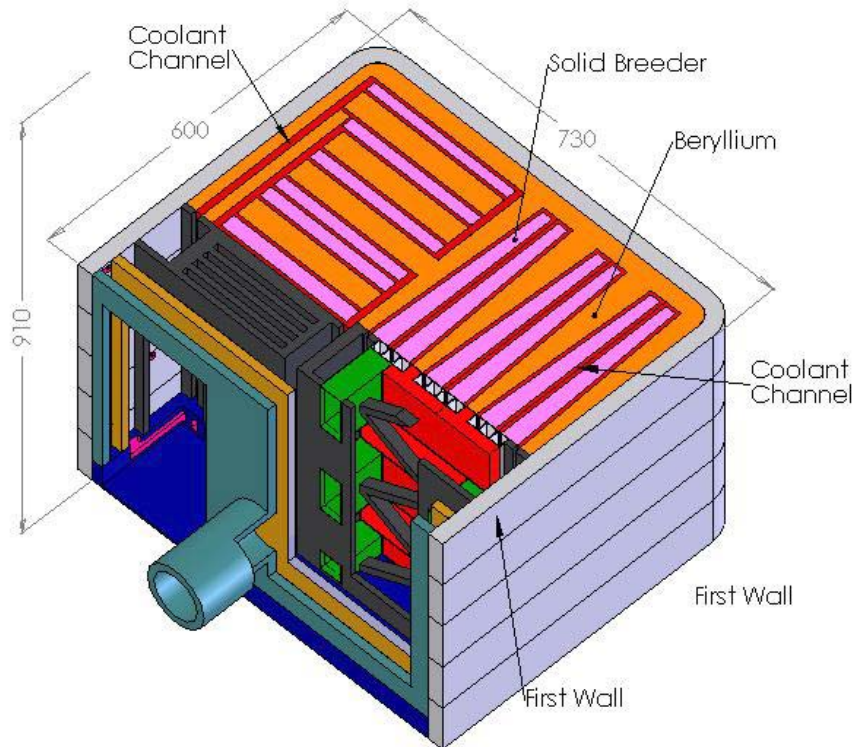
**M. Abdou, S. Sharafat, M. Youssef,
T. Sketchley, P. Calderoni, M. Ni,
A. Abou-Sena, J. An, W. Guo, P. Rainsberry, R. Hunt**

**CBBI-12
Karlsruhe, Germany
Sep. 16, 2004**

Recent Activities on Solid Breeder Blanket Areas

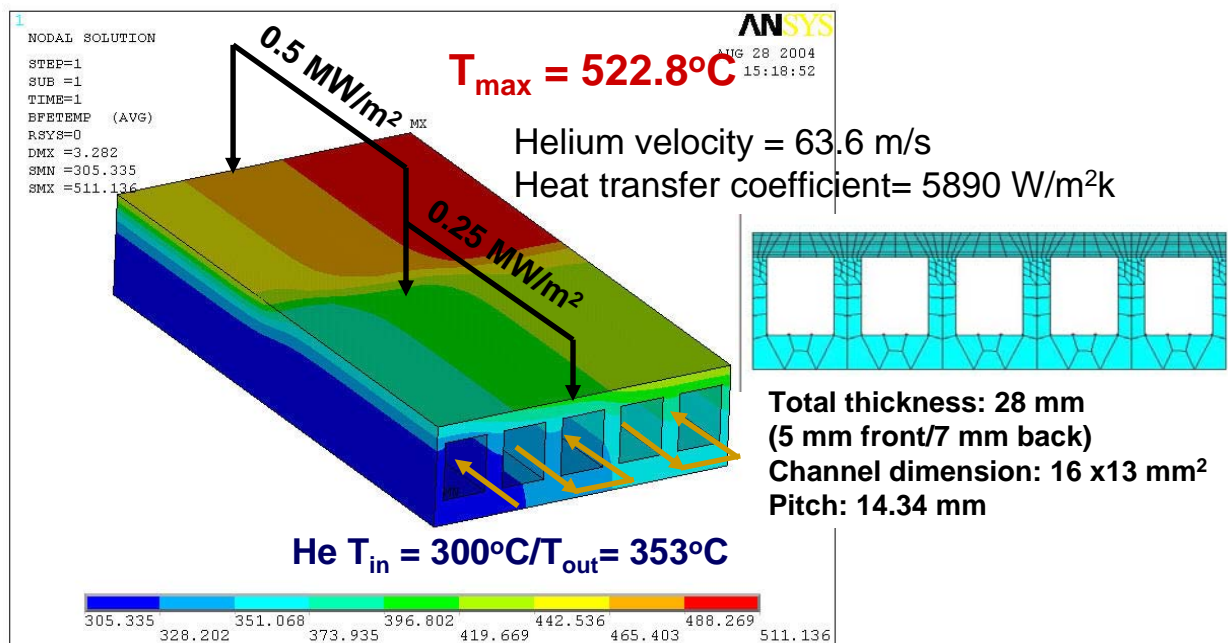
- Solid Breeder TBM Design and Analysis
- Modeling development for Ceramic Breeder Pebble Bed Thermomechanics
- Evaluation on the data of the effective thermal conductivity of ceramic breeder pebble beds
- Experimental activities
 - Interface conductance
 - Time-dependent creep deformation study
 - Creep rate data
- Tritium permeation analysis

Solid Breeder Test Blanket Submodules Design and Analysis

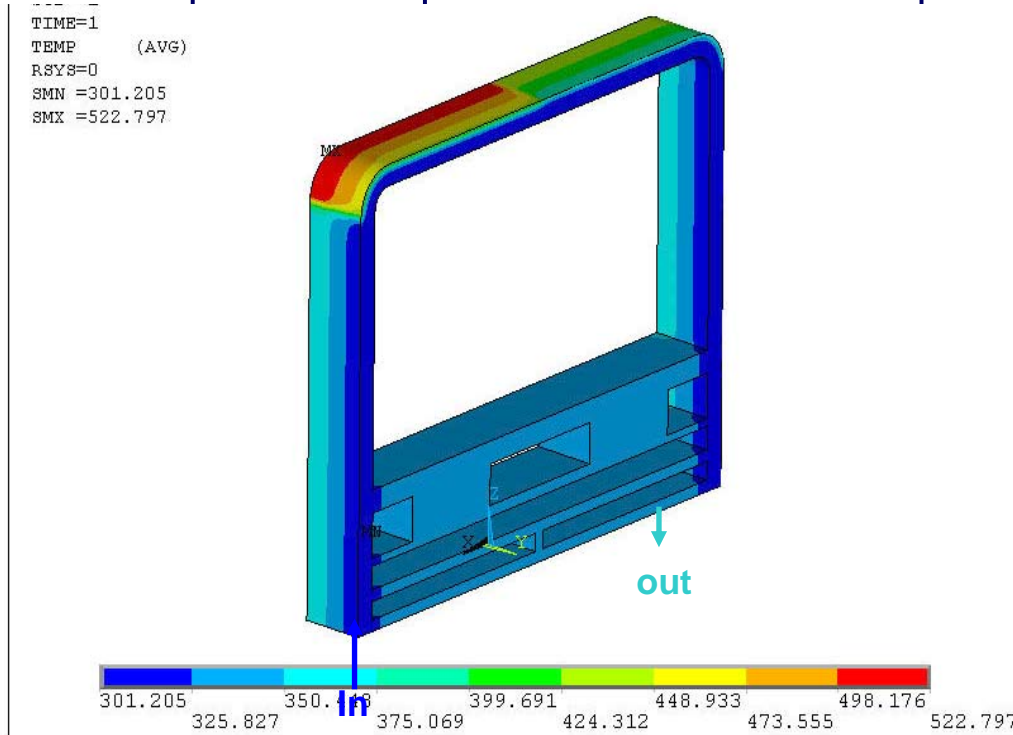


First wall thermo-mechanical analysis- temperature analysis

One flow path consists of 5 coolant channels connected in series

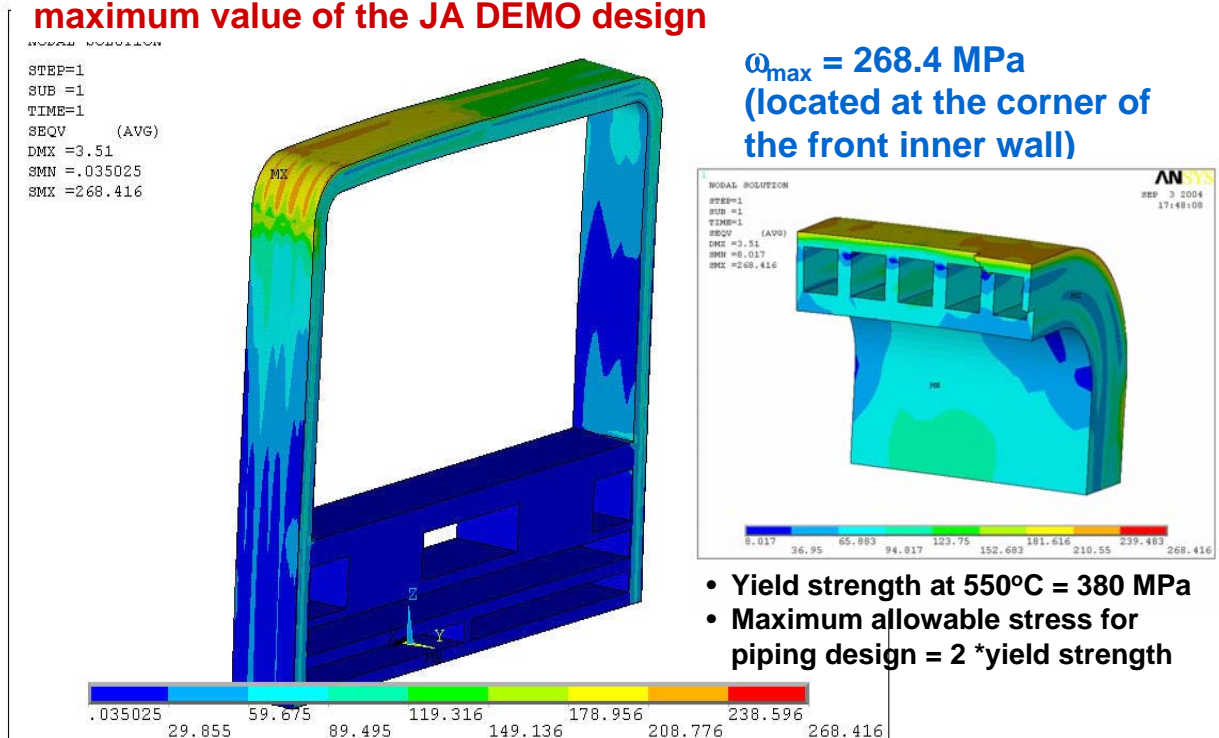


First wall thermo-mechanical analysis- temperature profile for one flow path



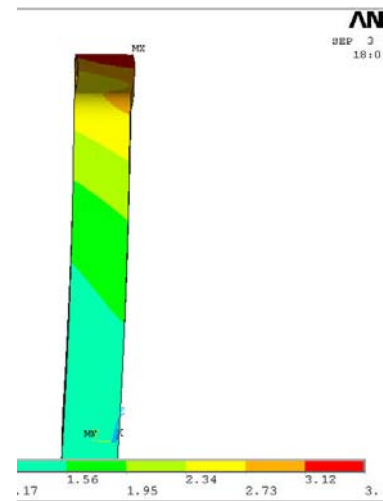
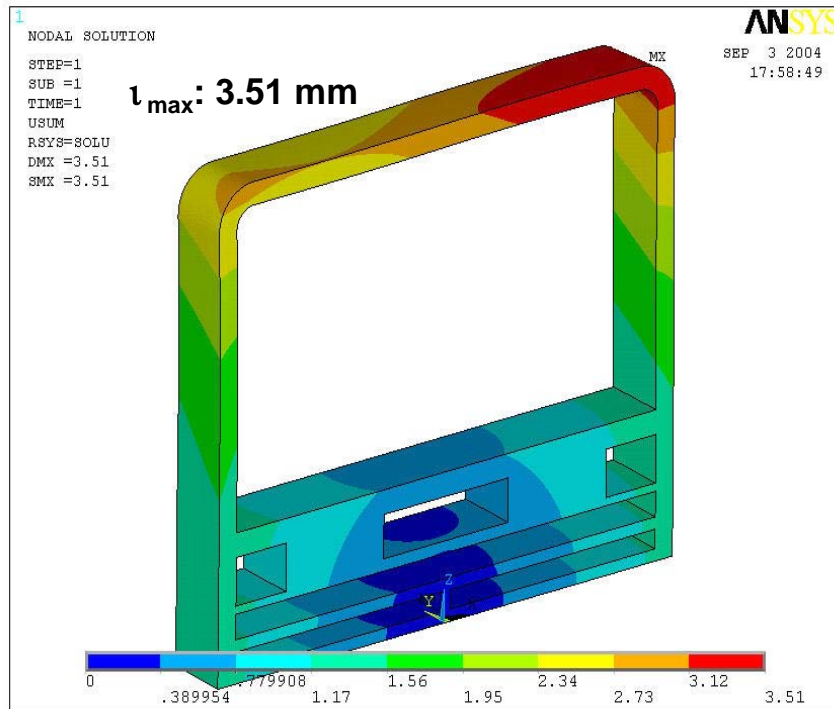
First wall thermo-mechanical analysis- Stress profiles

Maximum stress is lower than the stress limit and is similar to the maximum value of the JA DEMO design

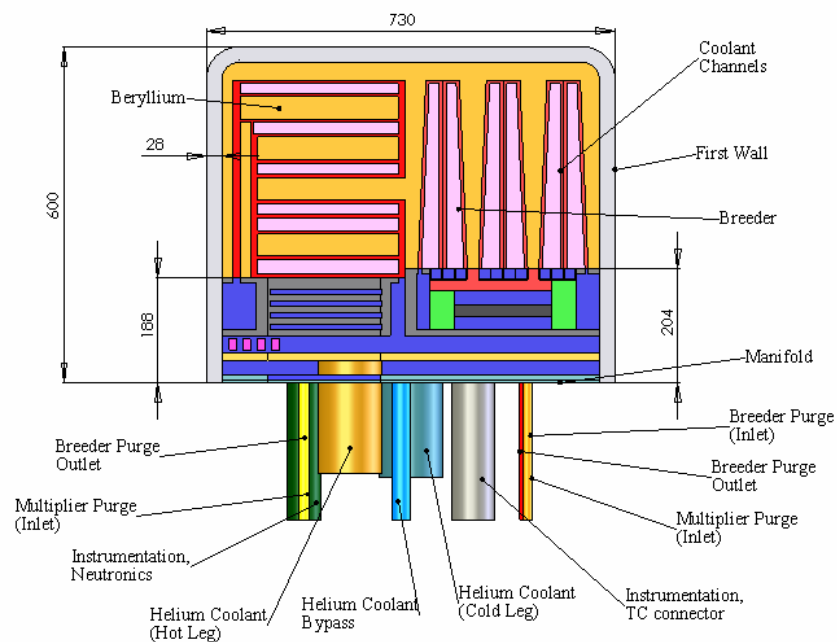


First wall thermo-mechanical analysis- Displacement profiles

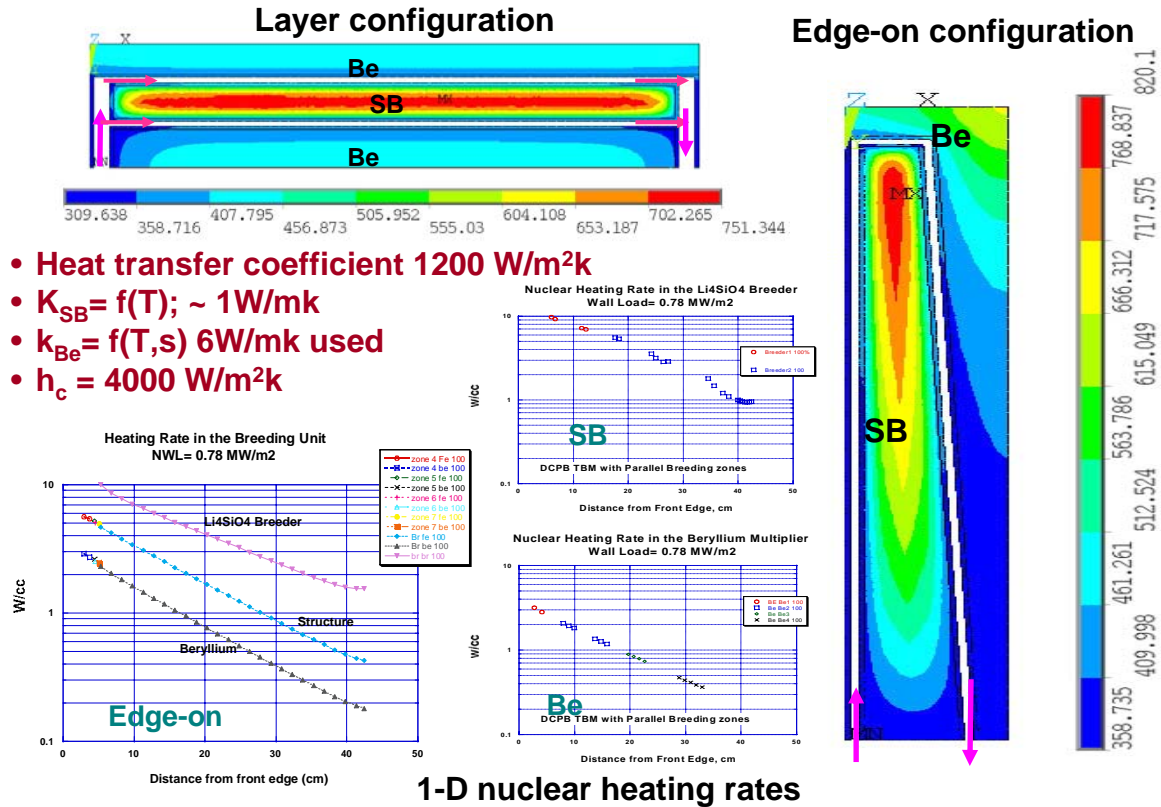
- A Non-uniform displacement due to a non-uniform heating (a non-prototype condition?)



Analyses have been performed for TBM designs to preserve key prototype parameters



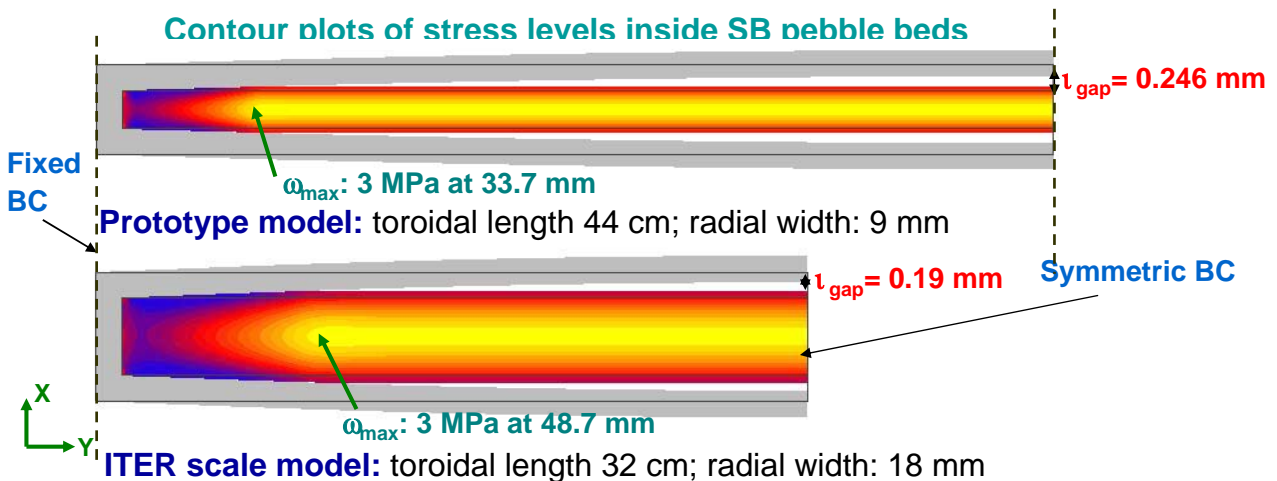
Thermal analysis for breeding unit shows that prototype temperatures have been preserved



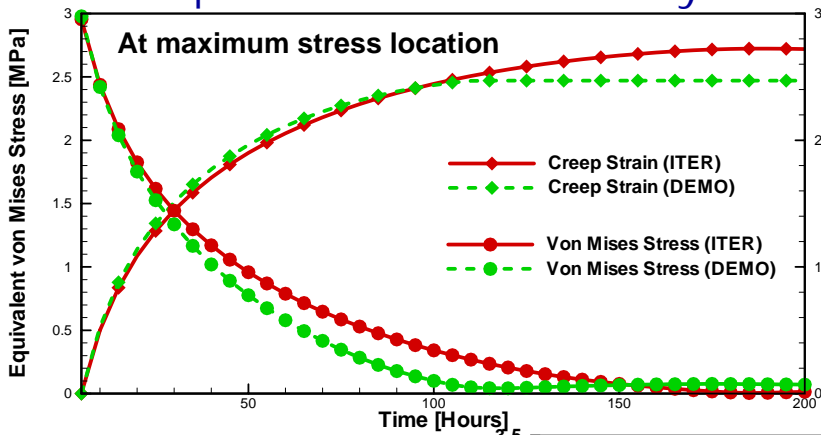
Prototype stress levels have been preserved in the scale model (layer configuration)

- FEM analysis using experimentally derived ceramic breeder pebble bed modulus, stress-strain consecutive equations
- Similar stress levels found in prototype and scale models with a maximum stress in the bed of about 3 MPa.
- The coolant plate deformation is a combined effect of thermal expansion, mechanical constraints, and dimensions.

Laboratory R&D goal is to predict thermo-mechanical parameters accurately.

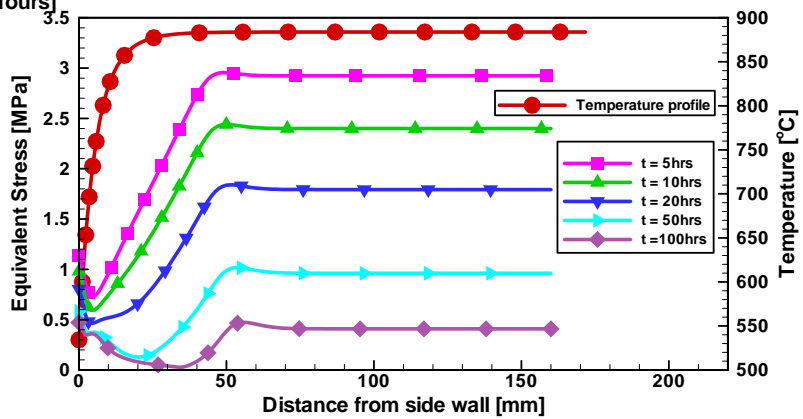


Creep and stress relaxation evolutions are preserved under steady state operations



- A R&D goal is to address and model the effect of pulsed operations on the pebble bed integrities and performance

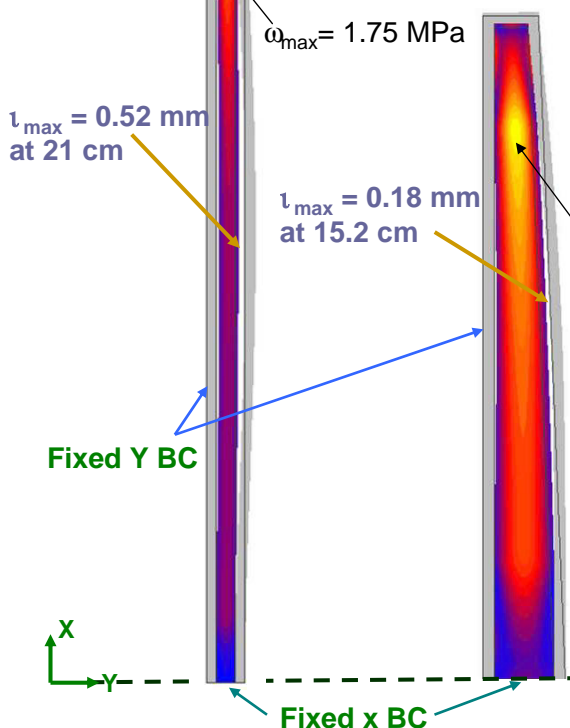
Von Mises stress evolution at the mid-plane of the ITER scale model



Stress profiles show concentration with 2-D characteristics for edge-on configurations

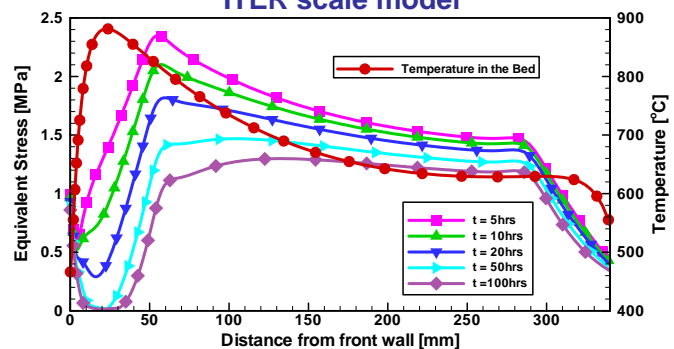
Prototype model (EU design)
47 cm radial length
1 cm toroidal width

Li₄SiO₄ pebble bed considered



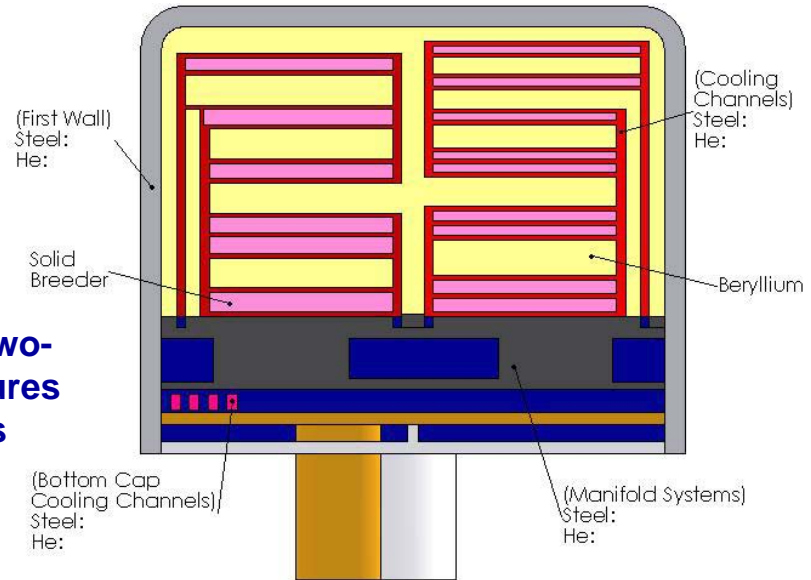
Modified ITER Scale model
reproducing temperature magnitudes
35 cm radial length (**geometric constraint**)
1.8 cm toroidal width near FW
3.2 cm toroidal width at the back

Stress evolution at mid-plane of ITER scale model



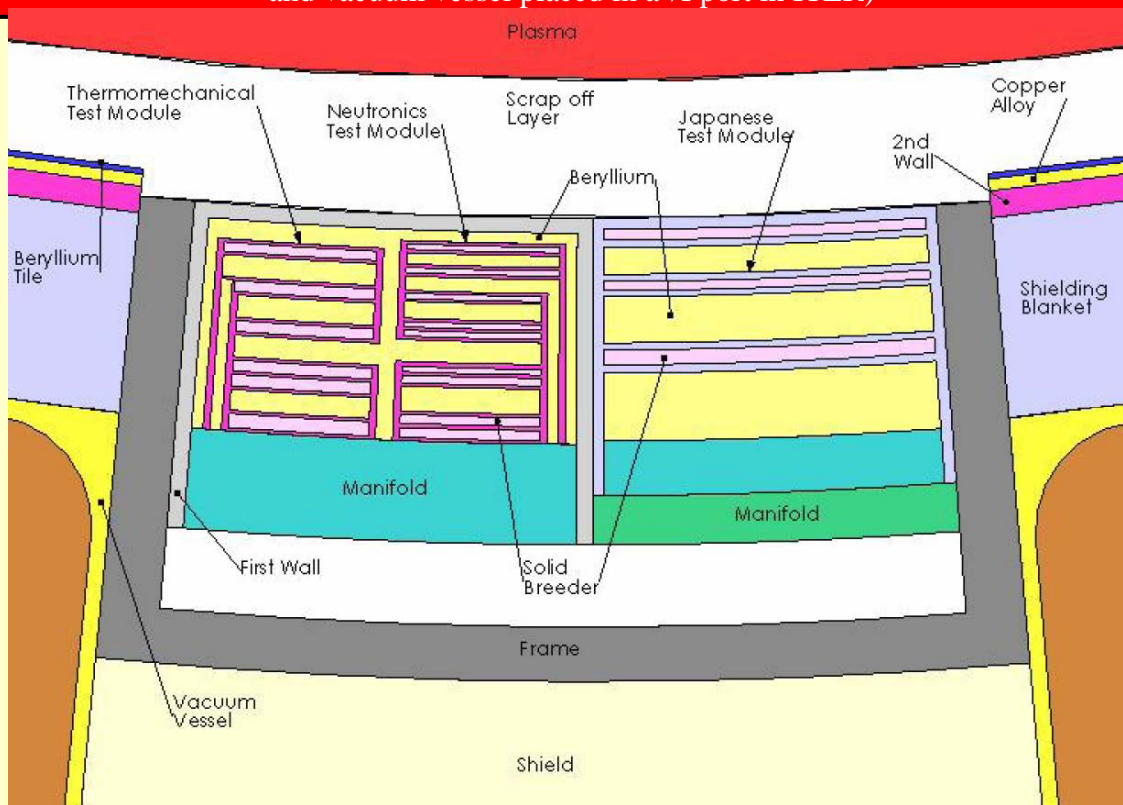
Neutronic submodule is designed to perform initial check of neutronic code and data (tritium production and heating generation rates)

- **The submodule incorporates two layer design configurations: one thermally acts alike and the other looks alike**

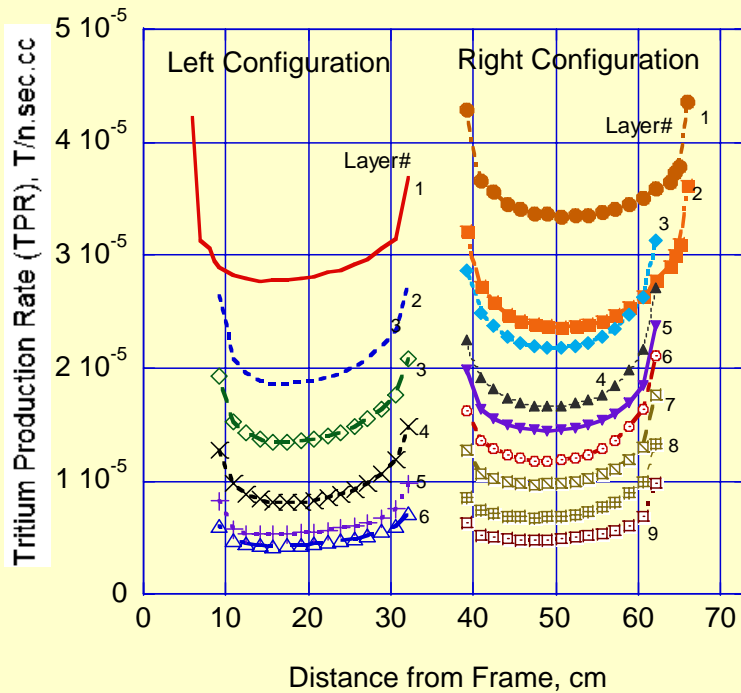


- **Complex one- and two-D performance features for code evaluations**

Top View of the 2-D nuclear model
 (The model includes neutronic submodule and its neighboring submodule, frame structure and vacuum vessel placed in a 1/2 port in ITER)



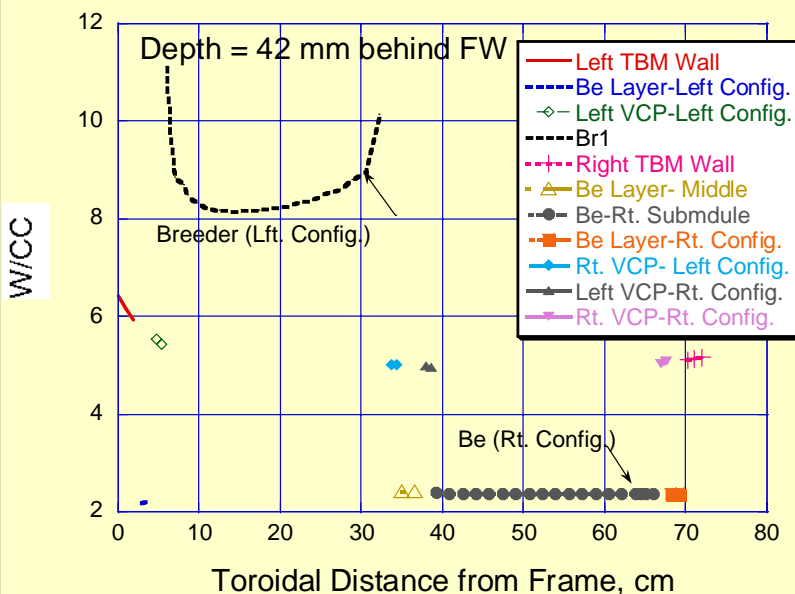
Toroidal Profile of Tritium Production Rate (TPR) in each Breeder Layer of the Two Test Blanket Configurations



- Profiles of the TPR is nearly flat over a reasonable distance in the toroidal direction where measurements can be performed (10-16 cm in the left Config. and 10-20 cm in the right Config.).

- Steepness in the profiles near the ends of layers is due to presence of Be layer and to neutrons reflected by the structure contact in the vertical coolant panels (VCP). This is more pronounced at the outer VCP. TPR values are larger at these locations by a factor of 1.4-1.5

Nuclear Heating Across the U.S. Two Test Blanket Configurations in the Toroidal Direction at Depth 42 mm Behind the FW



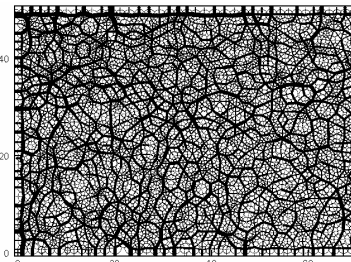
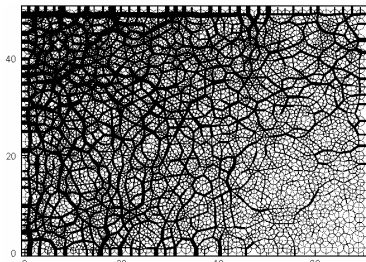
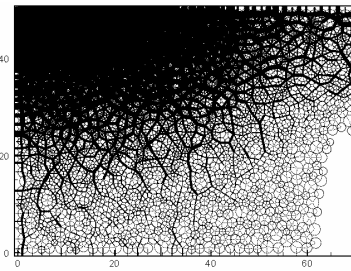
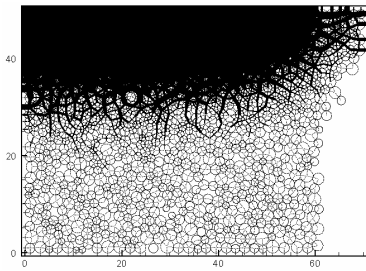
- Heating rate in the breeder of the Lft. Config. is a factor of ~4 larger than in Be of the Rt. Config. and is flat over ~10 cm. It peaks near the vertical coolant panels.

- Heating profile in beryllium is flat over the entire layer. This feature is applicable to other beryllium layers (not shown)

- The features shown indicate the heterogeneity effect which can't be produced with 1-D model

DEM model is under refinement-Initial packing simulation

Initial state



Final equilibrium state

2-D simulation of force distribution inside the pebble beds during the initial packing process*

(*The black lines stand for the contact force, and the width is proportional to the force magnitude.)

Fusion Engineering Science



Criterion of the equilibrium

Utilizing discrete element method to simulate the pebble bed, each element stands for one pebble, and it has variables to represent for the geometry and material properties of the pebble material. All the elements will be rearranged according the contact force and contact model. The pebble bed will be updated until achieving the pebble beds equilibrium state. At equilibrium state, the contact force distribution will follow Ngan's model.

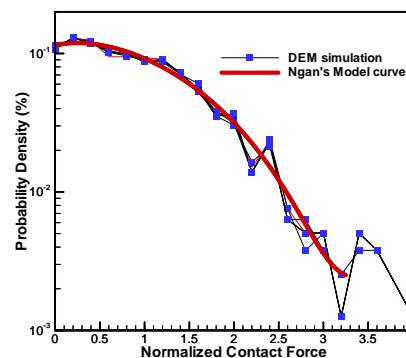


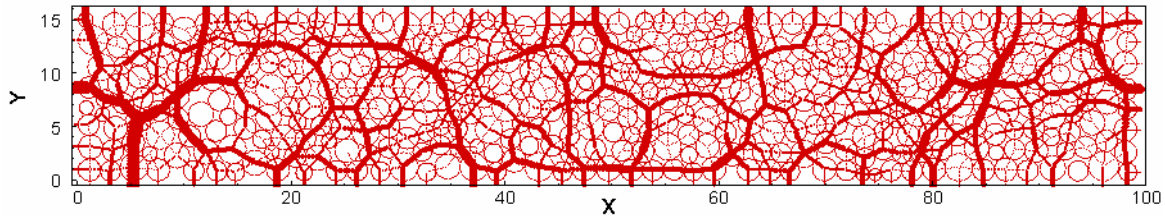
FIGURE: DEM simulation results of contact force distribution in 2-D (Contact forces are normalized by the mean value)

Fusion Engineering Science



2-D simulation of force distribution inside the pebble beds

Force distribution at the equilibrium state



(The line stands for the contact force, and its width is proportional to the force magnitude.)

As pressure is applied, the effect of high temperatures is to promote interparticle mass transport, which results in deformation starting with the contact.

- In general, deformation for ceramics can be evaluated by the sum of linear and power-law creep terms^[Billone]

$$\dot{\kappa} = A_1 \exp(4Q_1 / RT) \omega^2 + A_2 \exp(4Q_2 / RT) \omega^n$$

where A's and Q's are material properties and are functions of grain size, particle density, fabrication techniques, etc. and T is temperature in K, ω is the von Mises stress in MPa, n is the stress exponent and κ is the creep rate in s⁻¹. A stress exponent of around 6.5 was found^[Billone].

The difficulty is lack of material creep properties at high stresses for use in DEM simulation.

Reference: M. C. Billone, Y. Y. Liu, R. B. Poeppel, J. L. Routbort, K. C. Goretta, D. S. Kupperman, Elastic and Creep Properties of Li₂O, J. Nucl. Mater. 141-143 (1986) 282-288.

Stress distribution inside the pebble

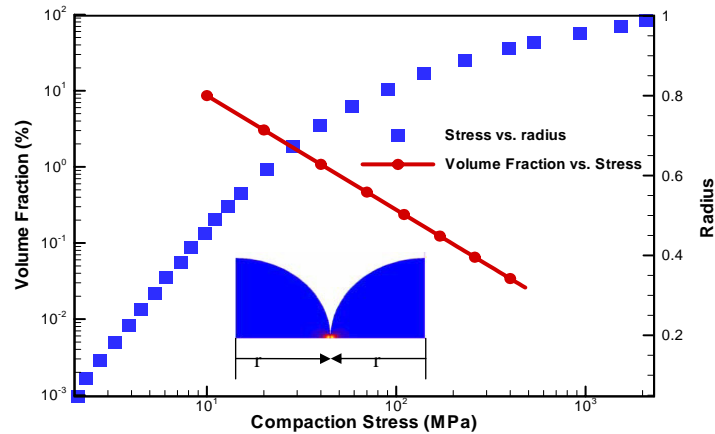

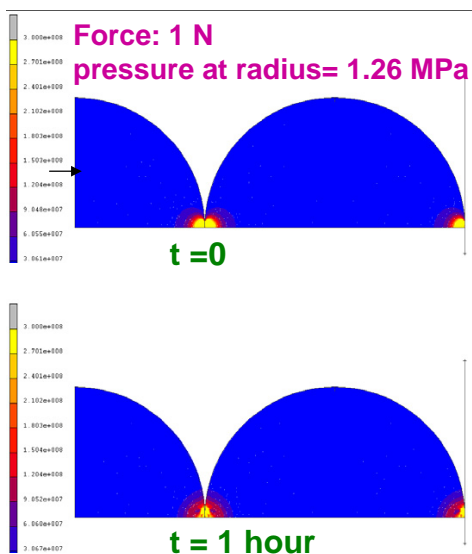


FIGURE: Stress profile of the contact balls under elastic deformation. The square dot line is stress distribution along the radius; the red line with circle shows the relationship between volume fraction and the stresses of the contact balls. (The compaction stress on the balls is 2.0 MPa.)

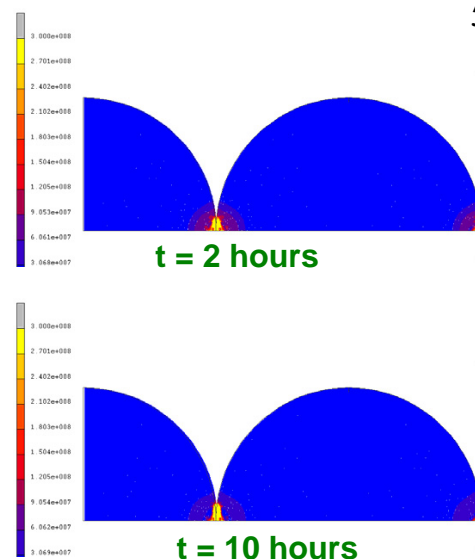
Fusion Engineering Science 

DEM approach shows that stress magnitude at contact exceeds ultimate compressive strength

Evolution of stress distribution at contact at different creep stages



$$|\kappa| = 4.82 \times 10^5 (14 P^{2/3})^{44} \exp(45.15 \times 10^4 / T) \omega^4$$



$$50 \Omega \omega \Omega 167 \text{ MPa}$$

$$973 \Omega T \Omega 1073 \text{ K}$$

$$0.25 \Omega P \Omega 0.28$$

v-LiAlO₂
creep
rate from
ITER
Solid
Breeder
Material
Database

$$\omega_c | \exp(410p) d_g^{40.5} \ln(2200/T) x 10^3$$

Calculated ultimate compressive strength $\omega_c = 298 \text{ MPa}$ at $T = 800^\circ\text{C}$

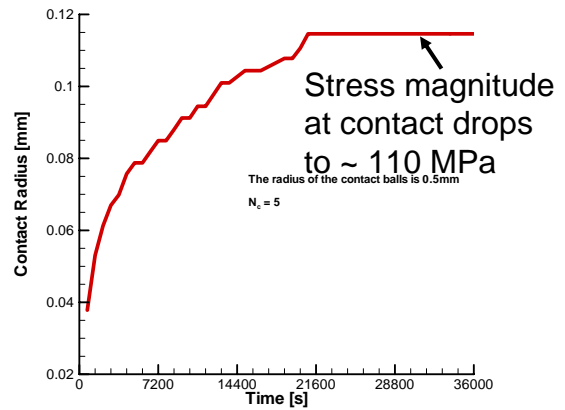
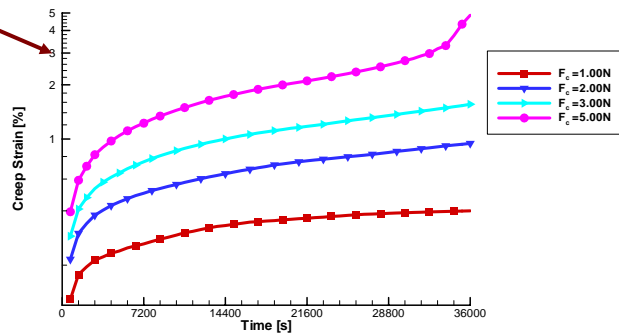
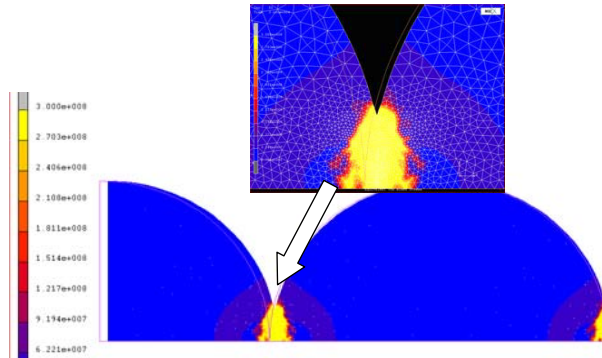
2-Pebbles DEM Creep Simulations

Creep rate becomes much smaller 2 hours after creep initiates

Stress limited at ultimate compressive strength (298 MPa)

Stress characteristics at contact after 10 hours of creep

Force: 2 N

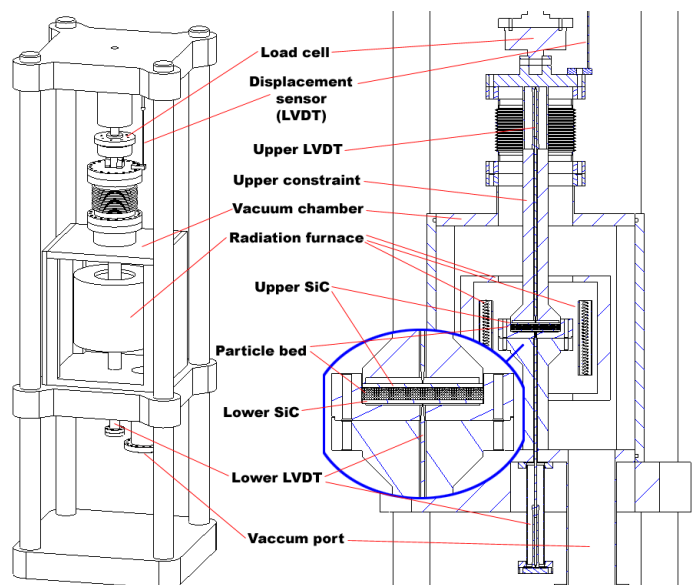
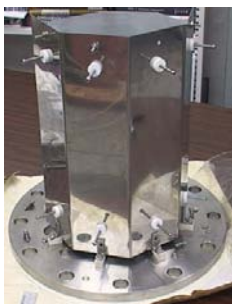
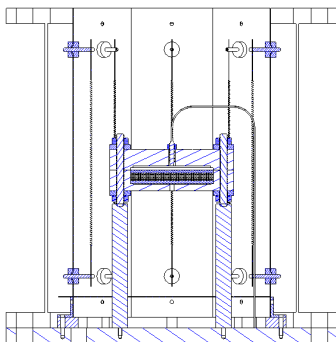


High temperature controlled atmosphere furnace under assembly

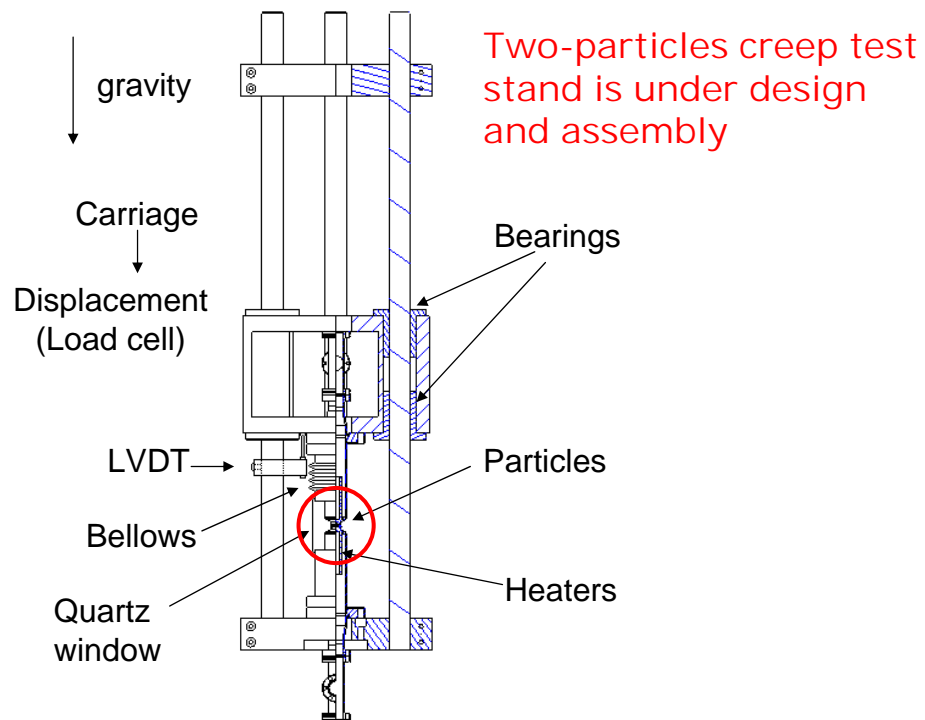
1st step

- Differential thermal expansion
- Capacitance sensor for clad deformation measurement

Later this year Controlled mechanical constraint with expanded diagnostics capability

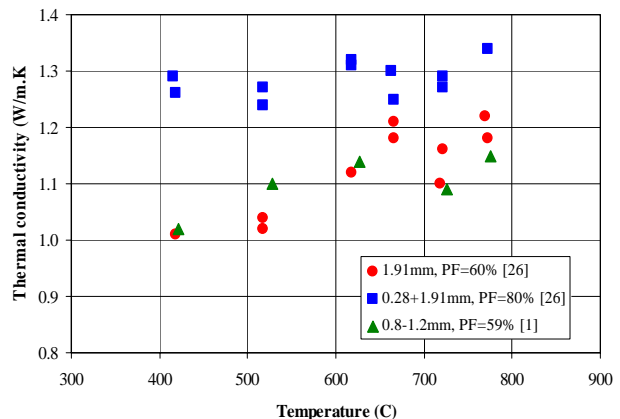


Creep rate data at high stress magnitudes is needed for DEM simulation



Effective Thermal Conductivity Of Lithium Ceramic Pebble Beds For Fusion Blankets: A Review Results of $\text{Li}_2\text{TiO}_3/\text{He}$ Pebble Beds

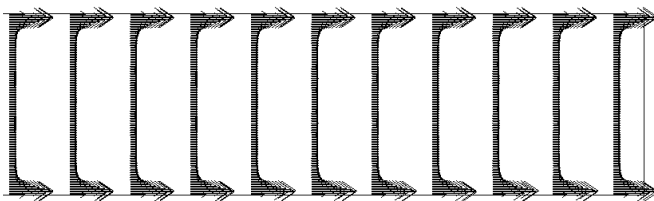
- k_{eff} of Li_2TiO_3 single size bed²⁶ increases from 1 to 1.22W/m.K over a temp. range of 420-775°C. While it increases from 1.26 to 1.34W/m.K with the binary size bed²⁶ for the same temp. range.
- Increasing packing fraction (from 60 to 80%) of Li_2TiO_3 pebble beds²⁶ leads to an increase in k_{eff} by 25% at 420°C and 14% at 775°C.
- k_{eff} of Li_2TiO_3 pebble bed¹ increases from 1.02 to 1.15W/m.K over a temp. range of 425-775°C.
- All the data have the same trend of increasing k_{eff} with the increase of temp. It is observed that values of k_{eff} of Li_2TiO_3 pebble bed oscillate with the increase of temp. from 620 to 775°C.



Tritium permeation study Motivation

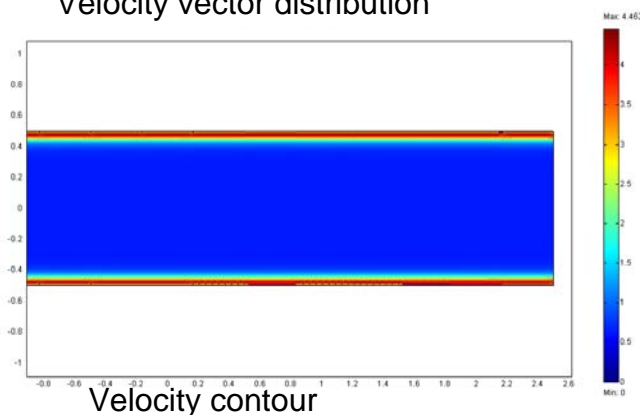
- There is a need to re-examine the tritium control issues for solid breeder blanket designs based on recent concerns raised by Dr. Sze.
- Previous modeling capability is somewhat limited.
- The goal is to develop a model which captures all phenomena involved including the effects of diffusion, convection, purge flow characteristics temperature distribution, and hydrogen swamping on tritium permeation.

One numerical result by considering the effect of porous of
a pebble bed



This result is acquired by solving 2D Navier-Stokes equation with a source term non-uniformly distributed inside the flow area

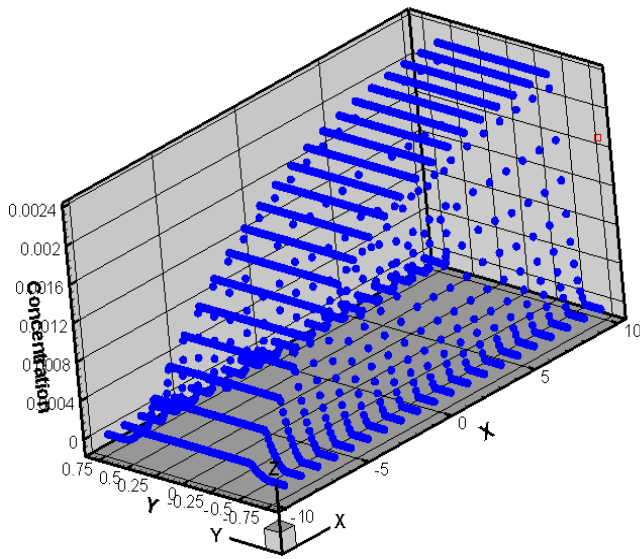
Velocity vector distribution



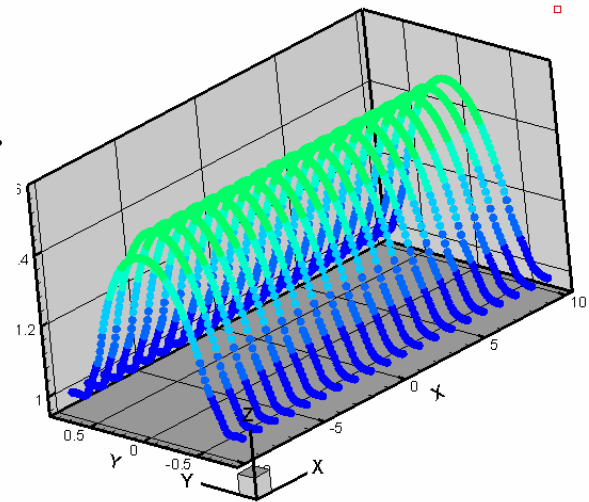
This result is very consistent with the analytical result of Cheng & Hsu

$$Re \approx 0.1 \quad \nu \approx L_y/d_p \approx 10$$

Concentration and Temperature Distribution



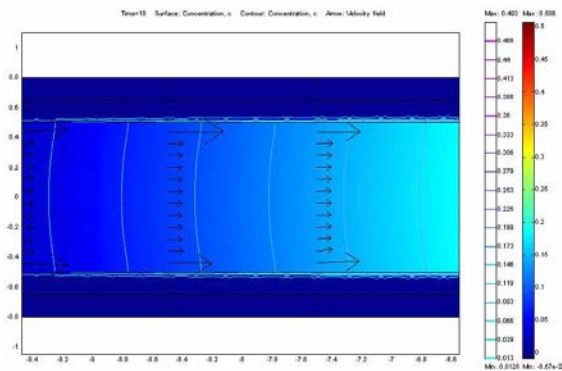
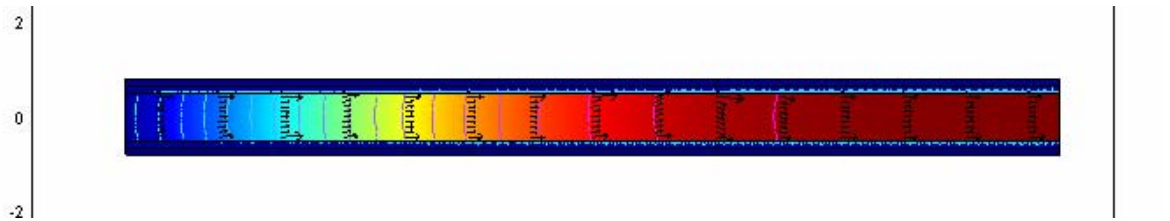
Concentration



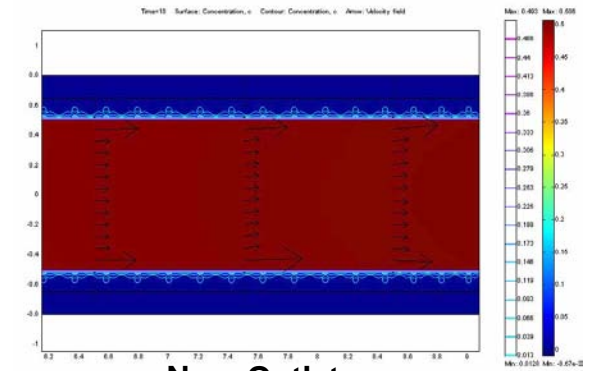
Temperature

for jet velocity

Concentration Profile



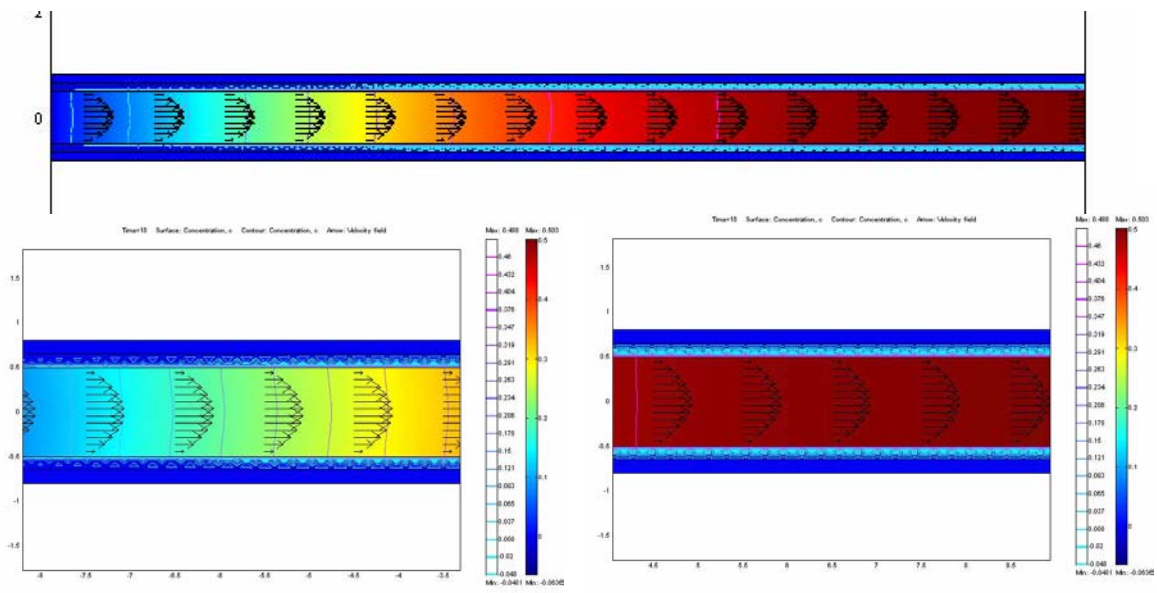
Near Inlet



Near Outlet

For Jet Velocity

Concentration Profile-Con't

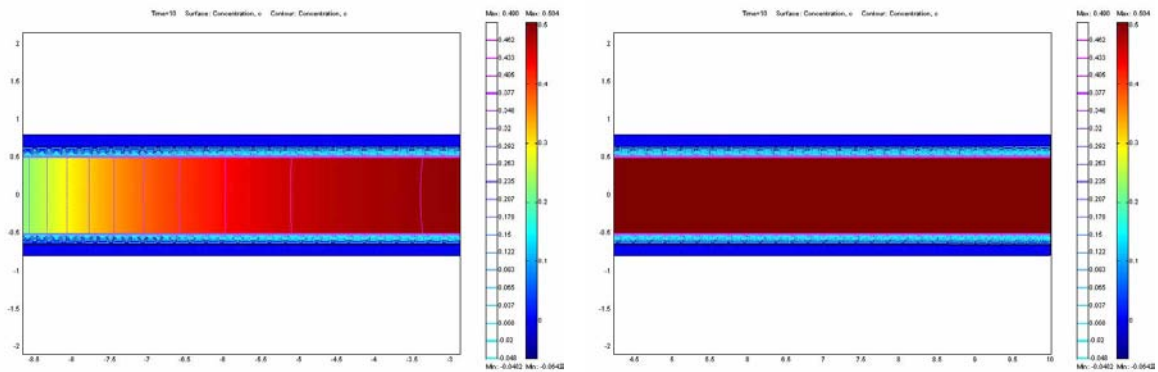


Near Inlet

Near Outlet

For Parabolic Velocity

Concentration Profile-Cont I

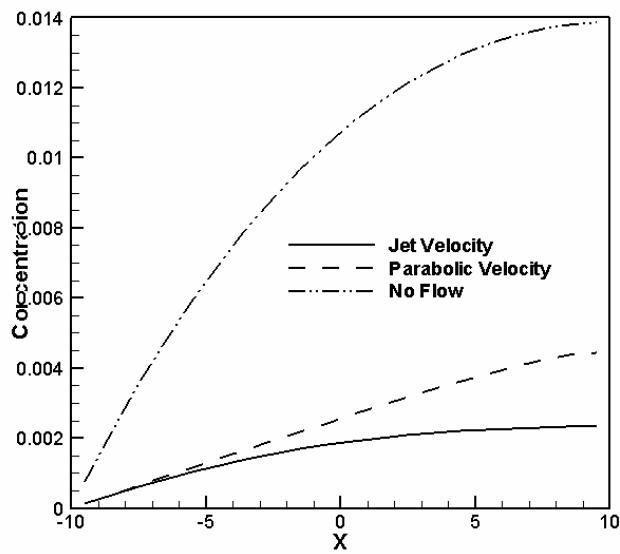


Near Inlet

Near Outlet

Without convective term

Concentration along the centerline with different velocity profiles



The concentration for noflow condition is much higher than the concentration of the other two cases, while the concentration with jet flow profile owns the smallest value

Characterisation of Orthosilicate ex Hydroxide Pebble Beds and Mechanical Cycling of Different Types of Ceramic Breeder Materials

J. Reimann¹); H. Harsch²)

1) Forschungszentrum Karlsruhe, Institut für Kern- und Energietechnik,
P.O. Box 3640, D-76021 Karlsruhe, Germany

2) Goraieb Versuchstechnik, In der Tasch 4a, D-76227 Karlsruhe, Germany

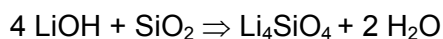
Abstract

Uniaxial Compression Tests (UCTs) were performed with pebble beds consisting of the new batches of OSi ex hydroxide at temperatures between ambient and 850°C. Compared to previous results obtained with pebbles produced from Li_4SiO_4 and SiO_2 , the pebble beds with the new material show a softer behaviour, that is, for a given uniaxial stress, strains are larger. Thermal creep strains become significantly larger for high temperatures and large creep times.

Furthermore, experiments are presented where pebble beds consisting of metatitanate or different kinds of orthosilicate pebbles were subjected to mechanical cycling with pressure amplitudes of up to 7MPa. These experiments were performed both at ambient temperature and elevated temperatures (750 or 840°C) where thermal creep occurred. It showed that also for ambient temperature at the end of the experiments (more than 100 cycles) the final compression state is not reached. At elevated temperatures, the compaction is significantly increased because of thermal creep. These experiments – although being not blanket relevant – should be well suited to validate pebble bed codes developed for the thermal-mechanical description of the interaction between pebble beds and blanket structures.

1. INTRODUCTION

For the European Helium Cooled Pebble Bed (HCPB) blanket slightly overstoichiometric lithium orthosilicate pebbles ($\text{Li}_4\text{SiO}_4 + \text{SiO}_2$) have been chosen as one optional breeder material. This material is developed in collaboration between Research Centre Karlsruhe (FZK) and the Schott Glas, Mainz. In the past, the not enriched pebbles were produced from a mixture of Li_4SiO_4 and SiO_2 powders, but because enriched Li_4SiO_4 is not available on the market, a new production route was pursued using LiOH powder which is also commercially available in the enriched state, based on the following, simplified reaction:



These pebbles designated as OSi ex hydroxide had been characterised in detail by [1].

In the present paper, the thermal-mechanical characterisation is described consisting of uniaxial compression tests (UCTs) in order to determine stress-strain relationships during pressure (uniaxial stress) increase and decrease and thermal creep correlations for elevated temperatures. These data are compared with pebble bed data for the formerly investigated batches of orthosilicate pebbles designated as OSi ex silicate.

In the second part of the paper, experiments are described where OSi and MTi pebble beds were mechanically cycled between a pressure close to zero and maximum pressures of either 4.3 or 6.5 MPa. These experiments were performed at elevated temperature where thermal creep occurs, and, for comparison, also at ambient temperature. The experiments at elevated temperatures were considered to be valuable for validation of pebble bed codes, because in these experiments thermal creep occurs in a condition where stress is not constant but a function of time.

It should be clearly stated, that these mechanical cycling tests are not considered to be blanket relevant because in fusion reactor operation thermal cycles will occur. Due to stress relaxation processes, the mechanical loads will decrease very fast. Only if due to gap formation and movement of particles due to gravity ratcheting effect could occur, the effects could be similar. Thermal cycling experiments in vertical beds were performed in Brasimone [2].

2. EXPERIMENTAL CONDITIONS

Both types of experiments were performed in the Uniaxial Compression Test Set-up of the Forschungszentrum Karlsruhe, see Fig.1, used already extensively in the past, compare e.g. [3-6]. In these tests, pebble beds in a cylindrical cavity are compressed in the direction of the cylinder axis and both the uniaxial stress σ and the uniaxial strain ε (defined as ratio of bed deformation to initial bed height) are measured. An important feature of the used test set-up is i) the use of blanket relevant shallow pebble beds (bed height $H \approx 10\text{mm}$ considerably smaller than the bed diameter $D=60\text{mm}$), and ii) the measurement of bed strain by four displacement transducers in order to control if the bed filling is homogeneous (if this is not the case, the piston inclines during compression causing different signals of the displacement transducers). UCTs are used i) to determine for the first stress increase period the σ - ε relation, respectively, the modulus of deformation $E = \sigma/\varepsilon$, and ii) to elaborate thermal strain correlations for $\sigma = \text{const.}$

Figure 2 shows the appearance and microstructure of the OSi ex hydroxide pebbles (from [1]), examined by optical microscopy. Most of the pebbles appear 'pearl white', but there are also some small glassy pebbles (Fig. 2a). The cross sections in Fig. 2b reveal only a small amount of cracks and pores for OSi 03/1-3, although a few pebbles exhibit larger pores. The batch OSi 03/1-4 has a larger amount of cracks and pores.

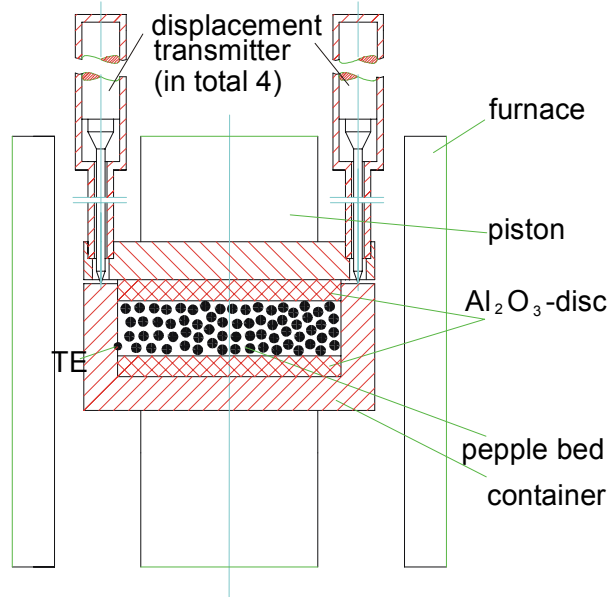
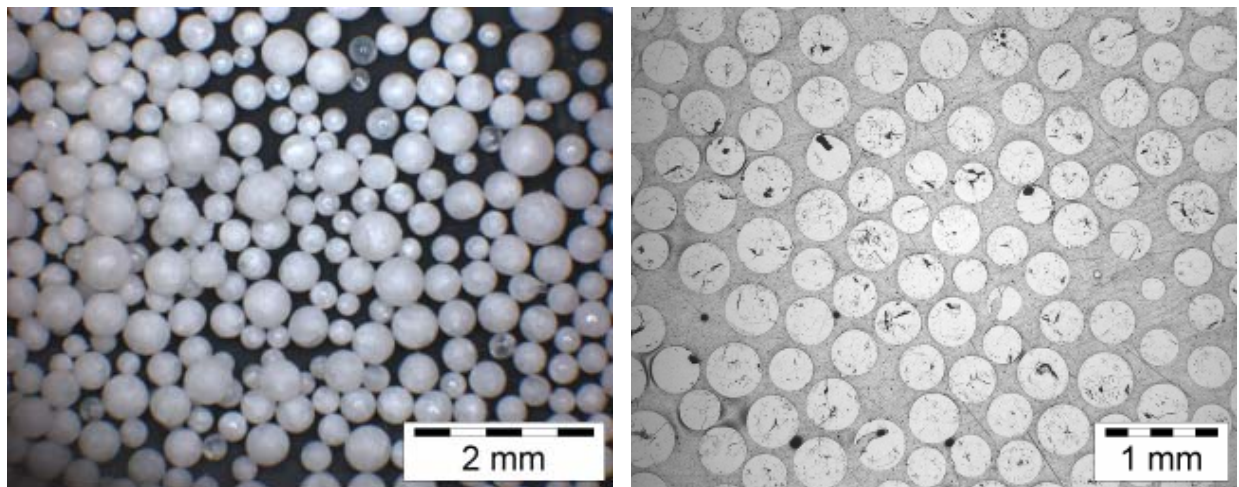


Fig. 1. Uniaxial compression test set-up.



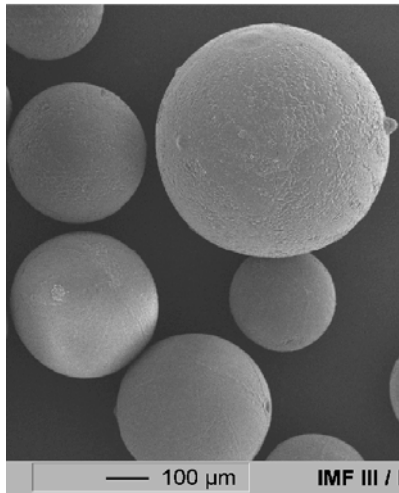
a)

b)

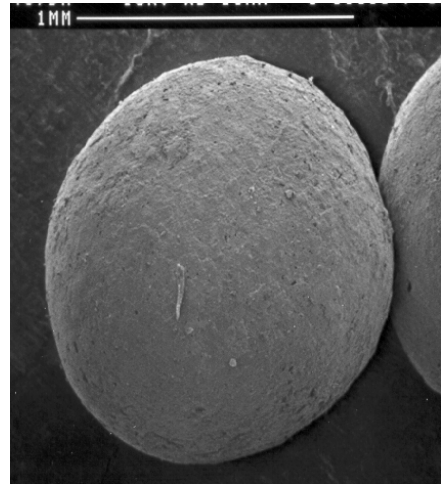
Fig. 2. Shape and cross-section of OSi ex hydroxide pebbles (from [1]).

For the thermomechanical tests, described in the first part of the paper, the OSi pebbles were annealed at 1000°C in air in order to decompose the metastable high-temperature phase $\text{Li}_6\text{Si}_2\text{O}_7$ into lithium orthosilicate and metasilicate. The sample OSi ex silicate were annealed for 2 weeks, whereas the batch OSi 03/1-3 ex hydroxide were treated for 4 weeks.

For the mechanical cycling tests, primarily, pebbles from older batches were used: the OSi pebbles originated from batches from 2001; diameters are, as usual, between 0.23 and 0.6 mm. As metatitanate pebbles, pebbles from batch D, compare [3], were used with diameters between 0.8 and 1.2 mm, see Fig. 3.



a) OSi pebbles batch 2001



b) batch D MTi pebbles

Fig. 3. Pebbles used in mechanical cycling experiments (from[3]).

3. CHARACTERISATION OF PEBBLE BEDS WITH OSi EX HYDROXIDE PEBBLES

Figure 4 shows that at ambient temperature the presently developed OSi ex hydroxide (batch 03/1-3) behaves softer (larger strains for a given stress value) than the OSi ex silicate produced until 2002. In agreement with previous measurements, the pebble beds become softer with increasing temperature; at $T=850^{\circ}\text{C}$, this effect is significantly influenced by thermal creep occurring during the stress increase period (stress ramp $\approx 0.6\text{MPa}/\text{min}$). After reaching $\sigma_{\text{max}} \approx 4\text{MPa}$, the stress was kept constant for about 10mins in all experiments; at 850°C strain increases remarkably due to thermal creep whereas at ambient temperature strain increases marginally due to relocations of pebbles.

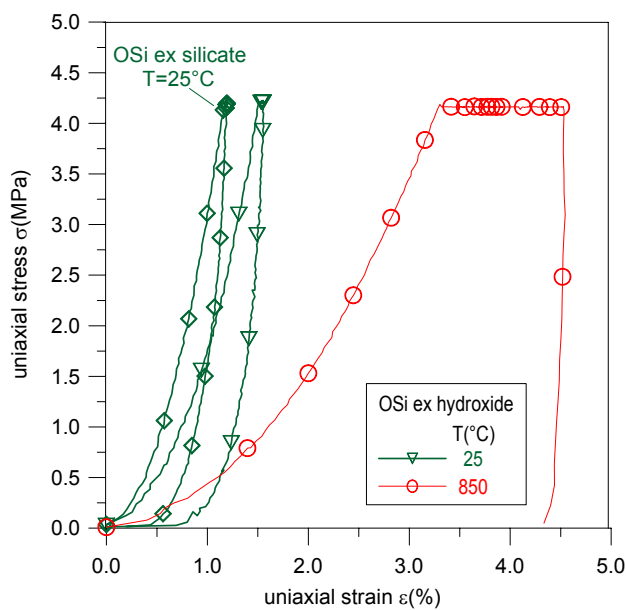


Fig. 4. Characteristic UCT results.

Figure 5 contains results obtained from experiments at different temperatures for the deformation module E for the first stress increase phase as a function of stress: for a wide range of σ , the slopes of the curves are fairly constant and independent of temperature; the curves can be well fitted by an expression of the type $E = C\sigma^m$, with $m = 0.5$ and about $C = 125$ for ambient temperature. With increasing T , C decreases as generally observed for all kinds of ceramic granular materials (compare [4]). In [5], the prefactor C was expressed as a function of temperature; however, in a subsequent paper [6] it was recommended for pebble bed modelling to use the value of C for ambient temperature and to describe the bed softening by the thermal creep model. For the new OSi pebbles the temperature dependence is larger than for the OSi ex silicate pebbles. However, again, for pebble bed modelling the procedure according to [6] is proposed.

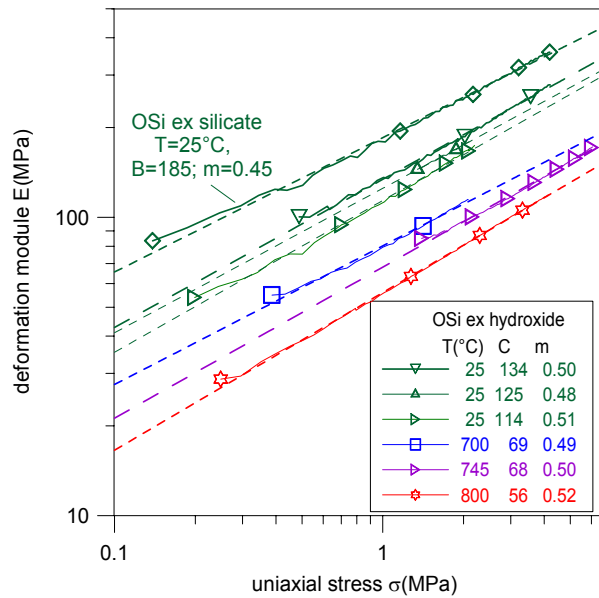


Fig. 5. Deformation module E for first stress increase as a function of temperature.

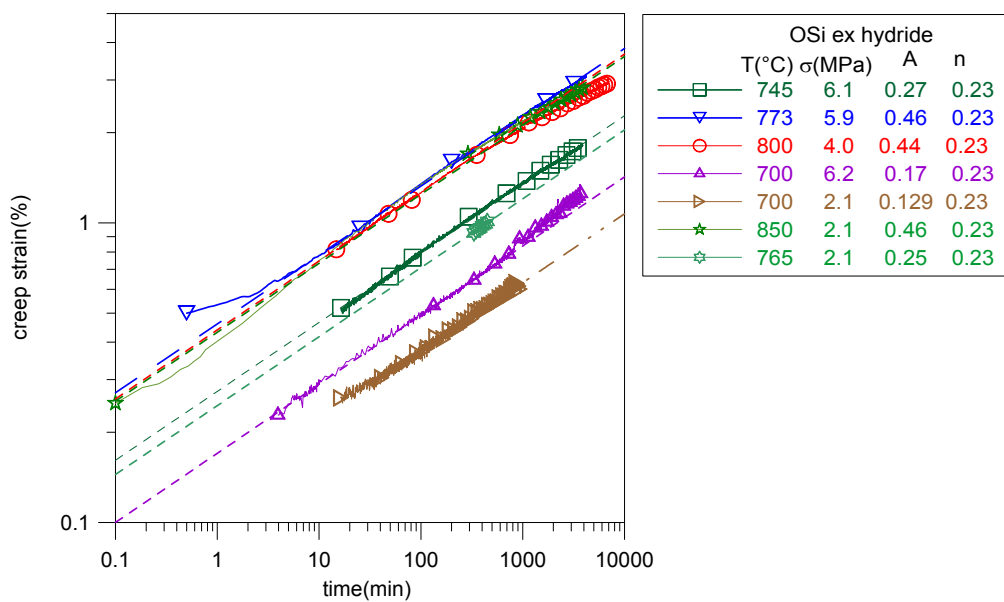


Fig. 6. Thermal creep strain ϵ_{cr} as a function of time t .

Thermal creep strain results for $\sigma = \text{const}$ and different temperatures T are presented in Fig. 6. In this plot the initial creep strain during the pressure increase period was taken into account (compare [6]). Then, the slopes of the curves become again fairly constant for nearly the total range of creep times and are also independent of temperature and stress which means $\epsilon_{cr} \sim t^n$. The temperature and stress dependence is determined using an Arrhenius plot shown in Fig. 7. For the temperature dependence a straight curve is assumed; the pressure exponent m is determined in such a way that the deviations from the mean curve become minimum. The final correlation of the type $\epsilon_{cr} = A \exp(-B/T(K)) \sigma(\text{MPa})^p t(\text{s})^n$ is given in Table 1, together with the values for OSi ex silica. Figure 8 shows a comparison for both granular materials: thermal creep

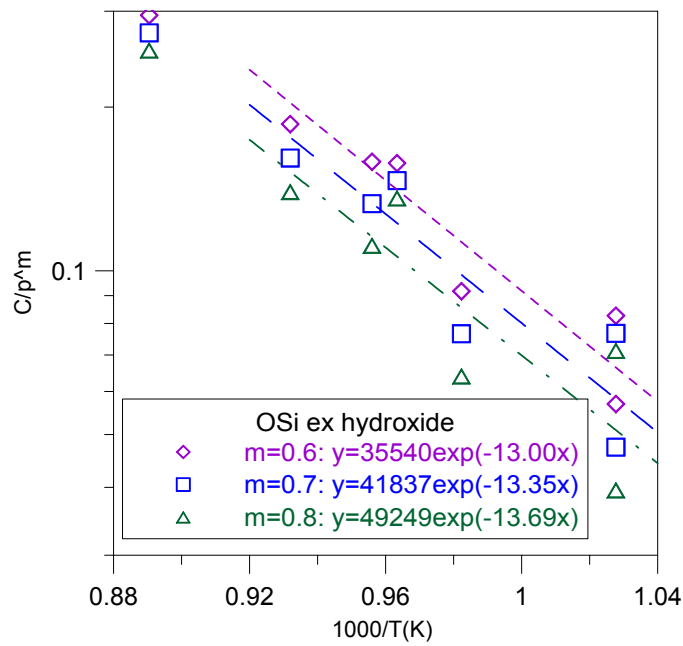


Fig. 7. Temperature and stress dependence of thermal creep strain.

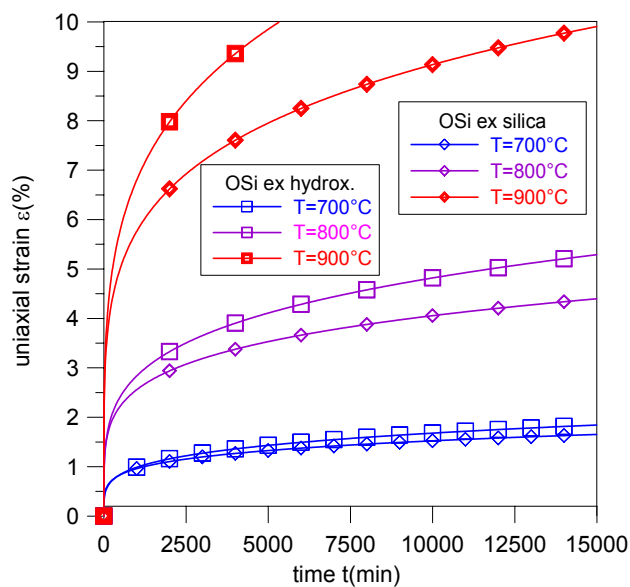


Fig.8. Comparison of creep stains for OSi ex silica and OSi ex hydroxide.

strain is slightly larger for the new OSi ex hydroxide and the temperature dependence is somewhat more expressed (for $t=10^5$ s: $\epsilon_{cr}/\epsilon_{cr\ OSi\ ex\ silicate} = 1.05, 1.16$ for $T= 700^\circ\text{C}$ and 850°C , respectively).

Table 1: Correlations for modulus of deformation, E, and thermal creep strain, ϵ_{cr} .

Granular material	$E(\text{MPa})=C\sigma(\text{MPa})^m$		$\epsilon_{cr}(1) = A \exp(-B/T(K)) \sigma(\text{MPa})^p t(\text{s})^n$			
	C	m	A	B	p	n
OSi ex silicate [12-14]	180*	0.47	12.1	10220	0.65	0.20
OSi ex hydroxide (OSi 03/1-3)	125*	0.50	20.1	11005	0.65	0.23

* $T=25^\circ\text{C}$

4. MECHANICAL CYCLING TESTS

In the planned tests of test blanket mock-ups (TBMs) in ITER, these TBMs will be subjected to many thermal cycles. However, stresses are expected to relax in a quite small period of time [7] because of thermal creep, during the following cycles, the stress build-up will be very much reduced.

In the mechanical cycling experiments, described in the following, in each cycle the maximum stresses are varied between a value close to zero and the maximum value. These conditions are, therefore, not blanket relevant. The objectives for performing these tests were

- to improve the general understanding of pebble beds,
- to provide data to validate codes which describe thermal creep behaviour.

Table 2 shows details of these experiments: the experiments were performed using the same material both at ambient temperature and at 750°C (OSi1 and 2, MTi 1 and 2). In these experiments, the pressure ramps during the pressure increase and decrease period was about 0.86 MPa/min and the dwell time at p_{\max} was about 0.3 mins. With OSi ex hydroxide pebbles, an experiment was performed at 850°C a smaller pressure ramp and a significantly larger dwell time (10 mins) compared to the other experiments.

Table 2: Cycling experiments

Pebble bed dimensions: height $H \approx 10.7\text{mm}$; diameter $D = 61\text{mm}$

Exp.	material	PF $\gamma(\%)$	T ($^\circ\text{C}$)	p_{\max} (MPa)	number of cycles	of cycles (min) $\Delta t_1/ \Delta t_2/ \Delta t_3$ ⁴⁾
OSi 1	OSi ex silica ¹⁾	63	25	4.3	117	5/0.3/5
OSi 2	OSi ex silica ¹⁾	63	750	6.5	337	7.5/0.3/7.5
MTi 1	MTi ²⁾	62	25	6.5	77	7.5/0.3/7.5
MTi 2	MTi ²⁾	62	750	6.5	166	7.5/0.3/7.5
OSi 3	OSi ex hydroxide ³⁾	66	840	4,1	112	7.5/10/10

¹⁾ Orthosilicate, batches from 2001, thermally unconditioned,

²⁾ Metatitanate, batch D

³⁾ Orthosilicate ex hydroxide, batch from 2003

⁴⁾ Δt_1 : p increase time
 Δt_2 : dwell time at p_{\max}
 Δt_3 : p decrease time

Figure 9 shows the results for ambient temperature in a σ - ε plot: The irreversible compaction is still continuing at the end of the experiments. It is not clear if this progressing compaction is only due to pebble relocation, or if pebble cracking is also occurring. For 750°C, Fig. 10, the compaction is considerably increased due to thermal creep. This is most expressed in the experiment at 840°C, see Fig. 11. The process of progressing compaction is illustrated in Fig. 12 where the strain values at p_{\max} are plotted as a function of time. The differences between OSi and MTi pebble beds are not significant. In Fig. 13, cycling tests are compared with thermal creep experiments with $p_{\max} = \text{const.}$ after the pressure increase period. As expected, the total strain during cycling is smaller than for $p_{\max} = \text{const.}$

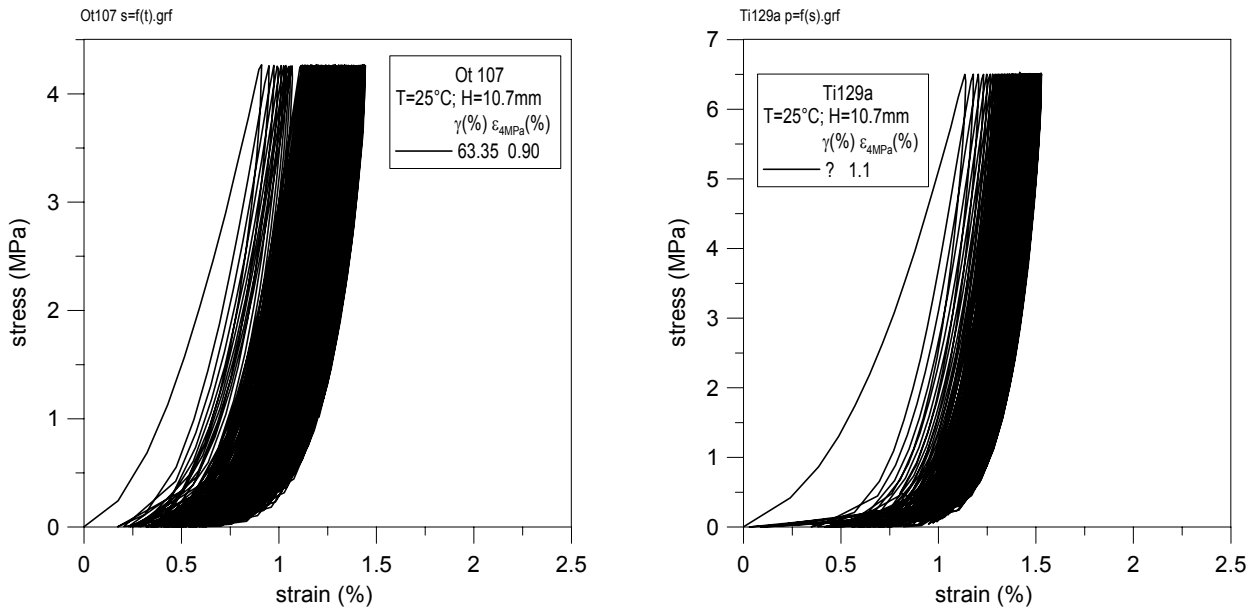


Fig. 9. Mechanical cycling of OSi and MTI pebble beds at ambient temperature.

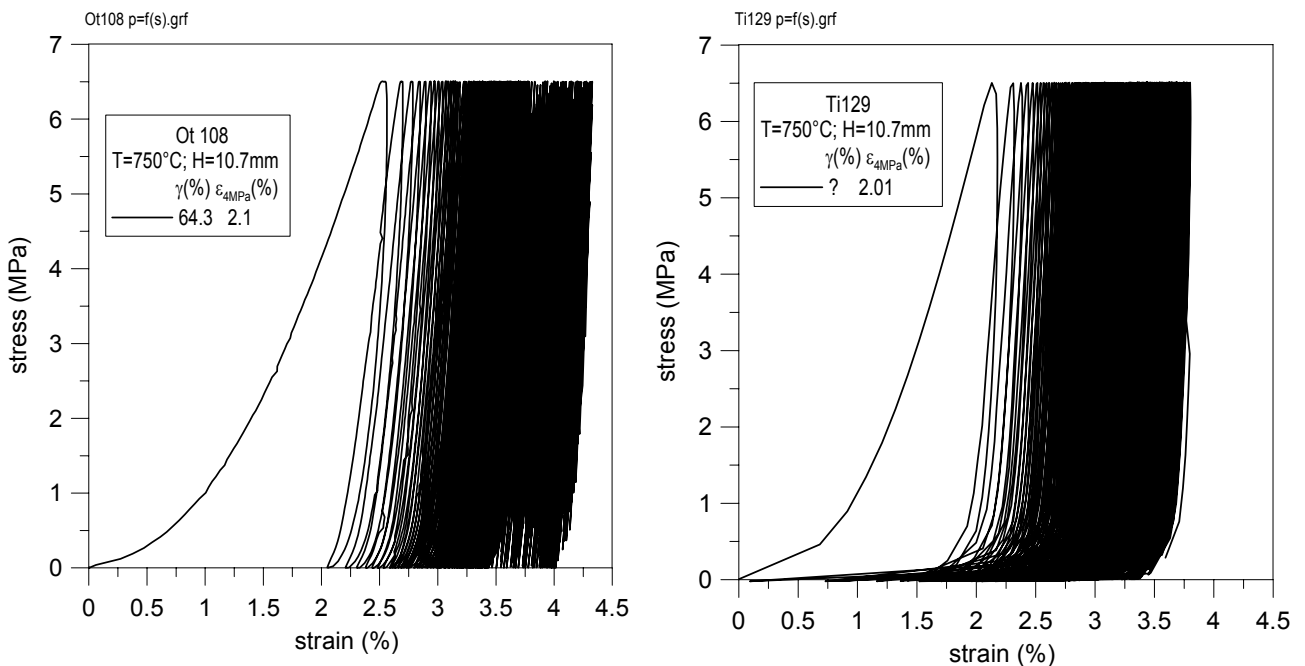


Fig. 10. Mechanical cycling of OSi and MTI pebble beds at $T=750^{\circ}\text{C}$.

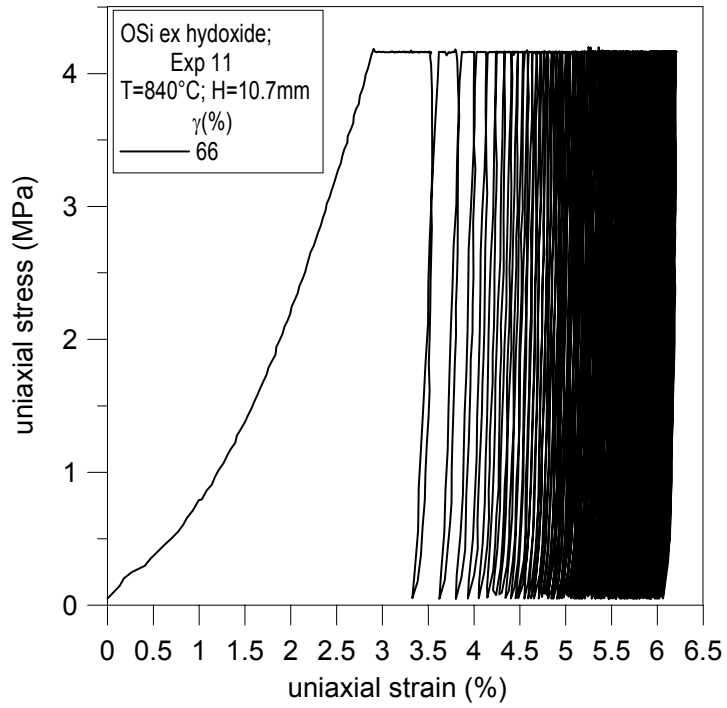


Fig. 11. Mechanical cycling of OSi ex hydroxide pebble bed at T=840°C

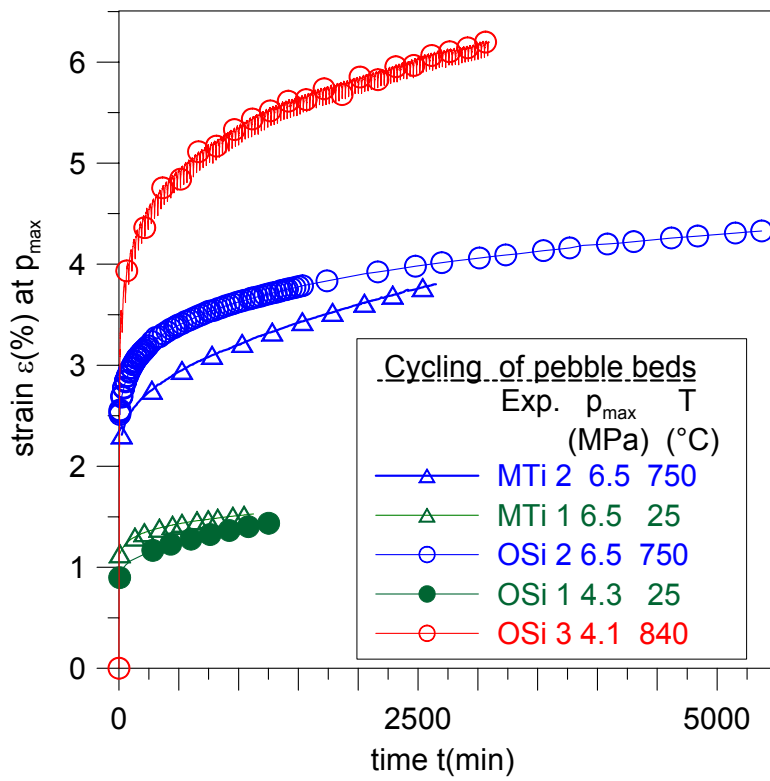


Fig. 12. Strain at p_{max} as a function of time.

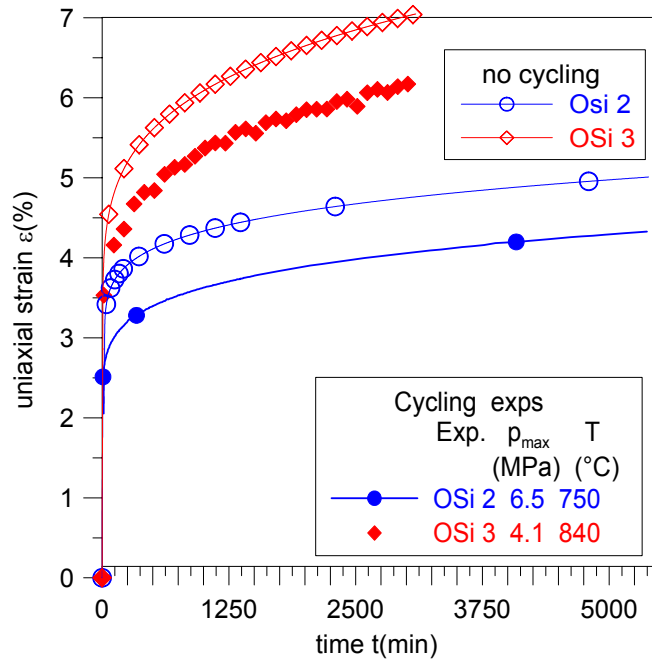


Fig. 13. Comparison of cycling tests with thermal creep experiments.

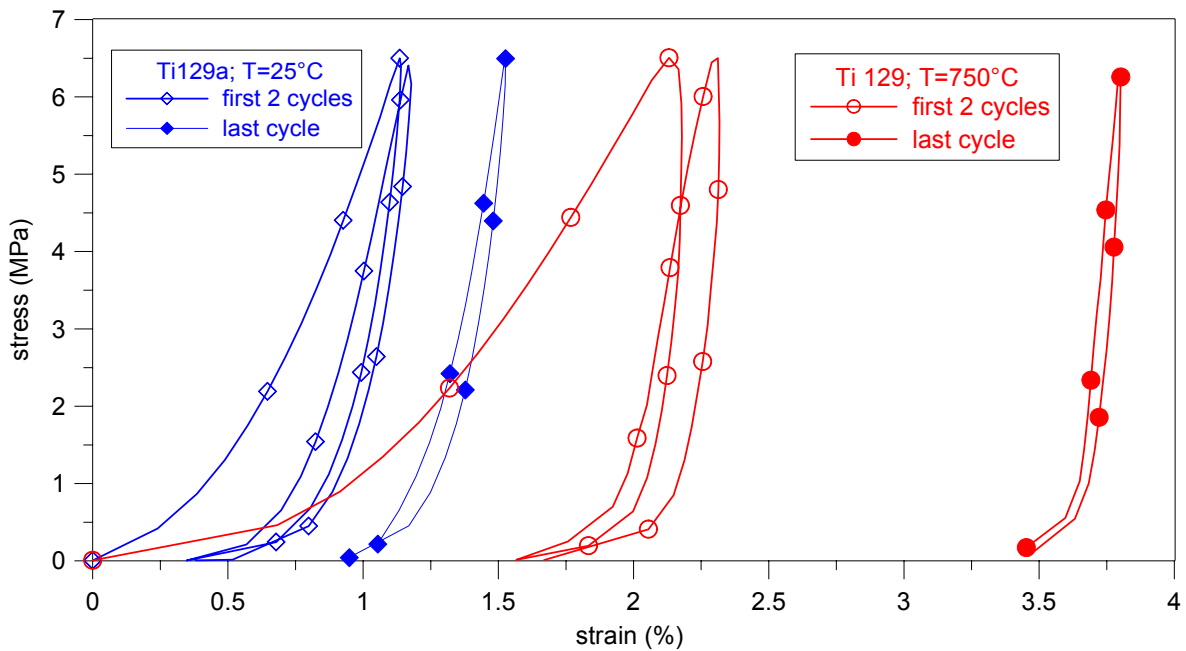


Fig. 14. Beginning and end of cycling for MTi pebble beds.

Figure 14 shows for the MTi pebble beds the strain for the first two cycles and the last cycle: for ambient temperature, the second cycle and the last cycle are very similar. For 750°C, the strain occurring during the first pressure increase phase is much larger due to thermal creep, the strain during the second stress increase is also larger than the strain occurring during the last cycle where the bed behaves very stiffly. These data are believed to be very suitable for the validation of pebble bed codes because creep is occurring when stress is changing with time.

CONCLUSIONS

The new pebble batches OSi 03/1-3 and 03/1-4 produced from lithium hydroxide and silica (OSi ex hydroxide) were subjected to uniaxial compression tests. Compared to the old material (OSi ex silicate), the OSi ex hydroxide pebble beds are characterised by a softer behaviour during the first pressure increase period and, to a smaller extent, in respect to thermal. A softer behaviour results in smaller stresses during the heat-up phase and faster stress relaxation processes at high temperatures; effects which are presumed to be favourable for blanket operation. In the future, more experiments are required in order to enlarge the pebble bed data base for this new material.

Furthermore, cycling tests were performed where different ceramic breeder pebble beds (metatitanate and different types of orthosilicate) were mechanically cycled between zero pressure and a maximum pressure which was, depending on the experiment between 4.3 and 6.5MPa. Temperatures were between ambient and 840°C. For ambient temperature, progressing compaction was still observable after more than hundred cycles). At elevated temperatures, the compaction was significantly increased because of thermal creep. These experiments should be well suited to validate pebble bed codes.

References

- [1] R. Knitter, G. Piazza, J. Reimann, P. Risthaus, L.V. Boccaccini, "Fabrication and characterisation of lithium orthosilicate pebbles using LiOH as a new raw material", CBBI-11, Dec. 15-17, 2003, Tokyo, Japan, in Proceeding of the 11th International Workshop on Ceramic Breeder Blanket Interactions, Ed. M. Enoda, Japan Atomic Energy Research Institute, 2004, 108-119.
- [2] G. Dell'Orco, A. Di Maio, L. Sansone, M. Simoncini, G. Vella, Experimental Test on Li-ceramic breeders for the Helium Cooled Pebble Bed (HCPB) Blanket Design, 22nd Symposium on Fusion Technology, Sept. 9-13, Helsinki, Finland, 2002.
- [3] J. Reimann; J.-D. Lulewicz; N. Roux; G. Wörner, Thermal Creep of Metatitanate Pebble Beds, CBBI-10, Oct. 22-24, 2001, Karlsruhe, Germany, in Proceeding of the 10th International Workshop on Ceramic Breeder Blanket Interactions, Ed. L.V. Boccaccini, FZKA 6720, June 2002.
- [4] J. Reimann, L. Boccaccini, M. Enoda, A. Ying. Thermomechanics of solid breeder and Be pebble bed materials. Fusion Eng. and Design, 61-62, (2002), 319-331.
- [5] J. Reimann, E. Arbogast, M. Behnke, S. Müller, K. Thomauske. Thermomechanical behaviour of ceramic breeder and beryllium pebble beds. Fusion Eng. and Design, 49-50, (2000), 643-649.
- [6] J. Reimann, G. Wörner. Thermal creep of Li₄SiO₄ pebble beds, Fusion Eng. and Design, 58-59, (2001), 647-651.
- [7] L. Bühler, J. Reimann, Thermal creep of granular breeder materials in fusion blankets, Journal of Nuclear Materials 307-311 (2002), 807-810.



FUSION

Forschungszentrum Karlsruhe
in der Helmholtz-Gemeinschaft

FZK – EURATOM ASSOCIATION

Modelling of ceramic breeder and beryllium pebble beds at FZK

D. Hofer, M. Kamlah

Forschungszentrum Karlsruhe, Institut für Materialforschung II

CBBI-12, September 16-17, 2004, D. Hofer, M. Kamlah, Forschungszentrum Karlsruhe



FUSION

Forschungszentrum Karlsruhe
in der Helmholtz-Gemeinschaft

FZK – EURATOM ASSOCIATION

Overview

- ∅ Basic Experimental results
- ∅ Drucker-Prager-theory
- ∅ Modification of the Cap hardening law
- ∅ PBA experiment

CBBI-12, September 16-17, 2004, D. Hofer, M. Kamlah, Forschungszentrum Karlsruhe



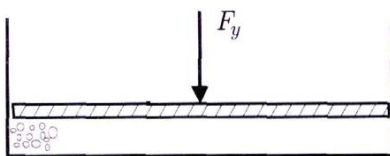
Basic experimental results

- Pebble size is small compared to bed dimensions
- Thermomechanical behaviour of ceramic breeder and beryllium pebble beds can be described by the same continuum-mechanical approach

CBBI-12, September 16-17, 2004, D. Hofer, M. Kamlah, Forschungszentrum Karlsruhe



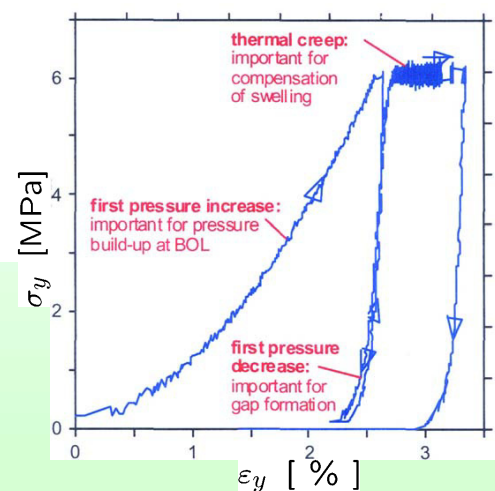
Basic experimental results: Oedometric test



Modelling strategy:

- 1) Model development on the basis of the oedometric test
- 2) Application to fusion relevant problems

LiOSi



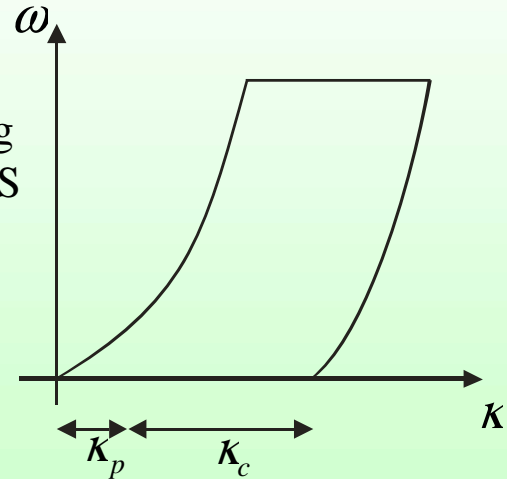
J. Reimann, L. Boccaccini, M. Enoeda, A. Y. Ying,
Fusion Engineering and Design 61-62 (2002) 319-331

CBBI-12, September 16-17, 2004, D. Hofer, M. Kamlah, Forschungszentrum Karlsruhe



Generalized Drucker - Prager - Model

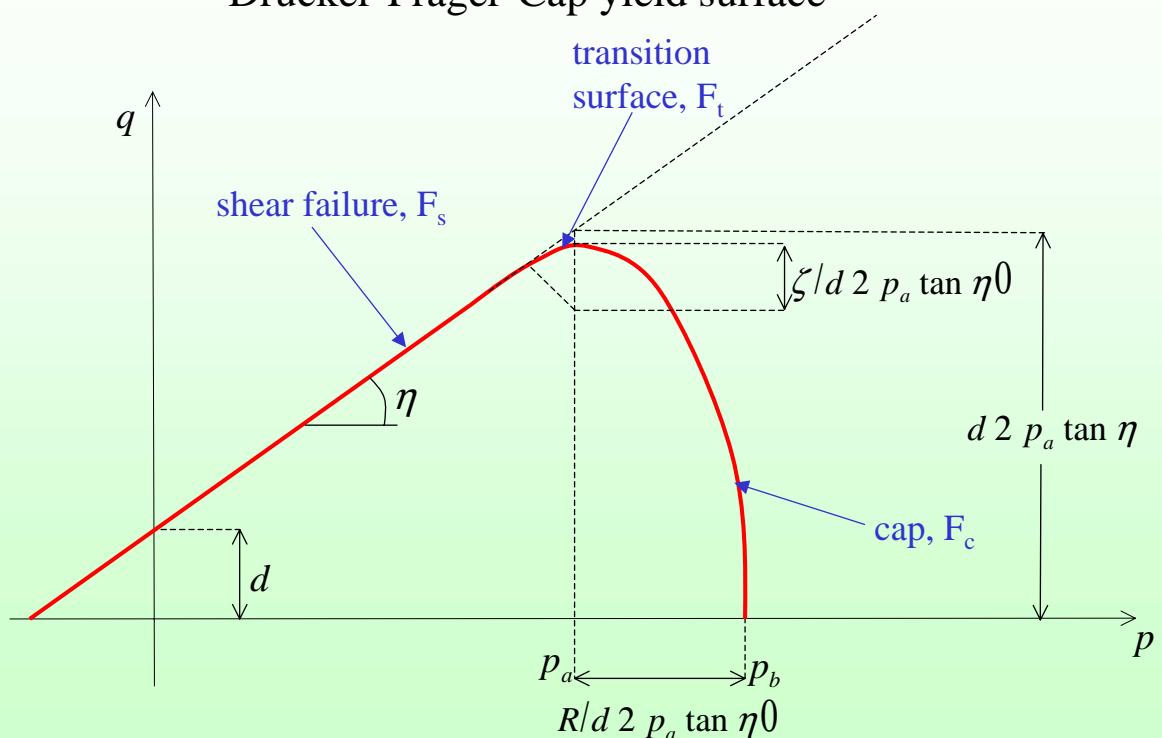
- Implemented in ABAQUS (FE Software)
- Nonlinear elasticity law (proposed by Coube, IWM Freiburg), implemented using the „user defined field“ option of ABAQUS
- Plasticity
- Hardening
- Volumetric creep



CBBI-12, September 16-17, 2004, D. Hofer, M. Kamlah, Forschungszentrum Karlsruhe



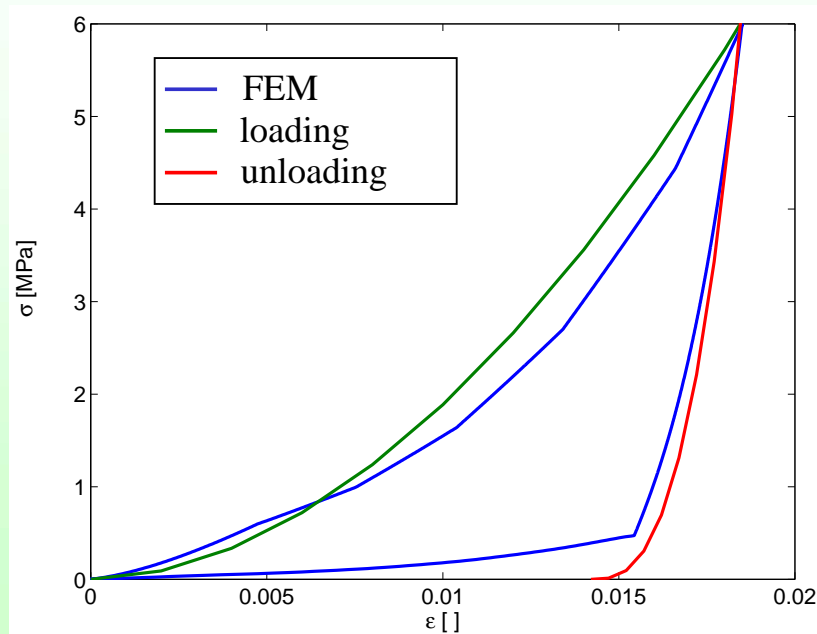
Drucker-Prager-Cap yield surface



CBBI-12, September 16-17, 2004, D. Hofer, M. Kamlah, Forschungszentrum Karlsruhe



Loading and unloading (Beryllium)



CBBI-12, September 16-17, 2004, D. Hofer, M. Kamlah, Forschungszentrum Karlsruhe



Creep mechanisms (strain-hardening)

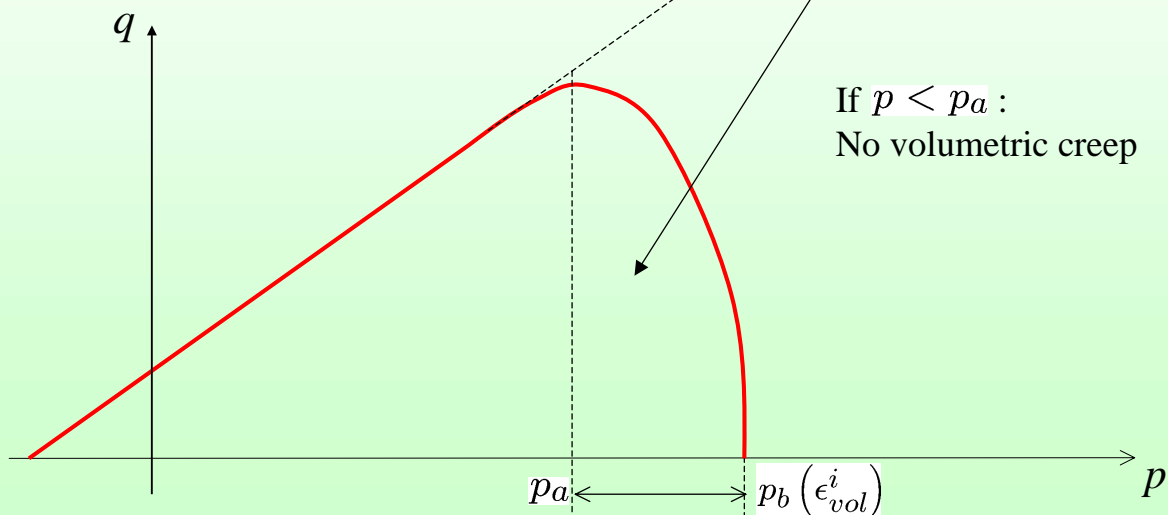
$$\dot{\bar{\epsilon}}_c = (A (\bar{p}_c)^n [(m+1) \bar{\epsilon}_c]^m)^{\frac{1}{m+1}}$$

consolidation creep:

$$\bar{p}_c = p - p_a$$

If $p < p_a$:

No volumetric creep

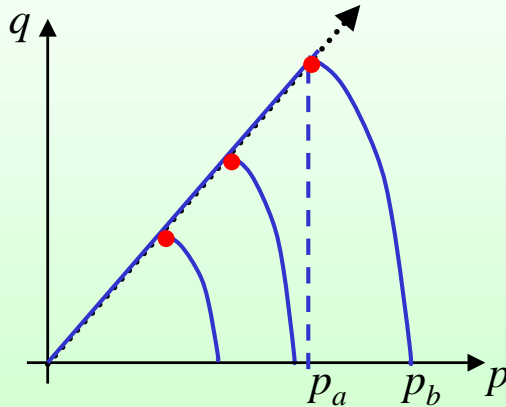


CBBI-12, September 16-17, 2004, D. Hofer, M. Kamlah, Forschungszentrum Karlsruhe

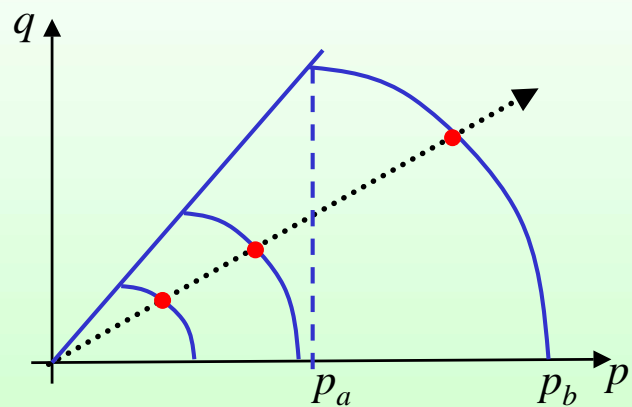


Influence of cap-geometry on creep behaviour

Shape of the cap-ellipse:



appropriate shape:

Effective creep pressure: $\bar{p}_c \mid p \ll p_a$ Hardening: $p_a \mid \hat{p}_a / \kappa_{vol}^p \approx 2 \kappa_{vol}^{cr} \epsilon$

CBBI-12, September 16-17, 2004, D. Hofer, M. Kamlah, Forschungszentrum Karlsruhe



Modification of the Cap hardening law

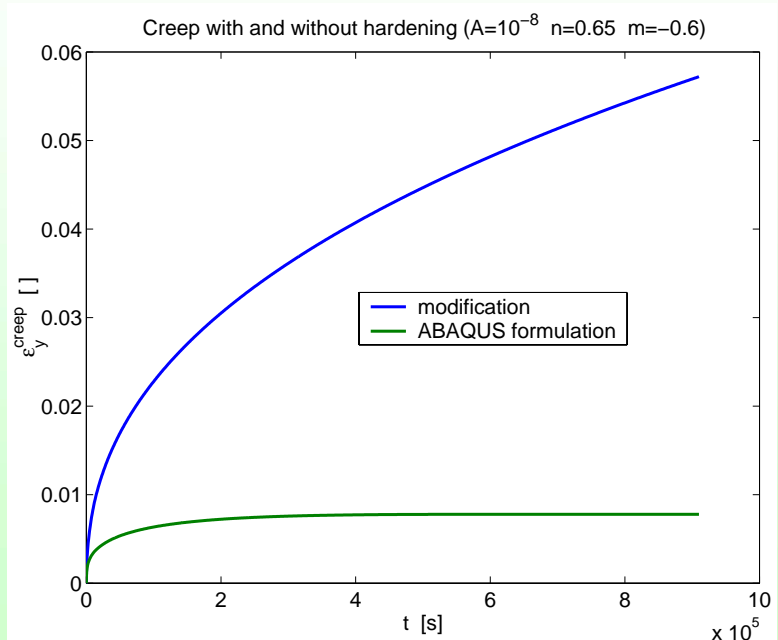
ABAQUS formulation:

$$p_b = \hat{p}_b (\epsilon_{vol}^i)$$

$$\epsilon_{vol}^i = \epsilon_{vol}^{pl} + \epsilon_{vol}^{creep}$$

Modification:

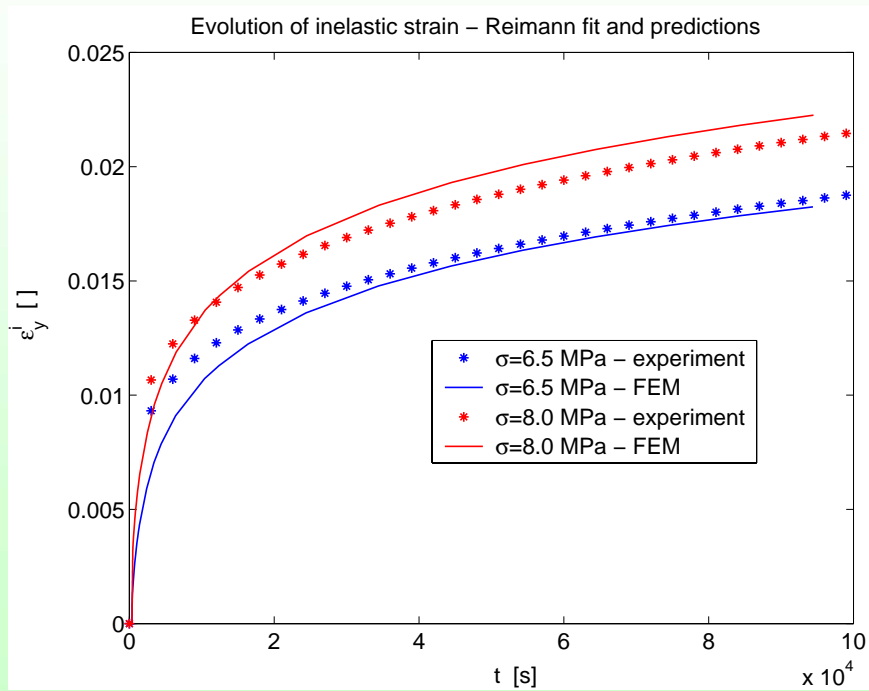
$$p_b = \hat{p}_b (\epsilon_{vol}^p)$$



CBBI-12, September 16-17, 2004, D. Hofer, M. Kamlah, Forschungszentrum Karlsruhe



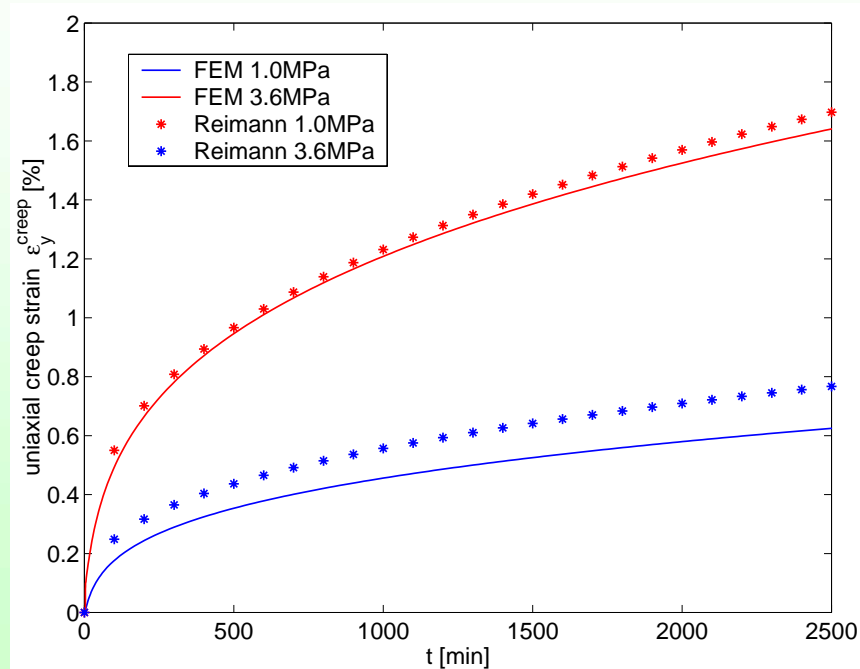
Fit to creep curves of LiOSi



CBBI-12, September 16-17, 2004, D. Hofer, M. Kamlah, Forschungszentrum Karlsruhe



Fit to creep curves of Be (605 °C)

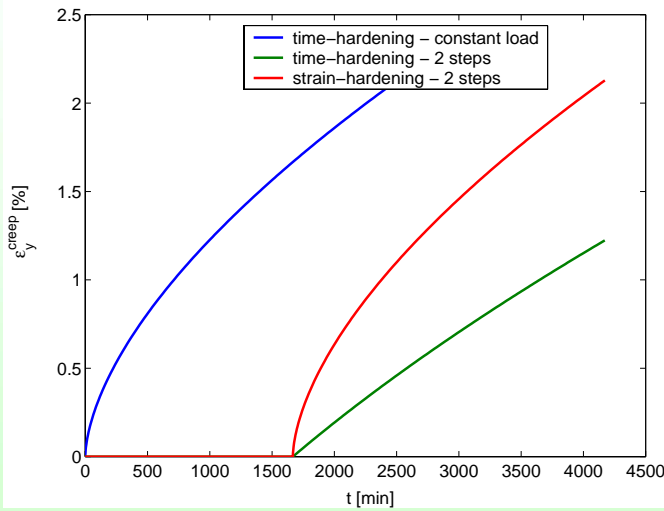


CBBI-12, September 16-17, 2004, D. Hofer, M. Kamlah, Forschungszentrum Karlsruhe

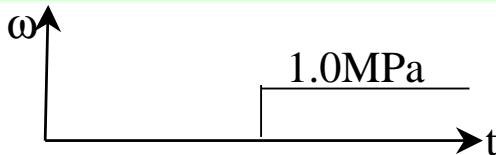
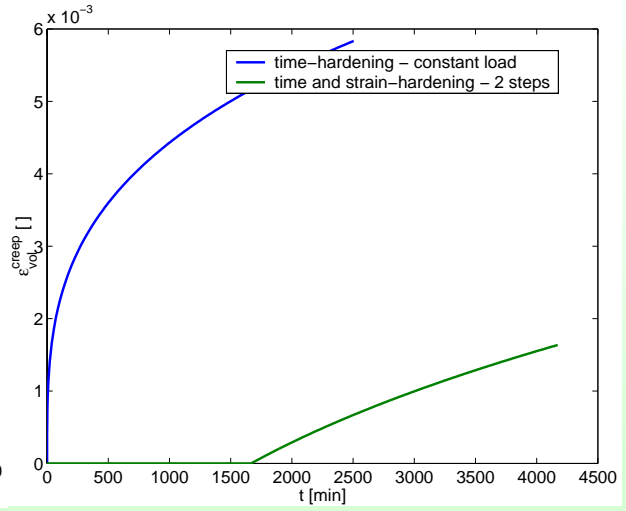


Remark: Time and strain hardening

*CREEP option



*CAP CREEP option

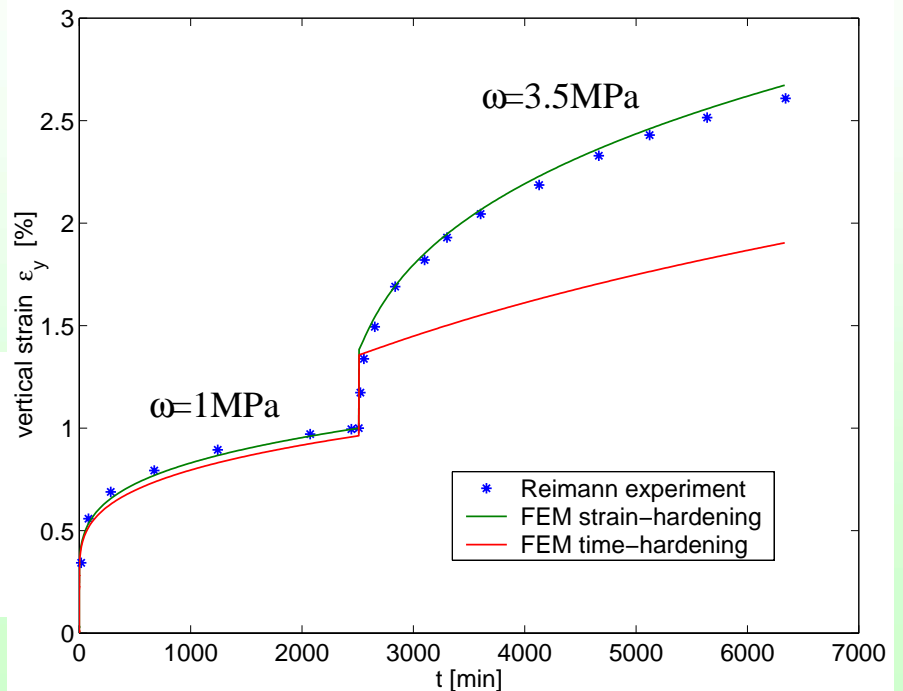
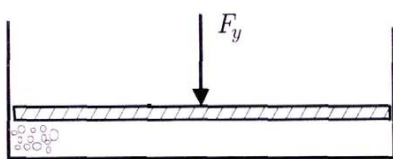


→ Bug in ABAQUS!



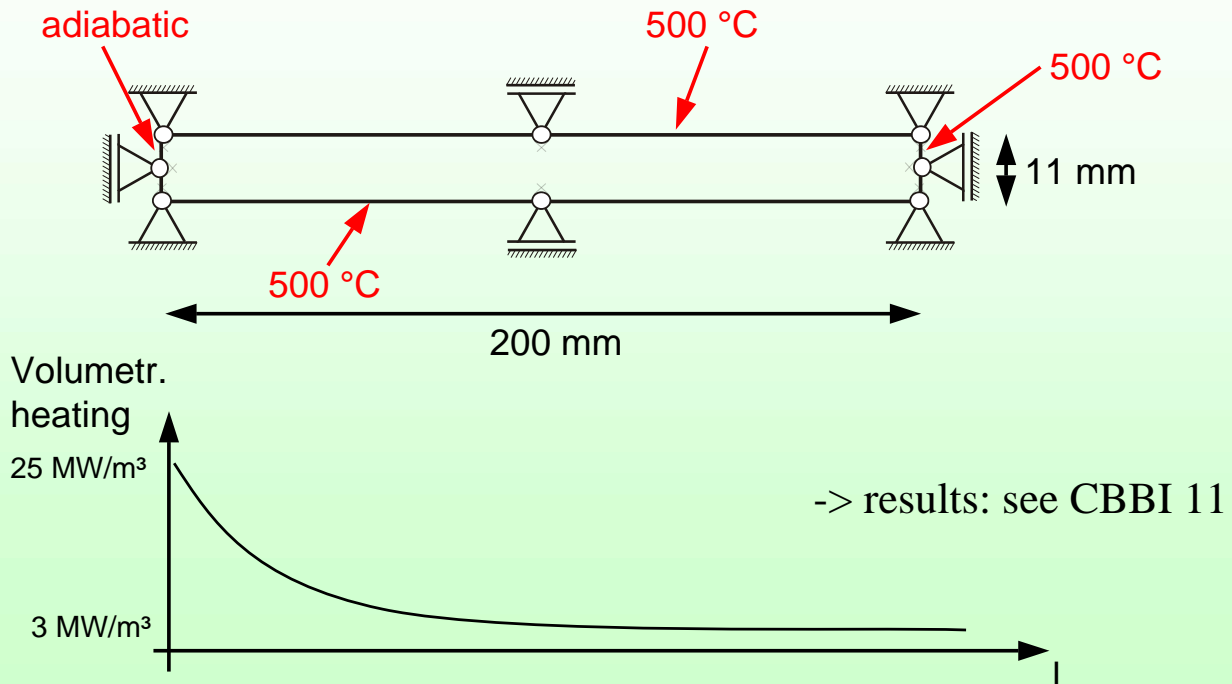
Example: 2-step creep experiment ($T=605^\circ\text{C}$)

bugfix: user subroutine CREEP

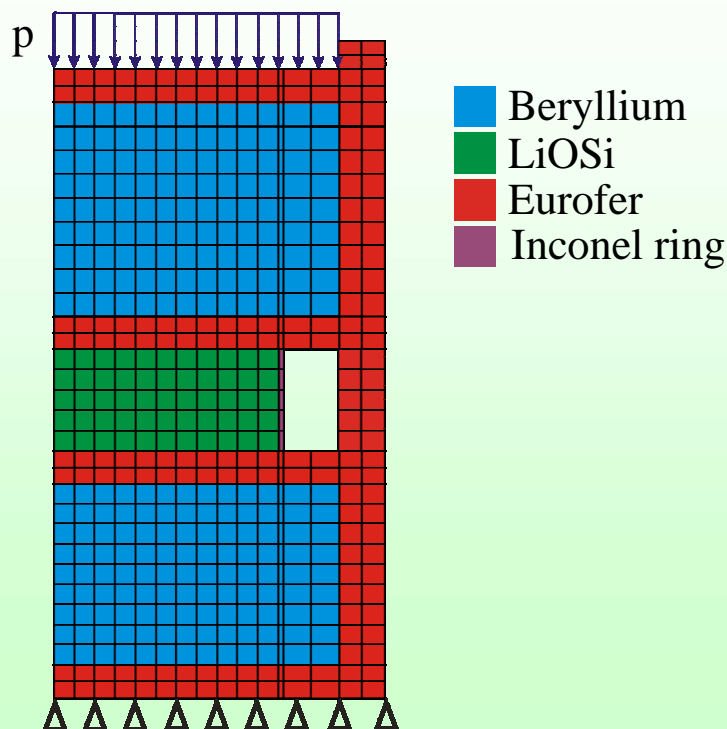




Simple application: Volumetric heating

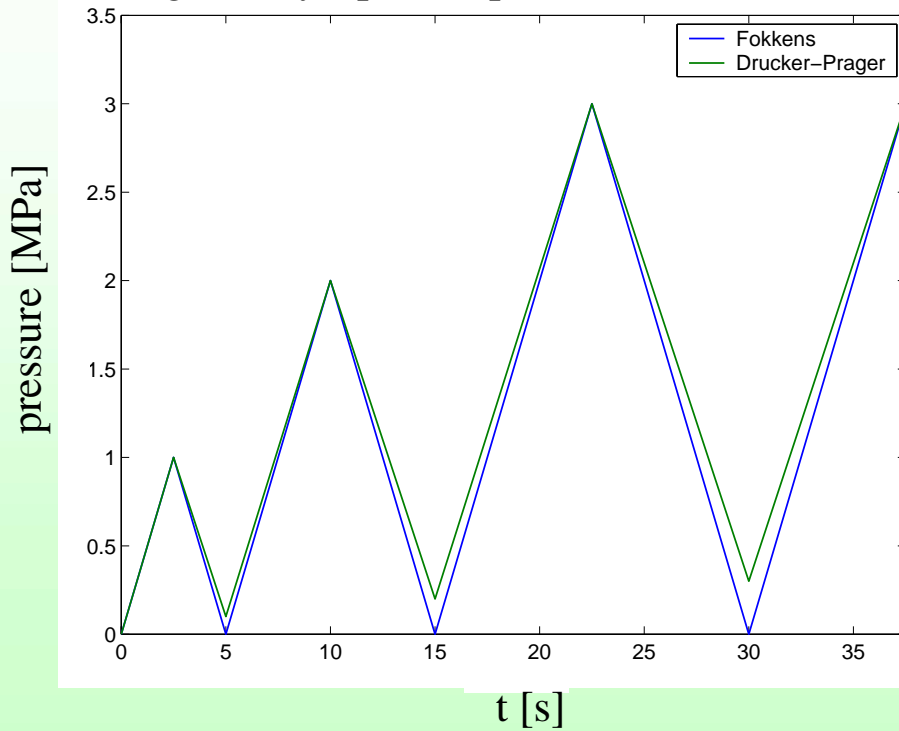


Example: PBA-experiment

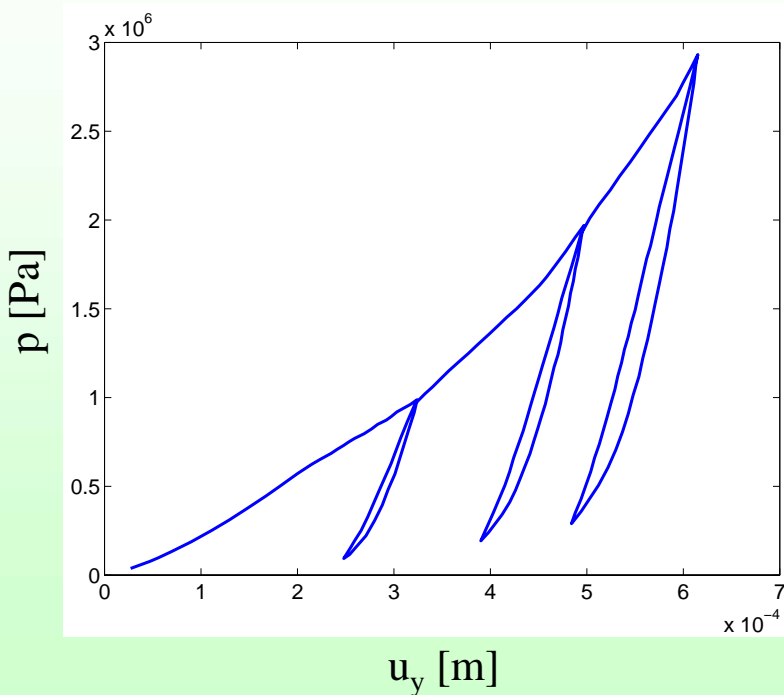




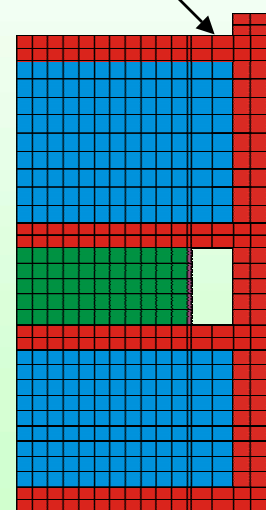
Loading history - precompaction 1 (Fokkens, NRG)



Displacement of pressure lid

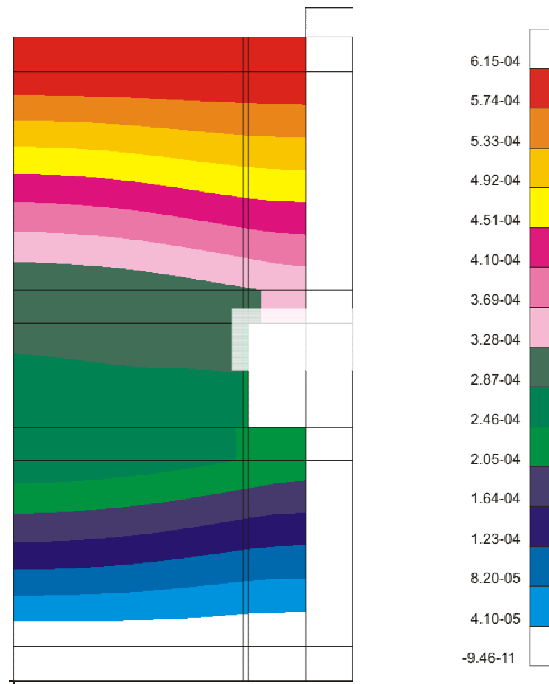


deformation
measurement





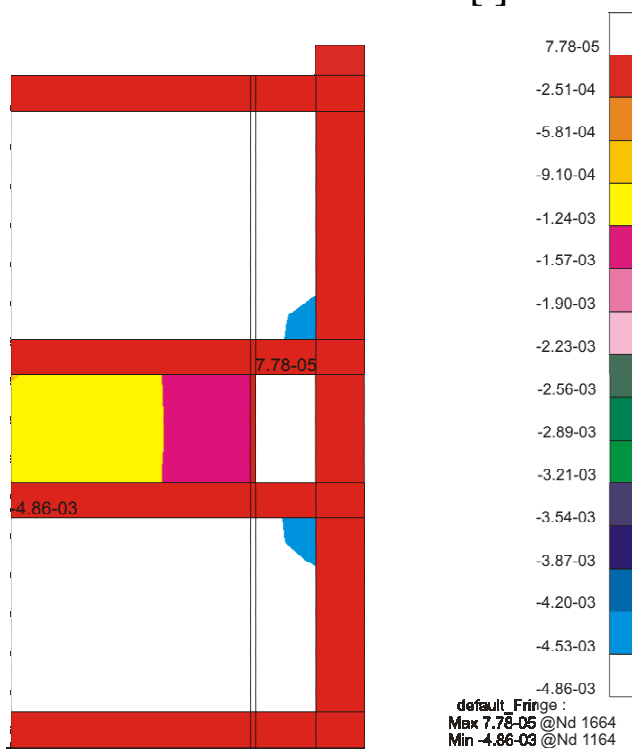
Displacement field [m]



CBBI-12, September 16-17, 2004, D. Hofer, M. Kamlah, Forschungszentrum Karlsruhe



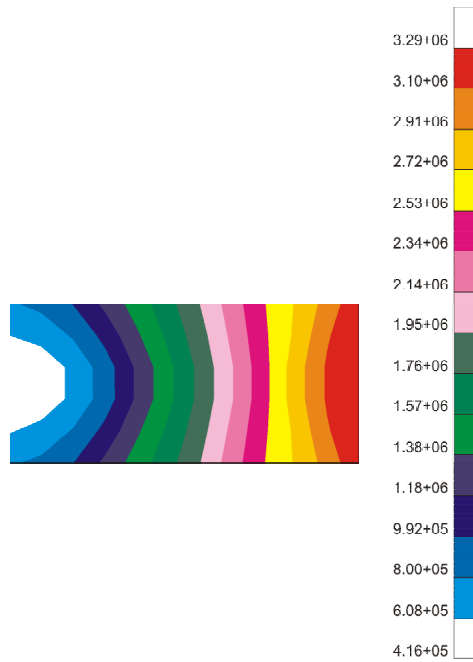
Volumetric strain []



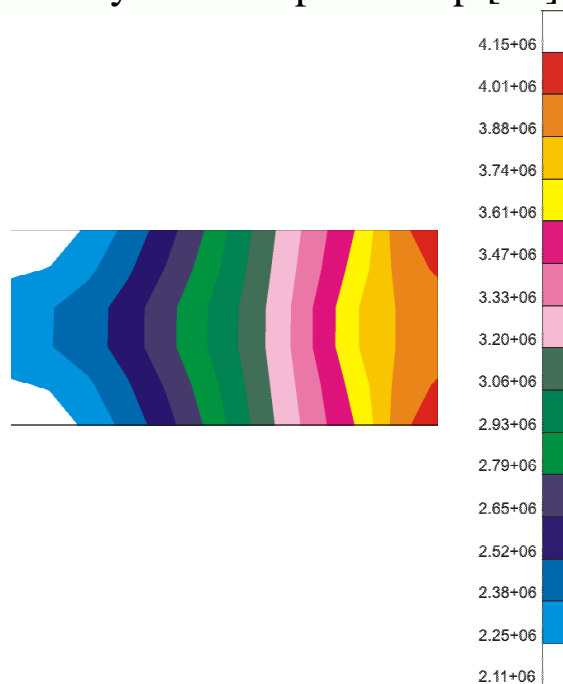
CBBI-12, September 16-17, 2004, D. Hofer, M. Kamlah, Forschungszentrum Karlsruhe



v. Mises stress q [Pa]



Hydrostatic pressure p [Pa]





Summary

- Continuum approach for modelling of pebble bed behaviour
- Implementation of a nonlinear elasticity law
- Drucker-Prager/Cap hardening yield surface
- Implementation of a modified creep law, ABAQUS bug in implementation of strain hardening fixed
- PBA benchmark

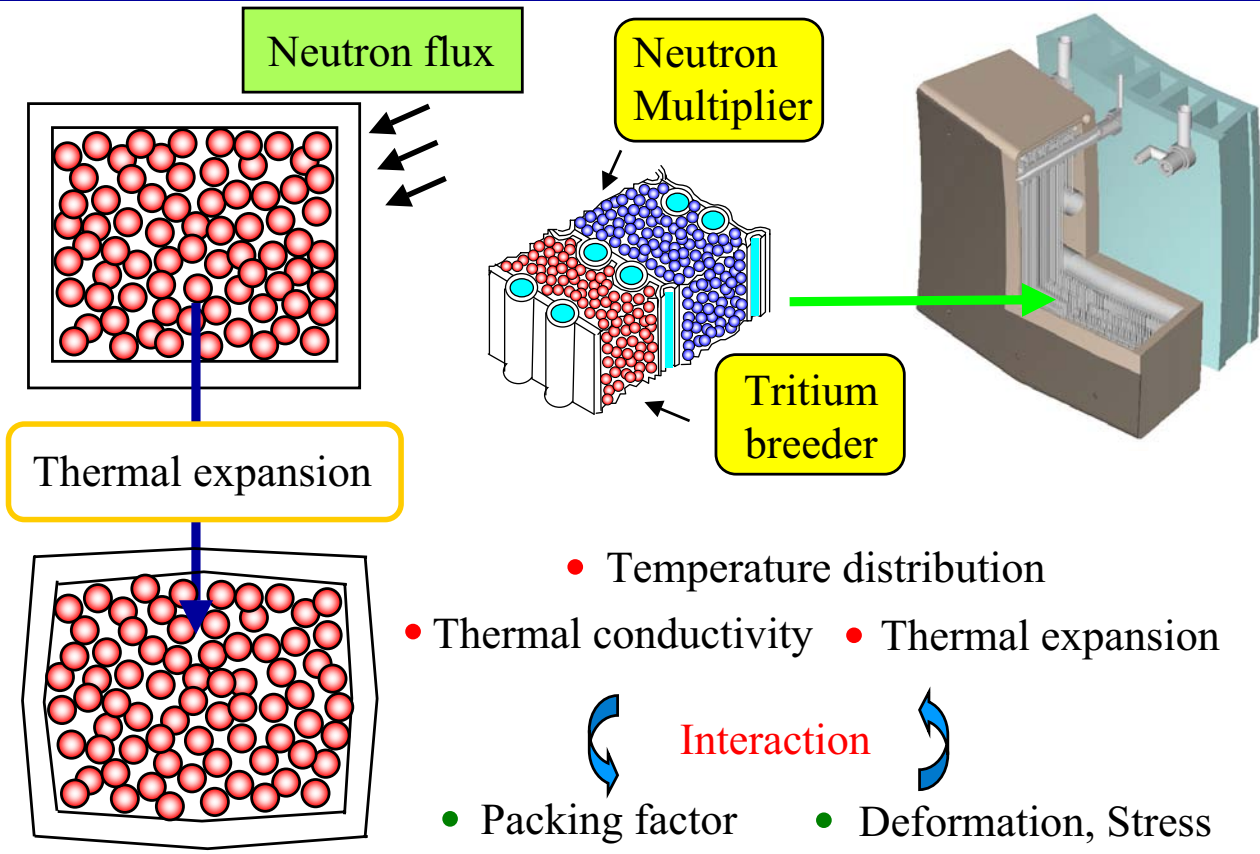
Effect of thermomechanical load on effective thermal conductivity of a Li_2TiO_3 pebble bed

H. Tanigawa, T. Hatano, M. Enoeda and M. Akiba

Blanket Engineering Laboratory, JAERI

Naka-machi, Naka-gun, Ibaraki-ken, 311-0193 JAPAN

Thermo-Mechanical properties of a pebble bed



Purpose and Progress of the study

Basic properties of a compressed bed

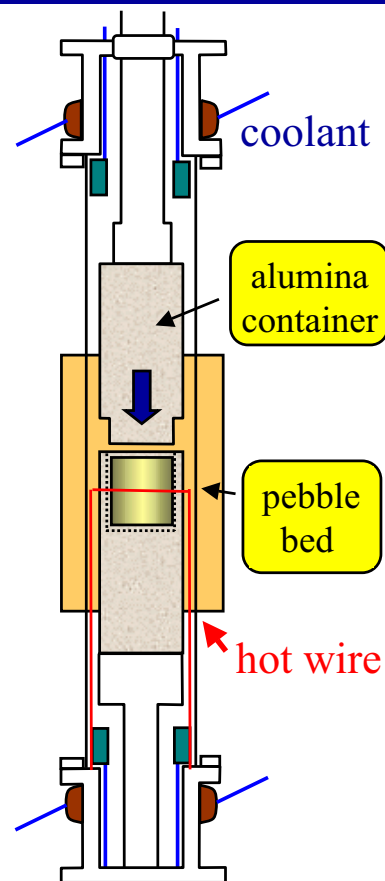
- Stress-Strain property
- Effective thermal conductivity

Simultaneous measurement



- Establishment of measurement system
- Basic correlation between stress and thermal conductivity
- Effect of cyclic load (Temperature, Stress)
- Effect of creep
- Interaction between pebbles and wall materials

Test apparatus

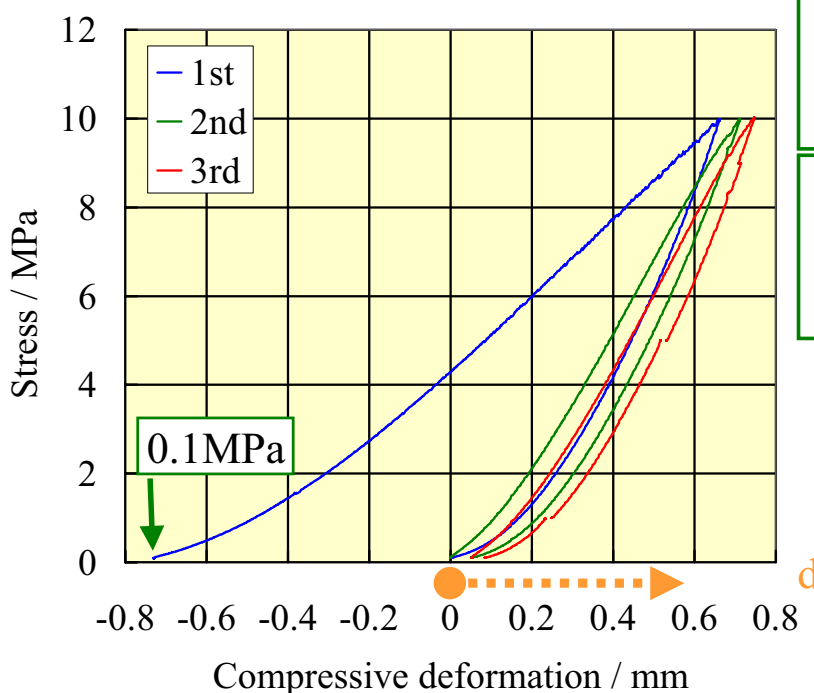


Experimental conditions

- Sample Li₂TiO₃ pebble; λ2mm
81.1% of T.D.
- Dimensions of packed bed λ75mm, h60mm; 265.1cm³
- Initial packing factor 67% (hand tapping)
- Atmosphere He; 1atm
purge rate; 30ccm
- Temperature 673 973K
- Stress-Strain 10MPa - 1%, 44kN

Definition of compressive strain

Strain is defined for compressions after the 2nd cycle, and the thermal conductivity was measured after the 3rd cycle.

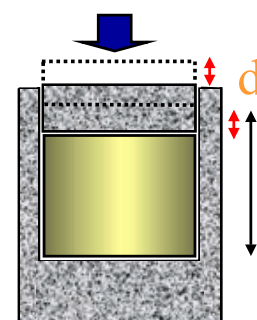


- Compressive strain

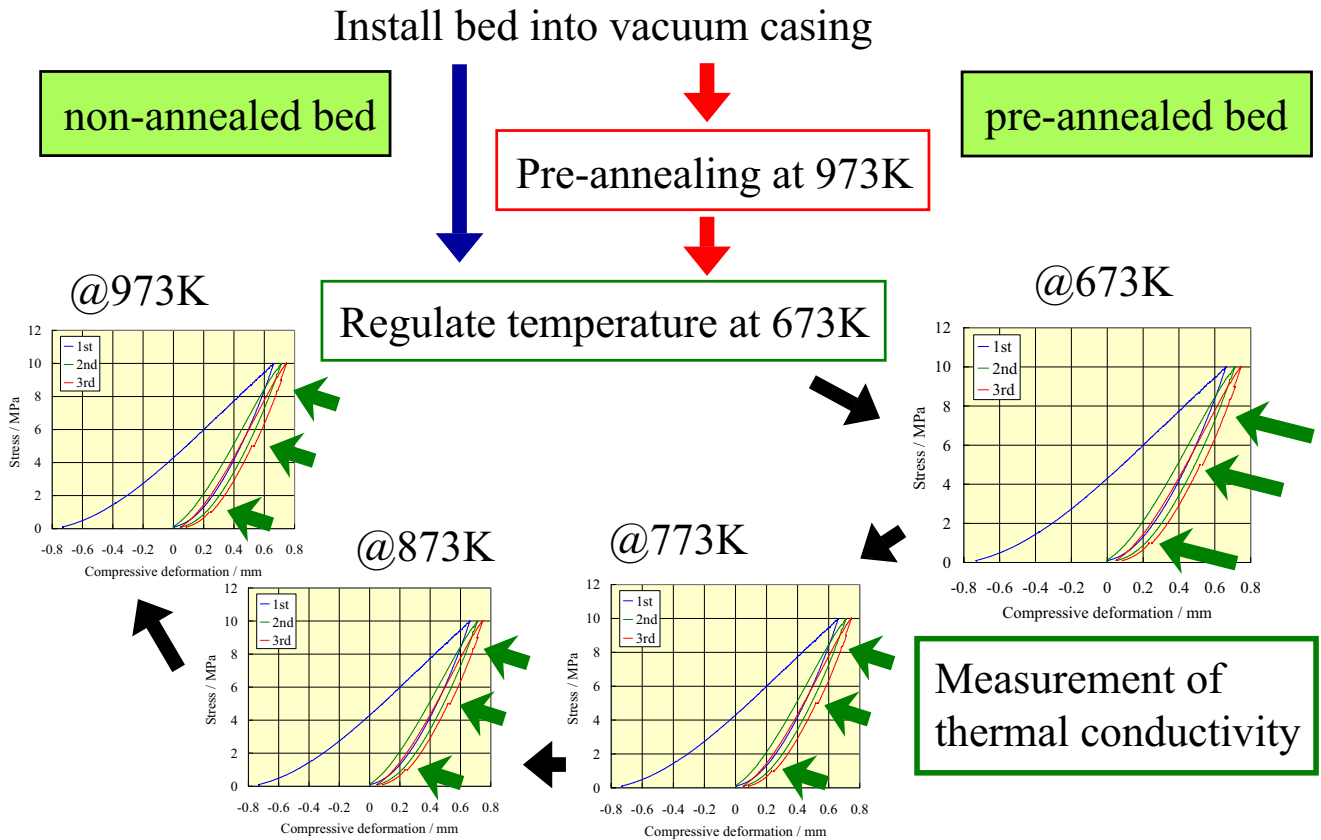
$$\frac{d}{: 60\text{mm}}$$

- Stress

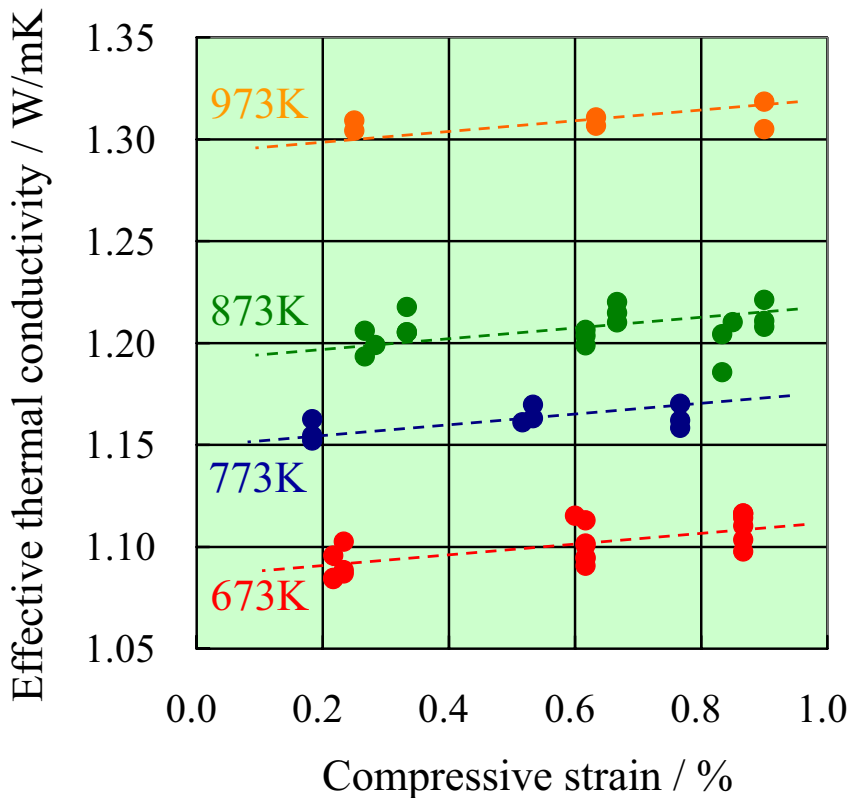
$$\frac{\text{load}}{\text{cross section of bed}}$$



Measurement procedure of thermal conductivity



Thermal conductivity of non-annealed bed



- Repeatability of obtained value
- Chemical stability of the hot wire

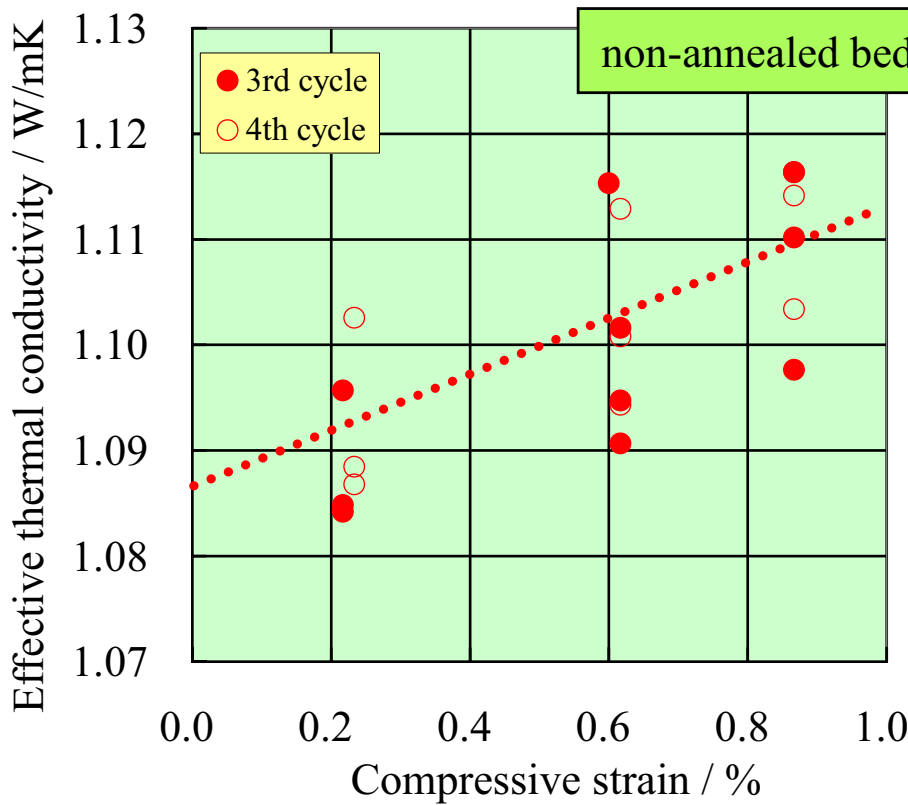


Establishment of measurement system

Dispersion of data: 2%

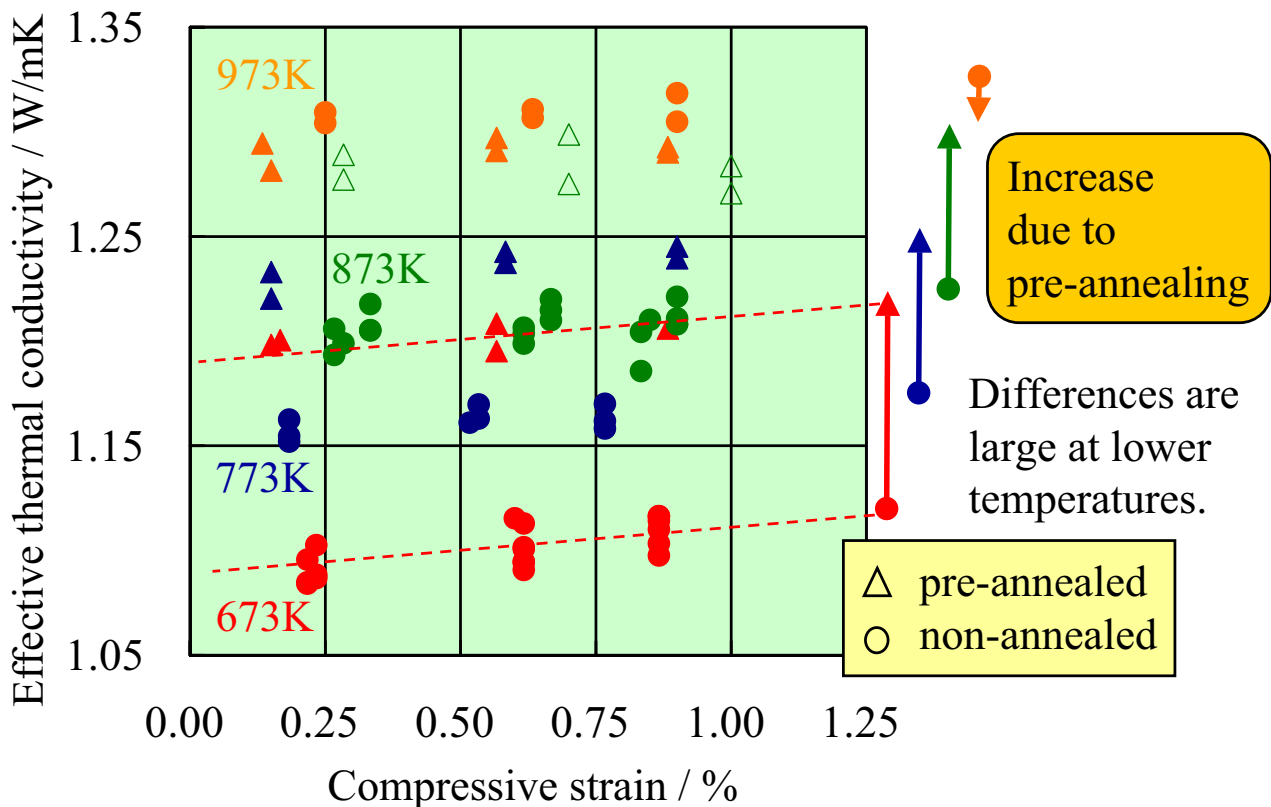
Experimental error: 10%

Correlation between compressive strain and effective thermal conductivity



In all conditions, compressive strain of 1% gave increase of about 3% (2.6%) in effective thermal conductivity.

Effect of pre-annealing

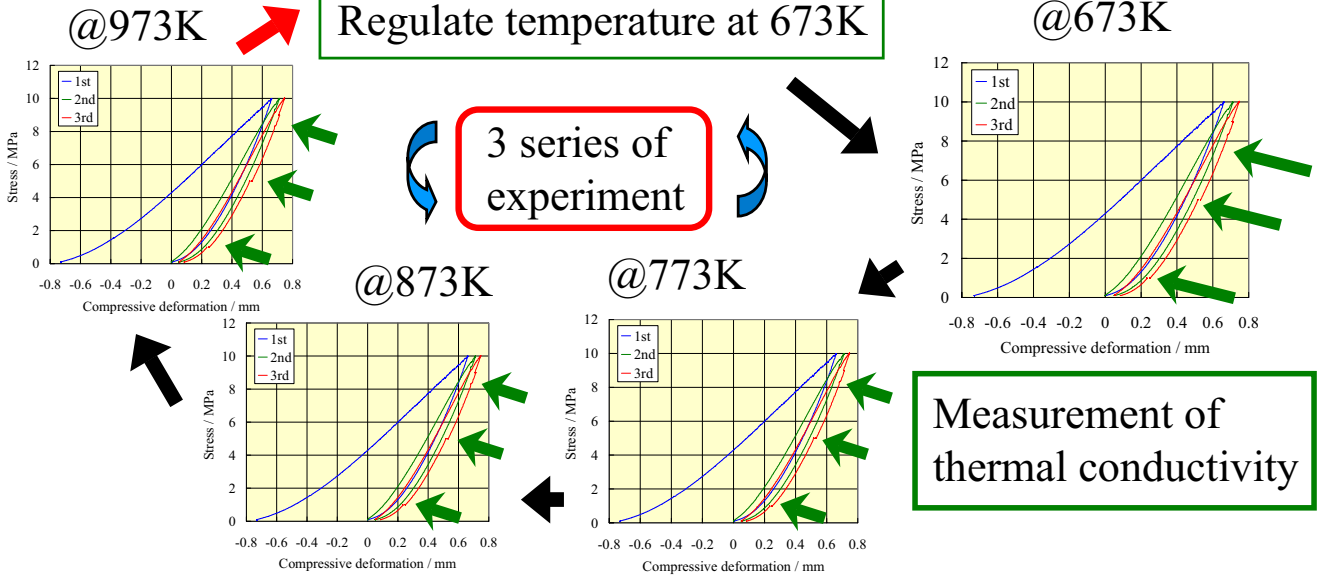


Pre-annealed bed with successive loads

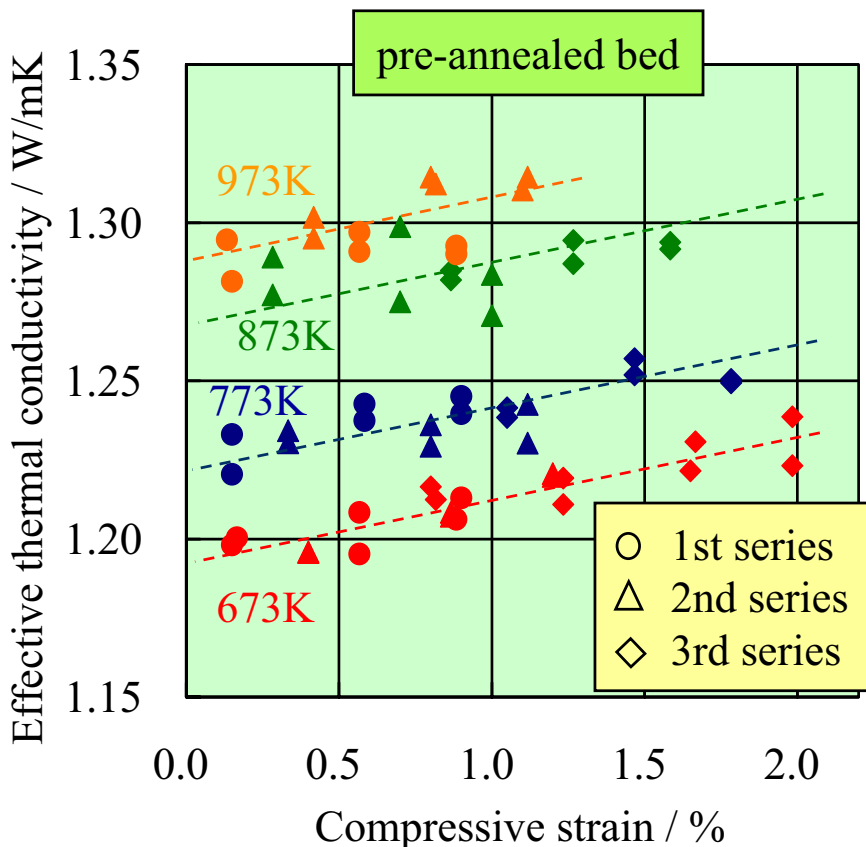
Install bed into vacuum casing

Pre-annealing at 973K

Regulate temperature at 673K



Effect of successive loads



History of thermal and/or mechanical loads on the beds affects effective thermal conductivity.

Convergent thermal conductivity of the bed with cyclic loads will be checked.

Summary

- Our new test apparatus for simultaneous measurements of stress-strain property and effective thermal conductivity is established.
- Dispersion of obtained data stands within 2%
(Experimental error will be 10%)
- Pre-annealing of the bed leads to increase in effective thermal conductivity.
- In all conditions, compressive strain of 1% gave increase of about 3% in effective thermal conductivity.
- When successive loads, heating-cooling or compression, work on the bed, effective thermal conductivity increased according to promotion of the compressive deformation.

Future works

- Analysis of obtained data using SZB model
- Effects of cyclic loads or thermal creep
- Effects of volume or shape of the packed bed
- Estimation of (effective) thermal expansion coefficient
- Difference in material for the container

4 Progress in Ceramic Breeder Material Development

4.1 Ceramic Foams: Inspiring New Solid Breeder Materials (P1)

S. Sharafat, N. Ghoniem, A. Ying, M. Savan, B. Williams, and J. Babcock

4.2 Fabrication of Lithium Orthosilicate Pebbles by Melt-Spraying – Reproducibility and Yield (P5)

R. Knitter and P. Risthaus

4.3 Preparation and Characterization of Li_2TiO_3 Pebble Using the Combustion Synthesis and the Dry-rolling Granulation Process (P12)

former title: Fabrication and Characterization of Li_2TiO_3 Pebble by the Combustion
Synthesis and the Dry-rolling Granulation Process

Choong-Hwan Jung, Ji Yeon Park, Weon-Ju Kim, Sang-Jin Lee and Woo-Seog Ryu

Ceramic Foams: Inspiring New Solid Breeder Materials

Shahram Sharafat, N. Ghoniem, A. Ying
Mechanical Engineering Department,
University of California Los Angeles, CA.

M. Sawan
University of Wisconsin- Madison, WI.

B. Williams, J. Babcock
ULTRAMET Inc., Pacoima CA.

12th International Workshop on
CERAMIC BREEDER BLANKET INTERACTIONS
Forschungszentrum Karlsruhe, Germany
Sept. 16-17, 2004



shahrams@ucla.edu

Outline

- **CERAMIC FOAM** and **CELLULAR MATERIALS** are being used in a wide variety of industries and are finding ever growing number of applications.
- Over the past decade advances in manufacturing of cellular materials have resulted in ceramics with highly uniform interconnected porosities ranging in size from a few μm to several **mm**.
- These relatively new ceramic foam materials have a **unique set of thermo-mechanical properties**, such as excellent thermal shock resistance and high surface to volume ratios.
- Based on **new advances in processing** ceramic foams, we suggest the development of ceramic foams or cellular ceramics for solid breeders in fusion reactor blankets.
- A cellular breeder material has a number of thermo-mechanical advantages over pebble beds, which can **enhance blanket performance**, **improve operational stability**, and **reduce overall blanket costs**.

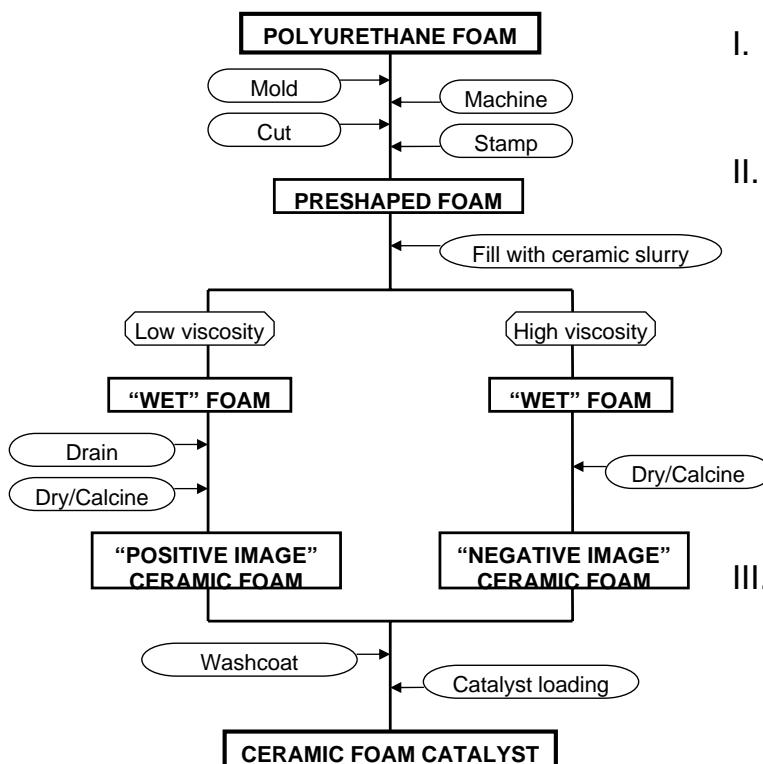


Ceramic Foams

- Al_2O_3 , ZrO_2 , SiC , Si_3N_4 , TiO_2 , Mullite, and Glass foams are made routinely.
- **APPLICATIONS:**
 - Metal melt filtration
 - Diesel engine exhaust filters
 - Flame stabilization - reduction in NO_x emission
 - Catalytic reactors
 - Solar based processes - direct CO_2 - CH_4 reforming
 - Solar Power Generations - volumetric receivers for concentrated solar radiation
 - Biotechnology - macroporous scaffolds for bone tissue engineering.
 - ...



Ceramic Foam Manufacturing: SPONGE REPLICATION



I. Use natural sponge or polyurethane foam as a form

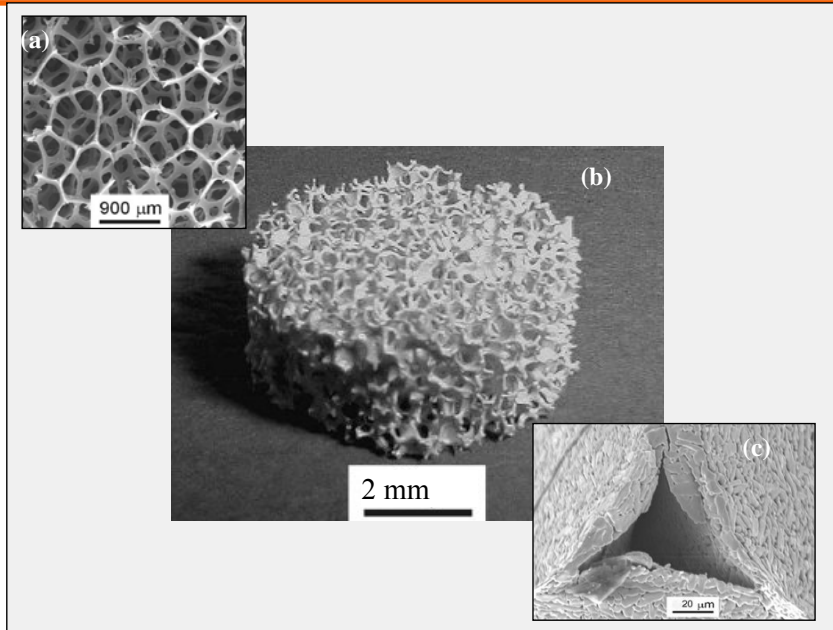
II. Infiltrated with ceramic slurry

Slurry consists of an aqueous solution of ceramic particles (Al_2O_3 , ZrO_2 , SiC , etc.) with diameters ranging between 0.1 and 10 μm , along with viscosity modifiers and dispersion stabilizers

III. Fire to form ceramic foam

This process can result in either "positive" or "negative" replicates of the original foam

TiO₂ Ceramic Foam



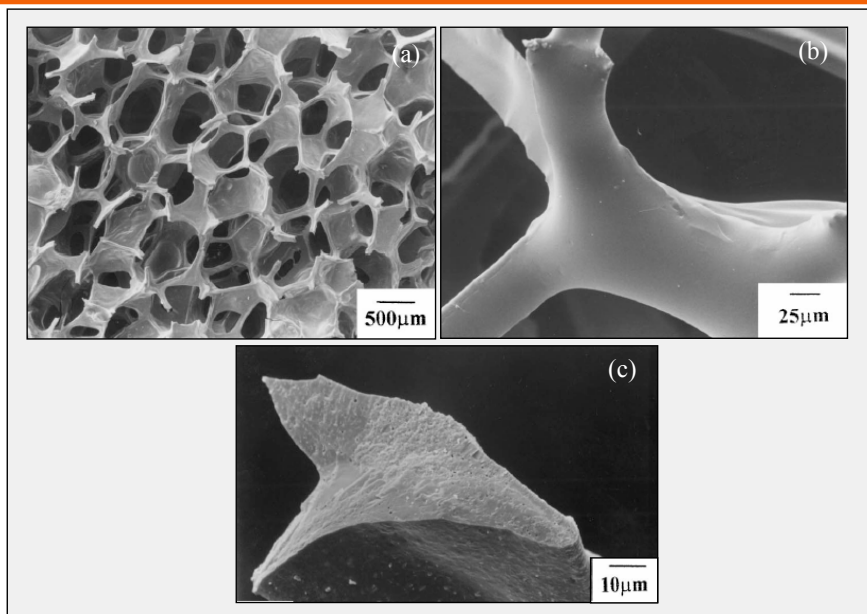
[Haugen-2004]

- (a) Fully reticulated polyester polyurethane foam with 45 ppi
- (b) TiO₂ foam: positive replicated of polyurethane foam,
- (c) Hollow TiO₂ foam ligament

polyurethane is removed during high temperature sintering of the TiO₂ slurry leaving behind hollow ceramic struts.

UCLA

SiC-Si₃N₄ Composite Ceramic Foam



Nangrejo 2000

Scanning electron micrographs of a pyrolyzed ceramic foam showing (a) cell structure of SiC-Si₃N₄ composite foam, (b) strut surface of SiC foam, and (c) strut cross-section of SiC-Si₃N₄ composite foam.

UCLA

Ceramic Foam Manufacturing: FOAMING Technique

- I. Based on gas bubbles in pre-ceramic melts
- II. Gas evolving constituents are added to the pre-ceramic
- III. During the treatment bubbles are generated, which cause the material to foam.

Foaming uniformity and cell geometry can be adjusted by careful selection of surfactants and foaming agents

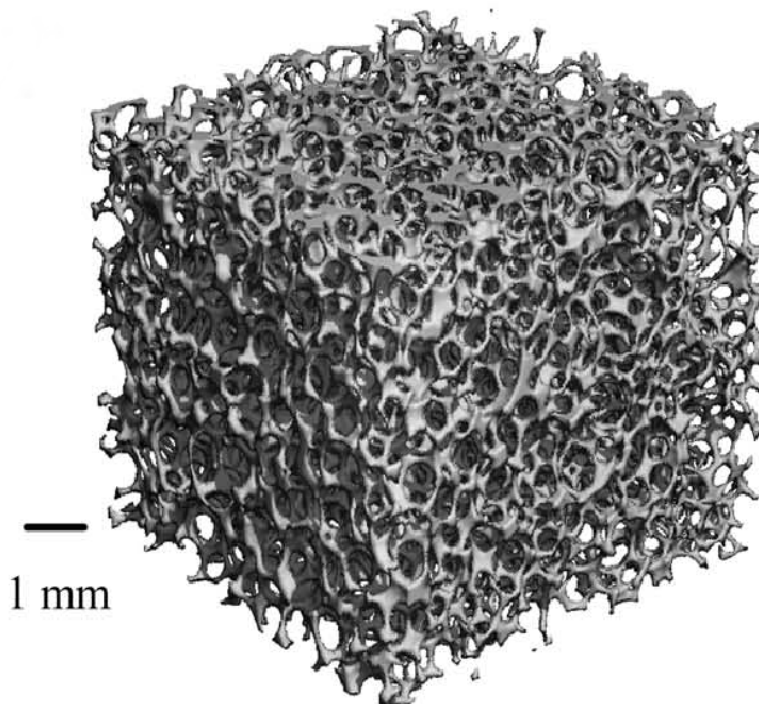
Surfactants are polar molecules that form bubbles inside a liquid, because one end of the molecule attracts liquid and other repels liquid.



[Zeschky 2004]



SiOC Ceramic Foam

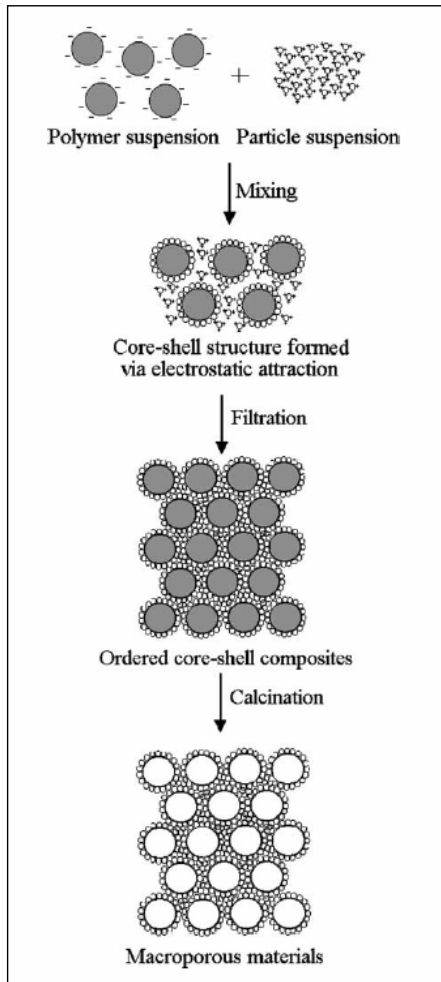


[Zeschky 2004]

Three dimensional micro computer tomography (μ CT) reconstruction of a SiCO ceramic foam prepared from preceramic polymer cured at 200°C



Ceramic Foam Manufacturing: SPACE HOLDER

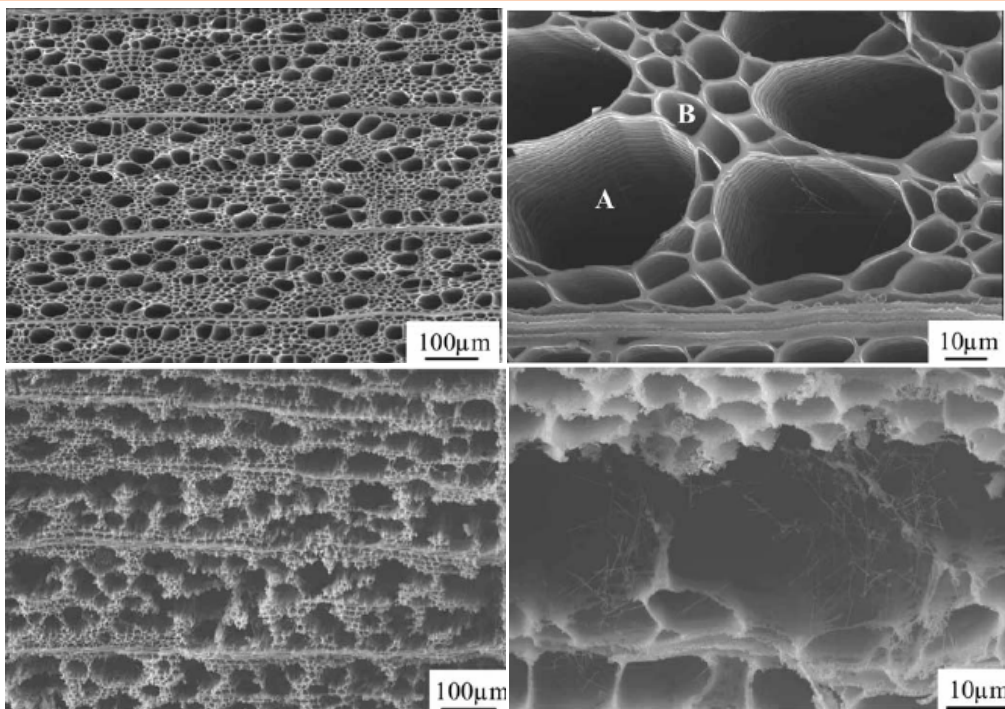


- I. Use a SPACE HOLDER, e.g., sodium chloride
- II. NaCl is sintered and compacted to form a porous space holders.
- III. Infiltrated with polycarbosilane.
- IV. Dissolve the salt and a polymer foam remains.
- V. The foam is then oxidized and pyrolyzed to form the SiC foam

[Tang, 2004]

UCLA

SiC Ceramic Foam

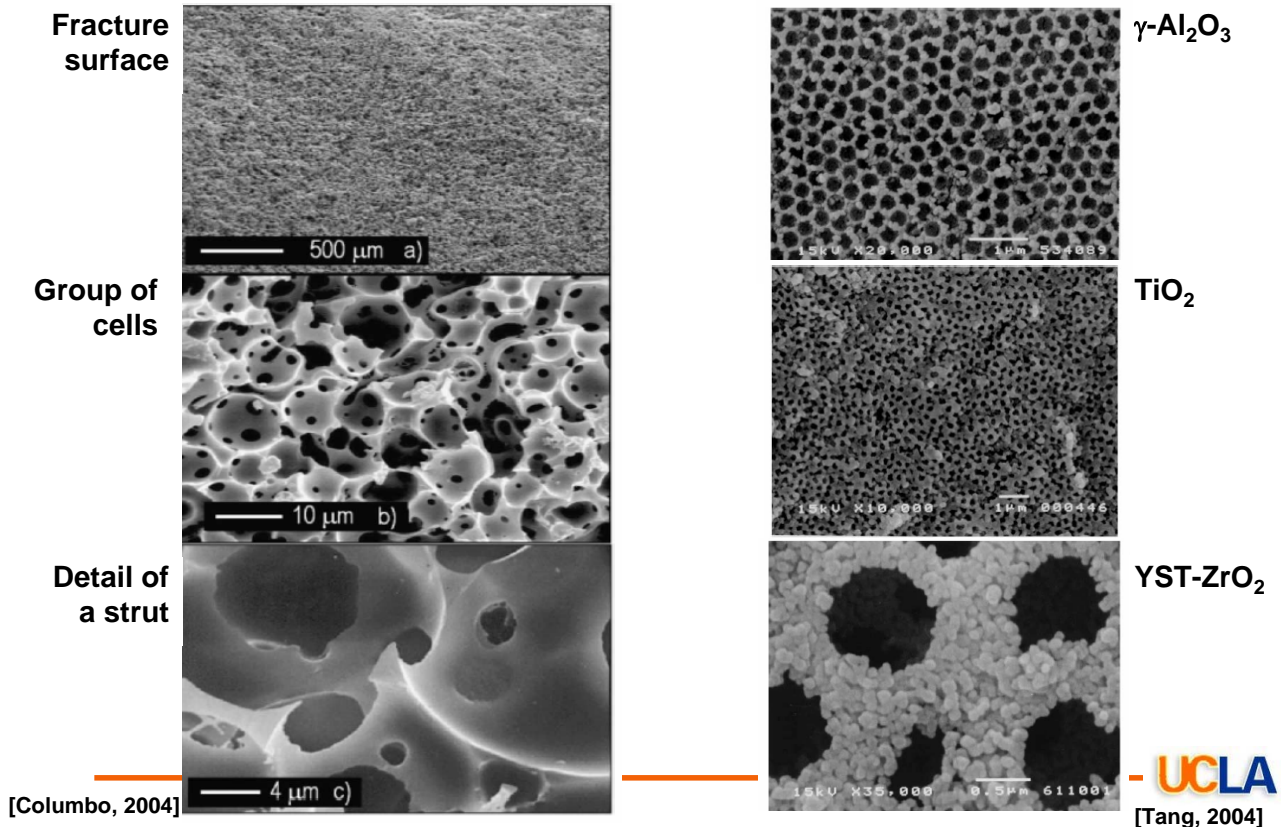


[Quin 2004]

SEM micrographs of (a)-(b) carbonized wood with cross sections perpendicular to axial direction, and SEM micrographs (c)-(d) of wood-like β -SiC ceramic manufactured by sol-gel and carbothermal reduction processing of wood templates.

UCLA

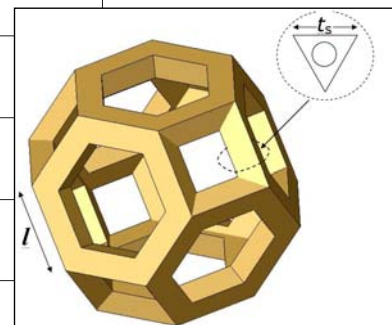
Microcellular SiOC Ceramic Foam



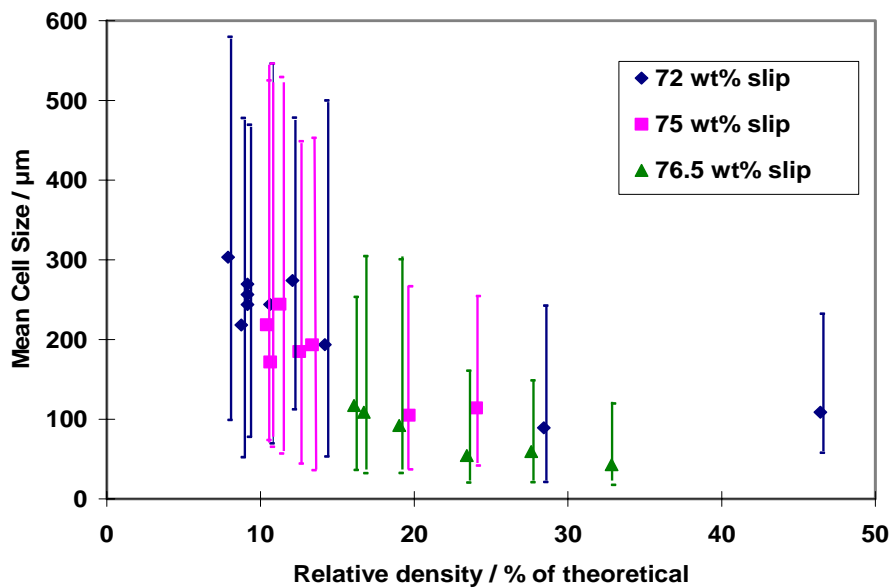
Tetrakaidecahedron Unit Cell

Property	Formula
Density	$\frac{\rho^*}{\rho_s} = C_1 \left(\frac{t}{l}\right)^2$
Stiffness	$\frac{E^*}{E_s} \approx 1.0 \left(\frac{\rho^*}{\rho_s}\right)^2$
Elastic Collapse Stress	$\frac{\sigma_{el}^*}{E_s} \approx 0.05 \left(\frac{\rho^*}{\rho_s}\right)^2$
Plastic Collapse Stress	$\frac{\sigma_{pl}^*}{\sigma_y} \approx 0.3 \left(\frac{\rho^*}{\rho_s}\right)^{3/2}$
Crushing Strength	$\frac{\sigma_f^*}{\sigma_{fs}} \approx 0.2 \left(\frac{\rho^*}{\rho_s}\right)^{3/2}$
Fracture Toughness	$\frac{K_{IC}^*}{\sigma_{fs}} \approx 0.65 \sqrt{\pi l} \left(\frac{\rho^*}{\rho_s}\right)^{3/2}$
Creep	$\frac{\dot{\epsilon}_f^*}{\dot{\epsilon}_0} \approx \frac{0.6}{(n+2)} \left(\frac{1.7(2n+1)\sigma^*}{n\sigma_0}\right) \left(\frac{\rho_s}{\rho^*}\right)^{(3n+1)/2}$
Thermal Conductivity	$\frac{\kappa^*}{\kappa_s} \approx 0.35 \left(\frac{\rho^*}{\rho_s}\right)$

C_1 is a constant which depends on cell geometry (l is the strut length and t strut thickness, see Table 1 for geometric constants).

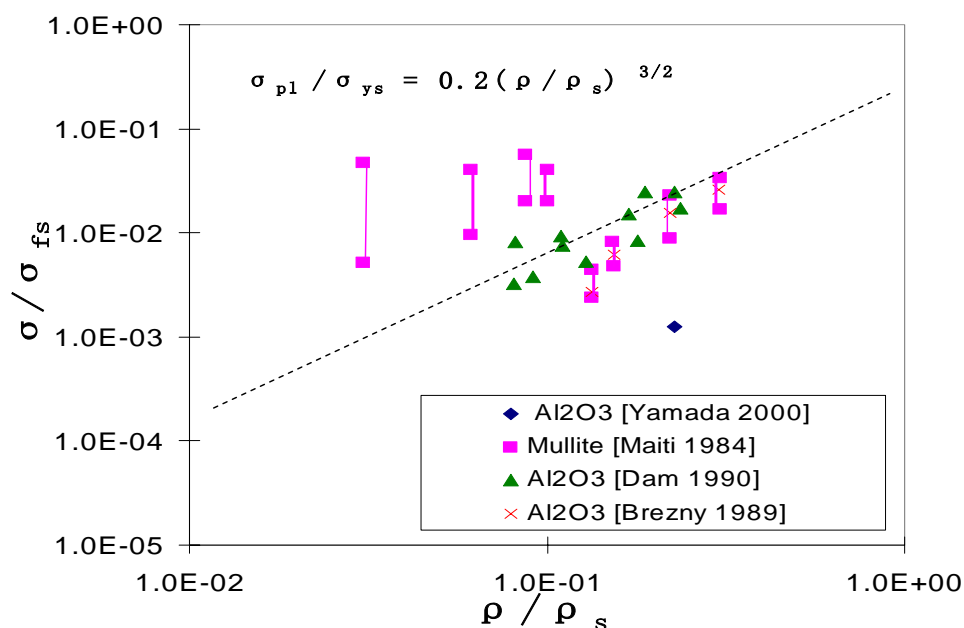


Ceramic Foam Properties: Density



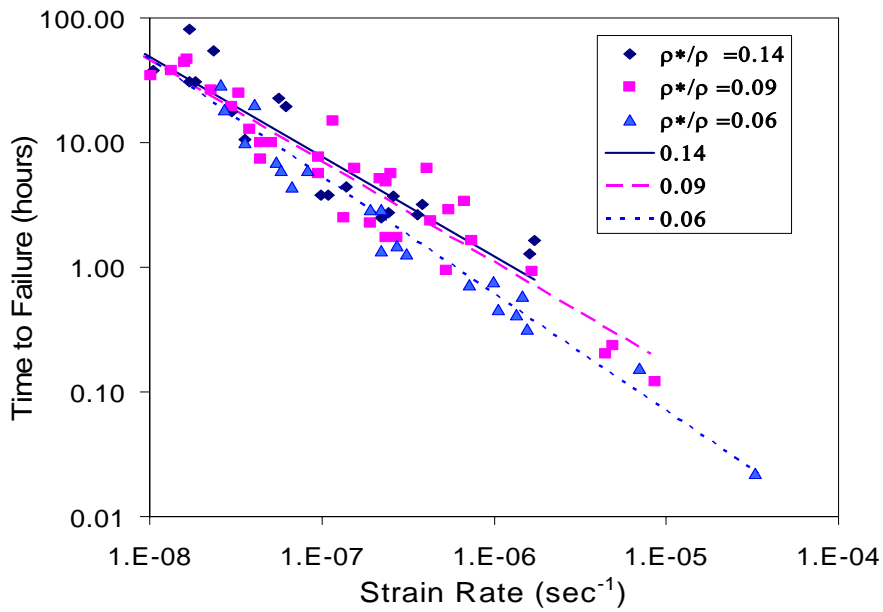
Cell size data retrieved from cell size histograms of ceramic foams at various relative densities showing mean cell size and cell size ranges [Sepulveda1999].

Ceramic Foam Properties: Strength



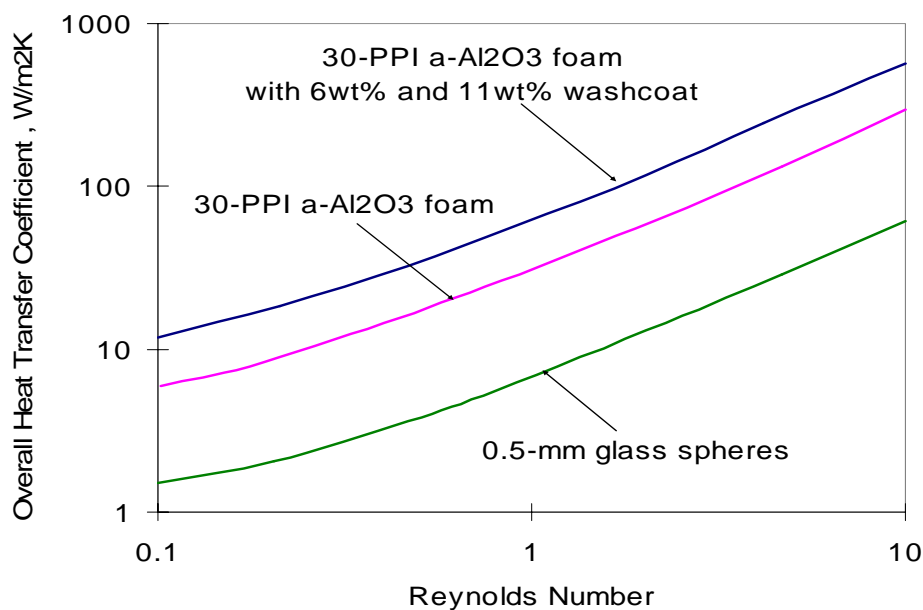
Variation of relative crushing strength as a function of relative ceramic foam density (dotted line is based on alumina solid fracture strength of $\sigma_{fs}=587$ MPa)[Yamada2000].

Ceramic Foam Properties: Creep



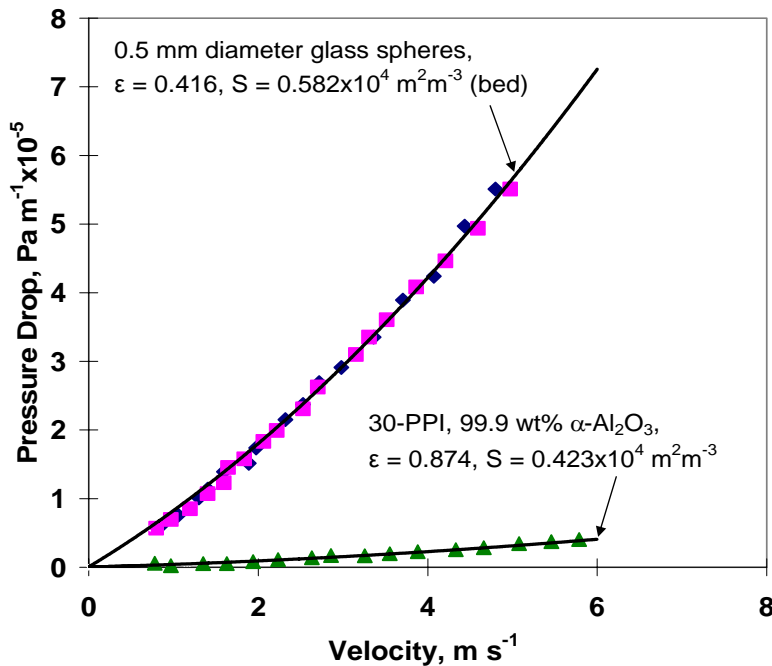
Time to failure of 6%, 9%, and 14% dense alumina foams plotted against secondary creep strain rate [Andrews 1999].

Ceramic Foam Properties: Heat Transfer Coefficient



Comparison between one-dimensional overall heat transfer coefficient of a sphere packed bed and an open cell alumina foam (bed: 0.5 mm glass beads; foam: 30 ppi Al₂O₃) [Peng 2004].

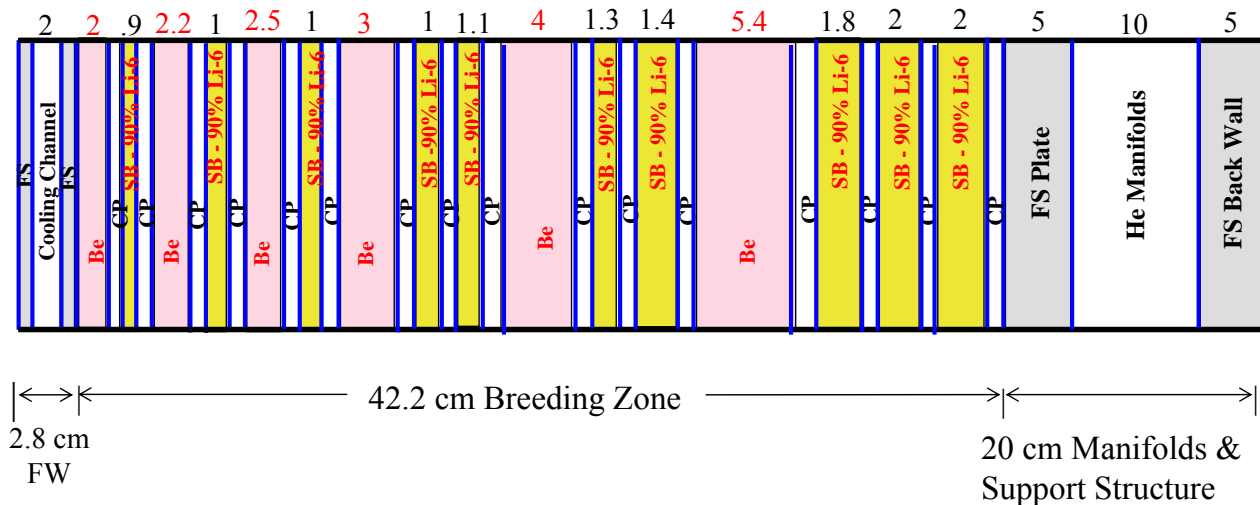
Ceramic Foam Properties: Pressure Drop



Comparison of pressure drop between a sphere packed bed of glass spheres (0.5 mm) and 30-PPI, 99.5 wt% alpha-Al₂O₃ without washcoat. [Richardson2000].



Schematic of 65 cm Thick Blanket



0.6 cm Thick Cooling Plates (CP)



Same TBR can be achieved with less Be

- With higher solid breeder conductivity it is possible to reduce structure content in cooling plates around SB
- Reducing the **structure** content in cooling plates by a **factor of 2** with the foam at 80% density yields **4.6%** higher TBR
- The same TBR as with pebble bed breeder can be maintained by reducing the Be zone thickness by 4.9 cm (**25% reduction in total amount of Be used**)

UCLA

Ceramic Breeder Foam Advantages

- **Densities** are not limited to packing fractions.
- Higher **thermal conductivity** due to a continuous strut network, instead of sphere-to-sphere point contacts.
- Increased breeder density and better thermal performance of foam **reduces structure volume** fractions and multiplier.
- **No sintering**; beginning-of-life and end-of-life configuration changes are primarily creep and swelling driven; reduced shifting of material.
- **Foam-to-wall contact** using brazing technology replaces low-conductivity sphere-to-wall point contacts of packed beds.
- Capability of **tailoring pore morphology**, could accommodate swelling
- Anisotropic foam: **porosity gradient** to achieve uniform heating and tritium release in blanket.
- **Self supporting structure**, no shift of material during operation.

IMPROVED PERFORMANCE AT A LOWER BLANKET COST

UCLA

Fabrication of Lithium Orthosilicate Pebbles by Melt-Spraying - Reproducibility and Yield

Regina Knitter and Peter Risthaus

Institute for Materials Research III

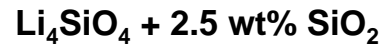
Outline



- **Fabrication of Li-Orthosilicate Pebbles**
- **Investigation of Process Parameters**
- **Quality Control of Reference Material**
- **Conclusions**

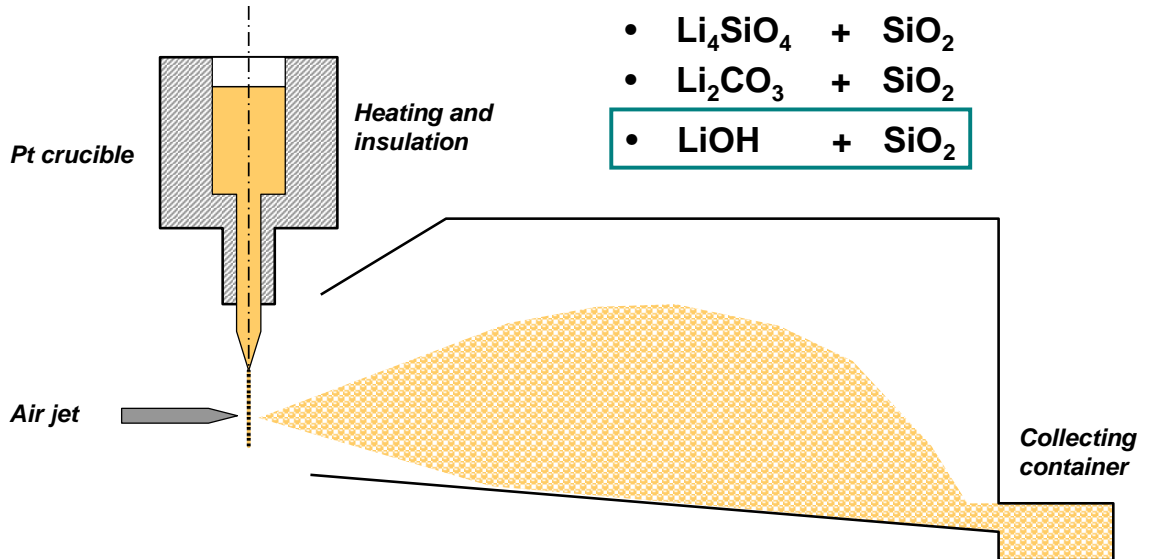
Fabrication of Li-Orthosilicate at Schott Glas

→ Aim



Raw Materials

- $\text{Li}_4\text{SiO}_4 + \text{SiO}_2$
- $\text{Li}_2\text{CO}_3 + \text{SiO}_2$
- $\text{LiOH} + \text{SiO}_2$



Melt-Spraying Facility at Schott Glas

Production 2 x 1.5 kg per day

Yield of screened pebbles ~50 % (250 – 630 μm)
200 – 300 kg per year

Drawbacks Batch processing
Limited control of fabrication parameters

→ Variation of batch properties

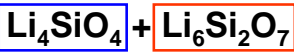
Advantage Recycling of material

Phase Diagram $\text{Li}_2\text{O} - \text{SiO}_2$

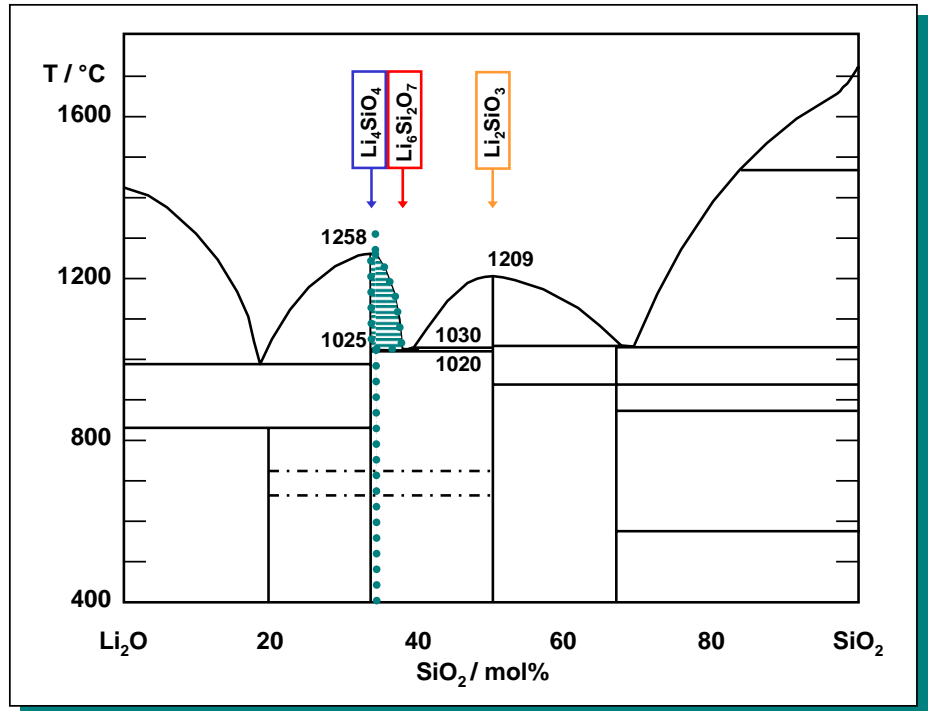
$\text{Li}_4\text{SiO}_4 + 2.5 \text{ wt}\% \text{SiO}_2$

Product phases:

as received



annealed



Investigation of Process Parameters

Influence of

Melt temperature / °C

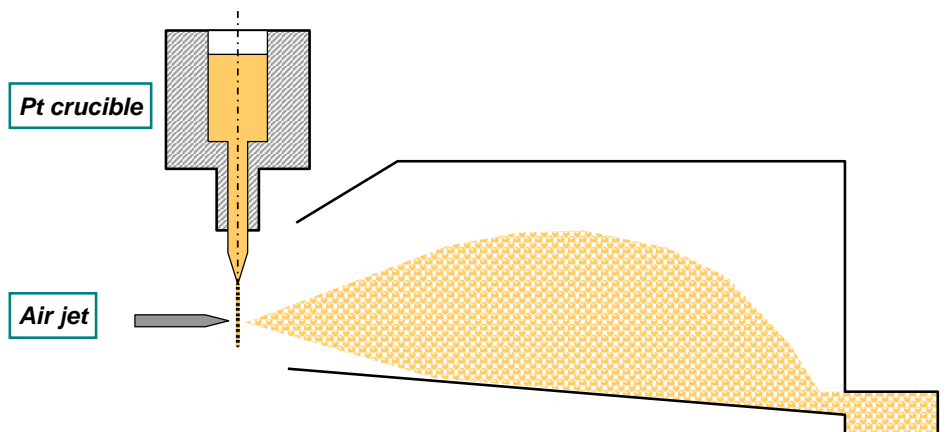
Air jet temperature / °C

Air jet pressure / bar

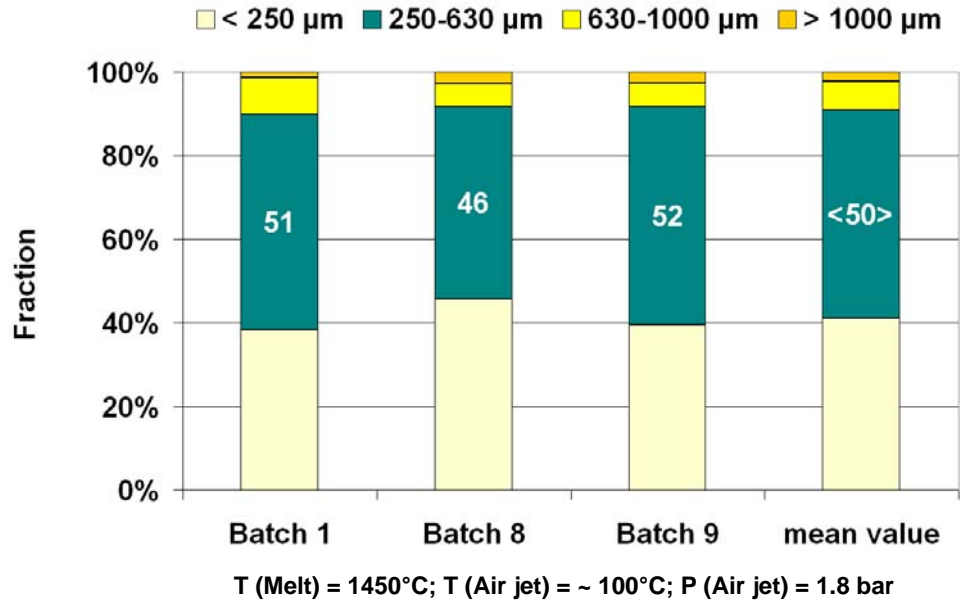
1350	1450	1550
~ 20	~ 100	
0.8	1.3	1.8
		2.4

“standard parameters“
for reference material

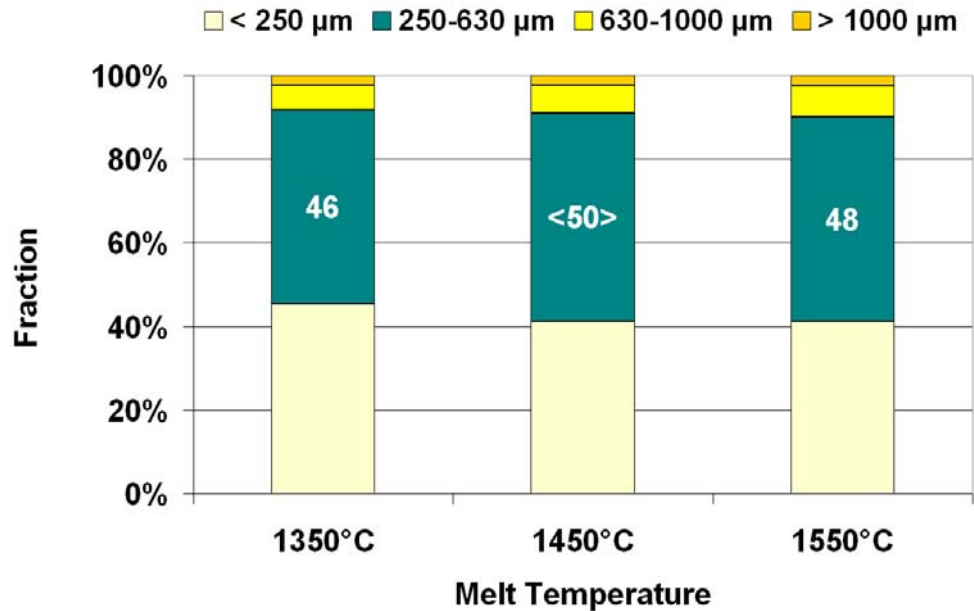
Process duration



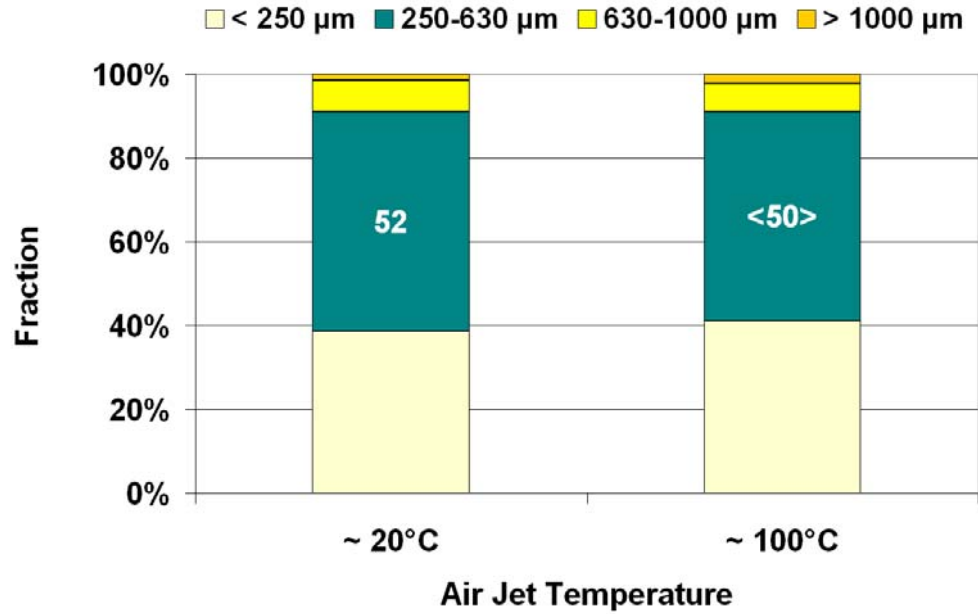
Yield of Reference Batches OSi 03/2



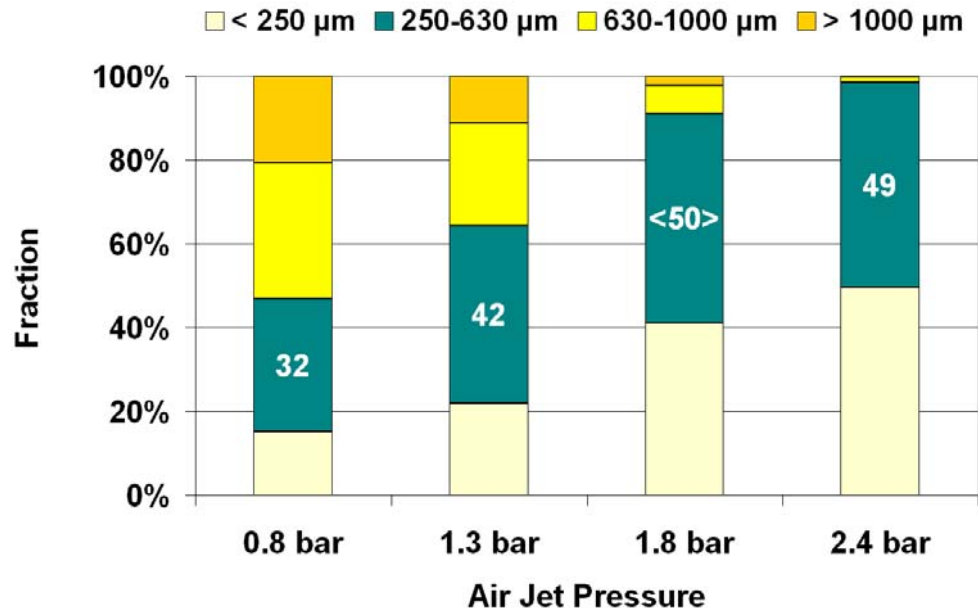
Influence of Melt Temperature on Yield



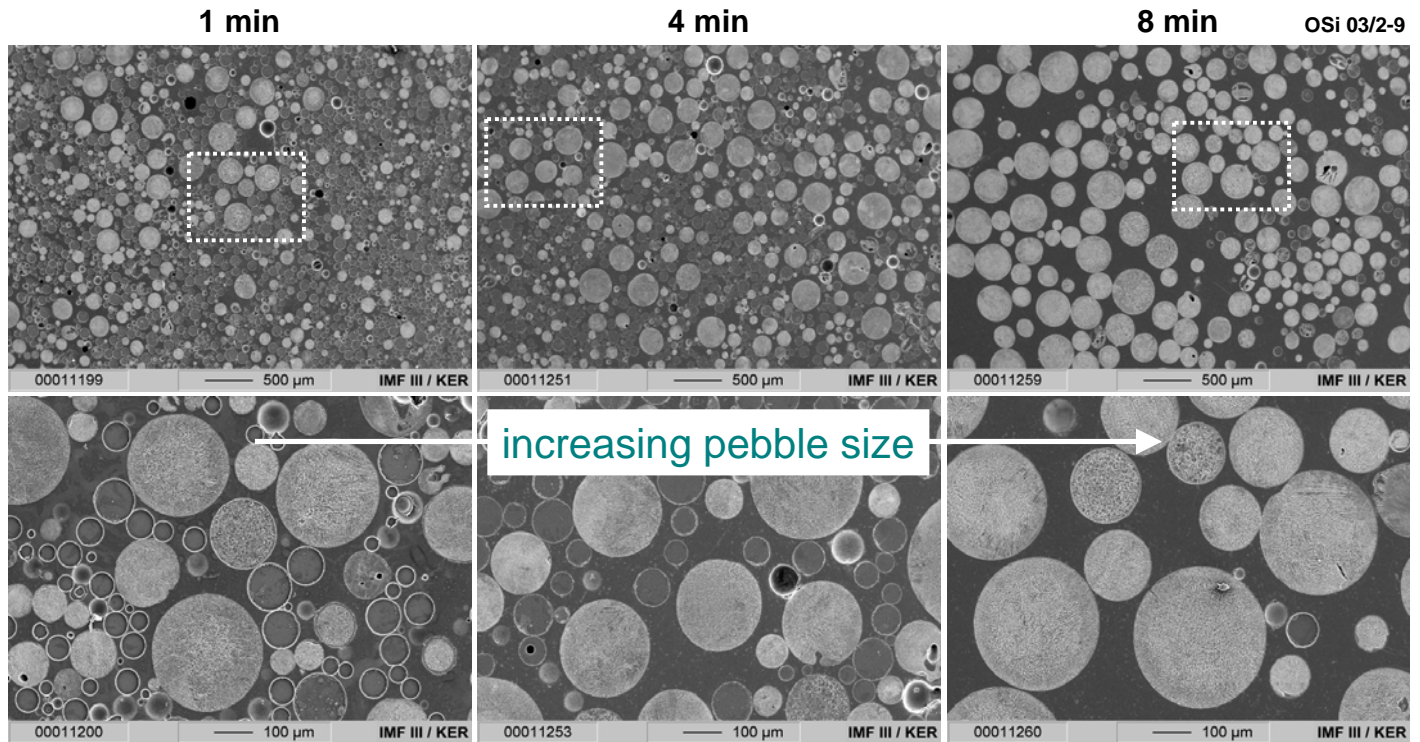
Influence of Air Jet Temperature on Yield



Influence of Air Jet Pressure on Yield



Influence of Process Duration



R. Knitter

CBBI-12, Sept. 16-17, 2004, Karlsruhe

IMF III / KER

Quality Control of Reference Material



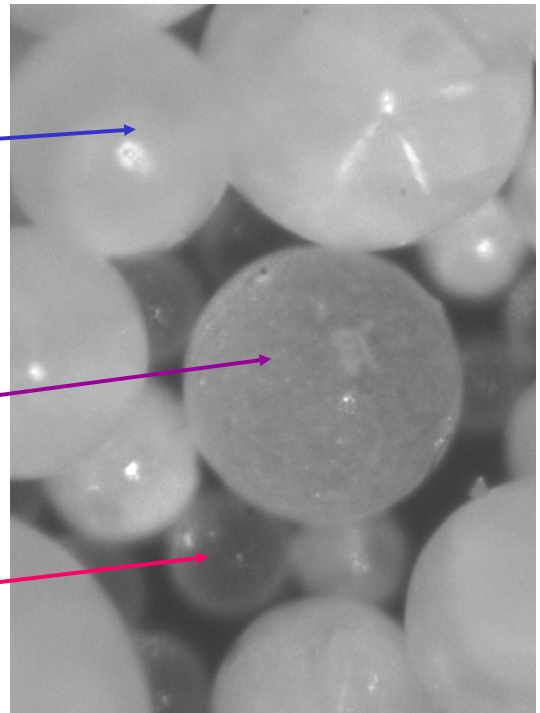
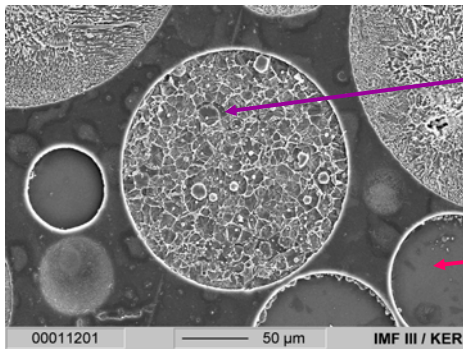
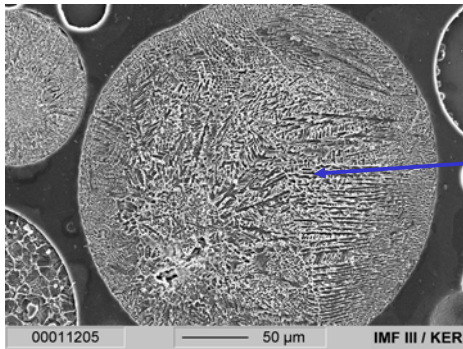
- **Microstructure**
- **Phase analysis**
- **Pebble size distribution**
- **Density and porosity**
- **Specific surface area**
- **Crush load**
- **Chemical analysis**

R. Knitter

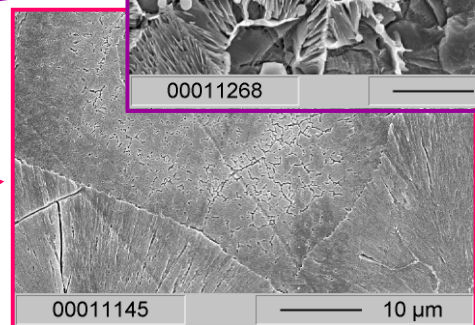
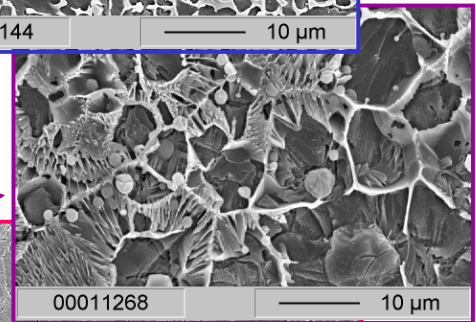
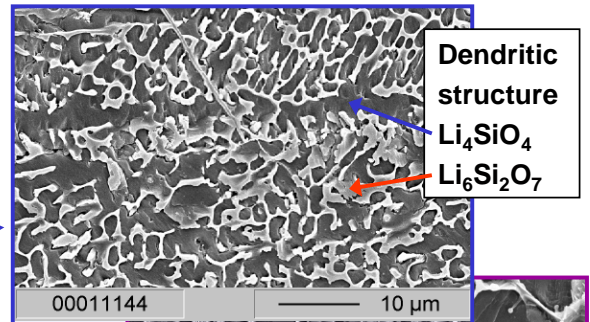
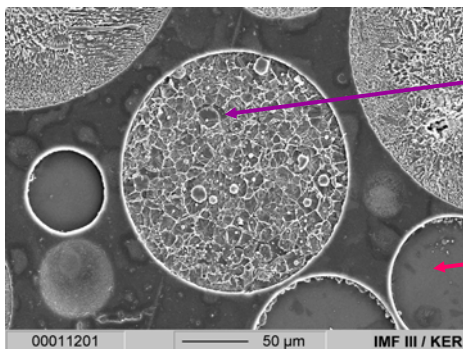
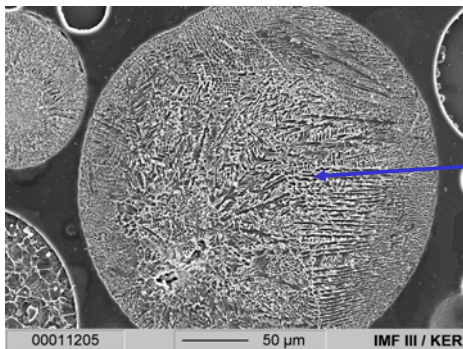
CBBI-12, Sept. 16-17, 2004, Karlsruhe

IMF III / KER

Microstructure

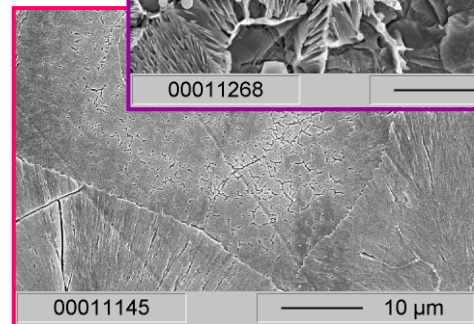
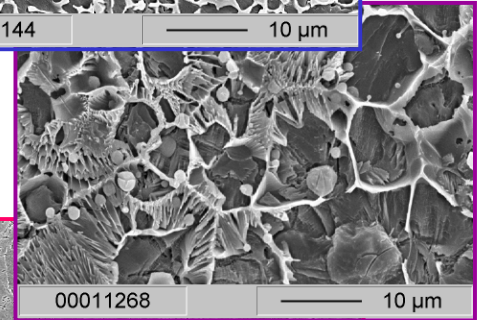
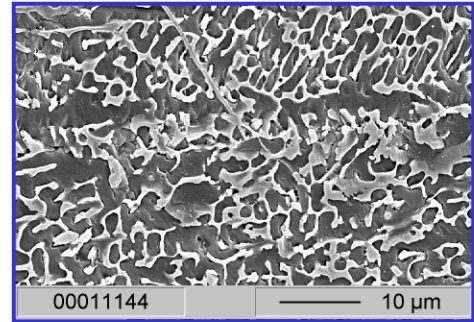
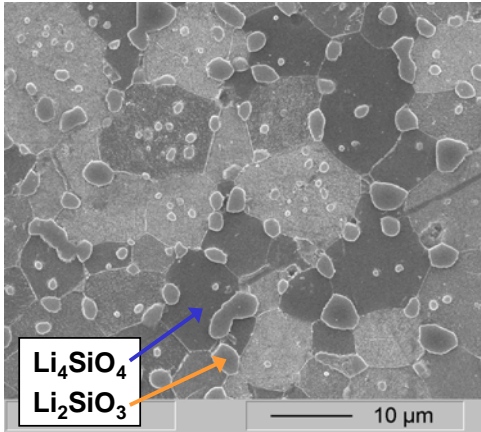


Microstructure



Microstructure

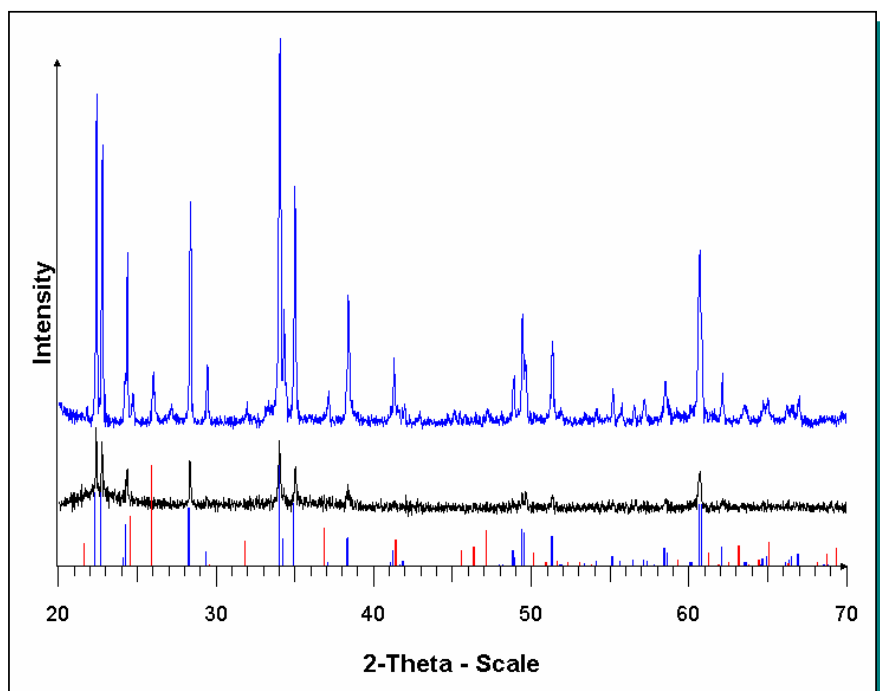
after annealing



X-Ray Powder Diffraction

OSi 03/2-9, large pebbles

OSi 03/2-9, small pebbles
(high amount of glassy pebbles)



X-Ray Powder Diffraction

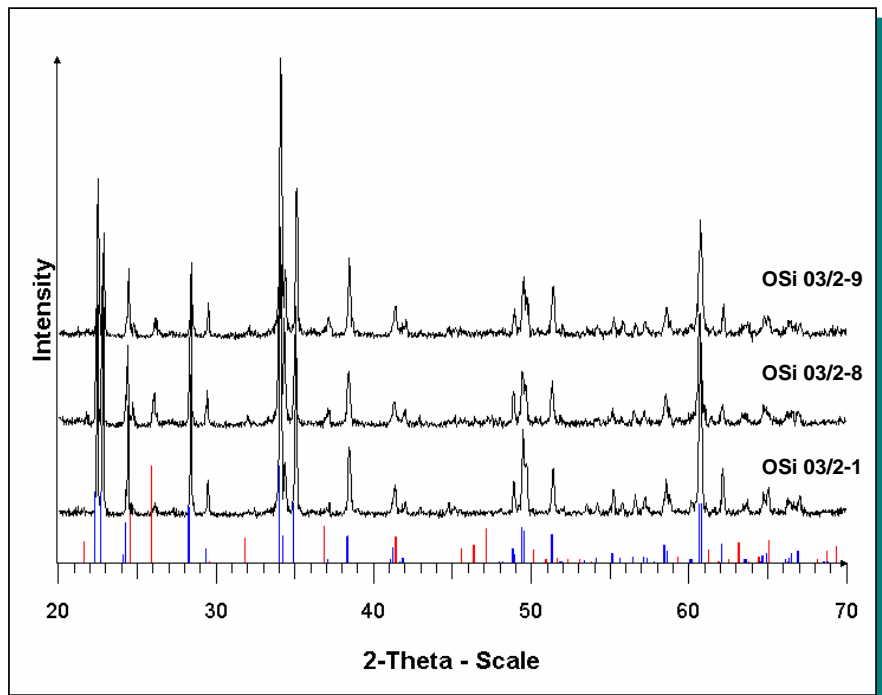
Phase analysis



+



(metastable HT-phase)



Chemical Analysis

Batch		OSi 03/2-1	OSi 03/2-8	OSi 03/2-9
Principal Constituents^(a)				
Li ₂ O	/ wt%	48.6 ± 0.1	48.1 ± 0.1	48.3 ± 0.1
SiO ₂	/ wt%	51.0 ± 0.1	51.6 ± 0.1	51.4 ± 0.1
excess SiO₂	/ wt%	2.16 ± 0.15	3.24 ± 0.06	2.85 ± 0.11
Impurities^(b)				
C	/ wt%	0.122 ± 0.001	0.117 ± 0.001	0.153 ± 0.005
Al	/ µg/g (≤ 60)	17.5 ± 0.5	15.2 ± 0.8	18.7 ± 0.2
Fe	/ µg/g (≤ 100)	3.4 ± 0.1	2.5 ± 0.05	2.8 ± 0.2
Zr	/ µg/g (≤ 70)	8.8 ± 1.7	4.8 ± 0.2	5.5 ± 0.8

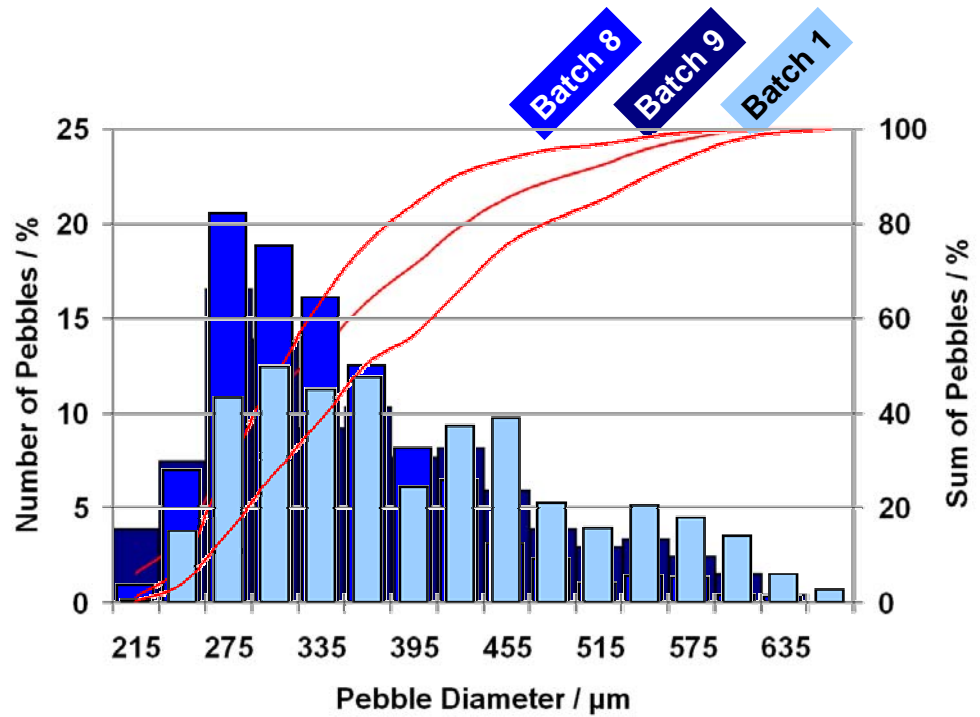
Pebble Size Distribution

OSi 03/2-

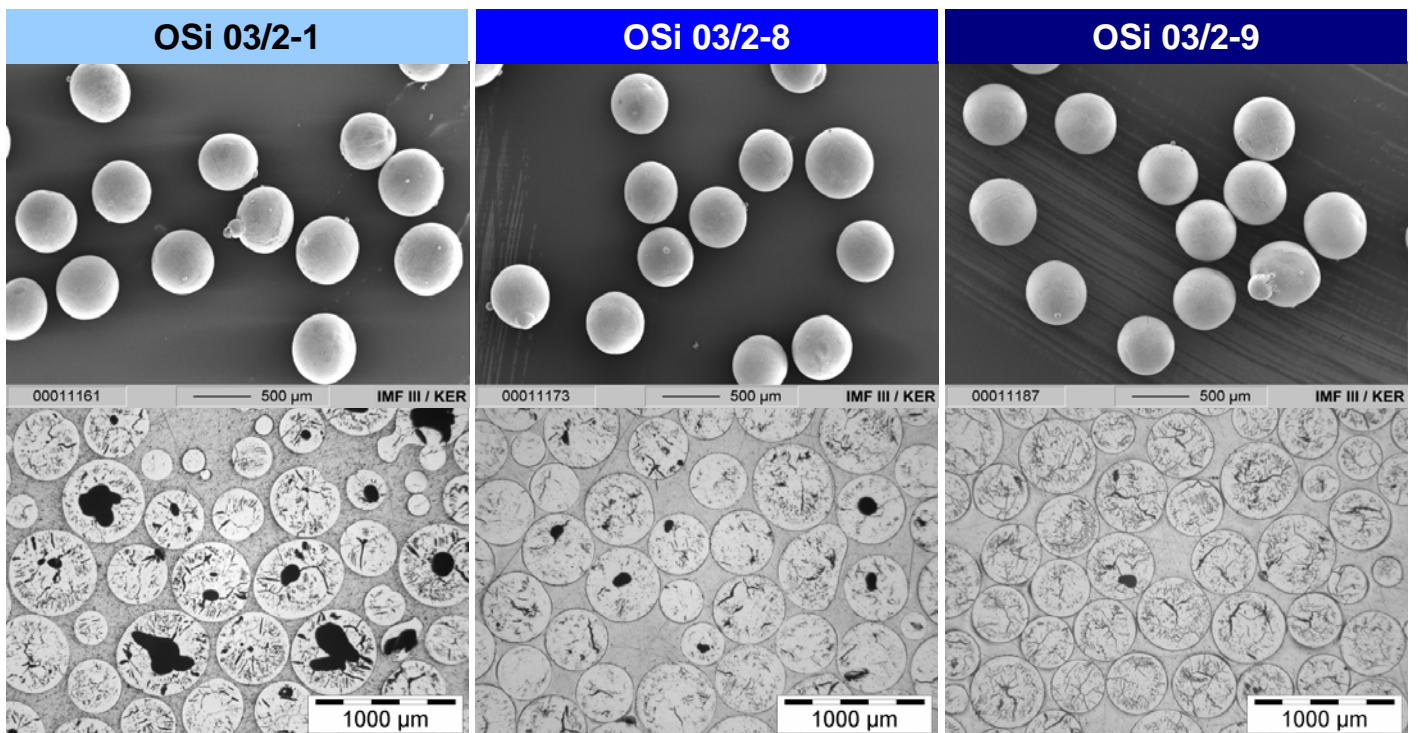
Batch 1 $d_{50} = 360 \mu\text{m}$

Batch 8 $d_{50} = 310 \mu\text{m}$

Batch 9 $d_{50} = 320 \mu\text{m}$



Microstructure



Density, Porosity and Specific Surface Area

Batch		OSi 03/2-1	OSi 03/2-8	OSi 03/2-9
He-pycnometry	inner density / g/cm ³	2.392	2.393	2.389
	closed porosity (calc.) / %	0.3 ± 0.1	0.3 ± 0.1	0.5 ± 0.1
Hg-porosimetry	density / g/cm ³	2.20 ± 0.04	2.25 ± 0.06	2.26 ± 0.02
	density / %	91.6 ± 1.5	93.7 ± 2.5	94.0 ± 0.8
	open porosity / %	6.7 ± 0.4	4.2 ± 0.7	5.2 ± 0.3
	inner density / g/cm ³	2.36 ± 0.03	2.35 ± 0.05	2.38 ± 0.02
	closed porosity (calc.) / %	1.8 ± 1.3	2.2 ± 2.0	0.9 ± 0.8
Specific surface area / m ² /g	0.11	0.13	0.09	

Crush Load

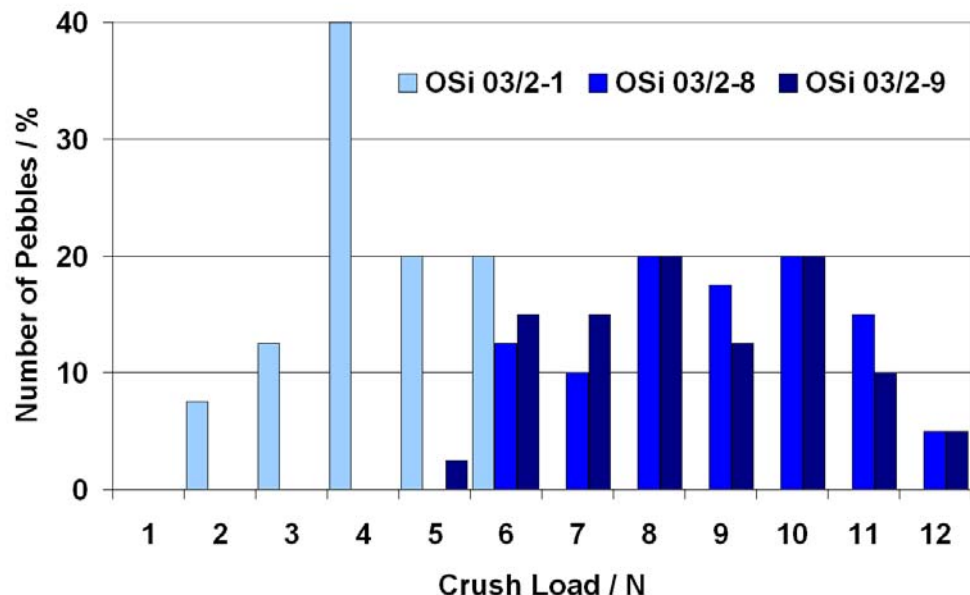
Pebble diameter 500 µm (dried at 300°C)

OSi 03/2-

Batch 1 4.3 ± 1.1 N

Batch 8 8.9 ± 1.8 N

Batch 9 8.5 ± 1.9 N



Conclusions

Fabrication of lithium orthosilicate pebbles in a melt-spraying process

- Yield**
- 50 % yield at standard process parameters for pebble sizes of 250 – 630 μm
 - air jet pressure has major influence on yield
 - pebble sizes vary during process duration
 - **will be increased by a continuous process**

- Reproducibility**
- limited control of the process
 - variations in batch properties
 - **will be improved by a continuous process**

- Advantages**
- material meets the specification of HCPB
 - single process for all required ^6Li enrichments
 - low impurities due to high-purity raw material
 - rejections and irradiated material can be recycled

CBBI-12 workshop
04. 9. 16. – 9.17. Karlsruhe, Ge

Preparation and Characterization of Li_2TiO_3 Pebble Using the Combustion Synthesis and the Dry-rolling Granulation Process

C.H. Jung, J.Y. Park*, W.-J. Kim, S.J. Lee[#], W.S. Ryu

Korea Atomic Energy Research Institute, Korea

[#] Mokpo National University, Korea

* jypark@kaeri.re.kr

Background (I)

Lithium titanate is one of the candidates for the solid breeder blanket for the D-T fusion reactor

Several synthesis methods of Li_2TiO_3 powder

- Solid State Reaction

$\text{Li}_2\text{CO}_3 + \text{TiO}_2 \rightarrow \text{Li}_2\text{TiO}_3 + \text{CO}_2$ (> 700°C calcination, milling step)

- Alkoxide Sol-Gel Process (Li and Ti-alkoxide, calcination step)

KAERI ; Combustion Synthesis Process (Li-salt and Ti salt + fuel)

Principle of the combustion process

- Self-propagating high temperature processing in a solution anionic oxidation-reduction method
- Using exothermic oxidation and reduction reaction between metal nitrates and fuels dissolved in water
- Precursor solution → heating → evaporation of water → self-ignition → production of powders
- A large amount of heat and large volume of gas produced in a short period of time → relatively 'soft' agglomerates

Advantages of the combustion process

- Very fine and homogeneous powder
- Easy control of stoichiometry
- Direct conversion from precursor solution to the final oxide product
- No formation of amorphous or intermediate crystalline phases
- Simple processing step
- Short time for completion of the process

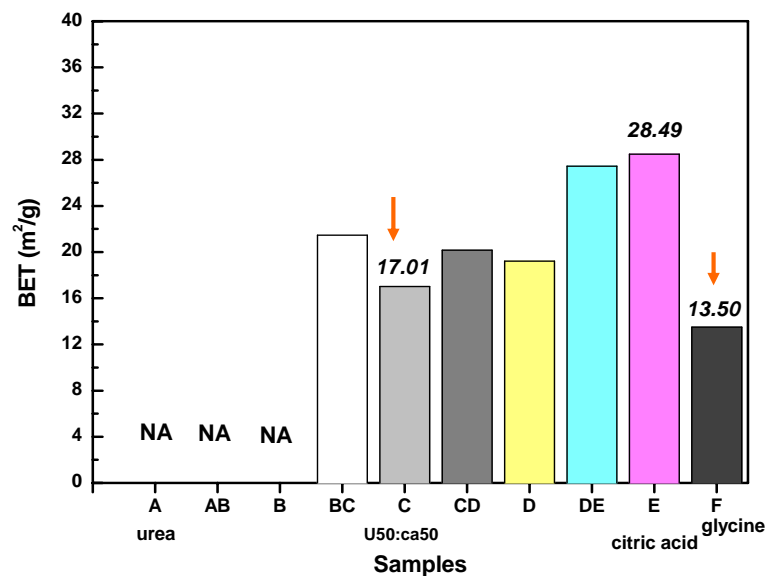
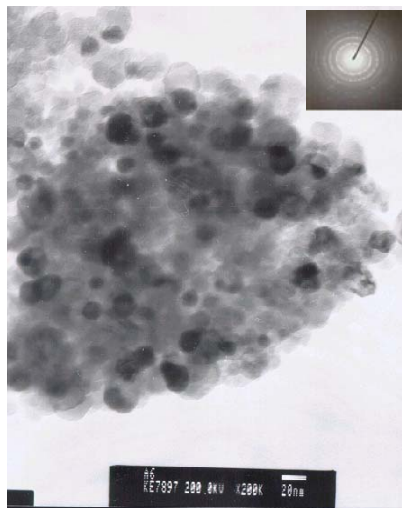


Combustion reaction

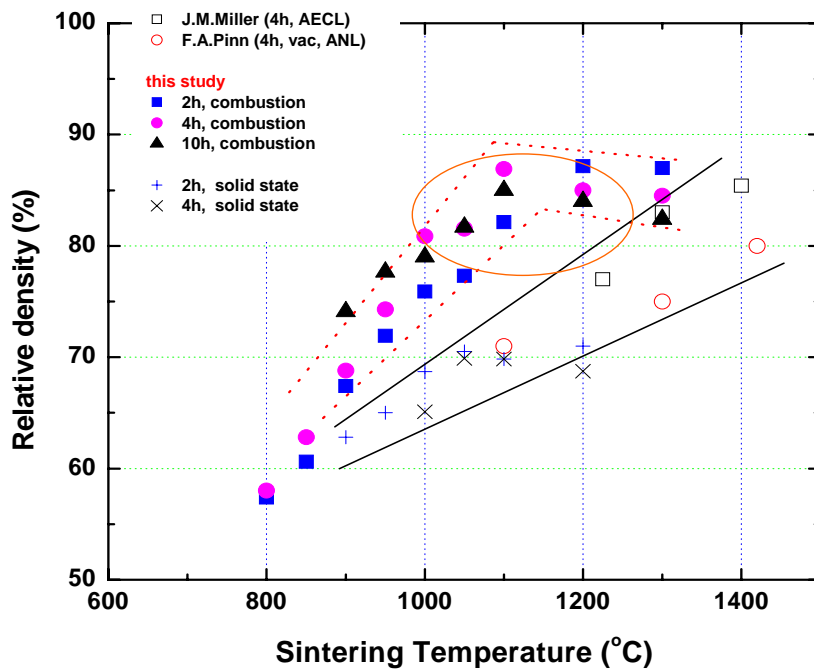
Effect of fuel types and compositions on the synthesis of Li_2TiO_3 powder

Composition of the fuel (mol) (based on 1mol of Li_2TiO_3)				Reactivity	Phase	Morphology & color
Sample	Urea	Citric acid	Glycine			
LT-A	10/3	-	-	No reaction (swelling)	Li_2CO_3 TiO_2 (anatase)	Cluster (yellow)
LT-B	8/3	2/9	-	No reaction (weak flame)	Li_2CO_3 TiO_2 (anatase)	Cluster (yellow)
LT-C	5/3	5/9	-	strong reaction	Li_2TiO_3	Powder (white)
LT-D	2/3	8/9	-	moderate reaction	Li_2TiO_3 (?) (impurity)	Powder (black gray)
LT-E		10/9	-	weak reaction	Li_2TiO_3 (?) (impurity)	Powder (black gray)
LT-F			20/9	very strong reaction	Li_2TiO_3	Powder (white)

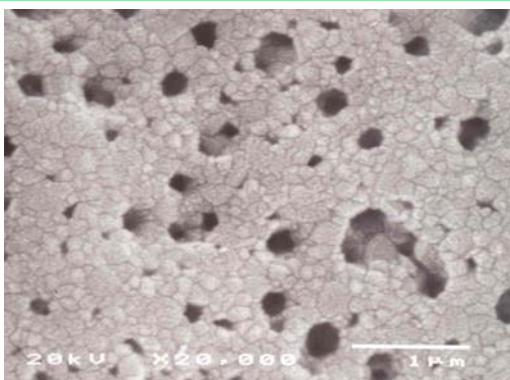
Microstructure and Specific Surface Area of Synthesized Li_2TiO_3 Powder by the Combustion Process



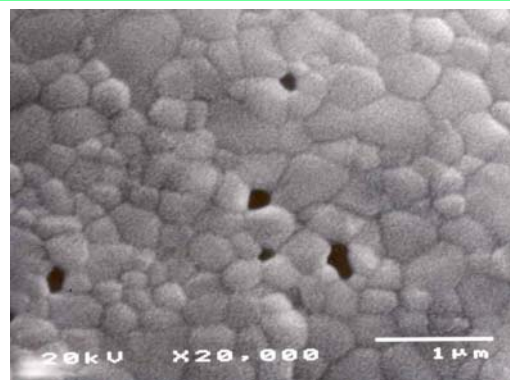
Sintered density of synthesized Li_2TiO_3 powder



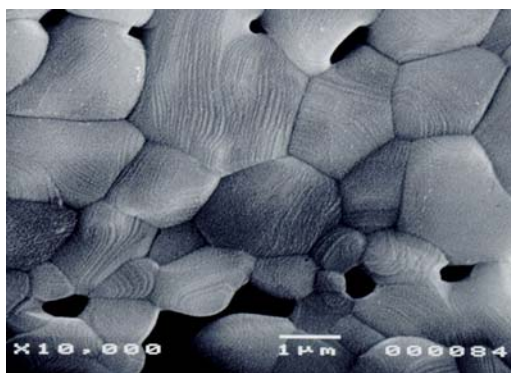
SEM micrographs of the sintered Li_2TiO_3 pellets using combustion synthesized powders



(A) 850°C



(B) 950°C



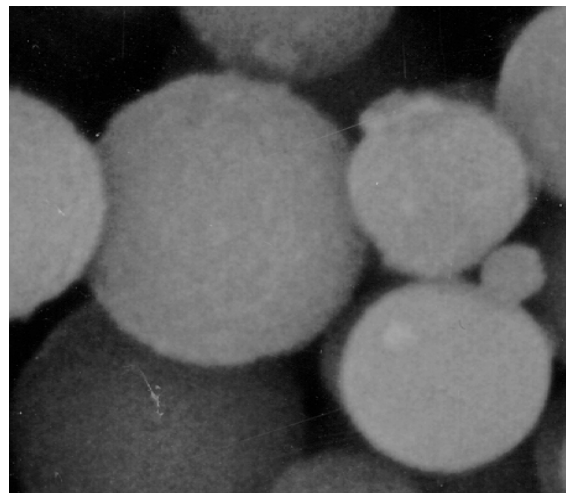
(C) 1000°C

Background (II)

Ultrasonic Mist Combustion Process (UMCP)

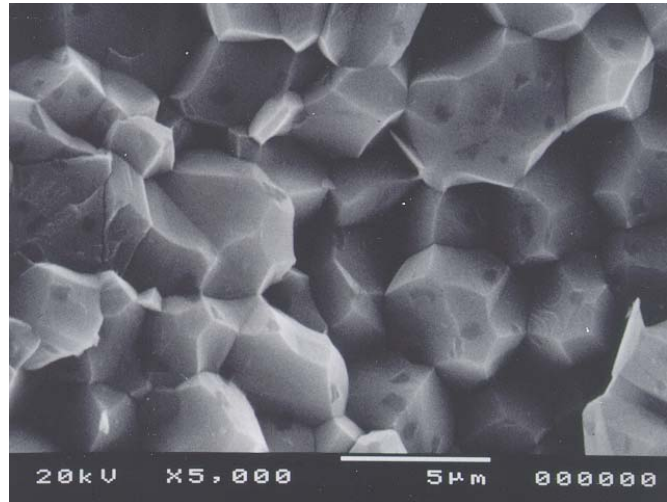
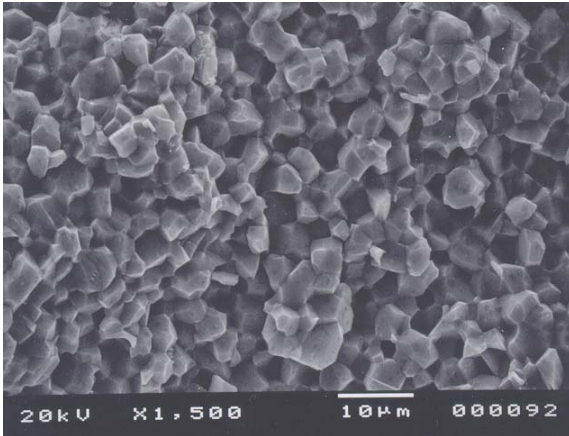
- **Spray Pyrolysis + Combustion Process**
- **Using ultrasonically generate mist to enhance the reactivity**
- **Continuous process**
- **Production of spherical powder**
- **Safe and economic process**

Microstructure of synthesized Li_2TiO_3 powder by the ultrasonic mist combustion process



Magnified photograph

Fracture surface of the sintered Li_2TiO_3 pellets prepared by ultrasonic mist combustion



1100°C, 2h, in air

Fabrication of Li_2TiO_3 Pebbles (KAERI)

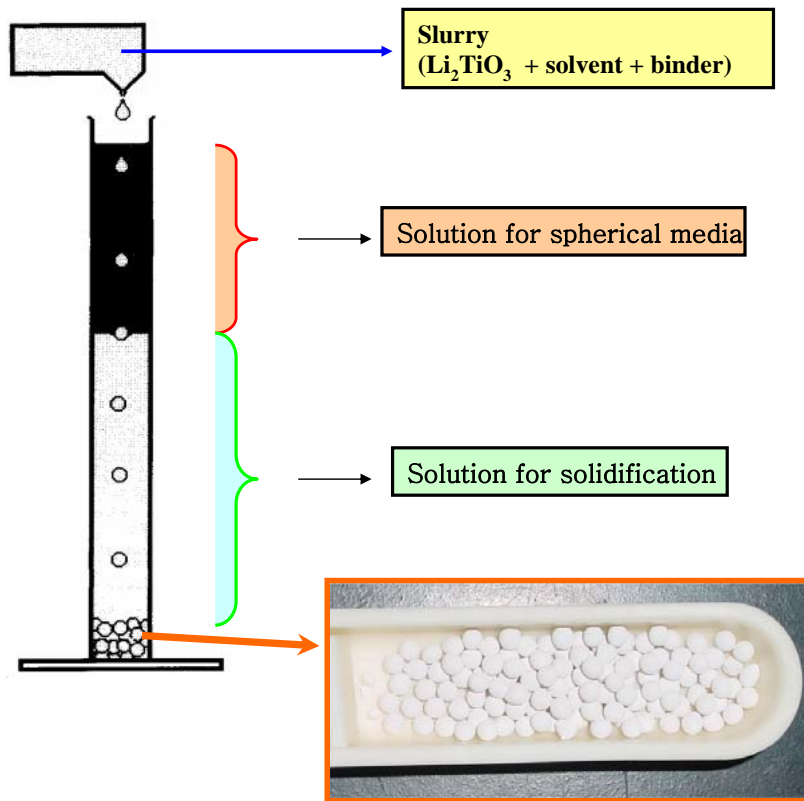
Reported Pebble Fabrication methods

- Wet process (sol-gel method) : JAERI
- Extrusion- Spheronisation-Sintering Process : CEA

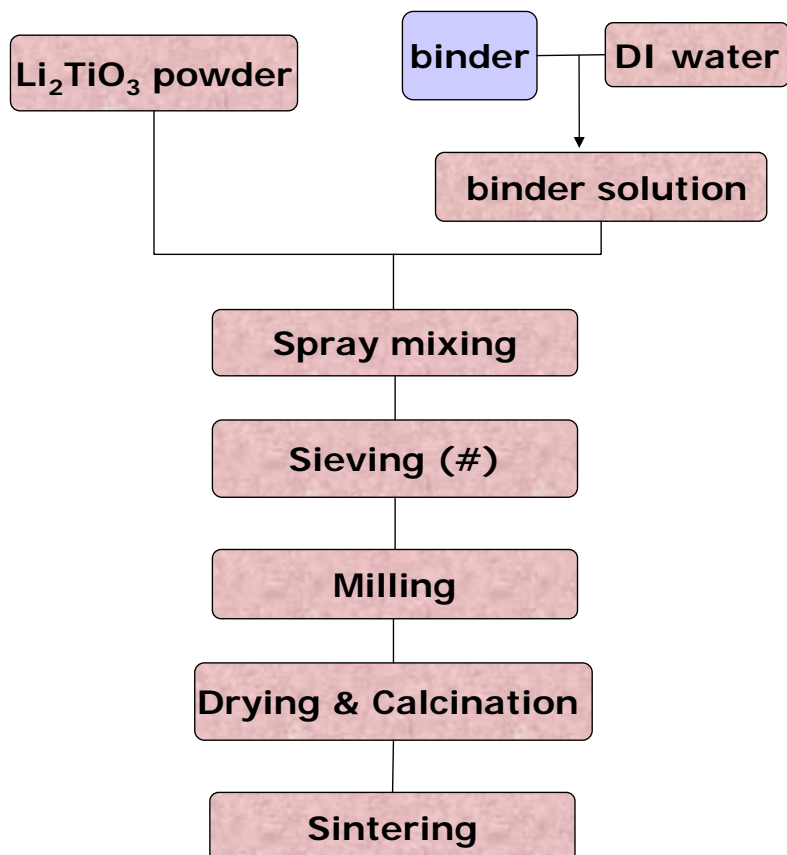
We have considered two processes for the fabrication of Li_2TiO_3 pebble ;

- Slurry Dropping –Sintering Process
- Dry-rolling Granulation – Sintering Process

Slurry dropping process

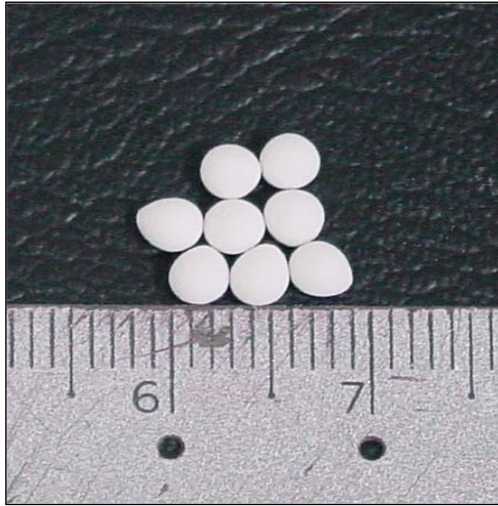


Dry-rolling granulation process

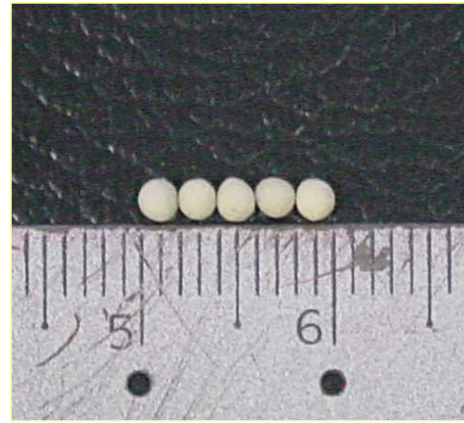


Preliminary Result (I)

Li_2TiO_3 pebbles using combustion synthesized powder and heat treated at 1200°C for 5h

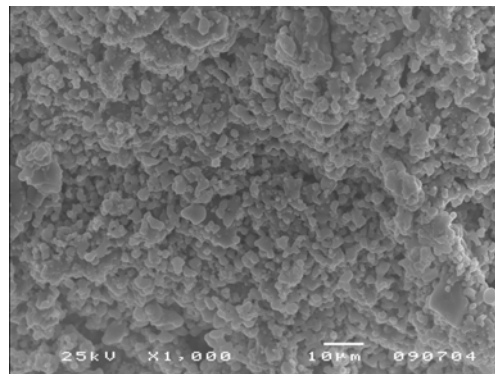
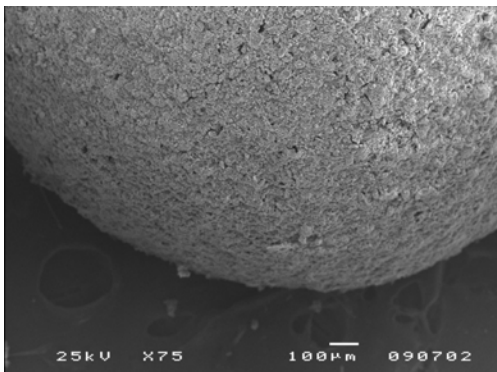


Slurry Dropping Process

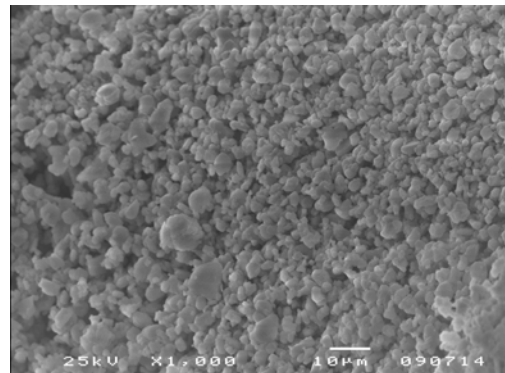
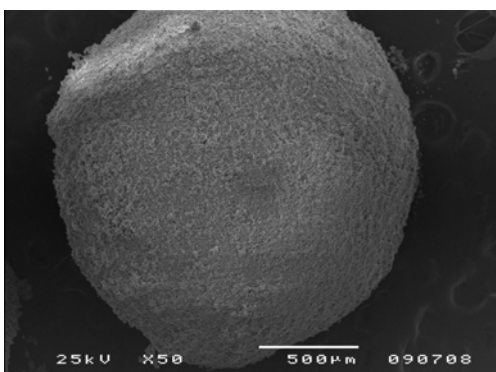


Dry-rolling granulation process

Preliminary Result (II)



Slurry dropping process



Dry-rolling granulation process

Summary & Future works

- Li_2TiO_3 powder with ultra-fine grains could be easily obtained by the combustion process.
- Spherical Li_2TiO_3 powders could be also made by the ultrasonic mist combustion process.
- The slurry dropping process and the dry-rolling granulation process are developing for the fabrication of Li_2TiO_3 pebbles.

- Future work
 - Optimization of both pebble fabrication methods
 - Evaluation of thermomechanical properties of pebble and pebble pac

5 Irradiation Testing

5.1 Behaviour of Blanket Ceramic Materials under Irradiation at High Temperature (P2)

G. Kizāne, J. Tīliks, A. Vītiņš and J. Tīliks Jr.

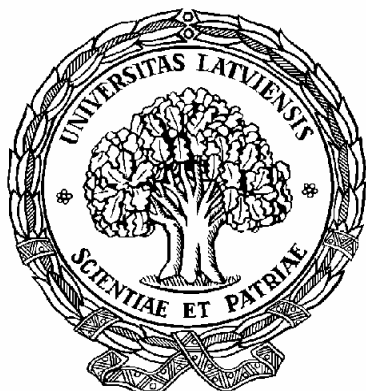
5.2 A High Fluence Irradiation of Ceramic Breeder Materials in HFR Petten, Test-matrix and Design of the Irradiation Capsule (P10)

J.B.J. Hegeman, J.G. van der Laan, S. Kamer, and S. de Groot

5.3 In Pile Behavior of the Pebble Bed Assemblies in the HFR, Results and First Data Analyses (P17)

A.J. Magielsen, J.G. van der Laan, J.H. Fokkens and M.P. Stijkel

Behaviour of blanket ceramic materials under irradiation at high temperature



Tel.: +371-7033883; fax: +371-7033884; e-mail: radchem@kfi.lu.lv

Gunta Kizāne, Juris Tīliks, Aigars Vītiņš, Juris Tīliks Jr.

Laboratory of Solid State Radiation Chemistry,
Department of Chemistry, University of Latvia,
Kronvalda bulvāris 4, LV-1010 Riga, Latvia

The breeding of tritium in HCPB is related to many complex physicochemical processes in the blanket ceramic materials. The simultaneous action of high temperature (600 – 850 °C), fast neutron radiation (up to $10^{19} \text{ n}\cdot\text{m}^{-2}\cdot\text{s}^{-1}$) and external magnetic field (6 – 9 T) affects the processes in the blanket ceramic materials. In order to predict the stability of the reference ceramic materials (Li_4SiO_4 and Li_2TiO_3 pebbles) during their long-term operation up to 20,000 hours under the DEMO relevant conditions, a long-time irradiation of these materials under high temperatures in high-flux fission reactors (e.g. HFR in Petten, the Netherlands) is carried out. However, the present irradiation technique does not enable in these experiments to apply an external magnetic field (MF) similar to that of the real HCPB conditions. The MF effect on several physicochemical processes (e.g. radiolysis) in ceramic materials has been proved experimentally [1, 2]. Evaluation of the MF effects on the tritium release, the corrosion of the ceramic materials with the structural materials, the tritium permeability, etc. requires further studies.

The stimulating MF effect on the formation of radiation-induced defects and products of radiolysis (e.g. colloid lithium), which can bind tritium, is significant up to 600 °C. There are no studies of this kind for the high-temperature (above 600 °C) radiolysis yet, where free oxides and O_2 can form.

In the middle nineties, MF was observed to affect the tritium release at thermoannealing of the Li_4SiO_4 ceramic pellets having a great grain size [3]. The delaying MF effect on the tritium release is related to lengthening of the diffusion path of charged tritium forms (T^+ , T^-) in the grain volume and is proportional to the grain size and to the MF intensity. Developing the manufacturing technology of the blanket ceramics, the grain size of the unirradiated ceramics is decreased to 1 – 10 μm . The MF effect on the tritium release

from the ceramics of this kind does not exceed 5-10%. However, the increase of the grain size can take place during a long-term radiolysis at a high temperature as it is characteristic for UO_2 ceramics [4]. One of the tasks of this study was to investigate the reference ceramic materials (Li_4SiO_4 and Li_2TiO_3 pebbles) after the thermal or radiation thermal treatment and the MF effect on the tritium release from the treated materials. The second task of this study was to investigate the MF effect on the tritium release at thermoannealing of the Li_4SiO_4 pebbles irradiated under the real conditions (the EXOTIC-8 experiment), where the structural changes have taken place in the pebbles. The Li_4SiO_4 pebbles irradiated in EXOTIC-8 were received in our laboratory in the end of 2003 with the assistance of EFDA (Dr. A. Cardella) and FZK (Dr. E. Rabaglino). The first results obtained in our laboratory about the irradiated Li_4SiO_4 pebbles were reported at the CBBI-11 workshop [2]. The results obtained point to the importance of the problem predicting the tritium release under the real DEMO conditions. The third task of this study was evaluation of the mutual corrosion of either of the two kinds of the reference ceramics (Li_4SiO_4 and Li_2TiO_3 pebbles) with EUROFER-97 under irradiation at a high temperature in MF. The experiment of this kind was performed for the first time and the results obtained should be considered as approximate. Assuming that the corrosion of this kind is based on the formation of soluble chemical compounds on the metal surface in the reactions between the metal and the radiolysis or thermolysis products (oxides, oxygen) of the ceramics, the parameters of surface roughness were used as the criteria. The roughness of surface was determined by atomic force microscopy (AFM). The results obtained characterise the initial stage of the chemical reaction and synergistic action of the external factors (temperature, radiation, MF).

References

1. J. Tiliks, S. Tanaka, G. Kizane, A. Supe, V. Grishmanov, A. Abramenkovs, and J. Tiliks Jr. Proc. Int. Workshop on CBBI – 5, Rome, Italy, (1996), 143.
2. G. Kizane, J. Tiliks, A. Vitiņš, E. Kolodinska. Proc. Int. Workshop on CBBI – 11, December 15-17, 2003, Tokyo, Japan / Ed. M. Enoeda, JAERI-Conf 2004-012, July 2004, 120-129 pp.
3. J. Tiliks, G. Kizane, A. Abramenkovs, J. Tiliks Jr., V. Grishmanov, A. Ozols, and V. Vasilyev. Proc. of 17th SOFT, Rome, Italy, v. 1, (1992), 1528.
4. J. Robertson et al. Proc. 2th Inter. Symp. IAEA, Geneva, 1959, 464.
5. G. Kizane, J. Tiliks, A. Vitiņš, J. Rudzitis, J. Nucl. Mater. 329-333 (2004) 1287.

1. High-temperature electron irradiation of the ceramic pebbles

Task - to test the influence of the temperature, high-temperature irradiation on the grain size changes, the influence of the MF on the T release from the treated ceramics.

Samples

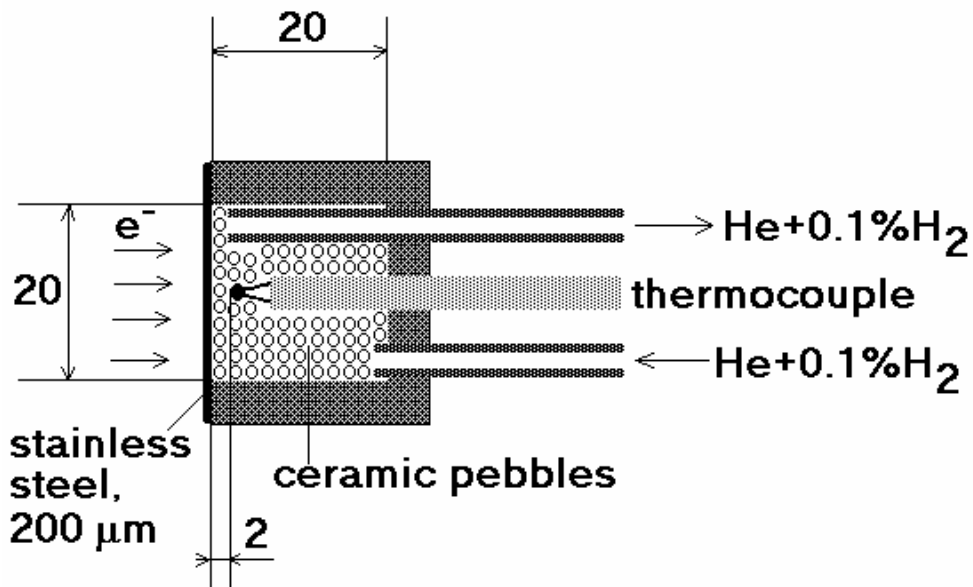
Material	Manufacturer	Batch code	Li-6, %	Grain size, μm	Pebble \varnothing , mm
Li_4SiO_4	FZK	00/2-3	20	10-15	0.25-0.63
Li_2TiO_3	CEA	CTI4C2Ti/100	7.5 (nat.)	1-3	1

Irradiation

Fast electrons ($E=5\text{ MeV}$), $P=80\text{-}100\text{ MGy}\cdot\text{h}^{-1}$, to the absorbed dose $1000\text{-}1200\text{ MGy}$ ($10\text{-}14\text{ h}$), maximum free path $2.55\text{ g}\cdot\text{cm}^{-2}$.

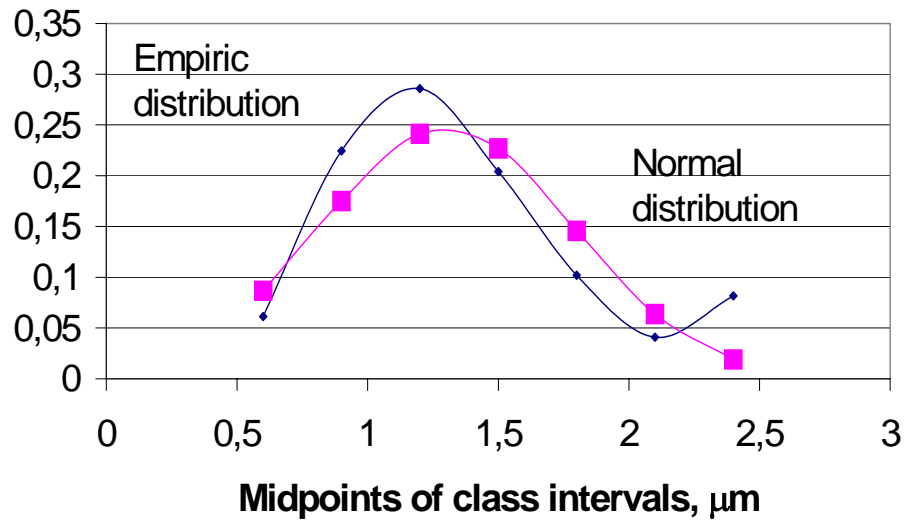
The temperature: $600\text{-}1000\text{ }^\circ\text{C}$. The gas flow: $\text{He} + 0.1\% \text{H}_2$. The treated samples were marked by tritium in the photoneutron source up to $2\cdot 10^{17}\text{ n}\cdot\text{m}^{-2}$.

Container (dimensions in mm).

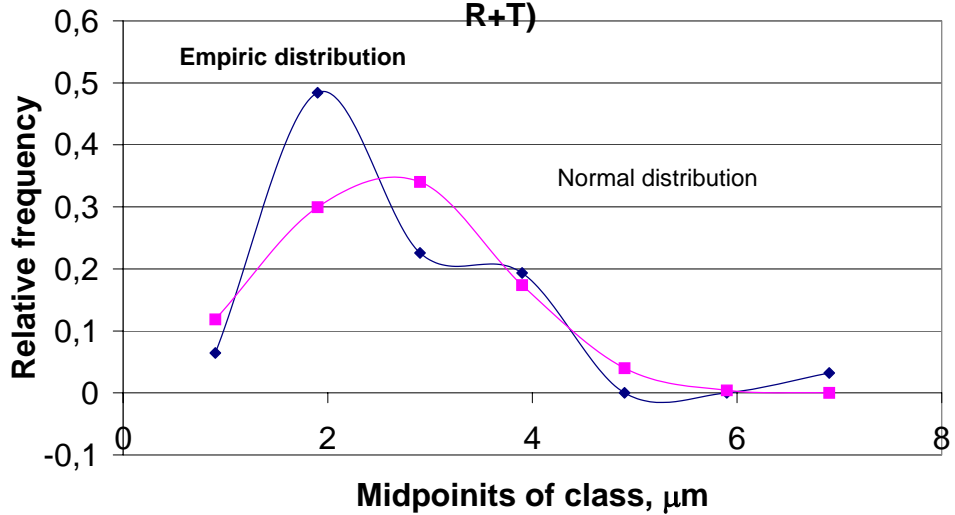


Analysis – structure of the etched and polished samples were investigated by SEM method, the T release parameters were obtained by isothermal annealing at a fixed temperature.

Distribution of the grain size for Li_2TiO_3 (before treatment)



Distribution of the grain size for Li_2TiO_3 (after R+T)



High temperature treatment of reference materials

Ceramics	Treatment	Time, h	T, °C	D, MGy	Average grain parameters		Grain characterisation	Composition	T, °C	(D/r ²).10 ⁶ , s ⁻¹	
					Grain size, μm	Layer thickness, μm				B=0 T	B=2.4, T
Li ₂ TiO ₃ (CEA) CTI 4C2Ti/100, natural Li-6 content	-	-	-	-	1-3	0.4	Lamellar structure, some grain boundaries appeared partly, pores both on grain boundaries and in grains	Li ₂ TiO ₃ + 5 wt. % TiO ₂	290	11.5	10
	thermal	12	970	-	3-5	0,4		Did not change	290	9.5	9.1
	radiation thermal	12	970	1200	3-7	1.2		Did not change	290	9.0	8.2
	-	-	-	-	-	10-15	-	Dendrite	Li ₄ SiO ₄ + 2wt. % SiO ₂ , some Li ₆ Si ₂ O ₇ , no Li ₂ SiO ₃	245	8.4
Li ₄ SiO ₄ (FZK) 00/2-3, 20 % enrichment Li-6	thermal	15	930	-	15-20	-	Irregular blocks, micro cracks	Decreased Li ₆ Si ₂ O ₇ , SiO ₂ content did not change	245	8.0	7.5
	radiation thermal	15	930	1100	20-25	-	Irregular micro increased	SiO ₂ content increases to 5-6 wt.%, some Li ₂ SiO ₃	245	7.8	7.4

CONCLUSIONS (1)

1. The following changes take place in the Li_4SiO_4 and Li_2TiO_3 ceramic pebbles at high temperature radiolysis ($T = 600\text{-}1000^\circ\text{C}$, $D = 1200 \text{ MGy}$):
 - The increase in the grain size was observed at the temperature above 900°C : from $10\text{-}15 \mu\text{m}$ to $20\text{-}25 \mu\text{m}$ in Li_4SiO_4 ,
from $1\text{-}3 \mu\text{m}$ to $5\text{-}7 \mu\text{m}$ in Li_2TiO_3 ,
 - Localisation of metastable radiation-induced defects in the ceramics investigated was observed only at the temperature below 600°C .
 - Products of radiolysis, SiO_2 (up to 7 %) and Li_2SiO_3 , form in Li_4SiO_4 at the dose 1200 MGy. Increasing the SiO_2 content decreases the melting point Li_4SiO_4 .
 - No changes in the composition were observed in the Li_2TiO_3 ceramics after the absorbed dose 1200 MGy at 1000°C .
2. The delay in the tritium release in the external magnetic field (2.4 T) from the samples radiolysed ($D=1200 \text{ MGy}$) at high temperature ($> 900^\circ\text{C}$) is within 10-15 %. That corresponds with a little increase in grain size.

2. Influence of the MF on the T release in the thermoannealing process from the Li_4SiO_4 pebbles irradiated in the EXOTIC-8 experiment

Task – to test the influence of the different MF intensity on the T release, to estimate the chemical form distribution of the tritium and the changes of the grain size

Material

The $\text{Li}_4\text{SiO}_4 + 1.4 \text{ wt.}\% \text{ SiO}_2$ (^6Li 50%). FZK – 42/93-2.

The pebbles have been fabricated by a melting-spraying method.

The pebble size: $\varnothing 0.25\text{-}0.63 \text{ mm}$.

The admixtures (wt.%): C – 0.358, Al – 0.068, Co - $<5 \cdot 10^{-4}$, Zn – $1.5 \cdot 10^3$.

The treatment before the irradiation: 1000°C , 2 weeks in air, 1 week in He.

The average crush load: before the irradiation – 5.66 N, after the irradiation – 7.23 N.

The characterisation of grains: a dendritic structure, length – approx. $100 \mu\text{m}$, width – approx. $20 \mu\text{m}$.

The irradiation: the years 1998-2001, HFR, Petten, the Netherlands, 18 FRC.

$\Phi_{\text{thermal}}=4.6 \cdot 10^{24} \text{ n} \cdot \text{m}^{-2}$, $\Phi_{>0.1 \text{ MeV}}=2.8 \cdot 10^{25} \text{ n} \cdot \text{m}^{-2}$, $T_{\text{irrad}}=640 \text{ }^\circ\text{C}$, Li burn-up – 11%, the atmosphere – He + 0.1% H₂.

The tritium activity: $1.9 \text{ GBq} \cdot \text{g}^{-1}$.

The activity of admixtures: $28 \text{ kBq} \cdot \text{g}^{-1}$.

Analysis - tritium release was investigated in the magnetic thermoannealing rig ($\beta = 2.5 \text{ K min}^{-1}$). The distribution of the tritium chemical forms was obtained by dissolving pebbles in the presence of the different acceptors. Tritium in the gaseous phase was measured by a proportional gas flow counter THM-2, in the liquid phase by liquid scintillation method.

Lyomethod for distribution the tritium chemical forms in Li₄SiO₄ pebbles.

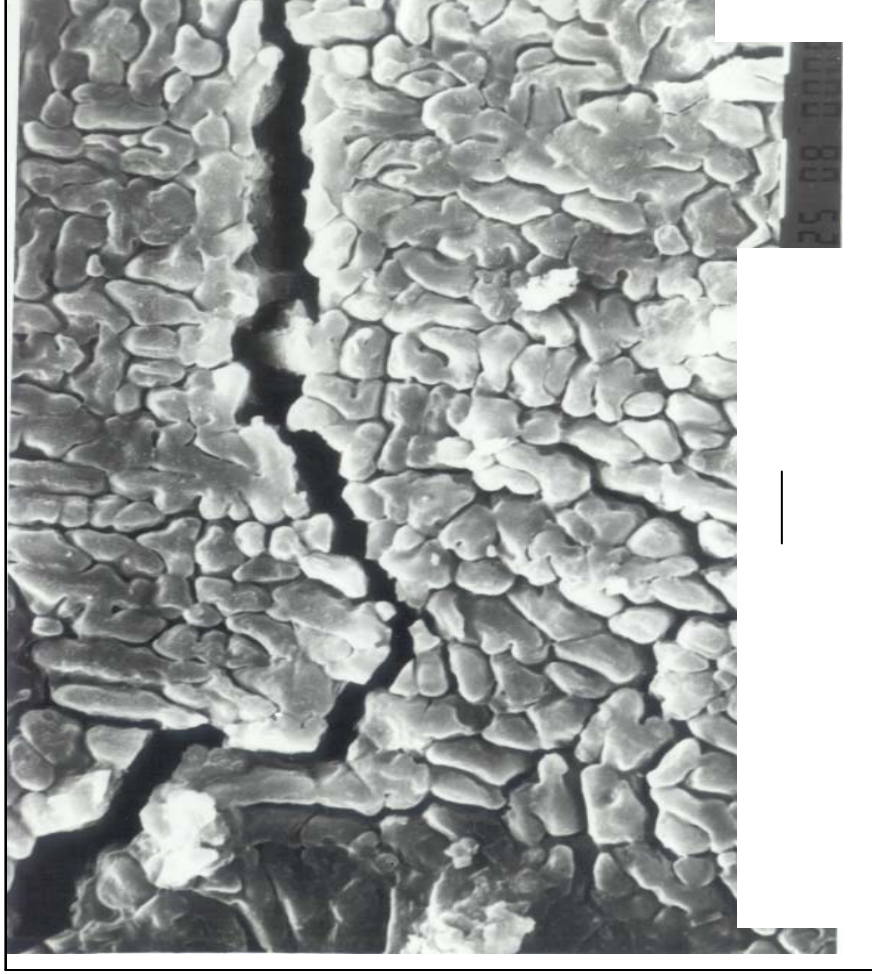
Lyosystem	T ₂ (HT)	T ⁺	T ⁰	T ⁻
Acid (0.4 M H ₂ SO ₄)	T ₂ (g)	T ⁺ (s)	T ⁰ +T ⁰ →T ₂ (g)	T ⁻ +H ⁺ →HT(g)
Acid + Ac	T ₂ (g)	T ⁺ (s)	T ⁰ +Ac→T ⁺ (s)	T ⁻ +Ac→T ⁺ (s)

T activity: g – in gaseous phase; s –in solution.

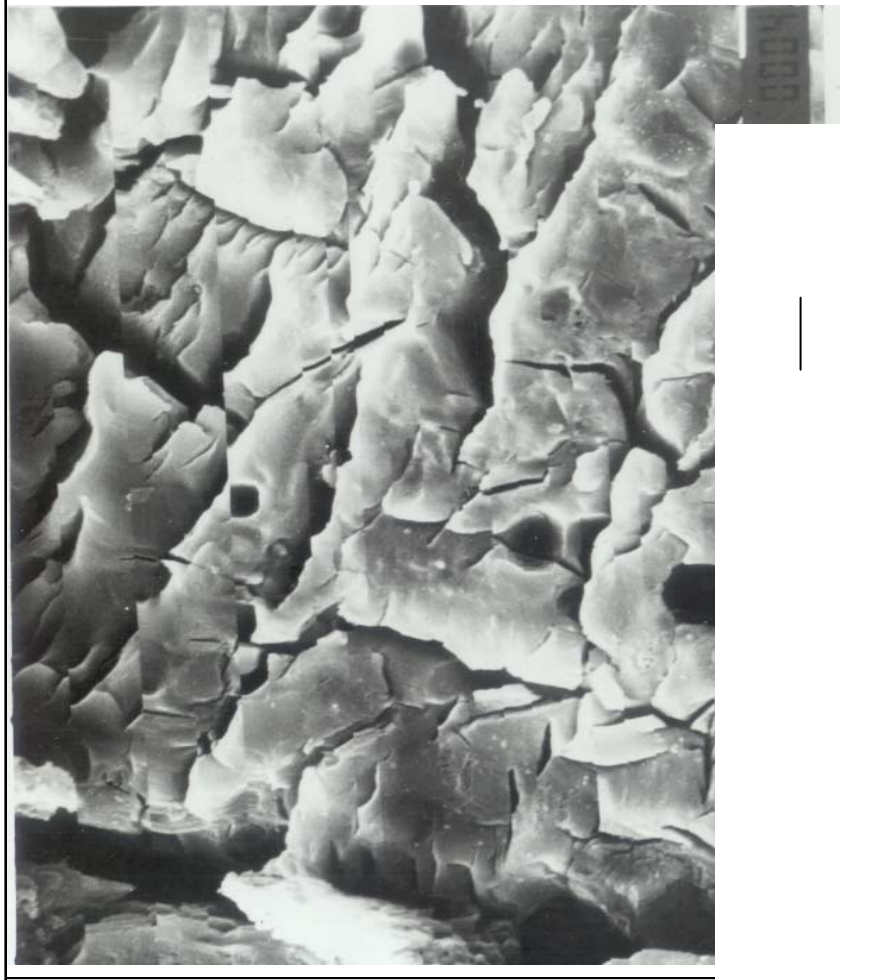
Ac – acceptors – may be used 0.1 M Ag⁺, Cr₂O₇²⁻, MnO₄⁻, NO₃⁻.

Irradiation and its conditions	Fractions of T forms, %			
	T ⁺ (OT ⁻)	T ⁻ (LiT)	T ⁰	T ₂ (HT)
Irradiated only with neutrons to 10^{17} n m^{-2} at RT	100	-	-	-
Irradiated with electrons (5 MeV) to 1000 MGy at 1100 K, after that with neutrons to $5 \cdot 10^{17} \text{ n m}^{-2}$ at RT	95±2	2±1	-	3±1
Irradiated with neutrons (> 1 MeV) to $2.4 \cdot 10^{25} \text{ n} \cdot \text{m}^{-2}$ in HFR (EXOTIC -8) at 900 K:				
➤ before thermoannealing	86±3	2±1	-	3±1
➤ after thermoannealing to 770 K without MF	75 ±5	5 ±2	-	20 ±2
➤ after thermoannealing to 770 K with MF (2,35 T)	65 ±5	8 ±2	-	27 ±2

The structure of grain size in the Li_4SiO_4 (FZK) pebbles by SEM method.

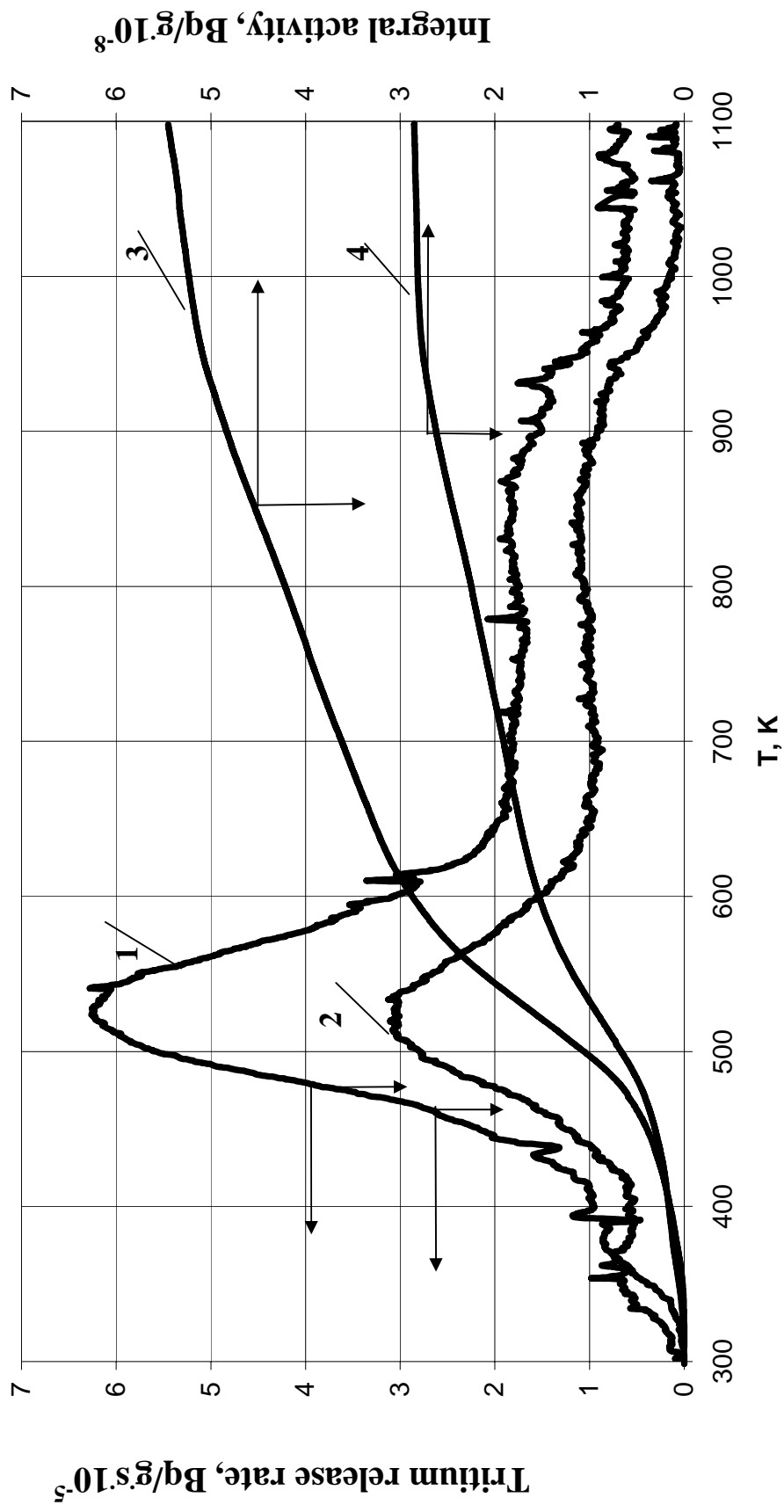


Before irradiation, 5 μm



After irradiation in the HFR Petten
(EXOTIC 8), $\Phi = 2.4 \cdot 10^{25} \text{ n. m}^{-2}$, 5 μm

Tritium release from strong irradiated Li₄SiO₄ pebbles (EXOTIC 8/8 experiments) in thermoannealing process (b= 2,7 K min⁻¹, purge gas -He +0,1 % H₂ : 1,3 without MF; 2,4 in MF 2.34 T



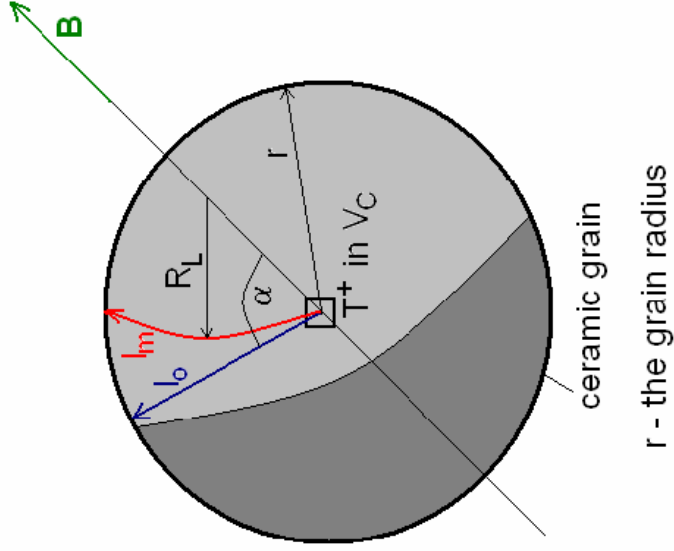
Scheme and formulae to simulate the effect of magnetic field on the volume diffusion of T^+ .

$$F = F_D + F_K \quad F_D = F_{D0} + F_{DM}$$

$$F_D = 6 \cdot \left(\frac{D \cdot t}{\pi \cdot l_0^2} \right)^{\frac{1}{2}} - 3 \cdot \frac{D \cdot t}{r^2}, \text{ for } F_D \leq 0.95$$

$$F_D = \frac{6}{\sqrt{\pi}} \cdot \sqrt{\frac{D}{l_0^2}} \cdot \sqrt{t}, \text{ for } F_D < 0.3$$

$$R_L = \frac{m \cdot v \cdot \sin \alpha}{e \cdot B}$$



CONCLUSIONS (2)

1. The following changes were observed in Li_4SiO_4 as a result of the neutron irradiation, $\Phi \approx 10^{25} \text{ n}\cdot\text{m}^{-2}$, at a high temperature (640 °C) in the EXOTIC-8 experiment:
 - increase of the grain size to 25-40 μm ;
 - formation of microcracks and closed pores in the volume of a pebble;
 - localised tritium concentrating in subsurface layer of a pebble (thickness up to 50 μm) – that correlates with the localisation of radiation-induced defects;
 - formation of tritium molecular forms (T_2 , HT) and tritide ions (T^-) up to 20%.
2. The tritium release from these samples at thermoannealing in the magnetic field appears as:
 - delay in the tritium release, the delay is proportional to the squared magnetic field intensity;
 - the magnetic field does not change the temperatures of maximum release rates and the activation energies;
 - increase in the abundance of tritium molecular forms at thermoannealing in the magnetic field.
3. The results obtained confirm the previous hypothesis about the role of magnetic field on the diffusion path of charged tritium forms in the grain volume and testify that the material produced in FZK can be operated under the ITER and DEMO conditions.

3. The mutual corrosion of the ceramic and structural materials under the action of temperature, radiation and magnetic field

Task –to test the process of the interface reactions under the influence of the temperature, radiation and MF between ceramics and metal.

Samples: Sandwich-type layer of the ceramics and the metal pressed under 3-5 $\text{kg}\cdot\text{cm}^{-2}$.

The metal – polished EUROFER plates 5×5 mm.

The ceramics – the reference Li_4SiO_4 (FZK) or Li_2TiO_3 (CEA) pebbles crushed into powder of the particle size approx. 50 μm .

Treatment: The temperature (T) – 650 °C.

The radiation (R) – fast electrons ($E=5 \text{ MeV}$), $P=10 \text{ MGy}\cdot\text{h}^{-1}$, $D=100 \text{ MGy}$.

The magnetic field (M) – 1.5 T.

The atmosphere – He + 0.1% H₂.

The treatment time – 10 h.

Chemical treatment: 30 min in 50 °C 20% hydrazine chloride solution, then in ethanol, drying.

Surface analysis: Atomic force microscopy (AFM).

The investigated area (M×N) – 100 μm².

The number of points in a line – 256.

Evaluation Roughness Parameters

1. **Roughness Average (DIN 4768), nm**

$$S_a = \frac{1}{MN} \sum_{k=0}^{M-1} \sum_{l=0}^{N-1} |z(x_k, y_l) - \mu|$$

$$\mu = \frac{1}{MN} \sum_{k=0}^{M-1} \sum_{l=0}^{N-1} z(x_k, y_l)$$

2. **Root Mean Square (ISO 4287/1), nm**

$$S_q = \sqrt{\frac{1}{MN} \sum_{k=0}^{M-1} \sum_{l=0}^{N-1} [z(x_k, y_l) - \mu]^2}$$

3. **Ten Point Height (ANSI B.46.1), nm**

$$S_z = \frac{\sum_{i=1}^5 (z_{pi} - \mu) + \sum_{i=1}^5 (z_{vi} - \mu)}{5}$$

The characterisation of the EUROFER-97 surface roughness, after T, R, M treatment in contact with ceramics

Ceramics	Treatment ^{a)}	S _a , nm	S _q , nm	S _z , nm
Metal	-----	11,7	15,6	104
Li ₄ SiO ₄	T	10,9	14,8	171
	T+M	12,4	19,1	214
	T+R	15,6	22,2	231
	T+M+R	20,0	28,0	300
Li ₂ TiO ₃	T	13,8	17,6	135
	T+M	12,6	16,3	127
	T+R	11,6	15,4	140
	T+M+R	18,6	27,4	269

a) – T - high temperature; M – magnetic field; R – radiation.

CONCLUSIONS (3)

1. A solid-state reaction takes place between the EUROFER-97 metal and the ceramics (Li_4SiO_4 or Li_2TiO_3) under high-temperature conditions. Nonuniform transition of the metal into reaction products was observed as a result of the reaction.
2. The dose of electron irradiation (100 MGy) increases the efficiency of this process only in the case of Li_4SiO_4 , but it has little effect in the case of Li_2TiO_3 .
3. The external magnetic field (1.5 T) facilitates the solid-state reaction in both the cases of Li_4SiO_4 and Li_2TiO_3 .
4. The processes at the metal-ceramics interface speed up considerably under the combined action of all the external factors (temperature, radiation, magnetic field) in both the cases of Li_4SiO_4 and Li_2TiO_3 .

A high fluence irradiation of ceramic breeder materials in HFR Petten, test-matrix and design of the irradiation capsule.

Hans Hegeman, Jaap van der Laan , Sander de Groot, Sander Kamer and Boudewijn Pijlgroms

CBBI-12, Karlsruhe, 2004

E-mail: hegeman@nrg-nl.com

HH1

Participants

- R. Conrad* JRC/IE, Petten, NL
- S. Kamer, M.A.G. Ooijevaar, B.J. Pijlgroms, M.P. Stijkel, S de Groot, L. Magielsen NRG Petten, NL
- L.V. Boccaccini, R. Knitter, J. Reimann FZK Karlsruhe, D
- J.D. Lulewicz CEA Saclay, F
- H. Kawamura JAERI, JA
- A.Y. Ying UCLA, USA

Outline

- Introduction
- Design of the high dose irradiation
 - Pebble-stacks & rig
 - Behaviour neutron shield
 - Ex-core section and out-of-pile instrumentation
- Material characterisations & test matrix
- Status

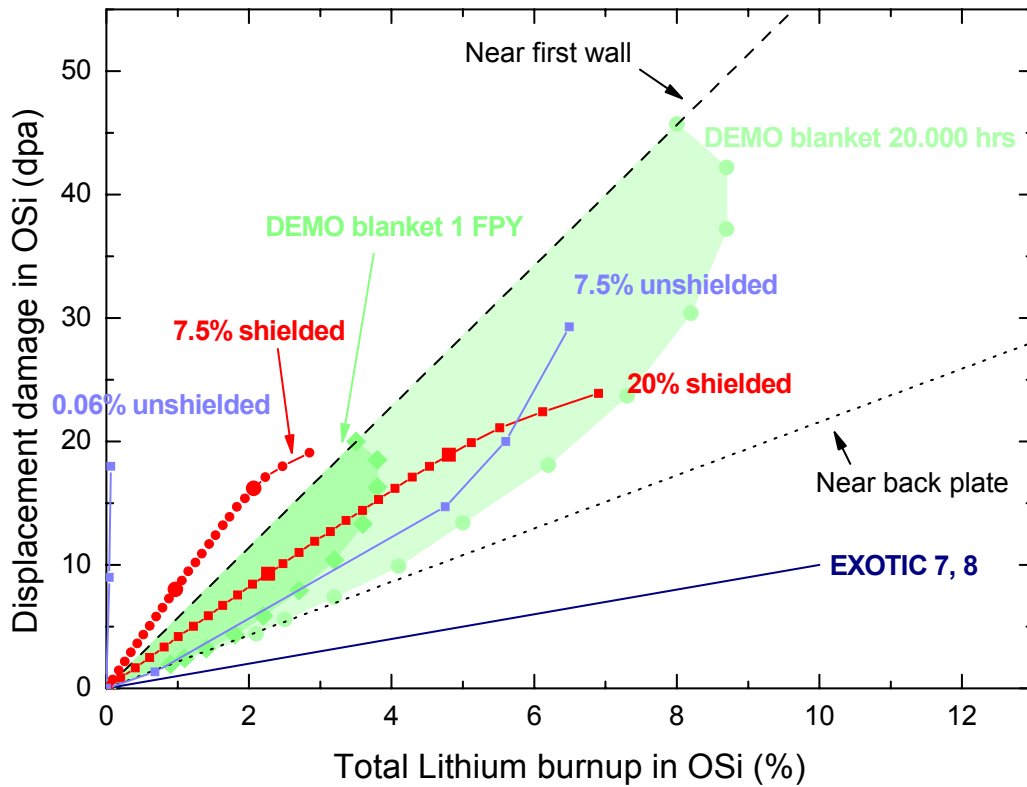
HH 3

Introduction

- **HICU test objective:**
“Investigation of
 - a) the impact of neutron spectrum and
 - b) the influence of constraint conditionson the thermo-mechanical behavior of breeder pebble-beds in a high fluence irradiation”
- The HICU project is part of the EFDA technology program for development of the HCPB concept. It has been adopted as subtask G within the IEA agreement on Fusion Nuclear Technology.

HH 4

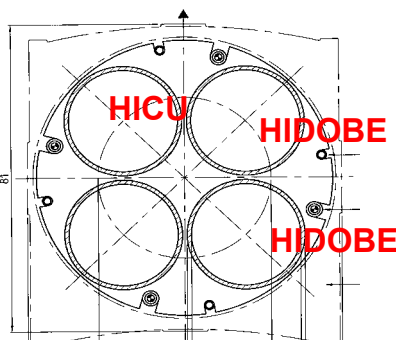
Burnup and displacement damage



HH 5

Irradiation

- Irradiation in HFR positions E/C-3/7 in a Quattro channel (diameter about 29 mm and about 400 mm total stack height)
- High reactivity by ^6Li , Cd and steel structure effects reactor operation scheme



Position shared with High Dose Be

		A	B	C	D	E	F	G	H	I
POOL SIDE FACILITY WEST	1	Be	Be	Be	Be	Be	Be	Be	Be	1 Be
	2	F	F	F	D2	F	F2	F	H2	2 Be
	3	F	F	C3	F	E3	F	G3	F	3 Be
	4	F	CR	F	CR	F	CR	F	H4	4 Be
	5	F	F	C5	F	E5	F	G5	F	5 Be
	6	F	CR	F	CR	F	CR	F	H6	6 Be
	7	F	F	C7	F	E7	F	G7	F	7 Be
	8	F	F	F	D8	F	F8	F	H8	8 Be
	9	Be	Be	Be	Be	Be	Be	Be	Be	9 Be

F Fuel element

CR Control rod

Be Reflectorelement

C5 Experiment position

HH 6

Irradiation parameters

- Lithium isotope compositions and spectrum tailoring measures are chosen so as to obtain in DEMO relevant dpa/burnup-ratios (~6 dpa/%) as well as (using higher ^6Li -enrichment) - DEMO relevant burn-ups (10-15 %).

	HICU
Fluence ($E > 0.1 \text{ MeV } 10^{26} \text{ n/m}^2$)	1.5
Fluence ($E > 1 \text{ MeV } 10^{26} \text{ n/m}^2$)	0.7
^6Li enrichments Li_4SiO_4 (%)	0.06, 7.5, 20
^6Li enrichments Li_2TiO_3 (%)	0.06, 11, 30
^6Li Burnup (%)	0.74 - 13
Neutron damage (dpa)	20-25
Temperatures ($^{\circ}\text{C}$)	600-650 750-800

HH 7

Design S(ev)olutions

- Complexity of the design due to:
 - High reactivity of the cadmium shield inside the HFR core
 - * Behaviour like an control rod (shield for thermal neutrons)
 - * Additional safety measures required
 - Low melting point of cadmium ($231 \text{ }^{\circ}\text{C}$) versus
 - * high expansion coefficient and 5 vol% expansion at melting
 - * High power densities inside capsule due to enriched materials
 - * Early burnup of cadmium leads to power increase and accelerated ^6Li burnup
 - * Manufacturing shield and containments without gas-gaps
 - Maximisation of pebble bed diameter to be representative
 - Optimising cladding to avoid chemical interaction, but achieve low attenuation factors to enable X-ray tomography
 - Limited space for instrumentation,
 - * but accurate estimation of temperatures required.
 - * Influence thermocouple on pebble stacking

HH 8

Design S(ev)olutions (2)

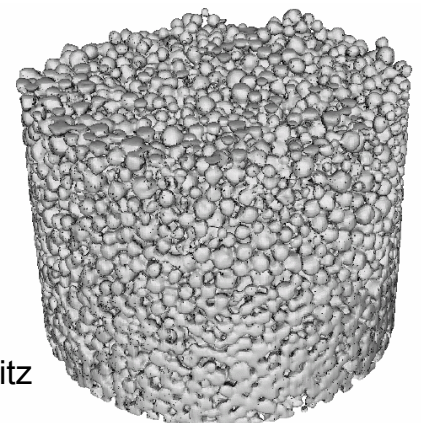
• Design solutions:

- High reactivity of the cadmium → Proposal submitted to the HFR safety committee
- Low melting point of cadmium (231°C) →
 - * Accommodate free expansion volume for Cd
 - * very small gas-gaps (80 µm) inside the capsule holder, only allow He purge gas in 2nd containment
 - * 2 fabrication routes currently investigated: explosive welding (perfect bond between containment and shield) and isostatic pressing, thermography (FzJ) will be employed to check the thermal resistance
 - * thickness Cadmium shield optimised using Hf wire and detailed nuclear analysis (MCNP)
- Maximisation of pebble bed diameter → maximum determined by thermal analysis and space $\sim \varnothing_{in} = 9 \text{ mm}$

HH 9

Design S(ev)olutions (3)

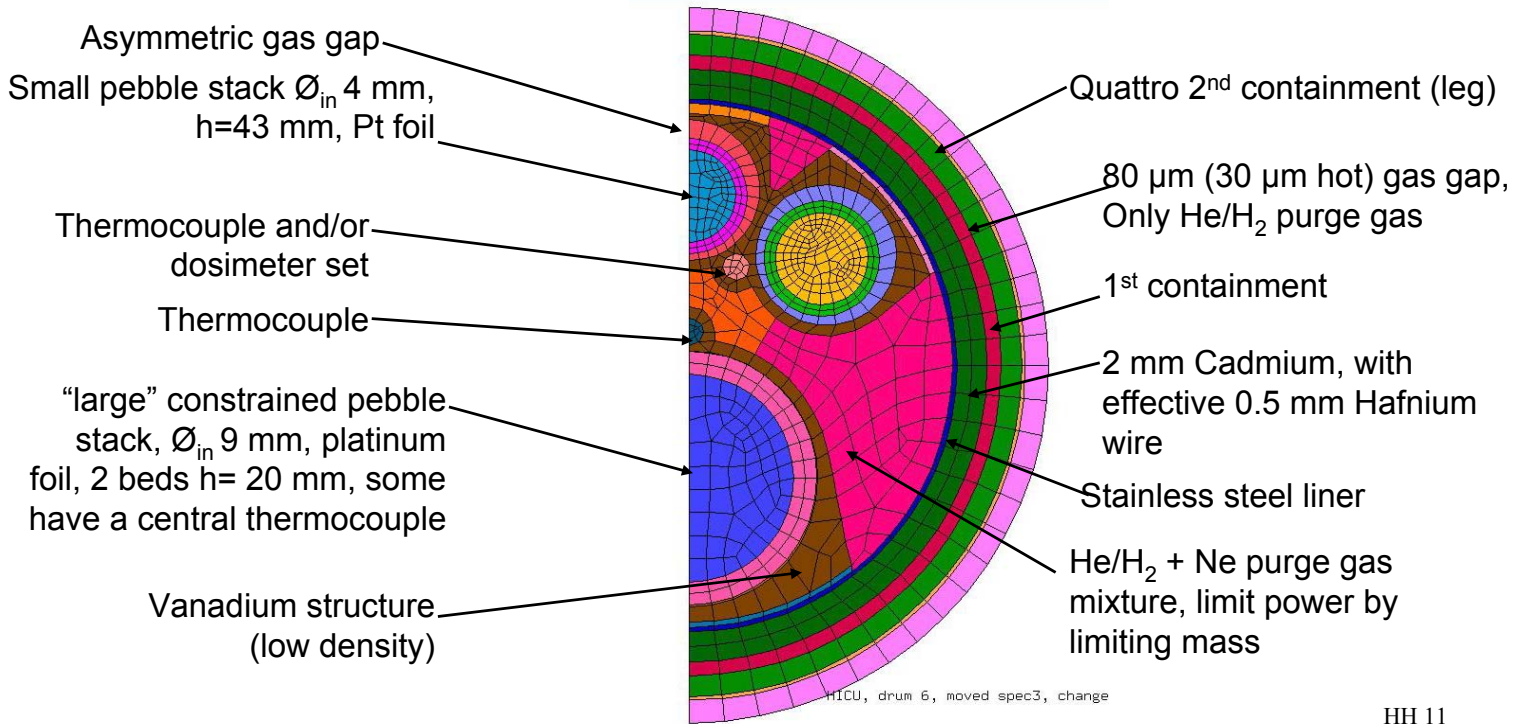
- Optimising cladding to avoid chemical interaction
 - * 0.05 mm Pt foil could be used, despite the low contrast of X-ray tomography images, pebble locations could be determined (R. Pieritz)
- Limited space for instrumentation
 - * Temperature measured at cladding (detailed thermal analysis should yield the actual temperatures)
 - * In some cases, pebble beds are equipped with a central thermocouple in addition to a on the cladding, tomography will help to interpret the measured thermal gradients



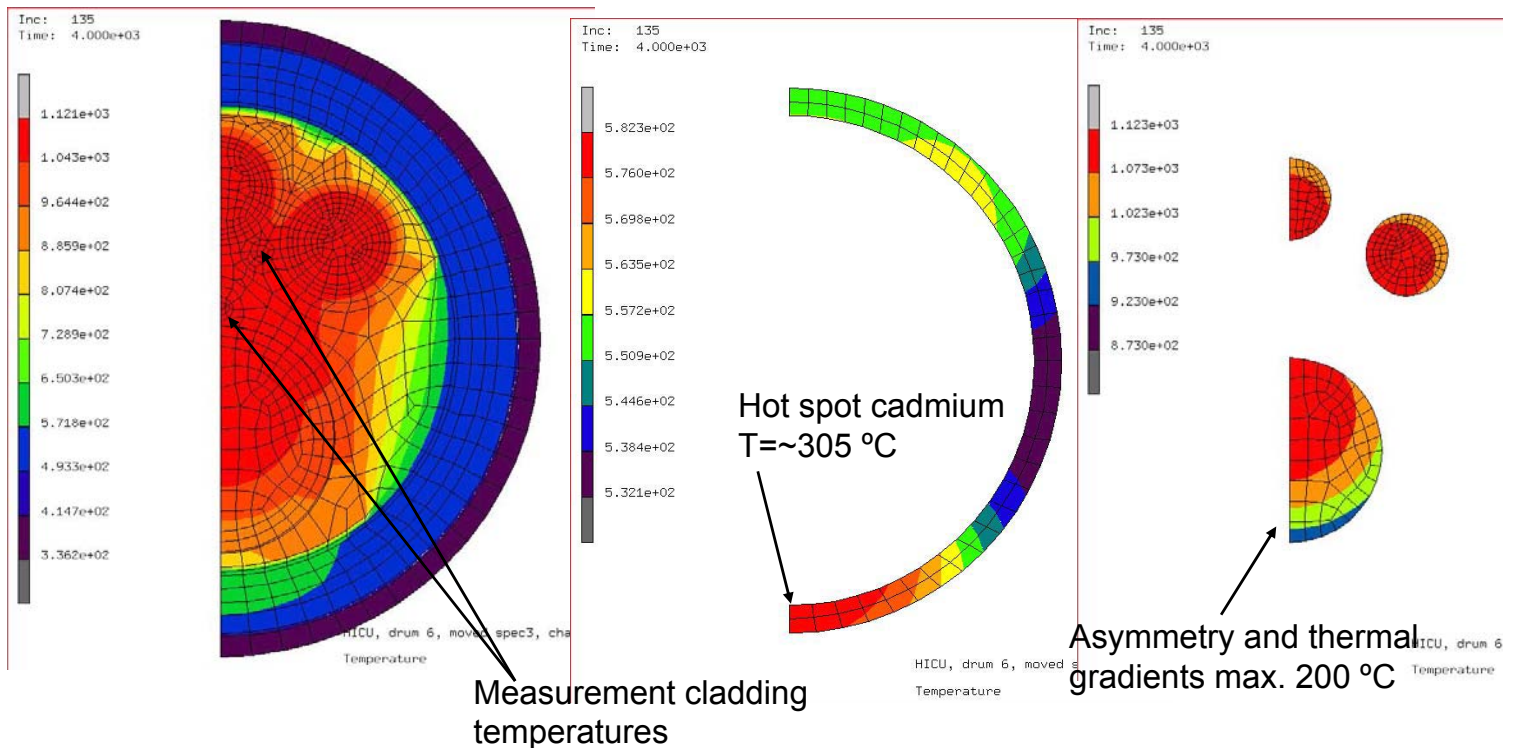
By R. Pieritz

Thermal analysis

- Design options limited by Cd-screen temperature ($T_m=320^\circ\text{C}$),
- n,α power up to 30 W/cm^3 , γ -heating up to 10 W/g

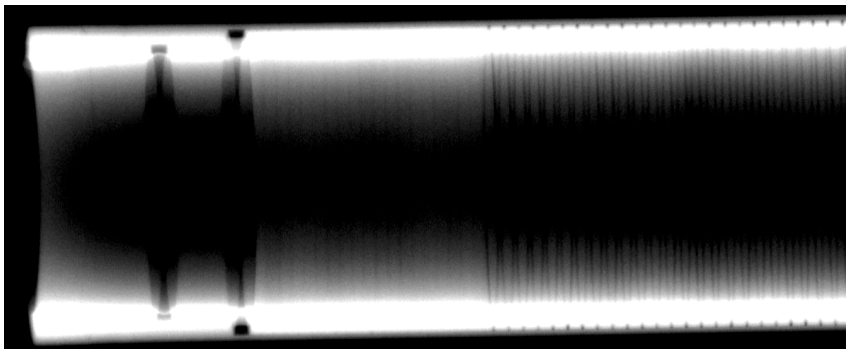
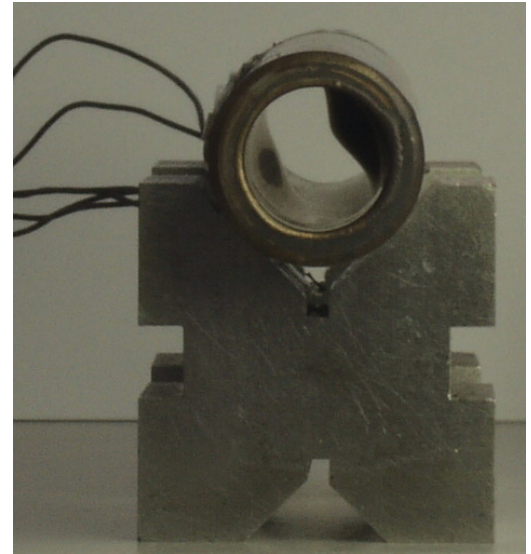


Thermal analysis (2)



Cd shield integration

- Double wall tube with Cd interlayer
 - high expansion coefficient ($>30 \times E-6$)
 - Low melting T (321°C)
- Prototypes
 - Testing manufacturing
 - * Isostatic pressing (1000 bar)
 - * Explosive welding
 - Testing thermomechanical behaviour

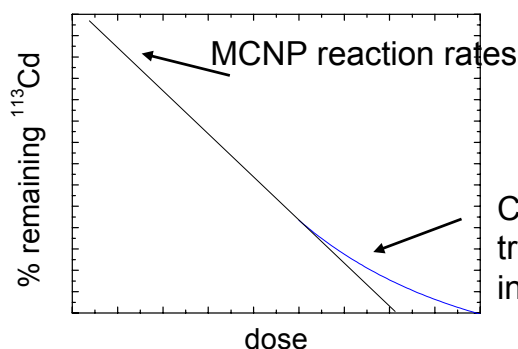


HH 13

Burnup of the cadmium shield

- Approximately linear burn-up (totally black for thermal neutrons)
- Gamma's from $(n, \text{}^{113}\text{Cd})$ absorbed where?

LI4SiO4-20%	Cd (mm)	W/cc	Cd burnup time (to 5%)
case 1	1.7Cd + Hf foil	26.13	1366
case 2	1.7Cd + Hf thread small pitch	27.48	1037
case 3	1.7Cd + Hf thread big pitch	30.38	437

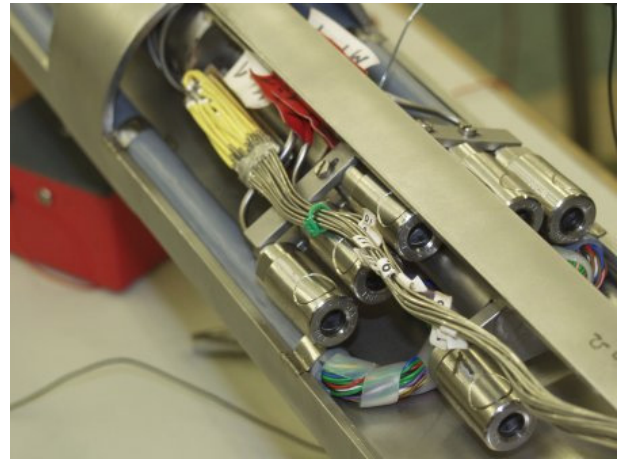
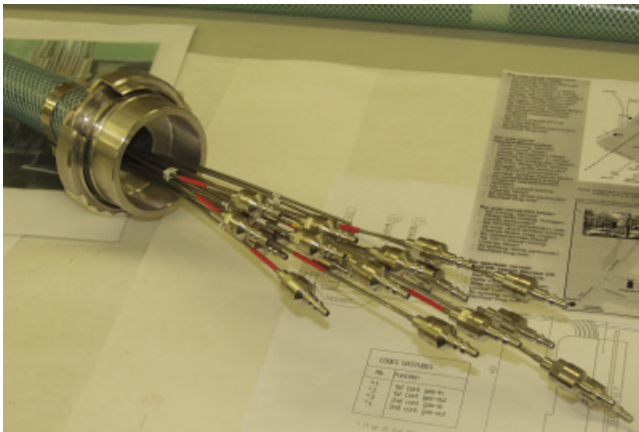


Low fluence rates, only relative differences

HH 14

Ex-core section & out-of-pile instrumentation

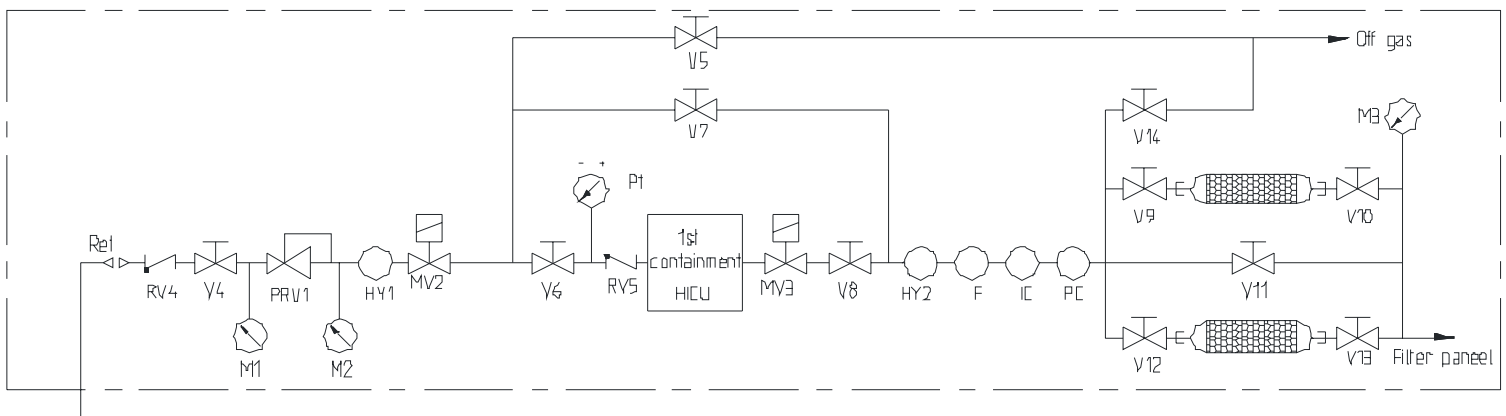
- Dedicated rig head modified for tritium producing experiments



HH 15

Gas supply system (1)

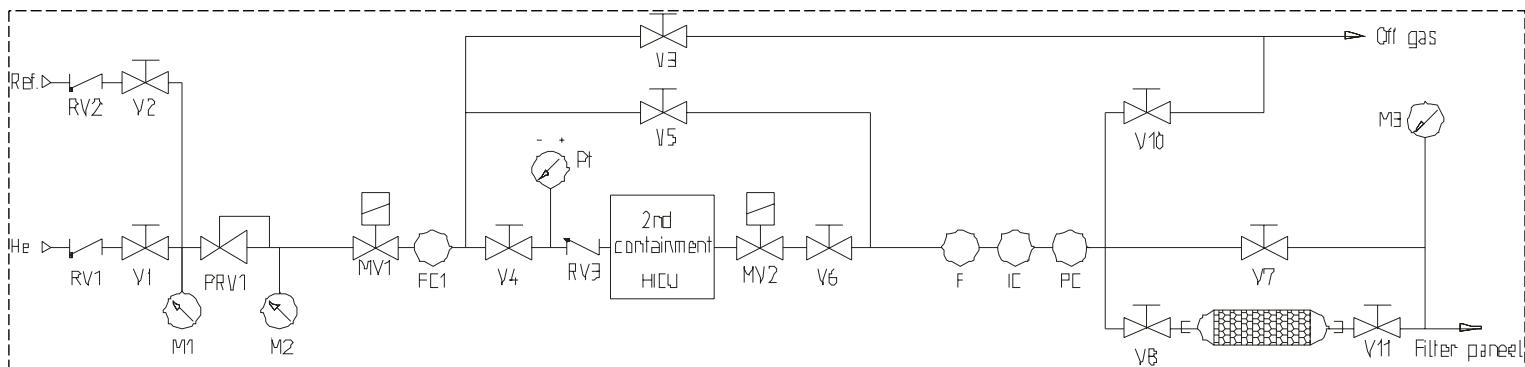
- First containment controlled from glovebox
 - Mixtures of He/H₂ and Ne gas (temperature control of ceramics)
 - Continuously purged
 - Measurement of pressure and flows
 - Measurement of Humidity and Tritium release by Ionisation chamber



HH 16

Gas supply system (2)

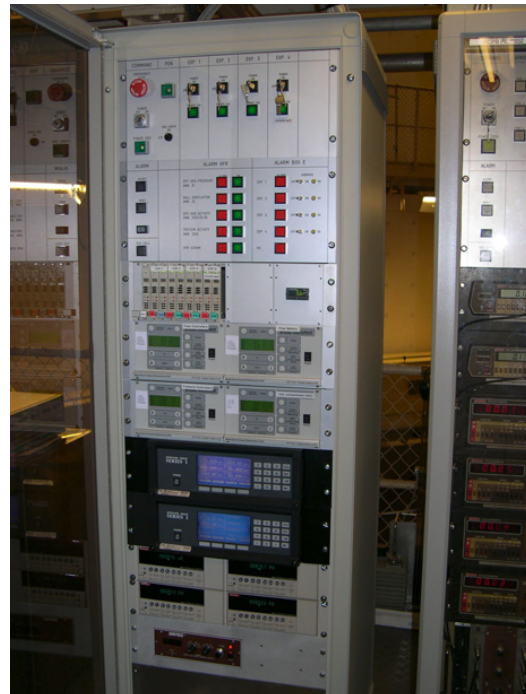
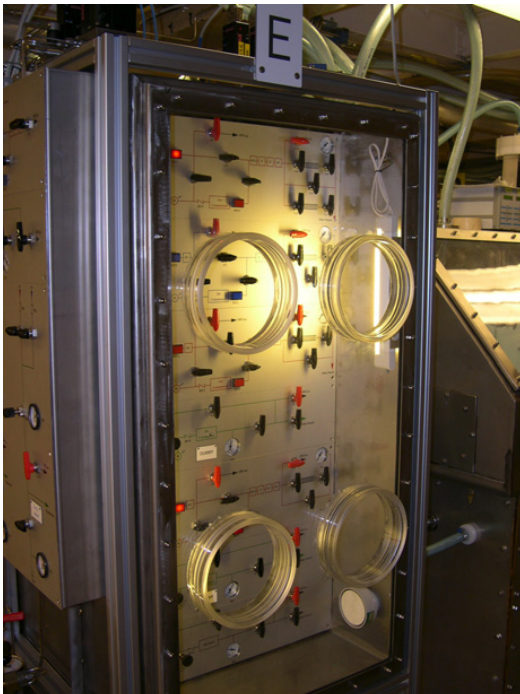
- Second containment, controlled from glovebox
 - Only He or He/H₂ gas (low temperature Cd shield required)
 - Continuously purged
 - Measurement of pressure and flows
 - Measurement of Humidity and Tritium release by Ionisation chamber



HH 17

Gas Supply system (3)

- Tritium glove box and control unit installed in the HFR Petten
- System is fully operational



HH 18

Test matrix and materials

NRG-ID.	Suppl.	% enrichment	High Constraint		Low Constraint		Total
			High T	Low T	High T	Low T	
NRG-126	FzK	OSi 20	2		1	1	4
NRG-125	FzK	OSi 7.5	2	1	1	1	5
NRG-129	FzK	OSi 7.5	1				1
NRG-124	FzK	OSi 0.06			1	1	2
			5	1	3	3	12
NRG-120	CEA	MTi 30	2		1	1	4
NRG-119	CEA	MTi 11	2	1	1	1	5
NRG-118	CEA	MTi 0.06			1	1	2
NRG-121	CEA	MTi 7.5			1	1	2
NRG-122	CEA	MTi 7.5	1		1		2
NRG-123	CEA	MTi 7.5			1	1	2
NRG-130	CEA	MTi 7.5	1	1			2
NRG-131	CEA	MTi 30			1	1	2
			6	2	7	6	21
NRG-115	JAERI	MTi 31	1		1	1	3
NRG-116	JAERI	MTi-5% 31	1	1	1	1	4
NRG-117	JAERI	MTi-10% 31	1		1	1	3
NRG-127	JAERI	MTi 7.5			1		1
			3	1	4	3	11
Total	Total		14	4	14	12	44
HiCon				18			
LoCon						26	

HH 19

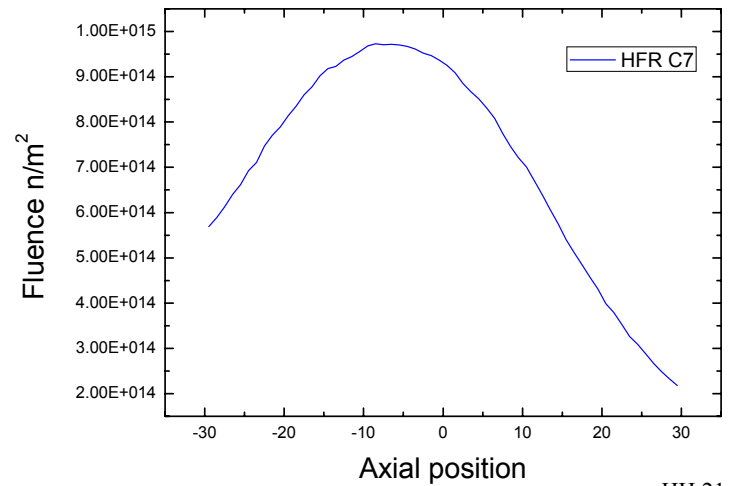
Axial distribution of the specimens

	material	T	density (g/cc)	Total Power		Ø _{in}	h						
				(W)	(W)								
DRUM 1	mti-ref+++ EU-CEA	LT	1.91	37.3	9	20		mti-ref+++ EU-CEA	1.91	91.3	9	20	
	mti-31-5% JP	LT	1.7	48.3	9	20	DRUM 5	osi-7.5+ EU-FZK	1.49	93.8	9	20	
	mti-31 JP	LT	1.75	21.1	4	43		osi-20 EU-FZK	1.49	51.1	4	43	
	mti-31-5% JP	LT	1.7	21.4	4	43		be-peb EU-Be	1.15	31.7	4	43	
	mti-31-10% JP	LT	1.68	21.7	4	43		mti-ref++ EU-CEA	1.91	41.0	4	43	
				377						822			
DRUM 2	mti-11 EU-CEA	LT	1.68	50.8	9	20	DRUM 6	osi-7.5 EU-FZK	1.49	94.8	9	20	
	osi-7.5 EU-FZK	LT	1.49	59.0	9	20		osi-7.5 EU-FZK	1.49	95.0	9	20	
	mti-30 EU-CEA	LT	1.73	31.0	4	43		be-peb EU-Be	1.15	32.6	4	43	
	mti-11 EU-CEA	LT	1.68	24.1	4	43		osi-7.5 EU-FZK	1.49	42.4	4	43	
	mti-0.06 EU-CEA	LT	1.68	23.9	4	43		osi-0.06 EU-FZK	1.49	35.4	4	43	
				504					829				
DRUM 3	mti-31 JP		1.75	83.3	9	20	DRUM 7	mti-11 EU-CEA	1.68	91.4	9	20	
	mti-31-5% JP		1.7	89.0	9	20		mti-11 EU-CEA	1.68	90.9	9	20	
	mti-31 JP		1.75	38.5	4	43		mti-ref EU-CEA	1.85	41.2	4	43	
	mti-31-5% JP		1.7	38.4	4	43		mti-11 EU-CEA	1.68	40.6	4	43	
	mti-31-10% JP		1.68	38.7	4	43		mti-7.5 JP	1.69	40.5	4	43	
				686					825				
DRUM 4	mti-30 EU-CEA		1.73	98.6	9	20	DRUM 8	osi-20 EU-FZK	1.49	107.7	9	20	
	mti-30 EU-CEA		1.73	104.0	9	20		osi-20 EU-FZK	1.49	104.9	9	20	
	mti-30 EU-CEA		1.73	45.9	4	43		be-disk EU-Be	1.85	34.6	4	43	
	mti-0.06 EU-CEA		1.68	35.6	4	43		osi-7.5 EU-FZK	LT	1.49	39.6	4	43
	mti-ref+ EU-CEA		1.82	36.7	4	43		osi-0.06 EU-FZK	LT	1.49	33.6	4	43
				788					823				
							DRUM 9	mti-ref+ EU-CEA	1.82	80.9	9	20	
								mti-31-10% JP	1.68	91.1	9	20	
								mti-ref EU-CEA	LT	1.85	34.6	4	43
								mti-ref++ EU-CEA	LT	1.91	34.8	4	43
								osi-20 EU-FZK	LT	1.49	42.1	4	43
									726				

HH 20

Nuclear Characteristics

- Nuclear characteristics (dpa, burnup, fluence) for all individual specimens are being calculated with MCNP and large model for HFR core. Calibration (a.o. PBA experiment) of code case is underway.
- Final arrangement of after thermal analysis and MCNP calculations



HH 21

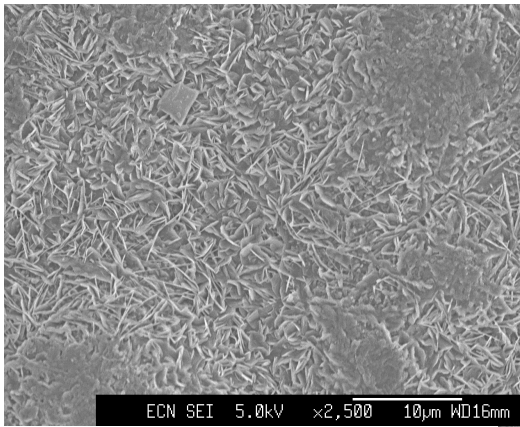
Materials & characteristics

NRG -ID	Material	suppl.	⁶ Li	Supplied density (g/cm ³)	He-pycnometry (g/cm ³)	Pebble size (µm)	closed porosity	crush load (N)
126	OSi 00/2-3	FzK	20	2.33 ^{*1}	2.305	< 630	2.7	4.18
125	OSi 97/3-1	FzK	7.5	2.372 ^{*1}	2.351	< 630	1.17	7.8
124	OSi 02/1-2	FzK	0.06	2.385 ^{*1}	2.357	< 630	0.62	5.74
129	OSi 03/1-3	FzK	7.5	2.34 ^{*1}	2.373	< 630	2.7	10.1
118	MTi CTI 1890 Ti 1100 CEA	CEA	30	3.28 ^{*2}	3.261	0.8 - 1.2	4.4	34
119	MTi CTI 2090 Ti 1140 CEA	CEA	11	3.26 ^{*2}	3.274	0.8 - 1.2	5.1	41
120	MTi CTI 2590 Ti 1100 CEA	CEA	0.06	3.23 ^{*2}	3.074	0.8 - 1.2	5.9	51
121	MTi CTI 942 Ti 1100 CEA	CEA	7.5	3.26 ^{*2}	3.267	0.6 - 0.8	4.9	31
122	MTi CTI 1271 Ti 1100 CEA	CEA	7.5	3.24 ^{*2}	3.260	0.8 - 1.2	5.5	40
123	MTi CTI 1532 Ti 1100 CEA	CEA	7.5	3.25 ^{*2}	3.267	0.8 - 1.2	5.3	31
130	MTi CTI 273 Ti 1100 CTI	CEA	7.5	3.25 ^{*2}	3.280	0.6 - 0.8	5.3	37
131	MTi CTI 1233 Ti 1100 CEA	CEA	30	3.23 ^{*2}	3.246	0.6 - 0.8	5.8	33
115	MTi-0% TiO ₂	JAERI	31	2.88 ^{*3}	3.192	1.05		24
116	MTi-5% TiO ₂	JAERI	31	2.80 ^{*3}	3.323	1.06		33
117	MTi-10% TiO ₂	JAERI	31	2.75 ^{*3}	3.328	1.05		24
127	MTi	JAERI	7.5		3.287			

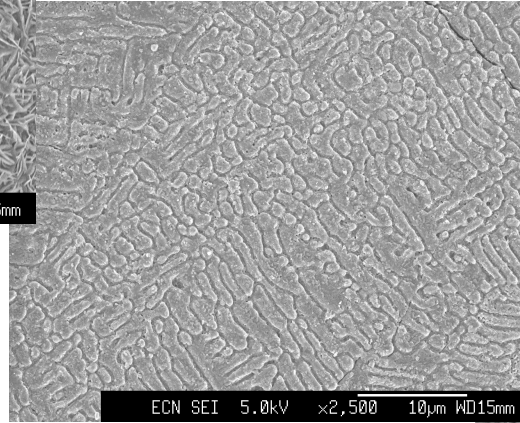
¹ reported values, ² calculated from closed porosity and 3.43 g/cm³ T.D., ³ calculated from % T.D.

Microstructure Osi pebbles

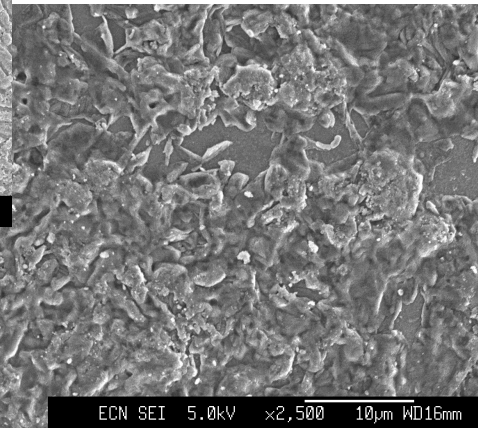
- OSi pebbles, melt spray by Schott Gmbh supplied through FZK (main process adapted to avoid CO₂ induced porosity)



OSi – 0.06% ⁶Li



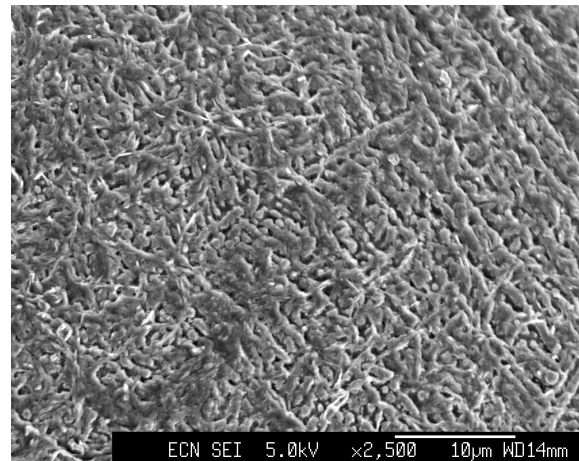
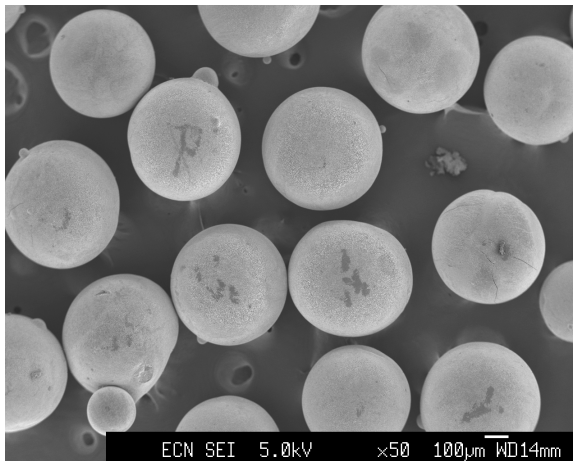
OSi – 7.5% ⁶Li



OSi – 20% ⁶Li

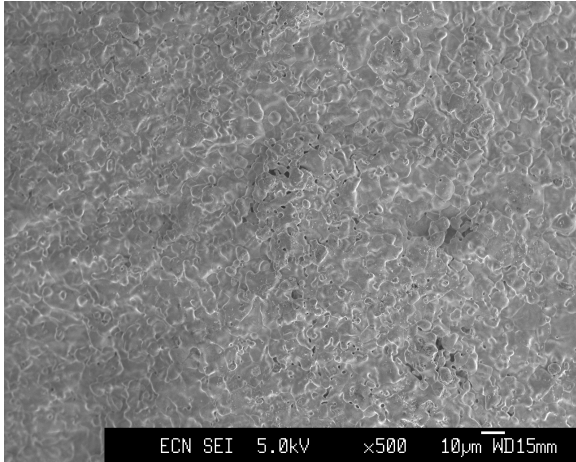
New Orthosilicate pebbles

- OSi pebbles, using the hydroxide processing

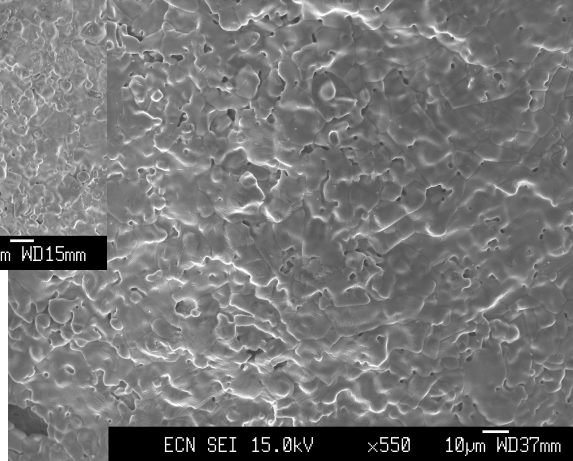


Microstructure MTi pebbles (CEA)

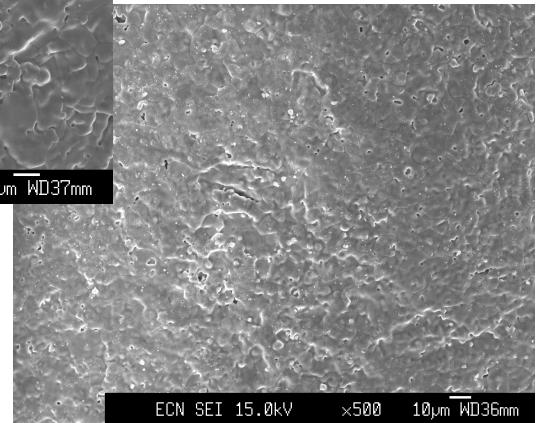
- MTi pebbles by extrusion-spheronisation method at CTI and CEA, supplied by CEA



MTi – 0.06% ⁶Li

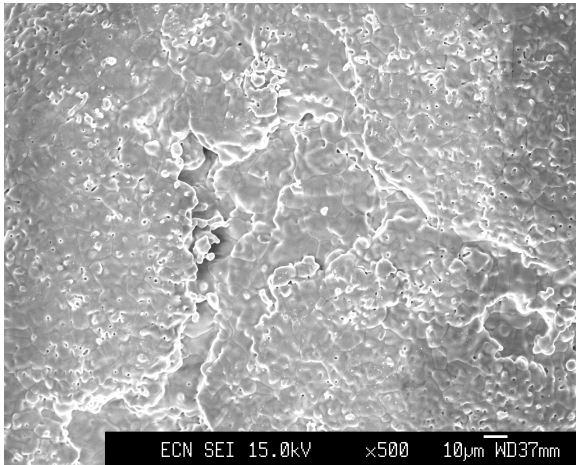


MTi – 11% ⁶Li

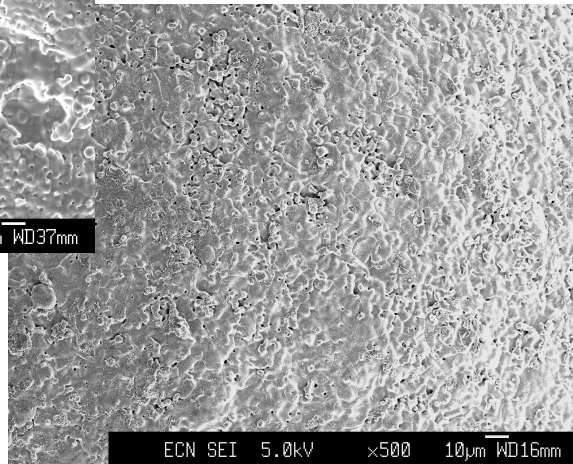


MTi – 30% ⁶Li

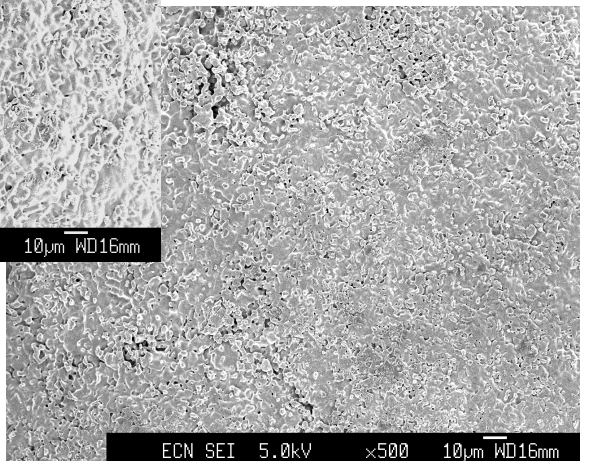
Microstructure MTi pebbles (CEA)



Smaller pebbles nat. enrichment



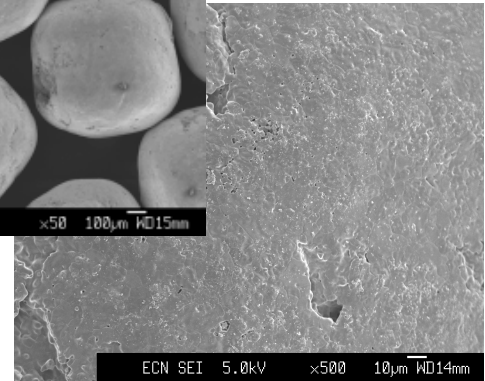
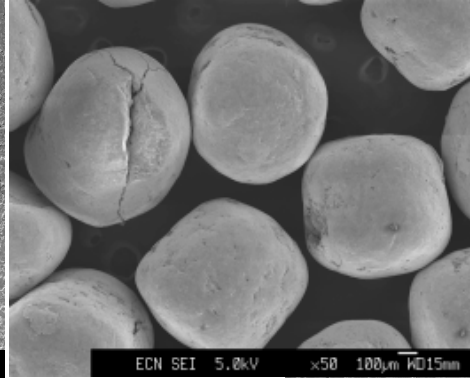
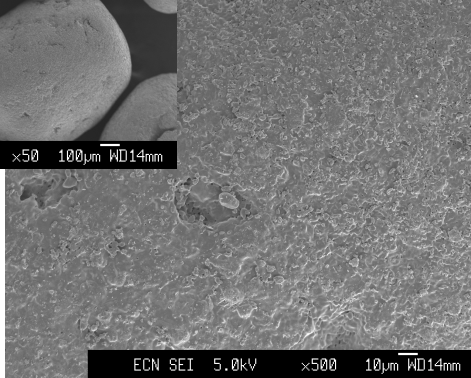
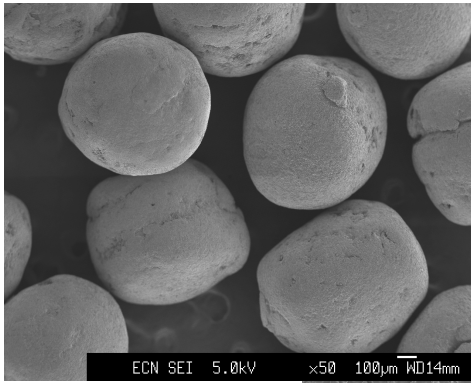
Same as in sub-module irradiation



Industrial batch, Nat. enrichment

Microstructure MTi pebbles (CEA)

Latest fabrication from CEA



Nat. enriched

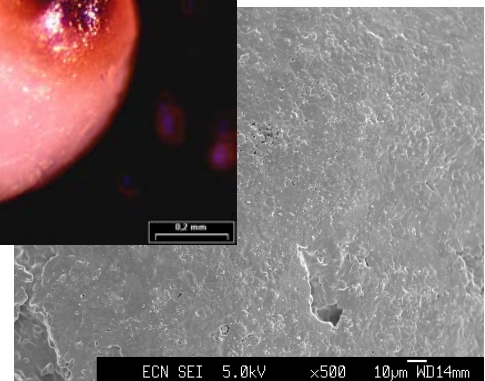
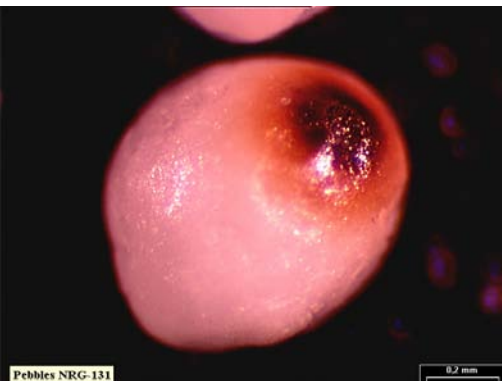
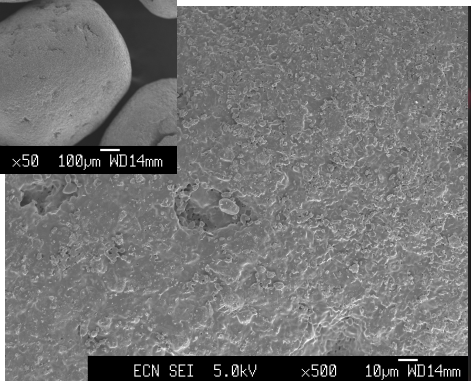
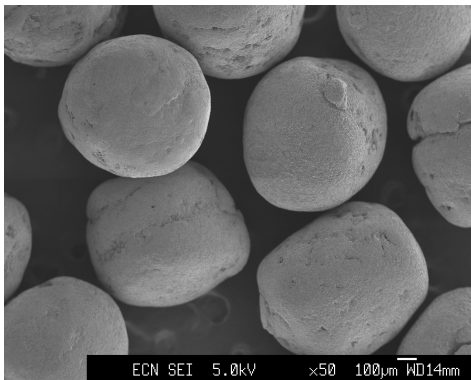
30% enriched

Some pebbles contain some glassy phase

HH 27

Microstructure MTi pebbles (CEA)

Latest fabrication from CEA



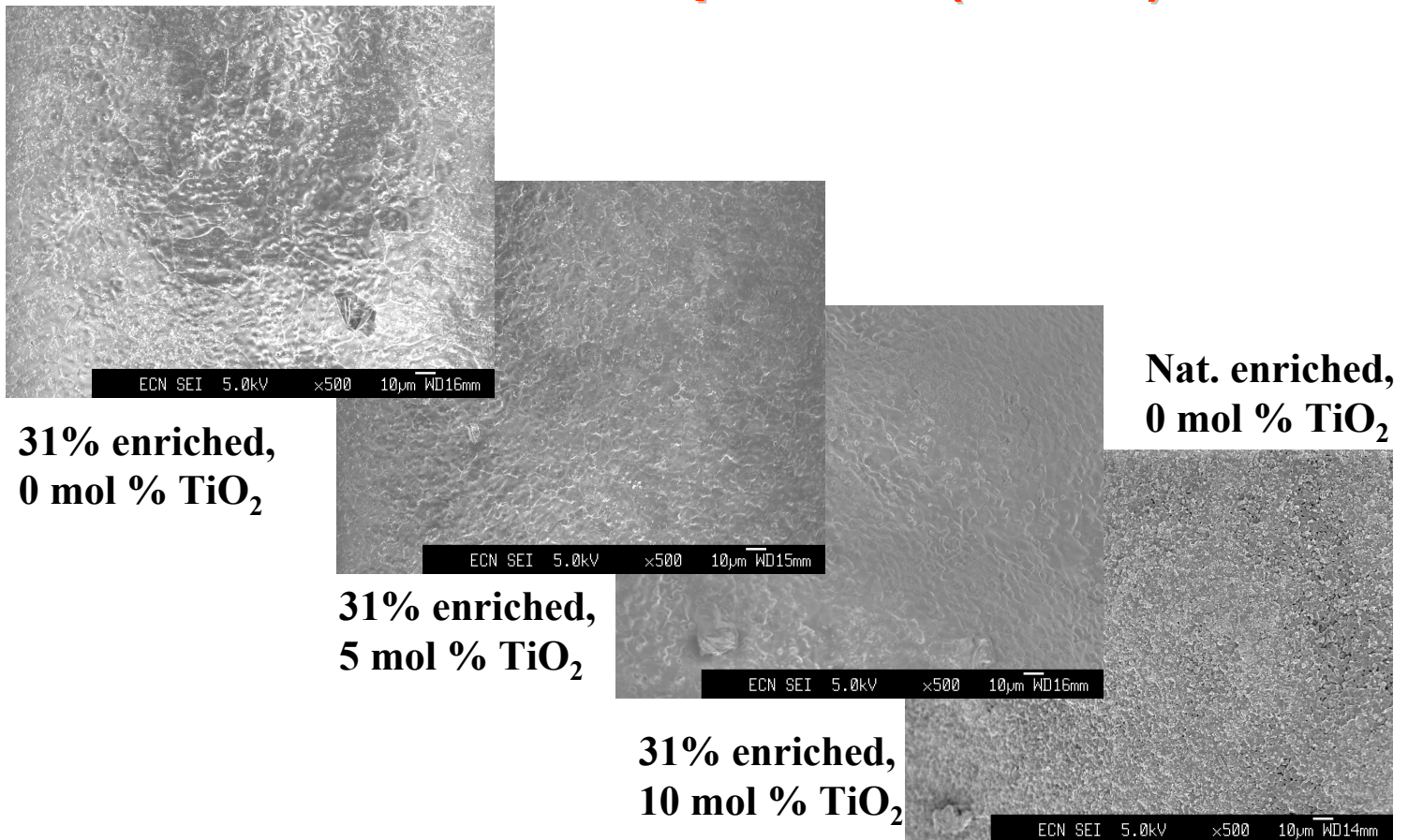
Nat. enriched

30% enriched

Some pebbles contain some glassy phase

HH 28

Microstructure MTi pebbles (JAERI)



Status

- Cd screen design is robust, and resistant to Cd melting. Manufacturing process is being elaborated, along with heat transfer test.
- Drum and specimen clamping schemes are detailed for thermal management of total assembly.
- Out of pile equipment is installed and operational at HFR
- Pre-testing HICU pebble stacks with X-ray tomography is finished, fabrication Pt-tubes, filling and X-ray tomography by the end of 2004. Materials loaded will be sieved, checked for fragments etc.
- Specimen loading and rig assembly, allow start of irradiation 1st QTR 2005

Materials (1)

Material	suppl	⁶ Li	density (g/cm ³)	Porosity (%)		pebble size (mm)
				open	closed	
OSi-ref	FZK	20	2.33 (1.5)		2.7	0.25-0.63
OSi-ref	FZK	7.5	2.372 (1.5)		1.17	0.25-0.63
OSi-ref	FZK	0.06	2.385 (1.5)		0.62	0.25-0.63
MTi-ref	CEA	30	1.73	7.5	5.9	0.8-1.2
MTi-ref	CEA	11	1.68	13.2	5.1	0.8-1.2
MTi-ref	CEA	0.06	1.68	12.5	4.4	0.8-1.2
MTi-ref	CEA	7.5	1.85	4.2	5.5	0.8-1.2
MTi-ref+ (indust)	CEA	7.5	1.82	6.0	5.3	0.8-1.2
MTi-ref++	CEA	7.5	1.91	2.0	4.9	0.6-0.8
MTi-ref-0%	JAERI	31				
MTi-ref-5%	JAERI	31				
MTi-ref-10%	JAERI	31				
MTi-ref-0%	JAERI	7.5	2.77			0.85-1.18

HH 31

Materials (6)

Material	suppl	⁶ Li cont. (%)	Pebble density (g/cm ³)	Open Porosity (%)		Closed porosity (%)	He-density (meas.NRG) (%)
OSi-ref	FZK	20	2.33			2.7	2.305 ± 0.001
OSi-ref	FZK	7.5	2.372			1.17	2.351 ± 0.002
OSi-ref	FZK	0.06	2.385			0.62	2.357 ± 0.001
MTi-ref	CEA	30		7.5		5.9	3.074 ± 0.004
MTi-ref	CEA	11		13.2		5.1	3.274 ± 0.004
MTi-ref	CEA	0.06		12.5		4.4	3.261 ± 0.007
MTi-ref	CEA	7.5		4.2		5.5	3.261 ± 0.006
MTi-ref+	CEA	7.5		6.0		5.3	3.267 ± 0.006
MTi-ref++	CEA	7.5		2.0		4.9	3.266 ± 0.006
MTi-ref-0%	JAERI	31					3.192 ± 0.007
MTi-ref-5%	JAERI	31					3.323 ± 0.007
MTi-ref-10%	JAERI	31					3.382 ± 0.007
MTi-ref-0%	JAERI	7.5	2.77				

HH 32

CBBI 12, Karlsruhe, 17-09-2004



In pile behavior of the Pebble bed Assemblies in the HFR, results and first data analyses

Presented by:
Lida Magielsen

Co-authors: J.G.van der Laan, J.H.
Fokkens, M.P. Stijkel

OUTLINE

- * INTRODUCTION
- * IN- PILE OPERATION
- * FIRST ANALYSIS RESULTS
- * CONCLUSION

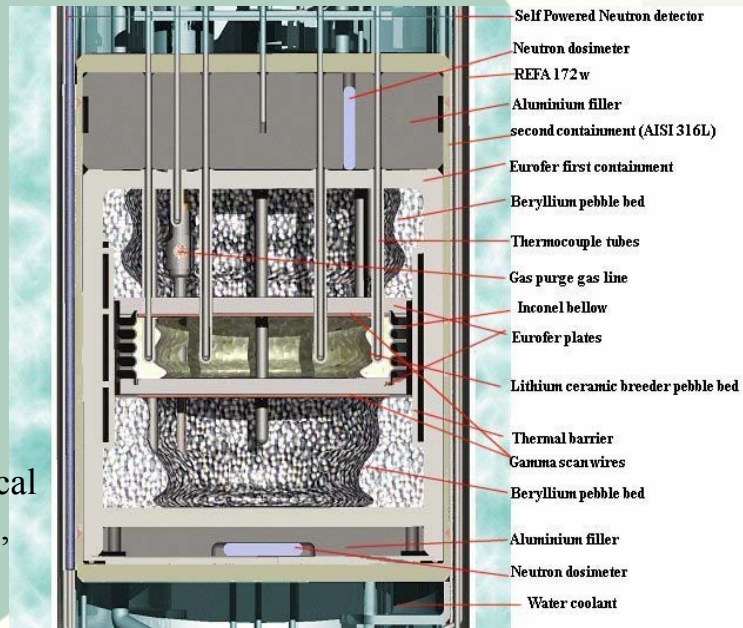


INTRODUCTION (1)

Design of Pebble bed Assemblies

INPUTS FOR DESIGN:

- Tests for determination of creep strain/ temperature dependent thermal conductivity of Be and Li ceramic pebble beds (performed by FZK)
- MCNP neutronic calculations
- Development of thermo mechanical model with out of pile test results, which also accounts for creep



INTRODUCTION (2)

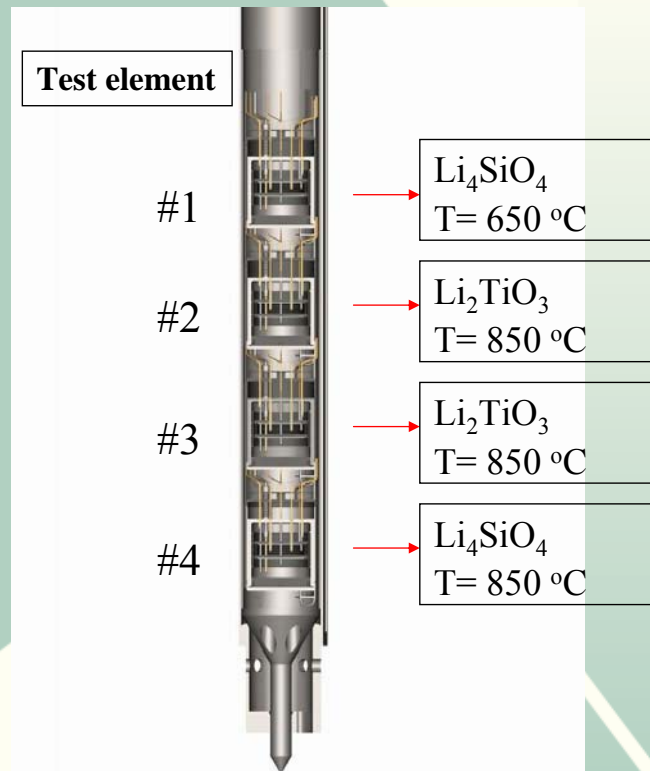
Test Matrix

Test element		1	2	3	4
Material		Li4SiO4	Li2TiO3	Li2TiO3	Li4SiO4
Supplier		FZK	CEA	CEA	FZK
NRG code		NRG 100	NRG 113	NRG 105	NRG 100
6 Li enrichment		7.5% (natural)			
Lithium burn up		plm. 3%			
Pebble dimensions	mm	0.25-0.63	0.8-1.2	0.8-1.2	0.25-0.63
Quantity of breeder material	g	24.94	32.28	32.62	25.17
Quantity of Beryllium	g	91.54	92.7	92.95	92.95
Beryllium supplier		NGK			
Beryllium pebble size	mm	0.9-1.1			
Purge gas 1st containment		He + 0.1 vol. % H2			
2nd containment		Mixture He/ Ne			
Gas flow 1st containment	ml/min	100			
2nd containment	ml/min	20-120			
Pressure 1st containment	bar	3			
2nd containment	bar	3			
Max. temperature breeder	oC	< 725	< 900	< 950	< 910
Temp. Floating plates	oC	< 450	< 580	< 600	< 585
Temp. Eurofer 1st containment	oC	< 200	< 285	< 300	< 290
Temp. Beryllium beds	oC	< 420	< 540	< 550	< 540

INTRODUCTION (3)

Operating conditions

- * Test element #1 and 4 same material at different temperature
- * Test element # 2 and # 3 different in grain size and creep behaviour
- * All first containments are continuously purged with He + 1000 ppm H₂ and optionally with Ne/He + 1000 ppm H₂ for extra T control



INTRODUCTION (4)

Fabrication and assembly

- Proto type assembly
- Development of precompaction procedure
- Filling and assembly of test elements
- Intermediate X-Ray examination
- Total assembly of four test elements

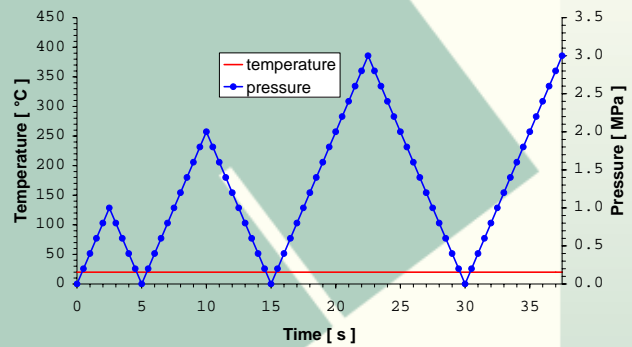


INTRODUCTION (5)

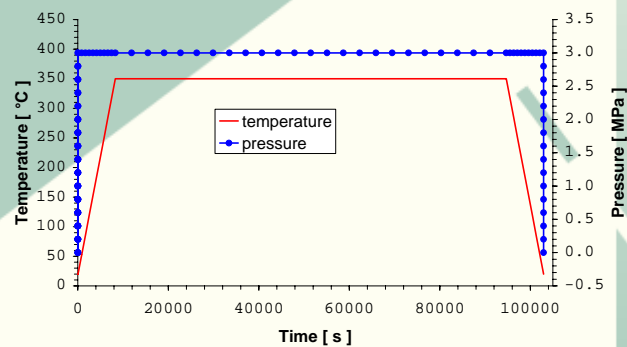
Pre compaction of the Pebble beds

- * First compaction step to 1 MPa
- * Afterwards compaction to 2 MPa and 3 MPa
- * Compaction of beds to 3 MPa
- * Heating of test element to 350 °C during 18 hours
- * Cool down
- * Screw toplid to test element

Pre-compaction procedure (1)

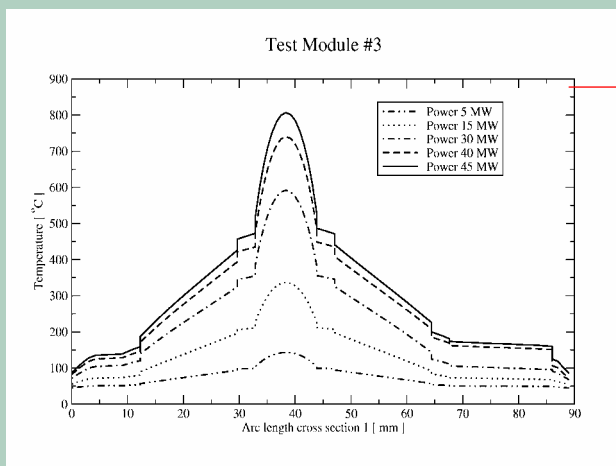


Pre-compaction procedure (2)



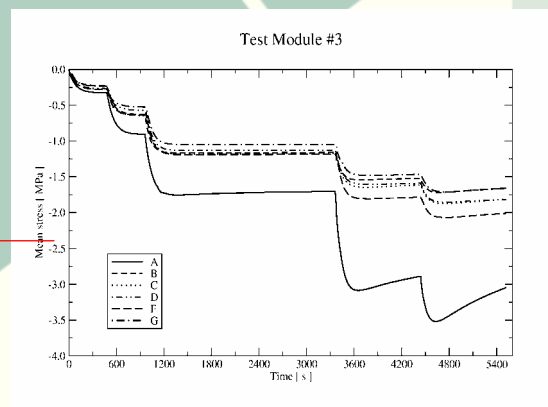
INTRODUCTION (6)

Pre irradiation calculations



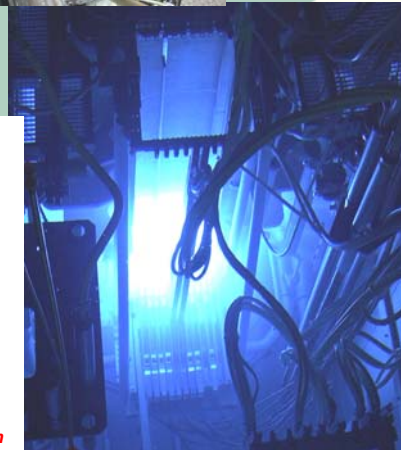
Temperature development during start-up in axial direction

Development of stress inside beryllium and breeder pebble beds during start up



IN-PILE OPERATION (1)

- * PBA are irradiated in HFR positions H4 and H6
- * Operation started April 17, 2003
- * Now irradiated up to 10 cycles

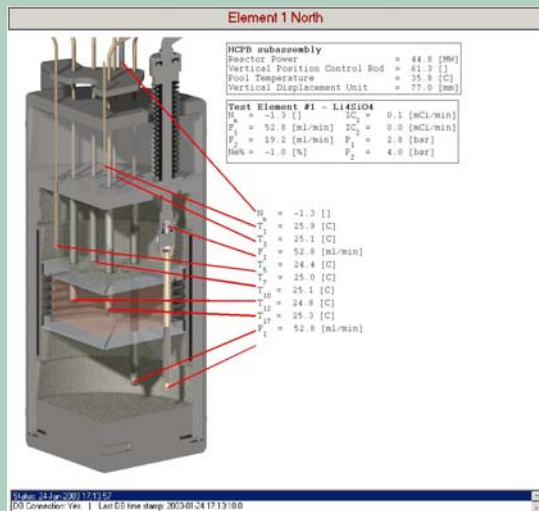


	A	B	C	D	E	F	G	H	I
1	Be	Be	Be	Be	Be	Be	Be	Be	Be
2	F	F	F	D2	F	F2	F	H2	Be
3	F	F	C3	F	E3	F	G3	F	Be
4	F	CR	F	CR	F	CR	F	H4	Be
5	F	F	C5	F	E5	F	G5	F	Be
6	F	CR	F	CR	F	CR	F	H6	Be
7	F	F	C7	F	E7	F	G7	F	Be
8	F	F	F	D8	F	F8	F	H8	Be
9	Be	Be	Be	Be	Be	Be	Be	Be	Be

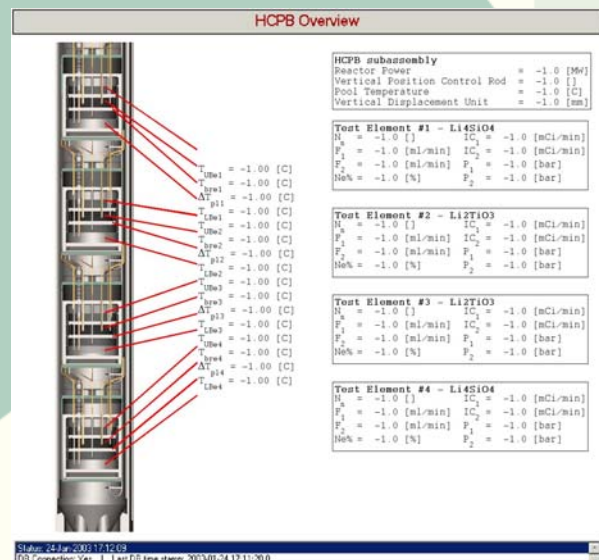
- F** Fuel element
- CR** Control rod
- Be** Reflector element
- E5** Experiment
- H4** HCPB PBA Irradiation

IN-PILE OPERATION (2) Operation monitoring

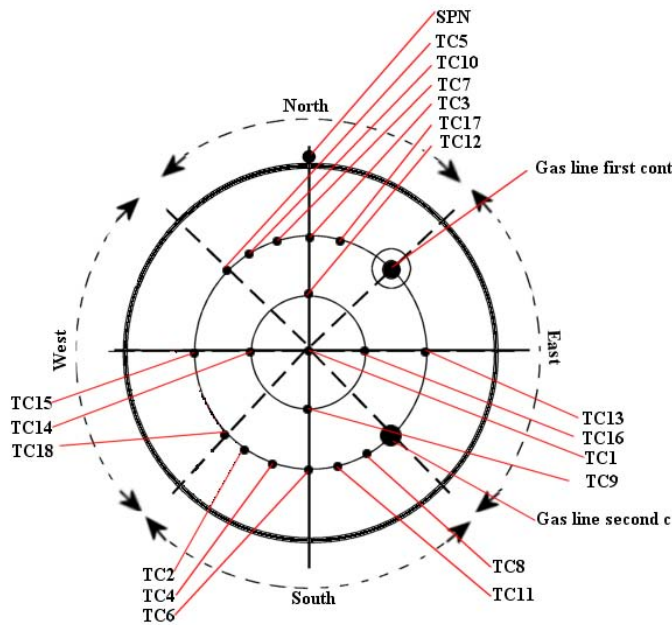
- * Development of an on-line and remote monitoring and analysis tool using MATLAB



- * Visualisation of all instrumentation in PBA
- * Real time monitoring of all operational parameters

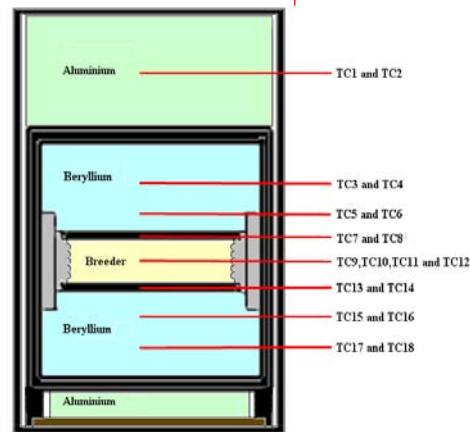


IN-PILE OPERATION (3) Temperature Measurement



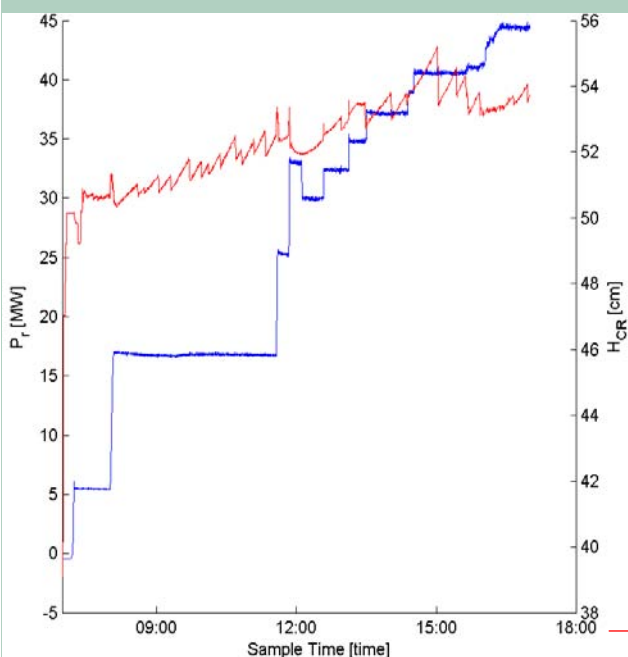
* Location of thermocouples inside test element

Radial distribution
Axial distribution



IN-PILE OPERATION (4)

Start up of first irradiation cycle



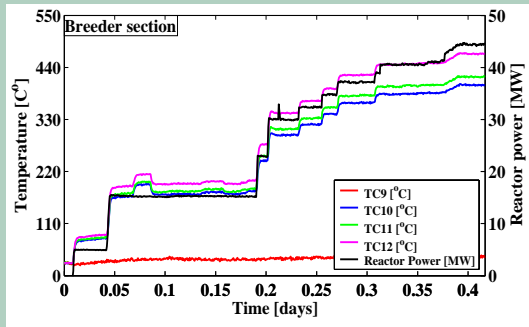
- * Special start up procedure was requested, including intermediate power steps to stabilise the pebble beds
- * At 15 MW tests were performed to obtain the temperature control range
- * Also longer hold times at 40 MW has been taken for creep compaction issues

Power evaluation and control rod movement during start up

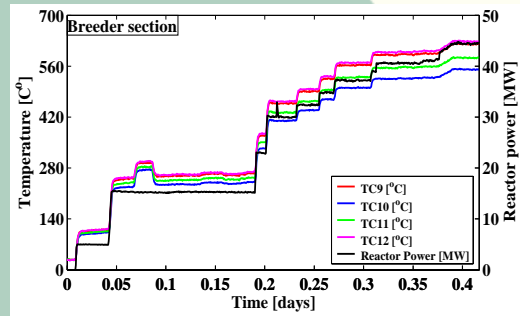
IN-PILE OPERATION (5)

Breeder section temperatures at start-up

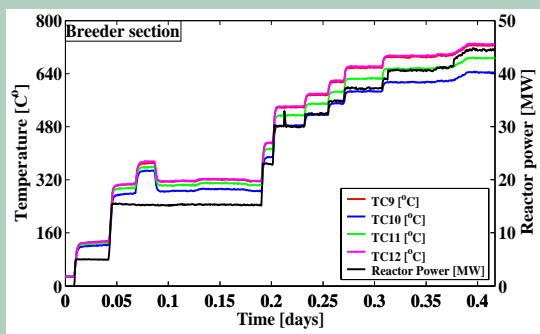
Test element #1



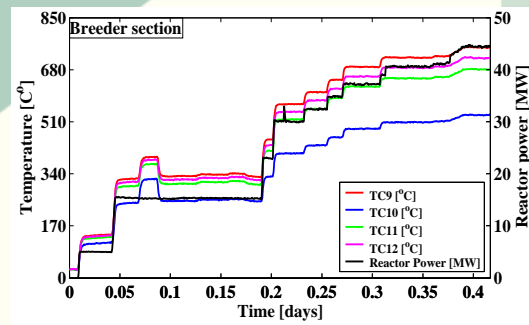
Test element #2



Test element #3



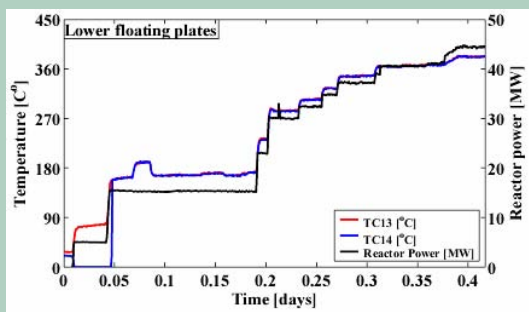
Test element #4



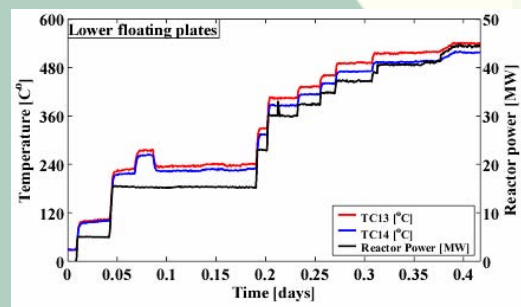
IN-PILE OPERATION (6)

Lower Floating plate temperatures at start-up

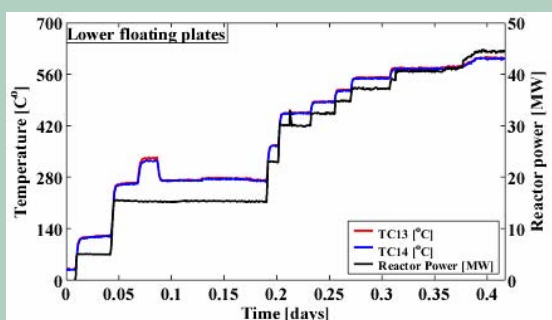
Test element #1



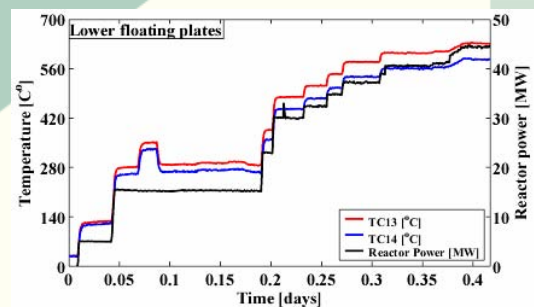
Test element #2



Test element #3



Test element #4



IN-PILE OPERATION (7)

Temperatures at 45 MW after start-up

- Temperature of breeder beds, TE-#1 to #4

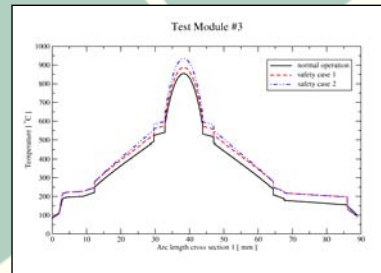
✓ $T_{av, \text{Test element 1}} = 440 \text{ } ^\circ\text{C}$

✓ $T_{av, \text{Test element 2}} = 600 \text{ } ^\circ\text{C}$

✓ $T_{av, \text{Test element 3}} = 660 \text{ } ^\circ\text{C}$

✓ $T_{av, \text{Test element 4}} = 680 \text{ } ^\circ\text{C}$

Very unsymmetrical Temperature profile



- Temperature of floating plates

✓ $T_{av, \text{Test element 1}} = 400 \text{ } ^\circ\text{C}$

✓ $T_{av, \text{Test element 2}} = 560 \text{ } ^\circ\text{C} (!)$

✓ $T_{av, \text{Test element 3}} = 625 \text{ } ^\circ\text{C} (!)$

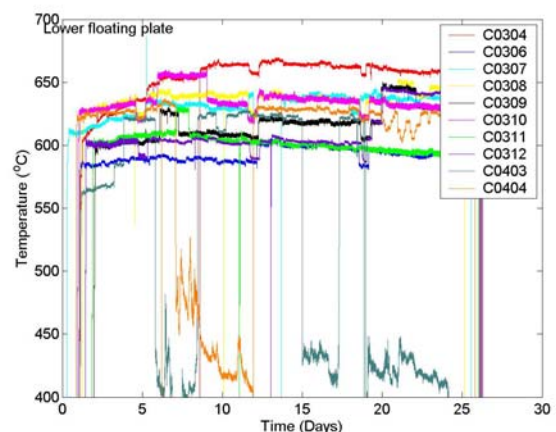
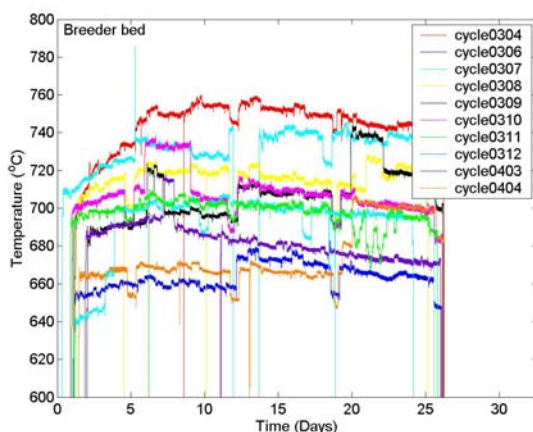
✓ $T_{av, \text{Test element 4}} = 600 \text{ } ^\circ\text{C} (!)$

	2nd containment	bar	3	3	3	3
Max. temperature breeder	oC	< 725	< 900	< 950	< 910	
Temp. Floating plates	oC	< 450	< 580	< 600	< 585	
Temp. Errorer 1st containment	oC	< 200	< 265	< 300	< 290	
Temp. Beryllium beds	oC	< 420	< 540	< 550	< 540	

IN-PILE OPERATION (8)

Continuation of irradiation

- * Other irradiation cycles started according to standard procedures
- * In the second irradiation cycle a shielding sample holder was used
- * Temperatures decreased due to ^6Li burn up
- * Floating plate temperatures continued to be high

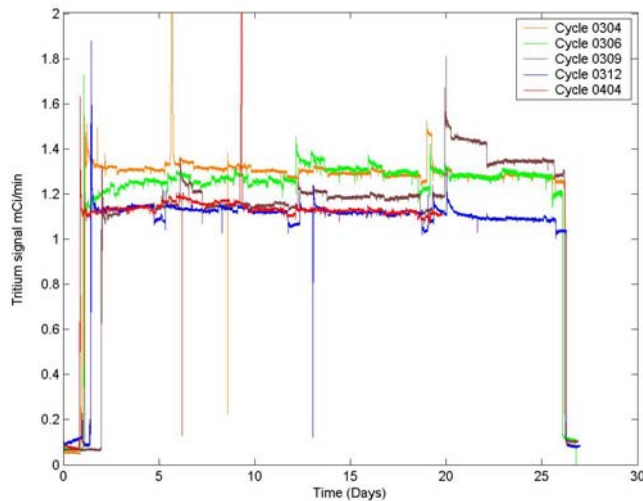


Evaluation of temperatures in Breeder and low. FP for TE#3

IN-PILE OPERATION (9)

Tritium measurement

- * Estimation of the ${}^6\text{Li}$ burn up is done with the ${}^3\text{H}$ measurement
- * Also used for estimation of neutron dose purpose
- * Difficult measurement because of Neon (different ionising potential, Jesse Effect)

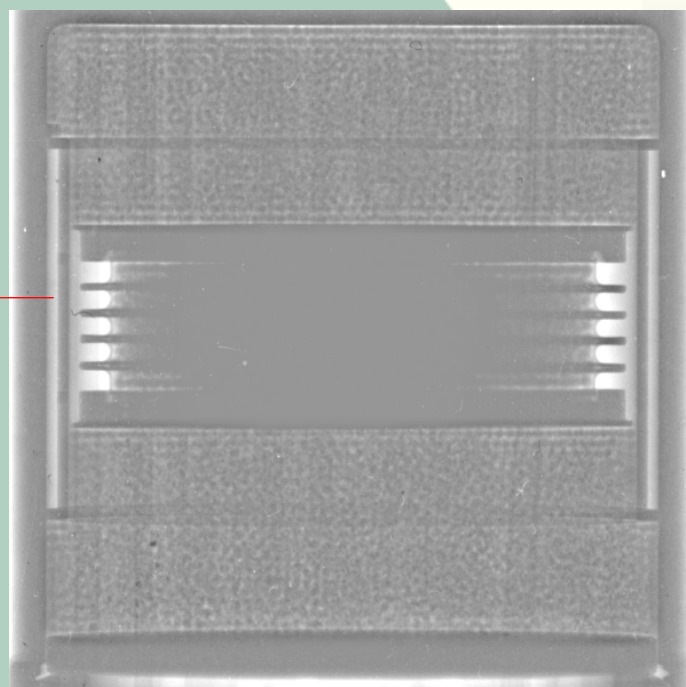


Tritium signals from some irradiation cycles for test element #3

IN-PILE OPERATION (10)

Neutron radiography

- * Before start of in-pile operation, after first cycle and after 8 cycles a radiograph was taken
- * TE-#3 gives best image for evaluation, parallax for other quite significant
- * Further image analysis to look for irradiation induced changes

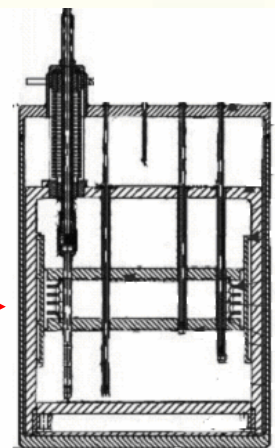


Evaluation after 10 irradiation cycles

- * Hot floating plate temperatures
 - * Relatively low breeder bed temperatures
 - * Gaps formation visualisation in neutroradiographics is not conclusive
 - * Thermo mechanics has to be evaluated
 - * Approx. 1.7 dpa in Eurofer
 - * $6 \cdot 10^{22}$ at T production
 - * Total lithium burn up 1.5 to 2.5 %
 - * Irradiation continued on September 9, after some interruption for another two months
- Subject to next presented thermal analysis

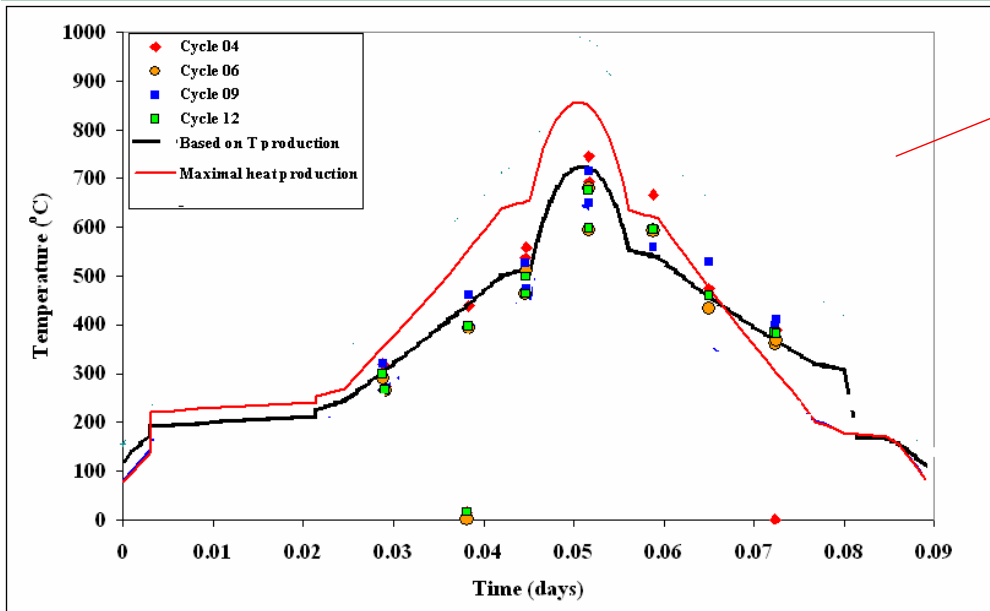
ANALYSIS OF DATA, FIRST RESULTS (1)

- * Analysis of unsymmetrical profile based on observations:
 - At the lower part eight heat interfaces instead of six in the upper part, with a probable gap between Lower Al filler and Eurofer
 - Neutronic calculations for n, α heating were overestimated
 - Thermocouple tubes take part in heat transport



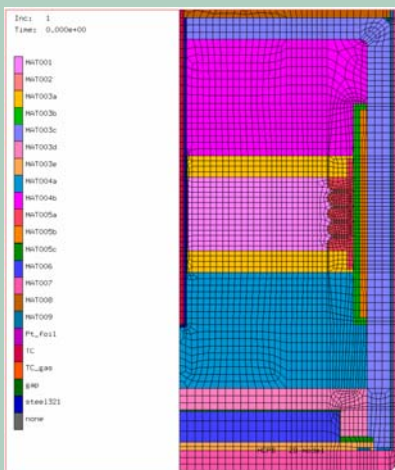
Comparison measured data and calculated temperature

- * Based on measured ^3H data
- * Gas gap between Al filler and Eurofer plate

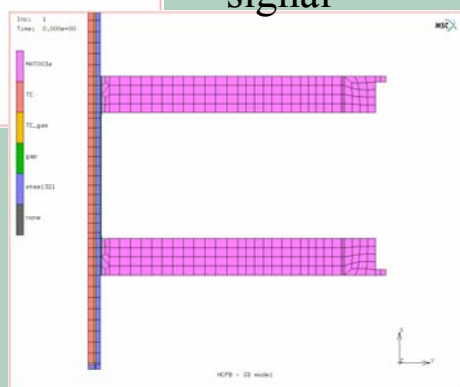


Still not accounted for high T in lower floating plate

Finite element model of test element #3

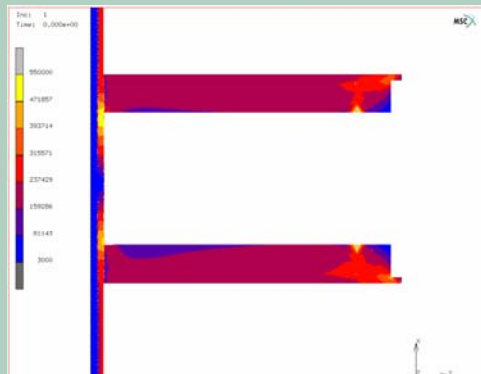


- * 2D axi symmetrical model
- * Thermocouple tube modelled at the center
- * Gas gap between Al filler and Eurofer
- * n, α heating from actual tritium signal

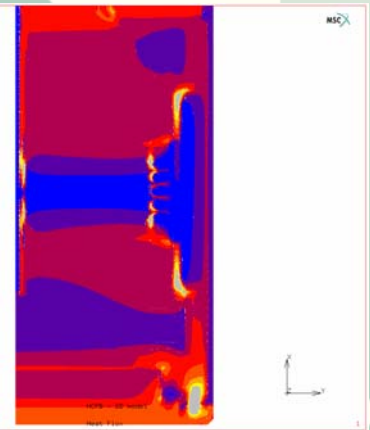
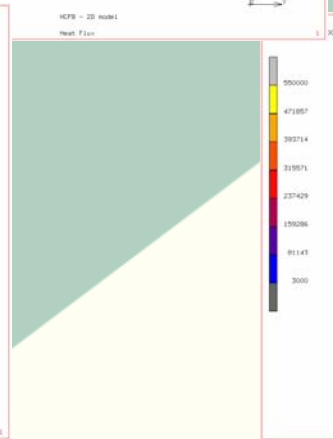
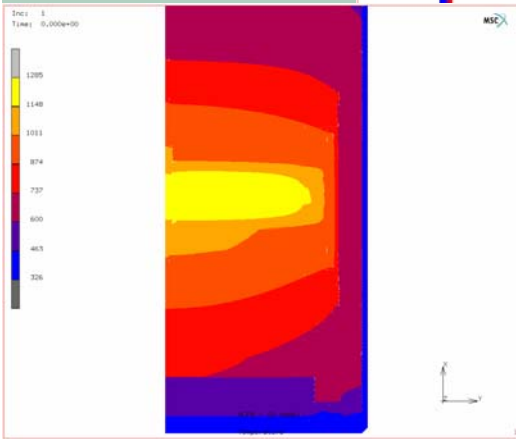


ANALYSIS OF DATA, FIRST RESULTS (4)

Heat flux through test element #3 [W m^{-2}]



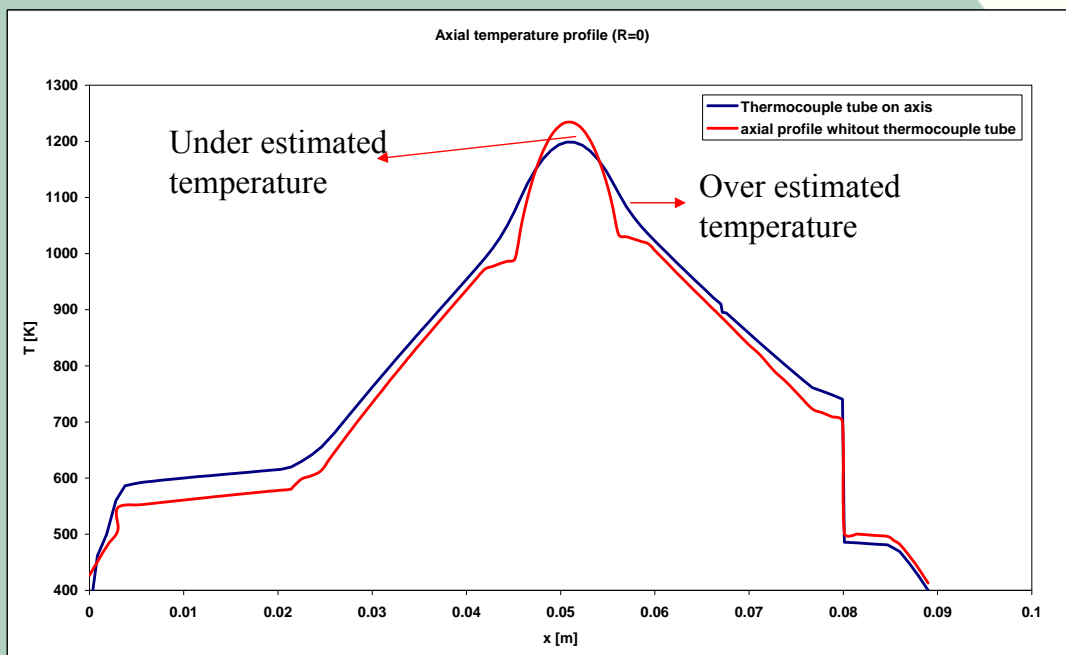
Removal of heat through tube:
Up to 550 kW m^{-2}



ANALYSIS OF DATA, FIRST RESULTS (5)

Axial T profile of test element #3 [W m^{-2}]

* Temperature profile on $r = 0$ with and without thermocouple tube



Future actions for analysis of in-pile data

- * The complete first irradiation cycle is to be calculated with the full coupled thermo mechanics model with the actual gas transients and nuclear data
- * First cool down test calculation has been done and is to be adapted for the cool down calculation of test element 3
- * Modelling of thermocouple tube in full coupled model
- * Expansion to 3D model to account for effect of tubes
- * More information is to be obtained from PIE

CONCLUSIONS

- * PBA irradiated 10 irradiation cycles, still 2 more to go
- * Gaps formation visualisation in neutroradiographics is not conclusive
- * Approx. 1.7 dpa in Eurofer
- * $6 \cdot 10^{22}$ at T production
- * Total lithium burn up 1.5 to 2.5 %
- * Thermocouple tubes interfere with the heat transport, giving underestimate readings for the breeder bed and overestimate readings for the lower floating plates